Investigation of Novel Thermoelectric Refrigeration Systems

By

Xiaoli Ma, BEng, MSc

Thesis submitted to the University of Nottingham

For the degree of Doctor of Philosophy

July 2004

THESIS CONTAINS CD/DVD

Contents

Abstract

Concern over global warming and depletion of the ozone layer has stimulated research to develop cooling methods that do not employ environmentally damaging working fluids such as CFCs and HCFCs. Two methods that have been considered are absorption and thermoelectric 'Peltier' cooling systems. Absorption systems, using H_2O/LiBr have the advantage of being able to use low-grade waste heat. However, the large volume, high capital cost and low performance of these systems have inhibited their widespread application.

Thermoelectric systems were developed in the 1950s and use of this technology for air-conditioning applications was investigated as early as the 1960s. However, the continued development of thermoelectric systems was slow owing to technical difficulties and the superior performance of vapour-compression systems in terms of coefficient of performance (COP). It is known however that most working fluids employed in vapour-compression systems are damaging to the environment, and as vapour-compression systems contain moving parts, they have the further disadvantage of being noisy and requiring regular maintenance. In recent years therefore, there has been stimulated interest in using thermoelectric "Peltier" cooling systems for domestic refrigerators and air conditioning.

Investigation of novel thermoelectric refrigeration systems was carried out in this research. The systems use thermoelectric "peltier" coolers (thermoelectric modules) to produce cooling or heating. Thermoelectric modules are solid state heat pump, which have the advantage of being environmentally friendly, being quiet, have no moving parts and can operate using direct current supplied from photovoltaic solar cells (PVs).

This work mainly investigated a passive technology based on integration of a thermal diode and thermoelectric modules for building integrated heat pump. The heat pump uses thermoelectric modules to produce cooling or heating, and the thermal diode to transfer heat in or out of the building, and prevent reverse heat flow in the event of power failure. The heat pump was designed to have the following features:

- Very compact and suitable for incorporation within the building structure;

- Does not require a plant room and simple to construct;
- Easily switched between cooling and heating modes;
- Can prevent reverse heat flow in the event of power failure;
- Low manufacturing cost;
- Environmentally friendly;
- Can be driven by solar photovoltaic panels.

This work also investigated the potential application of phase change materials (PCMs) in the thermoelectric refrigeration system. The system employs phase change material to improve the performance of a thermoelectric refrigerator as well as the cooling storage capability. The refrigerator employing phase change material was designed to have following features:

- Be able to overcome the peak loads and losses during door openings and power-off periods.
- Prevent reverse heat flow via thermoelectric modules in the event of the power being turned off by integrating the thermosyphon with the phase change material.
- Low manufacturing cost.
- Environmentally friendly.
- Can be driven by solar photovoltaic panels

The research initially involved the investigation of the performance of the components of the thermoelectric refrigeration systems, including thermoelectric modules, heat pipes and heat sinks. The analytical models were developed to evaluate the heat transfer and optimise the design of these components. Correlations between heat transfer and fluid flow inside the heat pipes were explored by computer modelling.

The research work further involved the design, modelling, construction and tests of a thermoelectric heat pump prototype. A computer model was developed to evaluate the performance of the heat pump system for two different modes, i.e., cooling and heating, under various operating and ambient temperatures. Laboratory tests were carried out to validate the modelling predictions and experimentally examine the thermal performance

of the heat pump. Comparison was made between the modelling and testing results, and the reasons for error formation were analysed and correction was given. Further experimental investigation showed that reducing the temperature of the condenser of the thermal diode could provide a significant improvement of the efficiency of the coefficient of performance (COP) of the system in cooling mode. This can be achieved by using the evaporation of water on the heat sink attached to the condenser.

The research work also involved the design, construction and tests of a thermoelectric refrigerator employing phase change material. The work intended to investigate the potential application of phase change materials (PCMs) in the thermoelectric refrigeration system. The system was first fabricated and tested using a conventional heat sink system as the cold heat sink. In order to improve the performance and the storage capability, the system was reconstructed and tested using an encapsulated PCM as a cold heat sink. Results of tests of the latter system showed an improved performance compared with the former system. However, to improve the storage capability, in particular during off-power periods, it was found necessary to integrate the PCM with a thermosyphons, which would allow heat flow in one direction only. Results of tests carried out on the system employing phase change material integrated with thermosyphons showed considerable improvement in the storage capability of the thermoelectric refrigeration system compared with the previous ones.

On the basis of the above investigation the further work for improving the performance of the thermoelectric refrigeration system was suggested, which is illustrated in Chapter 7, and its key technical issues are discussed.

Acknowledgement

I would like to express my gratitude and appreciation to my supervisor, Professor S.B.Riffat, for his unlimited support and assistance throughout the progress of my research work, and also for his technical instructions and advice during the whole period of the research.

I gratefully acknowledge the financial support by the University of Nottingham through the award of the PhD studentship.

I am indebted to my husband, Xudong, for his sincere moral support. He constructively supported me throughout my studies. He kept helping me in both my research and the house works.

I am also grateful to my colleagues and working partners, especially Dr Siddig Omer, Dr Guoquan Qiu, Dr Naresh Srivastava and Dr Yuehong Su, for their continued support. I would like to thank the technicians of the school for their tolerance and co-operation.

Nomenclature

Symbol	Term	Unit
A_b	Area of the base plate	m^2
A_c	Cross section area of the fin	m^2
A_f	Total surface area of a fin	m^2
A_l	Liquid area in the cross section of single hole	m^2
A_o	Total area of all the exposed regions of base plate	m^2
A_t	Total area exposed to coolant	m^2
A_v	Cross section area of vapour	m^2
A_{wall}	Total surface area of the box	m^2
C, C_1, C_2	Coefficient of vapour phase resistance calculation	
COP_1, COP_2	Coefficient of performance	
C_p	Specific heat of air	KJ/kg^oC
d_i	Equivalent diameter of the cross section	m
d_v	Diameter of cross section area of vapour	m
f_v	Frictional resistance coefficient of the vapour flow in the heat pipe,	0.014
G	Geometry factor (cross section area/length of thermoelectric element),	cm
G_f	Minimum filled liquid mass	kg
g	gravitational acceleration	m/s^2
h	Convective heat transfer coefficient	$W/m^{2o}C$
h_f	Liquid fill level (variable)	m
h_{fg}	Latent heat of vaporization	J/kg
h_{in}	Convective heat transfer coefficient of internal surface of the box	$W/m^{2o}C$
h_{out}	Convective heat transfer coefficient of outside surface of the box	$W/m^{2o}C$
I	Current	A
I_{opt}	Optimum current	A
J	Correction factor in relation to the heat resistance of the vapour flow	1
K	Coefficient for liquid phase resistance calculation	
k	Thermal conductivity of thermoelectric material	watt/cm Kelvin
k_e	Thermal conductivity of the wicked space	W/m^oC

k_{eff}	Effective thermal conductivity of the wicks	W/m°C
k_f	Thermal conductivity of fin	W/m°C
k_l	Thermal conductivity of the liquid	W/m°C
k_p	Thermal conductivity of the heat pipe wall	W/m°C
k_s	Shape factor of the heat pipe channel geometry	
L	Length of the fin	m
L_c	Corrected length of the fin	m
L_s	Length of finned heat sink	m
l_a	Length of adiabatic section of the heat pipe	m
l_c	Length of condensation section of the heat pipe	m
l_e	Length of evaporation section of the heat pipe	m
l_{eff}	Effective length of the heat pipe	m
l_p	Length of liquid column in the heat pipe	m
M_v	Mach number of vapour flow	N/m^2
N	Number of thermocouples in **3.1**; Number of fins in **3.4**	
P	Perimeter of the cross section of the fin	m
P_e	Power consumption	W
P_v	Vapour pressure	Pa
p	Resistivity of thermoelectric material	ohm cm
Q_a	Sensible energy of the air inside the refrigerator cabinet	W
Q_{allum}	Cooling energy stored in the aluminium block	W
Q_c	Heat flow at cold side (cooling capacity)	W
$Q_{c,e}$	Cooling energy produced by thermoelectric refrigerator	W
$Q_{cooling}$	Cooling capacity	W
Q_{cd}	Heat conduction from the hot side to cold side	W
Q_E	Power consumption	W
Q_f	Heat transfer from the fin	W
Q_{fs}	Heat transfer from finned heat sink	W
Q_h	Heat flow at hot side (heating capacity)	W
$Q_{heating}$	Heating capacity	W
Q_{input}	Electrical energy input to the thermoelectric modules	W
Q_J	Joule heat generation rate	W
Q_{load}	Heat load provided by lamps	W

Q_{loss}	Heat loss produced by the fan on the wall of the box	W
Q_{lpcm}	Latent heat of the PCM	W
Q_{sb}	Peltier heat pumping rate	W
Q_{spcm}	Sensible energy of the PCM	W
Q_w	Sensible energy of the water	W
Q_{wall}	Heat transfer from the environment to the interior of the box	W
$q_{b,m}$	Boiling limit for heat transport	W
q_c	Heat input	W
$q_{e,m}$	Entrainment limit for heat transport	W
$q_{s,m}$	Sonic limit for heat transport	W
$q_{v,m}$	Viscous limit for heat transport	W
R_c	Thermal resistance of the inside heat sink	K/W
R_e	Heat exchanger thermal resistance	K/W
Re_v	Reynolds number	
R_f	Thermal resistance of the fin	$^oC/W$
R_{fs}	Thermal resistance of finned heat sink	$^oC/W$
R_h	Thermal resistance of the outside heat sink	K/W
R_{hp}	Thermal resistance of the thermal diode	K/W
$R_{p,c}$	Condenser wall heat resistance	$m^{2o}C/W$
$R_{p,e}$	Evaporator wall thermal resistance	$m^{2o}C/W$
R_v	Thermal resistance of the vapour flow in the heat pipe	$m^{2o}C/W$
R_{vc}	Vapour constant (J/kg.K) (n-pentane: 115; HFE-7100: 31.5)	
R_w	Thermal resistance of condenser saturated wicks	$m^{2o}C/W$
R_{wall}	Thermal resistance of wall of the box	$m^{2o}C/W$
$R_{w,e}$	Heat resistance of evaporator saturated wicks	$m^{2o}C/W$
r_{ce}	Capillary radius	m
r_i	Equivalent radius of the cross section	m
$r_{i,c}$	Radius of the condensation section of the heat pipe (inner surface)	m
r_{ie}	Radius of the evaporation section of the heat pipe (inner surface)	m
r_{hl}	Hydraulic radius of liquid cross section	m
r_{hv}	Hydraulic radius of vapour cross section	m
$r_{h,w}$	Hydraulic radius of wicks with liquid	m
r_n	Critical radius of bubble generation	m

r_o	Radius of the evaporation section of the heat pipe (outer surface)	m
$r_{o,c}$	Radius of the condensation section of the heat pipe (outer surface)	m
r_v	Equivalent radius of the vapour area in the cross section	m
$r_{v,c}$	Radius of the vapour column in the condensation section of the heat pipe	m
S_a	Cross section area of the airflow of the fan on the wall	m^2
T_a	Ambient temperature (Kelvin in section 5.2)	°C
T_c	Cold side temperature	K
T_{cell}	Temperature of the PV cell	°C
T_h	Hot side temperature	K
T_{in}	Temperature inside the box (room) (Kelvin in section 5.2)	°C
T_m	$1/2(T_h+T_c)$	K
T_r	Temperature of fin base	°C
T_s	Temperature of the surrounding fluid over the fin	°C
T_v	Absolute temperature of vapour	K
U_w	Coefficient of heat transfer of the box	$W/m^{2o}C$
V	Voltage	V
V_a	Velocity of the wind of the fan on the wall	m/s
W	Width of the finned heat sink	m
Z	Figure of Merit ($a^2/(pk)$)	K^{-1}
ΔT	T_h-T_c	K
Δp_{ag}	Axial hydrostatic pressure drop	Pa
Δp_{cl}	Net capillary pressure difference	Pa
$\Delta p_{c,m}$	Maximum capillary force	Pa
Δp_l	Viscous pressure drop occurring in the liquid phase	Pa
Δp_{rg}	Radial hydrostatic pressure drop	Pa
Δp_v	Viscous pressure drop occurring in the vapour phase	Pa
α	Seebeck coefficient of thermoelectric material	Volts/K
σ	Surface tension	N/m
ε	Cofficient of performance for cooling	
ε_{opt}	Optimum cofficient of performance for cooling	
η	Coefficient of performance for heating	
η_f	Fin efficiency	

η_{fs}	Finned heat sink efficiency	
η_{opt}	Optimum cofficient of performance for heating	
δ	Thickness of the fin	m
δ_b	Thickness of base plate	m^2
μ_l	Liquid viscosity	$N.s/m^2$
μ_v	Vapour viscosity	$N.s/m^2$
ρ	Density of air	kg/m^3
ρ_l	Liquid density	kg/m^3
ρ_v	Vapour density	kg/m^3
γ	Specific heat ratio	
ϕ	Angle of inclination of the pipe relative to horizontal surface	deg
ψ	Angle of inclination of adiabatic section relative to horizontal surface	deg
θ	Wetting angle of liquid-vapour surface	deg
λ	Latent heat of working fluid of the heat pipe	J/kg

List of Figures

Chapter 6

List of Tables

Chapter 1. Introduction

1.1 Background

Concern over global warming and depletion of the ozone layer has stimulated research to develop cooling methods that do not employ environmentally damaging working fluids such as CFCs and HCFCs. Two methods that have been considered are absorption and thermoelectric 'Peltier' cooling systems. Absorption systems, using H_2O/LiBr have the advantage of being able to use low-grade waste heat. However, the large volume, high capital cost and low performance of these systems have inhibited their widespread application.

Thermoelectric systems were developed in the 1950s and use of this technology for air-conditioning and refrigerator applications was investigated as early as the 1950s-1960s. However, the continued development of thermoelectric systems was slow owing to technical difficulties and the superior performance of vapour-compression systems in terms of coefficient of performance (COP). It is now known however that most working fluids employed in vapour-compression systems are damaging to the environment and as vapour-compression systems contain moving parts, they have the further disadvantages of being noisy and requiring regular maintenance. In recent years therefore, there has been renewed interest in using thermoelectric modules for domestic refrigerators and air conditioning. Thermoelectric refrigeration systems are much more compact and lighter than absorption systems. Some thermoelectric modules, such as Melcor's Polar TEC^{TM} series thermoelectric modules, have been developed specifically for these low-cost, high volume, commercial applications. Many reports on the use of thermoelectric refrigerator, and some reports on use of thermoelectric air-conditioning for small-scale or specific applications can be found (Bojic M, 1997; Morrow R.C, 2000]. However, few reports exist on the use of a thermoelectric air conditioner for cooling/heating a room space, such as living rooms, restaurants, offices, or similar (Kim C.M, 2001).

The main aim of this research is to investigate a passive technology based on integration of a thermal diode and thermoelectric modules for a building-integrated heat pump. The system is very compact and suitable for incorporation within the building structure. This

research also investigated an improved thermoelectric refrigerator employing a phase change material to improve the overall performance of the system.

As a building heat pump, the system can be constructed as a flat unit suitable for mounting on the wall of a building. It also has the advantage that it can be easily switched between cooling and heating modes and adjusted to meet individual air conditioning requirements. Thermoelectric air-conditioning has the potential to achieve a higher COP as it requires a smaller temperature difference between the room and the ambient. These advantages make thermoelectric systems very attractive for building air-conditioning.

Although many improved thermoelectric refrigerators have been reported, the present thermoelectric refrigerators still have the problem of low coefficient of performance. One of the methods to solve the problem is to improve the overall performance of the system, by properly storing and releasing the available energy and utilizing it efficiently. Phase change materials (PCM) have long been identified as prime candidates for thermal energy storage systems, due to the high energy densities (MJ/m^3). A further advantage of PCM is that heat transfer normally takes place at a constant temperature (the transition temperature). This is appropriate for thermoelectric cooling, and refrigeration units, especially those used for food and medicine storage which require precise temperature control.

1.2 Description of the Research

Thermoelectric Heat Pump

The thermoelectric heat pump system utilised novel and integrated design concept for optimising system performance, size, reliability and costs. It was based on the integration of thermoelectric modules, a new type of thermal diode in one unit. The heat pump can be driven by mains power (DC) or PV solar cells (DC). The components and the operation of the heat pump are described, and the novelty is summarised as follow:

(a) Thermal Diodes

Thermal diode is a unidirectional heat pipe, which can transfer the heat in one direction. This consists of a closed container charged with a working fluid. When heat is applied to

the lower end of the heat pipe (evaporation section), the liquid boils and vaporises. As the vapour reaches the upper end of the tube, which is cooler (condenser section), it condenses and returns by gravity to lower end of the tube. Thermal diodes can be made in various shapes (e.g., tubes, panels) and sizes. A new type of thermal diode was designed, constructed and used in this system, as shown in Figure1-1. This thermal diode can rotate along its axis to change the operation mode from heating to cooling or the reverse. The external forms of the evaporator and condenser of the thermal diode are flat panels, which makes it easy to mount thermoelectric modules and heat sink units. The internal structures of the evaporator and condenser are holes that can undertake the high vapour pressure without changing the external forms. The holes connect each other to keep the working liquid in the same level.

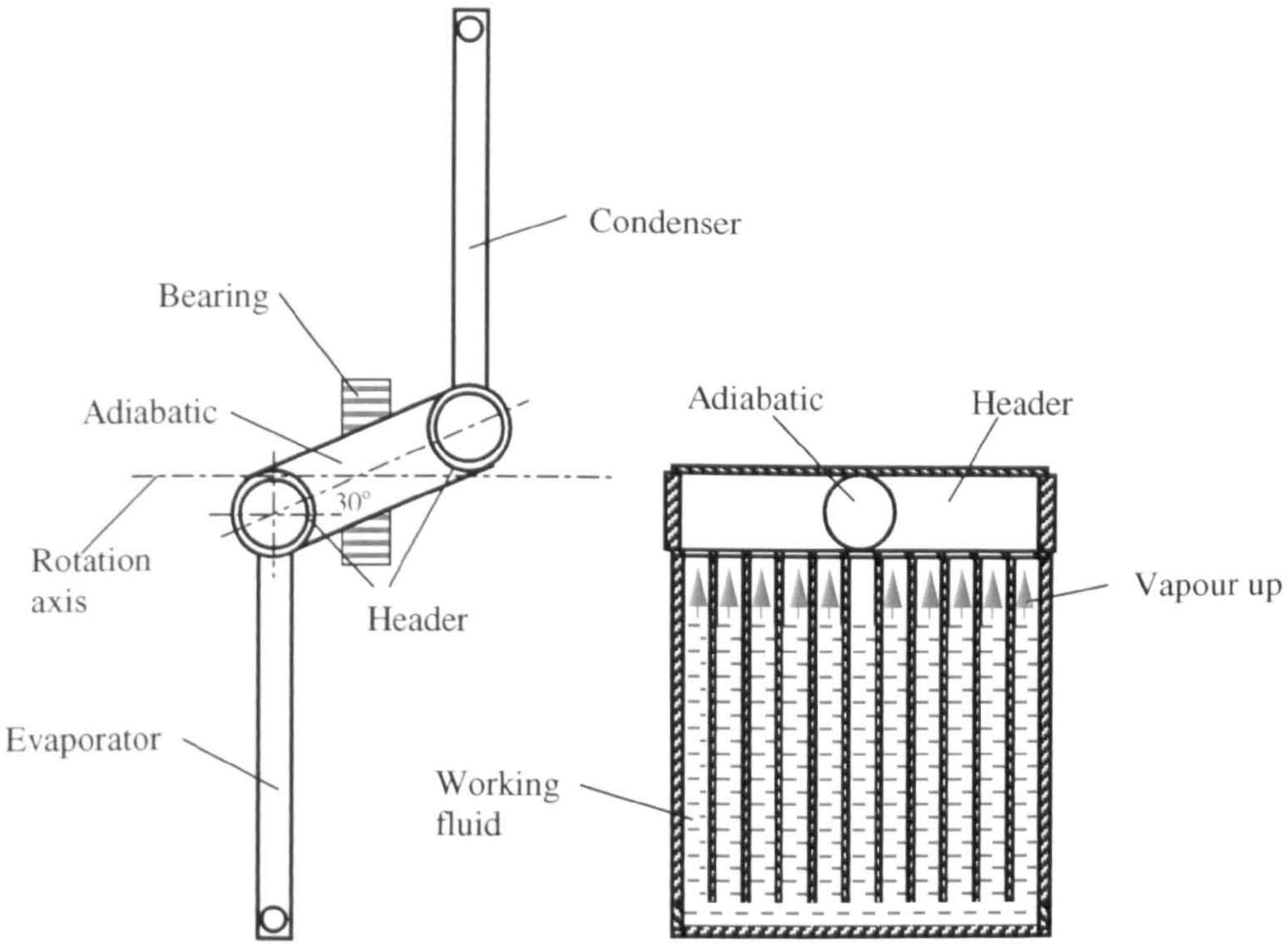

Figure 1-1. Schematic diagram of the new type thermal diode (a) Illustration of the thermal diode (b) Internal structure of the evaporator and condenser

(b) Thermoelectric Modules

A thermoelectric module is a simple solid-state device that converts electrical energy into thermal energy or the reverse. It consists of a number of couples of p- and n-type

semiconductor strips sandwiched between two ceramic plates, connected electrically in series and thermally in parallel, see Figure1-2. When supplied with a suitable electric current they can provide either cooling or heating depending on the direction of the current. Heat generation or absorption rates are proportional to the magnitude of the current and also the temperature of the hot and cold side. The amount of heat removed by the hot side corresponds to the cooling effect and the electrical power input.

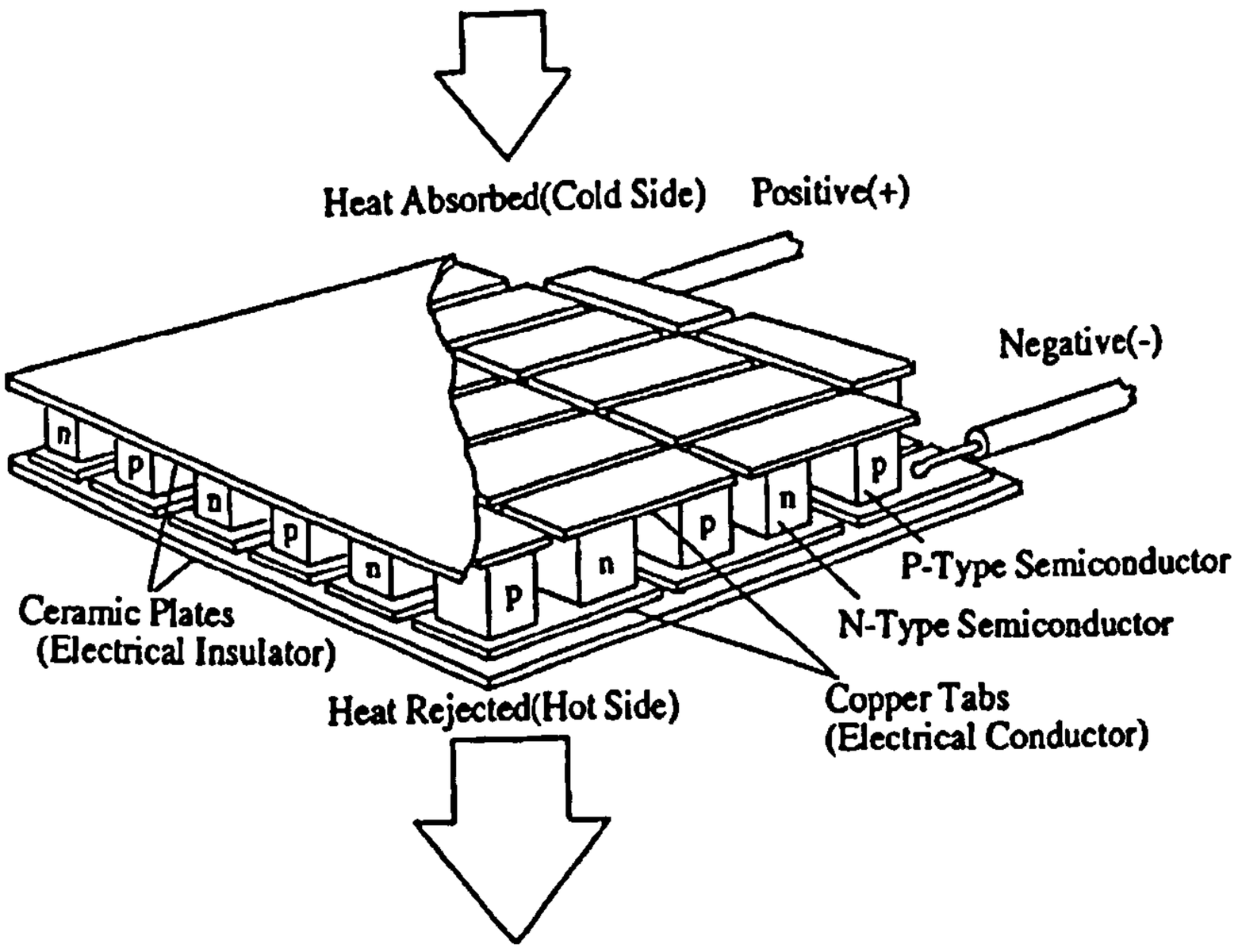

Figure 1-2. Schematic description of a thermoelectric (Peltier) module, showing details of element integration[Rowe D.M, 1995]

(c) Operation of the Heat Pump

The operation of the heat pump system was shown in Figure 1-3.

Cooling Mode [Figure 1-3(a)]: In summer, Heat from the building will be extracted by the thermoelectric modules. The heat causes the working fluid inside the thermal diode to boil and vaporise. As the vapour flows to the condenser section (situated outside the building) it condenses and releases heat to ambient with the help of the heat sink units.

Heating Mode [Figure 1-3(b)]: In winter, the thermal diode will be rotated along its axis to reverse the functions of the evaporator and condenser sections. Ambient heat extracted by the evaporator section of the thermal diode, causing the working fluid to vaporise. As the vapour flows to the condenser section of the thermal diode, it condenses

and releases heat to the thermoelectric modules. These upgrade the heat to a more useful temperature which can then used for space heating in the building.

The heat sinks in this system are used to help to dissipate the heat. The system can be driven by PV panels.

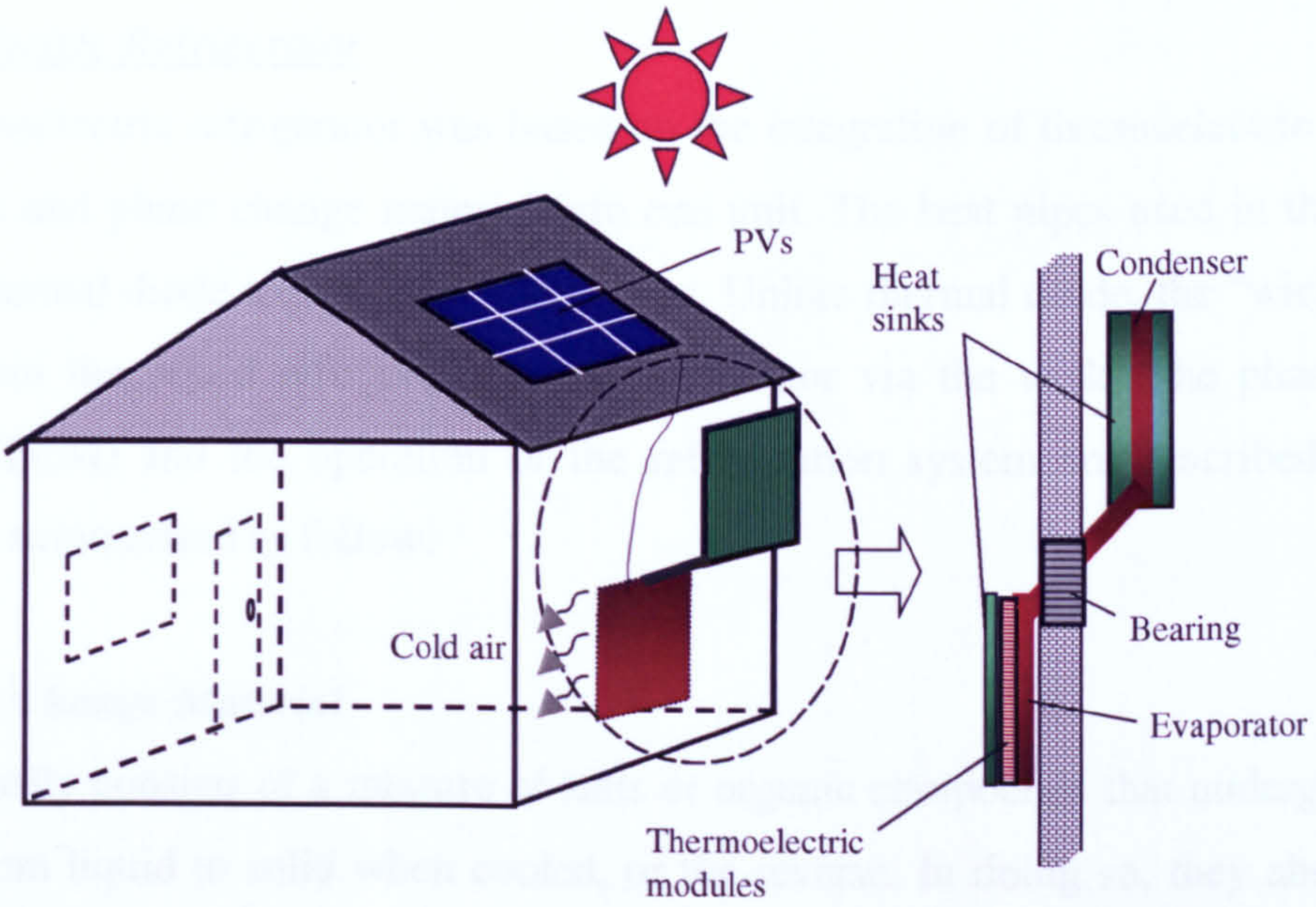

(a)

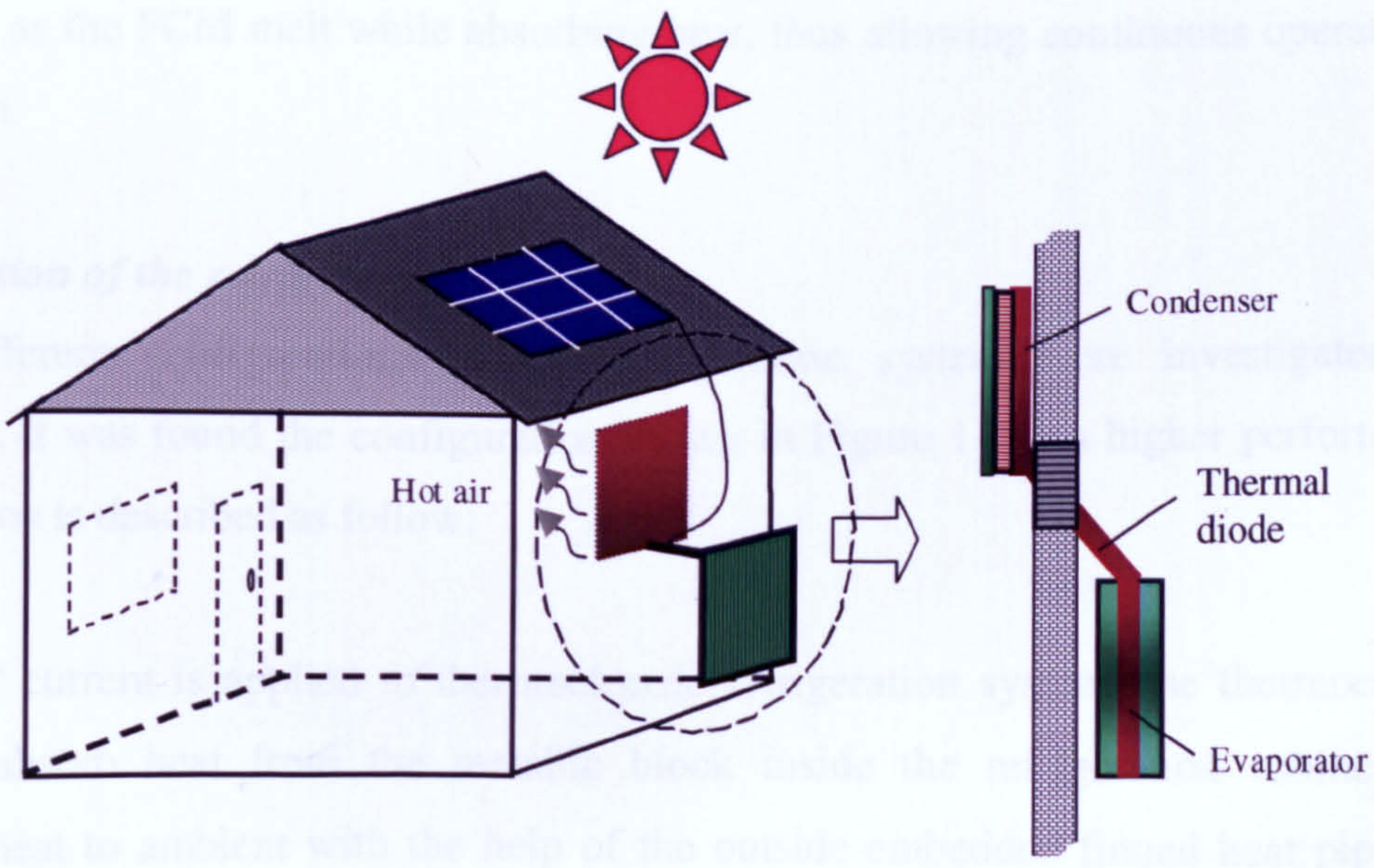

(b)

Figure 1-3. Operation modes of the heat pump (a) Cooling mode (b) Heating mode

(d) Novelty

- Integration of thermoelectric modules and thermal diode technology to produce a compact unit;
- Use of a new type of thermal diode;
- Method to allow operation of the thermal diodes in heating or cooling mode;

Thermoelectric Refrigerator

The thermoelectric refrigerator was based on the integration of thermoelectric modules, heat pipes and phase change material into one unit. The heat pipes used in this system include thermal diode and "wicked" heat pipe. Unlike thermal diode, the "wicked" heat pipes return the liquid refrigerant to the evaporator via the wick. The phase change material (PCM) and the operation of the refrigeration system are described, and the novelty is summarised as follow:

(a) Phase Change Material

This normally consists of a mixture of salts or organic compounds that undergo a phase change from liquid to solid when cooled, or the reverse. In doing so, they absorb large quantities of energy while remaining at an almost constant temperature. The use of a PCM in the system allows the cooling load to be stored for periods of peak loads or power off as the PCM melt while absorbing heat, thus allowing continuous operation of the system.

(b) Operation of the refrigerator

Three different configurations of the refrigeration system were investigated and compared. It was found the configuration shown in Figure 1-4 has higher performance, its operation is described as follow:

When DC current is applied to thermoelectric refrigeration system, the thermoelectric modules absorb heat from the metallic block inside the refrigeration cabinet, and dissipate heat to ambient with the help of the outside embedded finned heat pipe heat sink. On the cold side of the system, the working fluid in the evaporator of the thermal diodes absorbs heat from the PCM, producing cooling. The vapour produced in the evaporator travels to the condenser end where it condenses, whilst dissipating heat to the

cold side of the thermoelectric modules. When the power is turned off, the condenser of the thermal diodes gets hot, as a result of heat transfer from the hot side to the cold side of the thermoelectric modules. This stops the condensation to occur, and thus causes the operation of the thermal diode to cease, and therefore prevents heat transfer to the PCM.

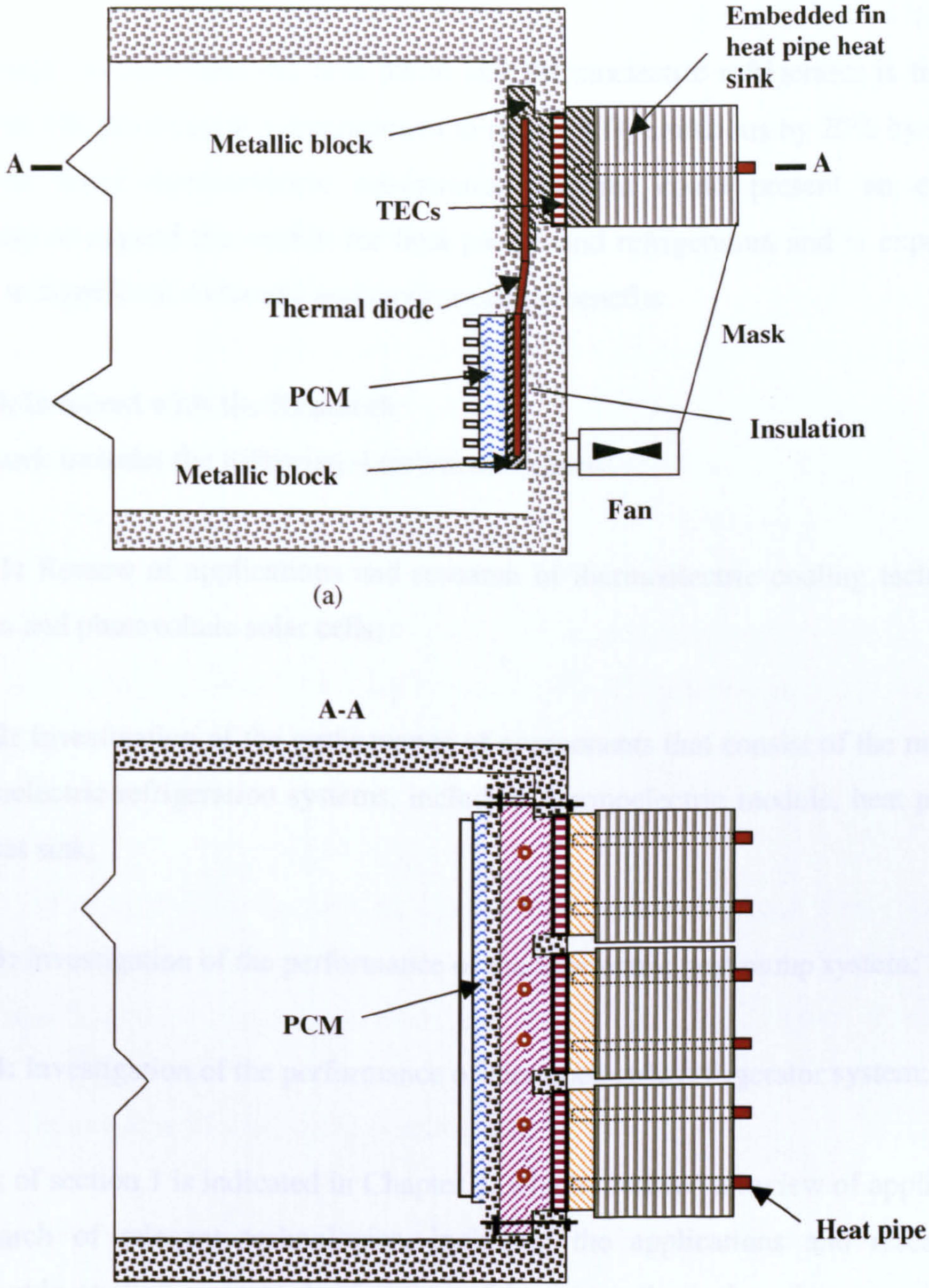

Figure 1-4. Schematic diagram of a thermoelectric refrigeration system employing PCM integrated with thermal diodes (a)Vertical section (b)Horizontal section

(c) Novelty

- The encapsulation of a PCM within heat pipe is a novel idea to enhance the heat input/output mechanisms.
- The integration of thermoelectric modules, a PCM, heat pipes and perhaps PV in a refrigeration unit is a novel idea to conserve energy supply.

The research on thermoelectric heat pump and thermoelectric refrigerator is timely in view of the UK government's commitment to reduce CO_2 emissions by 20% by the year 2010. The novel thermoelectric refrigeration systems could present an excellent opportunity to expand the market for heat pumps and refrigerators and is expected to give rise to significant economic and environmental benefits.

1.3 Work Involved with the Research

The research includes the following 4 technical sections:

Section 1: Review of applications and research of thermoelectric cooling technology, heat pipes and photovoltaic solar cells;

Section 2: Investigation of the performance of components that consist of the main part of thermoelectric refrigeration systems, including thermoelectric module, heat pipe and finned heat sink;

Section 3: Investigation of the performance of thermoelectric heat pump system;

Section 4: Investigation of the performance of thermoelectric refrigerator system;

The work of section 1 is indicated in Chapter 2, which involved a review of applications and research of relevant technologies, including the applications and research of thermoelectric cooling systems, heat pipes and heat pipe thermal performance analysis as well as the photovoltaic solar cells technology and their applications. Technical progress in these areas was examined, and the innovative aspects of this research were identified compared to the current technical status.

The work of section 2 is detailed in Chapters 3 and 4. Thermoelectric module performance was analysed and optimum selection (design) of thermoelectric modules for thermoelectric refrigeration systems was explored by computer modelling. The analytical model was validated by comparing the modelling results with the results from the design software of Melcor company. An analytical model of finned heat sink was developed and the modelling results provided a basis for designing the finned heat sink. An analytical model of the heat transfer of heat pipes was developed. The model was used for simulating the new type of novel cranked thermal diode in two cases, including the "wicked" thermal diode and "wickless" thermal diode. Results obtained were discussed. Experimental results were used to validate the analytical model.

The work of section 3 is detailed in Chapter 5. A building-integrated thermoelectric heat pump was designed and constructed. Computer modelling was used to evaluate the performance of the heat pump for various operating and weather conditions under two different modes, i.e., cooling mode and heating mode. Laboratory testing of the prototype was then carried out. The results obtained are used to assess real performance of the system. These were also compared to theoretical predictions to validate/modify the analytical model. Method for improving the COP of the thermoelectric pump system was explored in this research. Environmental and potential economical effects of the heat pump were illustrated.

The work of section 4 is detailed in Chapter 6. An experimental investigation of thermoelectric refrigerator employing phase change material was carried out. Three different configurations were fabricated and tested. The comparison of the three configurations showed an effect of employing a phase change material integrated with thermal diode in thermoelectric refrigeration system.

A number of conclusions derived from the research were arisen in Chapter 7. The merits of the proposed systems were highlighted, and the problems encountered with the research were illustrated. Opportunities for further study on this topic were also discussed.

Chapter 2. Review of Applications and Research of Thermoelectric Cooling Technologies, Heat Pipes and Photovoltaic Solar Cells

2.1 Applications of Thermoelectric Cooling Technology and Research on Thermoelectric Cooling Systems

2.1.1 Thermoelectric Cooling Technologies and Their Applications

This section gives the basic knowledge of the thermoelectric modules and an overview of these applications for the purpose of apprehending the progress in the thermoelectric cooling technologies.

Thermoelectric Modules

Thermoelectric modules can convert electrical energy into a temperature gradient—This phenomena was discovered by Peltier in 1834. The application of this cooling or heating effect remained minimal until the development of semiconductor materials. With the advent of semiconductor materials came the capability for a wide variety of practical thermoelectric refrigeration applications [Guy E.C, 1988].

A thermoelectric module consists of a number of couples p- and n-type semiconductor strips sandwiched between two ceramic plates, connected electrically in series and thermally in parallel. Figure 2-1 shows a diagram of a single pair consisting of n- and p-type semiconductor material. When DC current passes from the n- to the p-type semiconductor material, the junction of semiconductor become cold, and the other end become hot. The heat is transferred from the cold end to hot end and cooling the environment, see Figure 2-1(a). This phenomenon is called the Peltier effect. Reversing the direction of the current, the junction of semiconductor become hot, and the other end become cold, heat is dissipated to the environment, as shown in Figure 2-1(b).

Thermoelectric heat pumping at the cold end due to the Peltier effect is reduced by other unwanted heat sources, i.e., Joule heat and conducted heat. Current flow generates resistive or Joule heat in the thermoelectric material. 50 percent of the Joule heat goes to the cold end and 50 percent goes to the hot end. Due to the temperature difference

between the cold and hot end of semiconductor material, heat is conducted from the hot end to the cold end of the module through the thermoelectric material, called Seebeck effect.

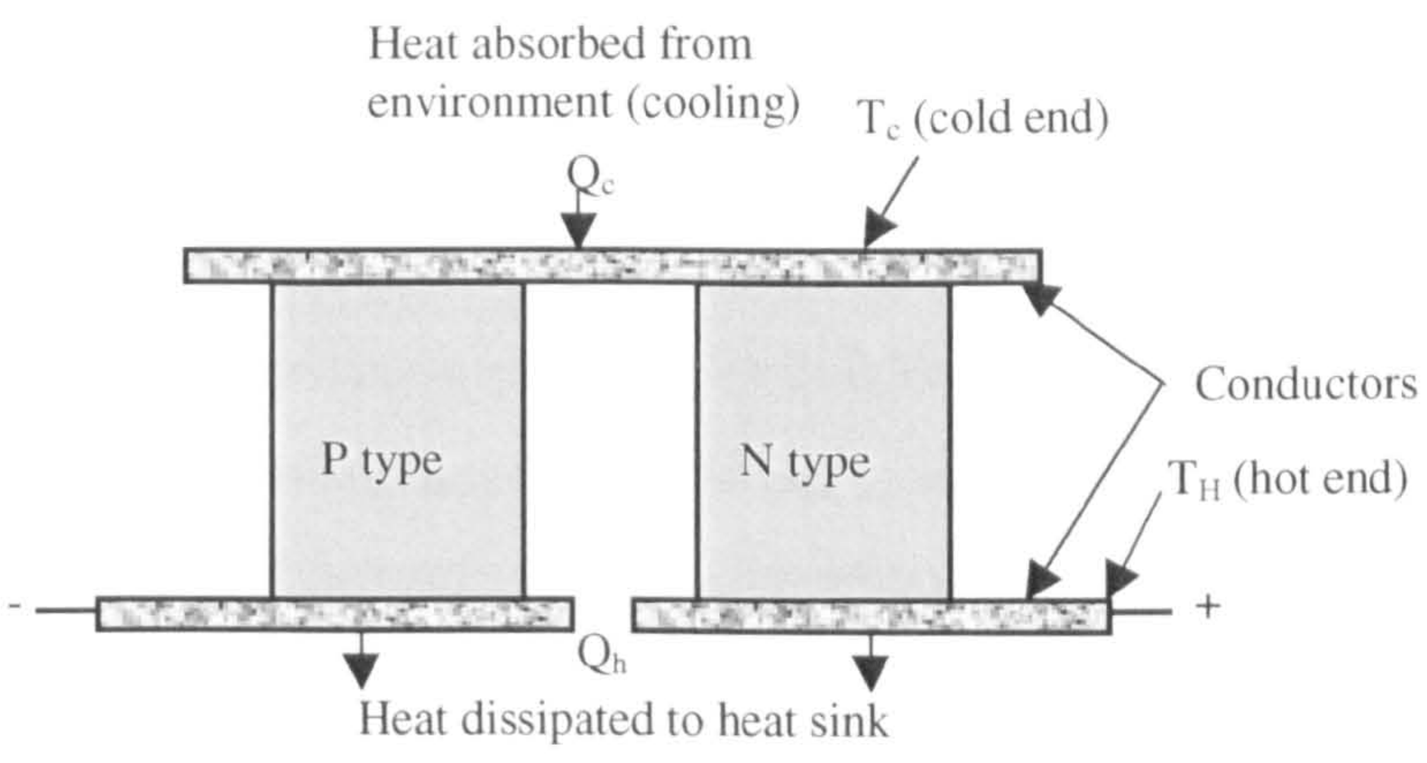

(a)

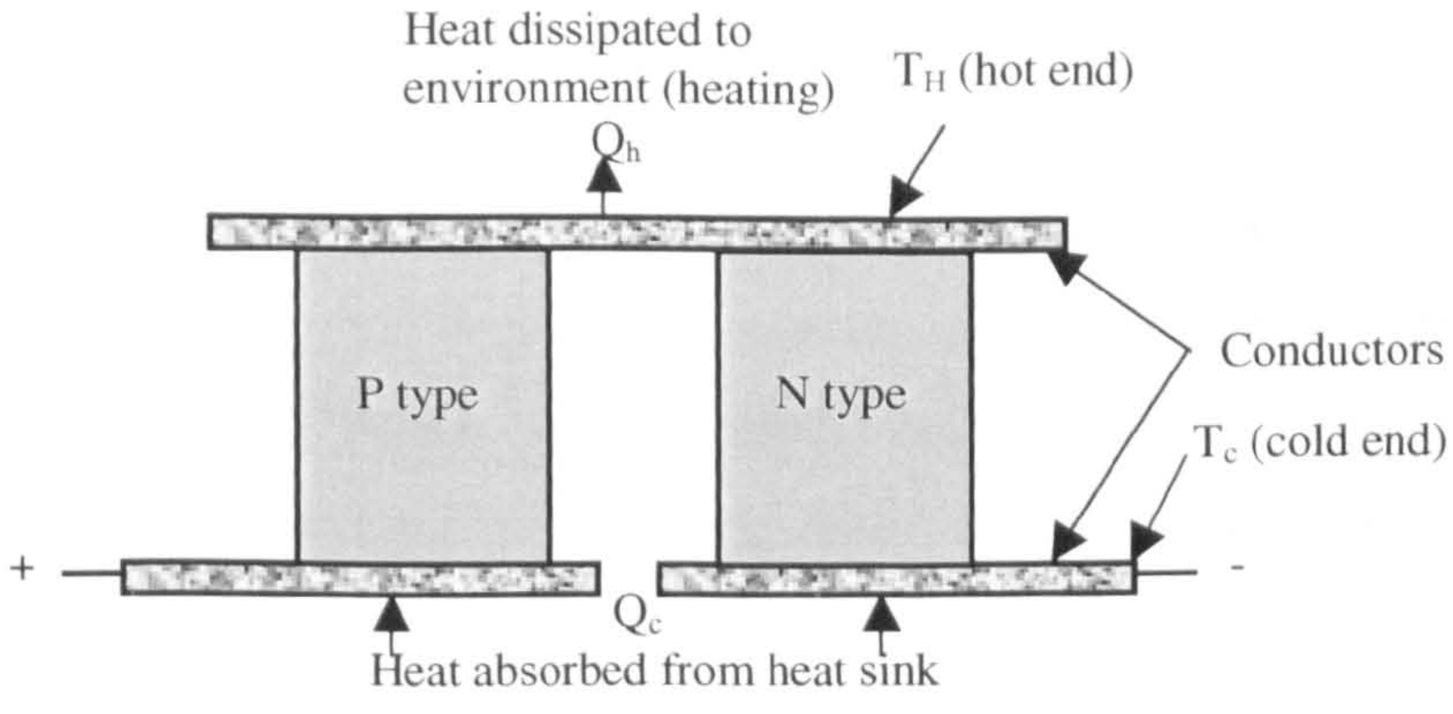

(b)

Figure 2-1. Schematic of thermoelectric module operation (a) cooling mode (b) heating mode.

As the current is increased, the temperature difference increases due to the increased Peltier cooling effect, and thus the Joule heat and conducted heat increase. Thermal equilibrium is established when the sum of one half the Joule heat and the conducted heat equals the Peltier heat, and the thermoelectric module no longer operates.

The electrical power consumption of a thermoelectric module is used to generate the Joule heat and overcome the Seebeck effect. The coefficient of performance used is defined as the net heat absorbed at the cold end divided by the applied electric power.

The cooling capability of a semiconductor material is dependent on the material's figure of merit. Figure of merit depends only on material properties, Seebeck coefficient, electric resistivity and thermal conductivity. Maximising the figure of merit is the major objective to increase the module efficiency.

The thermoelectric modules can also convert thermal energy from a temperature gradient into electric energy—this phenomenon was discovered in 1821 and is called "Seebeck effect." As mentioned above, when a temperature differential is established between the hot and cold ends of the semiconductor material, a voltage is generated, i.e, Seebeck voltage. Actually, the Seebeck effect is an inverse effect of Peltier effect. Based on this Seebeck effect, the thermoelectric modules can also act as power generators. As shown in Figure 2-1, if heat supplied at the one junction causes an electric current to flow in the circuit and electrical power is delivered. In practice a large number of such thermocouples are connected electrically in series to form a "module".

More than one pair of semiconductors are usually assembled together to form a thermoelectric module. Within the module each semiconductors is called a thermoelement, and a pair of thermoelements is called a thermocouple.

A typical thermoelectric module is composed of two ceramic substrates that serve as a foundation and electrical insulation for P-type and N-type Bismuth Telluride thermoelements that are connected electrically in series and thermally in parallel between the ceramics. Conventional thermoelectric modules have various specifications

for various applications; the dimensions vary from 3mm square by 4mm thick to 60mm square by 5mm thick, the maximum heat-pumping rate from 1 W to 125 W. The maximum temperature difference between the hot and cold side can reach 70°C. The modules contain from 3 to 127 thermocouples. There are multistage (cascade) series thermoelectric modules designed to meet requirements for large temperature differentials (up to 130°C). The lowest practically achievable temperature is about –100°C.

Because the cold side of the module contracts while the hot side expands modules with a footprint larger than 50 mm square usually suffer from thermally induced stresses, at the electrical connection points inside the module causing a short circuit, so they are not common. Long, thin modules want to bow for the same reason and are also rare. Larger areas than an individual module can maintain are cooled or have the temperature controlled usually by using multiple modules.

Two types of commercially available thermoelectric modules are shown in Figure 2-2. Type A was originally designed for cooling applications and possesses significant inter-thermoelement separation. In this type of module, n- and p-type semiconductor thermoelements are connected electrically in series by highly conducting metal strips and sandwiched between thermally conducting but electrically insulating plates. Type B has been developed recently for power generation and is densely constructed with very small inter-thermoelement separation to increase the power-per-area. However, the conducting metal strips in the latter device are not insulated and the module cannot be attached directly to electrical conductor, such as aluminium heat sink. [Rowe D.M et al, 1998]

Thermoelectric modules can not be used independently. They should be connected with heat exchangers to dissipate heat, which consist of thermoelectric cooling systems. The basic theory and operation of thermoelectric cooling systems have been developed for many years. Thermoelectric cooling systems are usually small heat pumps, which follow the laws of thermodynamics in the same manner as mechanical heat pumps, vapour compressors associated with conventional refrigerators, or other apparatus used to transfer energy.

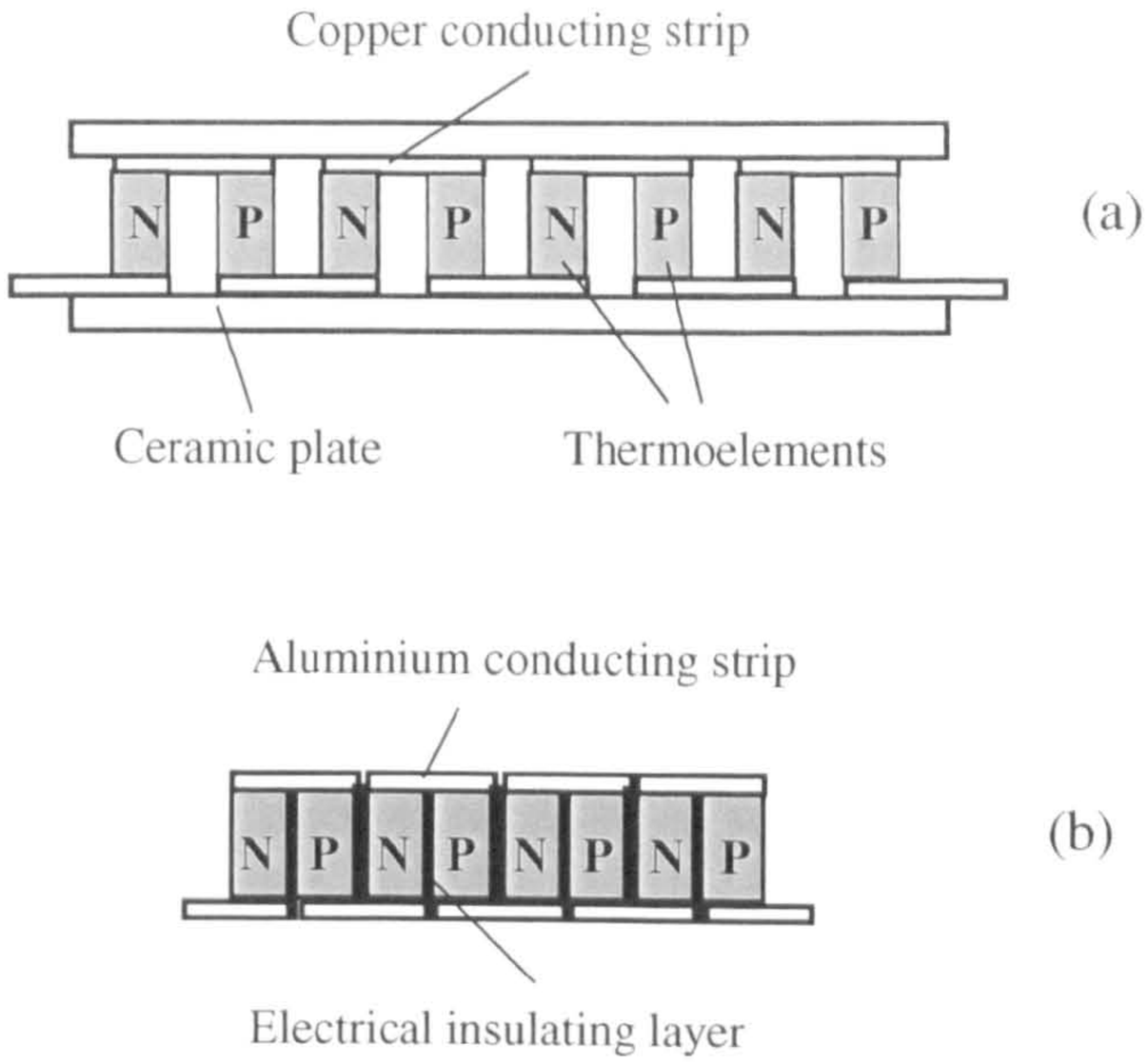

Figure 2-2. Schematic diagrams of two types of thermoelectric modules.
(a) Type A Configuration with ceramic insulating plates and large inter-thermoelement separation;
(b) Type B Configuration without ceramic insulating plate and with very small inter-thermoelement separation.

The thermoelectric modules offer several distinct advantages over other technologies:

- Thermoelectric modules have no moving parts and, therefore, need substantially less maintenance.
- Life testing has shown the capability of thermoelectric modules to exceed 100,000 hrs of steady state operation.
- Thermoelectric modules contain no chlorofluorocarbons or other materials that may require periodic replenishment.
- The direction of heat pumping in a thermoelectric system is fully reversible. Changing the polarity of the DC power supply causes heat to be pumped in the opposite direction--a cooler can then become a heater.
- Precise temperature control to within $\pm 0.1^{o}C$ can be maintained using thermoelectric modules and the appropriate support circuitry.

- Thermoelectric modules can function in environments that are too severe, too sensitive, or too small for conventional refrigeration.
- Thermoelectric modules are not position-dependent.

Due to all the above advantages, thermoelectric modules have found special applications in wide areas, such as military, aerospace, instrument and industrial or commercial products in the past decade. According to the working modes, these applications can be classified into three categories, which are coolers (or heaters), power generators or thermal energy sensors. The applications of thermoelectric modules as coolers (or heaters) are detailed below.

Applications of Thermoelectric Cooling Technologies

Commercially available thermoelectric modules are very reliable when used as coolers and operated at temperatures below room temperature. However, the results of a recent reliability study indicated that these modules might be less reliable when operated above room temperature as generators.[Rowe D.M, 1998]

Usually, thermoelectric coolers are used in cases where the system design criteria includes such factors as high reliability, small size, low weight, intrinsic safety for hazardous electrical environments, and precise temperature control. When thermoelectric coolers are used in niche applications (under 25 W), their low coefficient of performance is not an apparent disadvantage.

A thermoelectric cooling system has an electric circuit including a direct current power source providing direct current through the electric circuit, a thermoelectric module has at least one heat sink and at least one heat source capable of being cooled to a predetermined temperature range, and a control assembly. The use of a thermoelectric module in a cooling system has conventionally followed the basic arrangement shown in Figure 2-3.

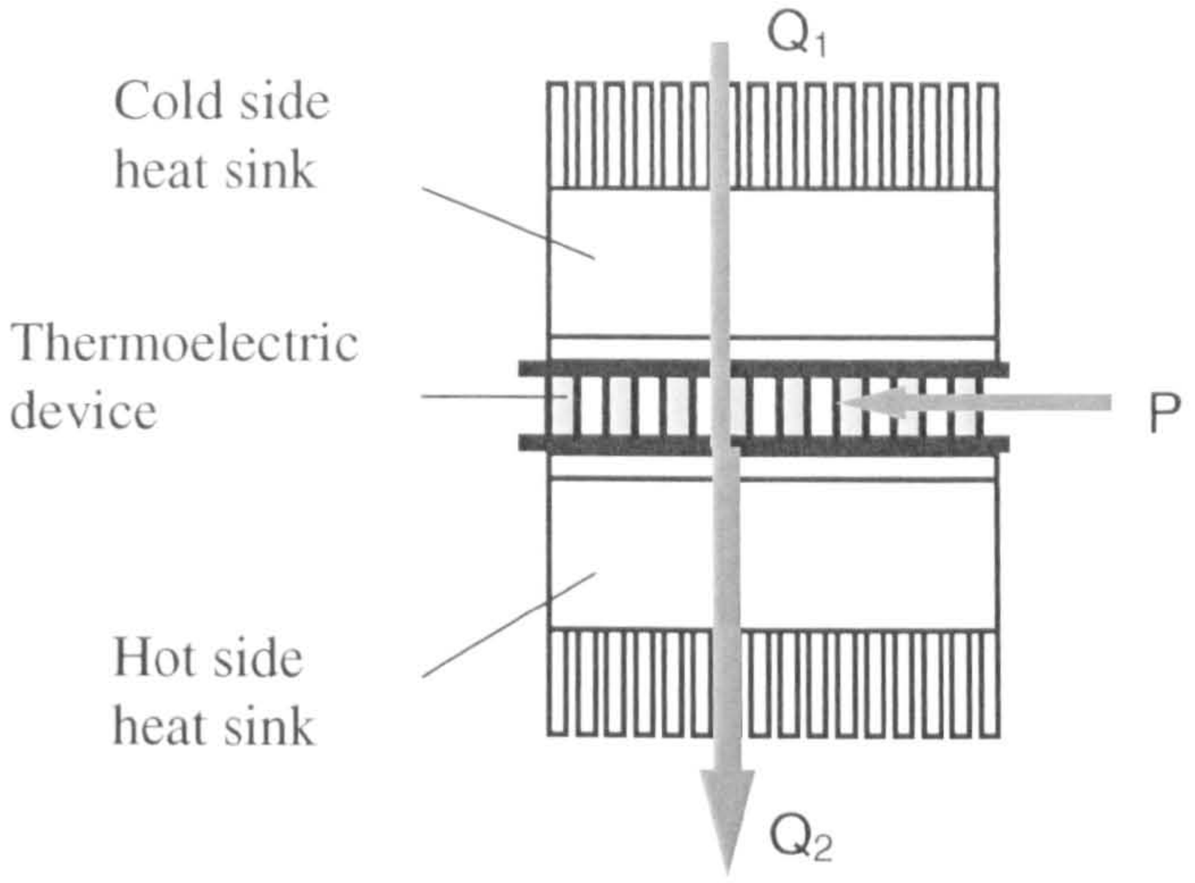

Figure 2-3. Conventional arrangement for thermoelectric cooler. Q_1 is the heat to be pumped, P is the electrical power supplied. Q_2 is the heat dissipated to the ambient.

Thermoelectric cooling systems are analogous to conventional refrigeration systems. For example, a conventional cooling system includes an evaporator, a compressor, and a condenser. In the evaporator or cold section, pressurised refrigerant is allowed to expand, boil, and evaporate. During the change of state from a liquid to a gas, energy in the form of heat is absorbed. In the next step, the compressor recompresses the gas into a liquid. Further, the condenser expels the heat absorbed at the evaporator and the extra heat added by the compressor to the ambient environment.

A thermoelectric cooling system has similar subassemblies. However, thermoelectric cooling is specifically the abstraction of heat from electronic components by the Peltier effect. Potential uses range from the cooling of electronic components to domestic refrigerators and air conditioner for cooling/heating a room space.

(a) Cooling Electronic Devices

Electronic devices often have specified cooling requirements. In this area, the thermoelectric coolers have important roles because the conventional bulk cooling systems are not fit for these niche applications. The following are examples of these applications.

One of the applications is cooling the heat-producing device to keep the device in normal operation. By using a thermoelectric cooler arranged as a super cooler, the heat is conducted and the temperatures of the devices are kept close to the ambient temperatures.

Another application is to reduce the thermal noise of the electric components and the leakage current of the electronic devices, which can improve the accuracy of the electronic instruments [Redus R.H et al, 2001; Bale G et al, 1999; Scruggs M.K et al, 2001]. One of the examples is a cooled CdZnTe detector for X-ray astronomy. Cooling between –30°C and -40°C reduces the leakage current of detector and allows the use of a pulsed reset preamplifier and long pulse shaping times, significantly improving the energy resolution. Although the heat is conducted from the very low temperature (–40°C) to the chilled water of 10°C, it is only necessary to use 3W of electrical power for this small capacity application.

In the aforementioned applications, an electronic device to be cooled is usually directly physically mounted on the cold side of one or more thermoelectric modules allowing maximum thermal transfer between the electronic device and the cold side. The hot side of the thermoelectric module is coupled to a heat sink and a fan or water is used to cool the hot heat sink. Nature convection is also used in some cases. A variable source of direct current connected to the thermoelectric coolers to allow them to lower the temperature of the electronic devices.

Applications of thermoelectric modules for cooling electric devices require very small and low current thermoelectric modules. The low-cost, general-purpose thermoelectric modules for cooling instrumentation, laboratory apparatus and consumer appliances etc are commercially available, such as FRIGICHIP CP Series thermoelectric modules provided by Melcor company.

Thermoelectric coolers are also widely employed in microelectronics to stabilise the temperature of laser diodes, to cool infrared detectors and charge-coupled devices (CCD), and to reduce unwanted noise of integrated circuits. For this application, the

conventional thermoelectric coolers are bulk and are incompatible with microelectronic fabrication processes. Therefore, the thin film thermoelectric coolers have been designed by using micromachining technology and can be integrated in microelectronic circuits. Figure 2-4 (a) and (b) are schematics of a proposed thin film thermoelectric cooler with infrared component integrated into cooled central region. This thin film thermoelectric cooler can be fabricated as follows: a very thin amorphous SiC film is 'laid down' on a silicon substrate using conventional thin film deposition and a 'membrane formed by removing the silicon substrate over the desired regions using micromachining. N- and p-type thermoelements are then deposited on the membrane to form thermocouples. Thermocouples are configured so that the central region which is to be cooled is surrounded by the cold junctions of the Peltier thermocouples, while the hot junctions are located on the outer peripheral area which rests on the silicon substrate rim. Heat is pumped laterally from the central region to the silicon substrate rim and then dissipated vertically through it to an external heat sink. Theoretical analysis indicates that the coefficient of performance and heat pumping capacity, when operating at a temperature difference of 20°C, are 0.6 and 1mW, respectively. The maximum temperature difference of 30°C can be obtained for a thermoelement length *l* of 0.15mm.[Gao M et al., 1999]

(b) Refrigerator and Air Conditioner

In addition to cooling the electronic devices, thermoelectric modules are widely used in other niche applications where the cooling demands are not too great (such as portable cooler boxes) or cases in which the energy cost is not the main consideration (such as military applications). However, their applications in cooling large thermal capacity components or spaces have been limited due to the relatively low COP and high energy cost. The COP of a present thermoelectric refrigerator is typically < 0.5 when operating at temperature difference $\Delta T \sim 20^{\circ}C$.

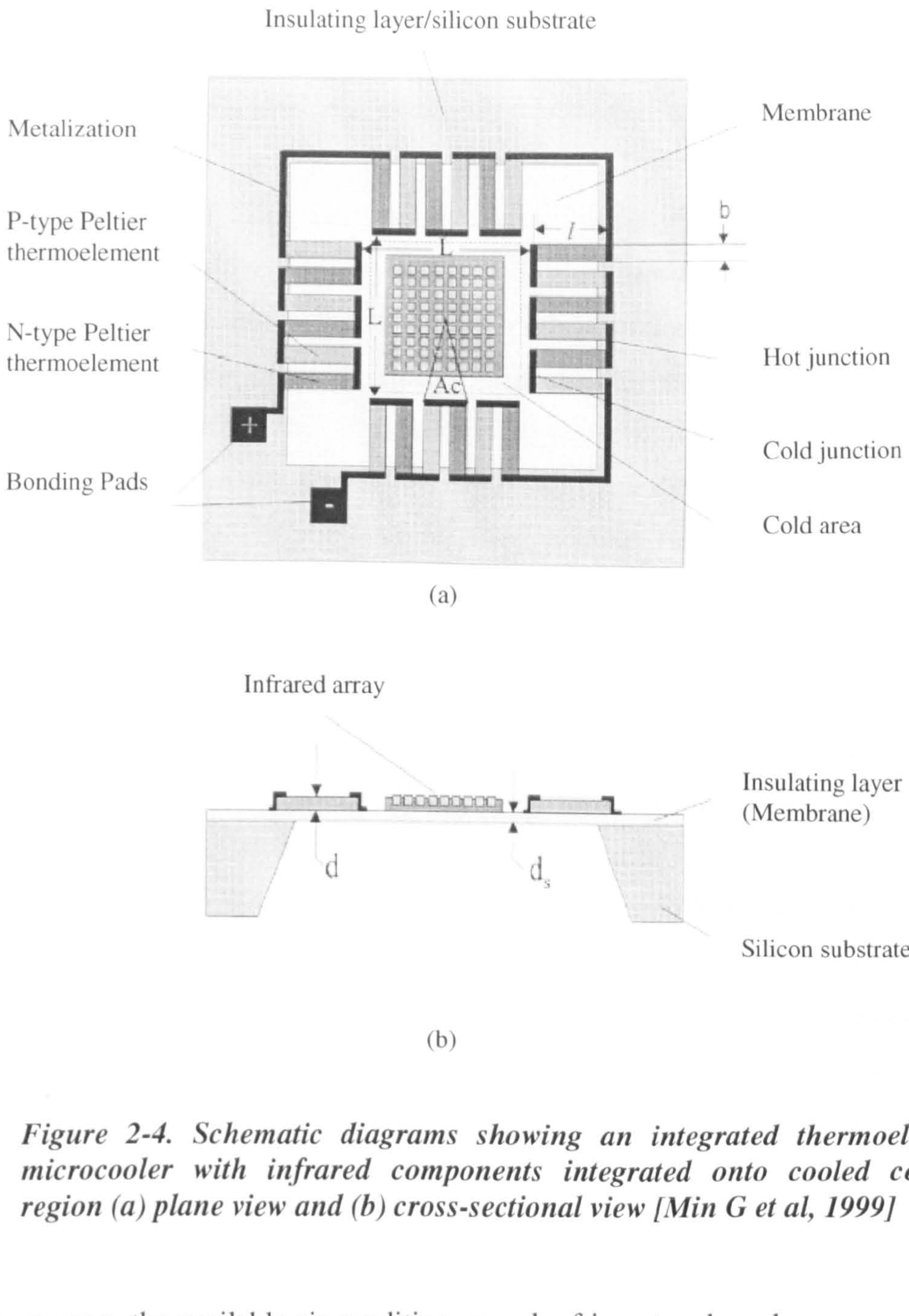

Figure 2-4. Schematic diagrams showing an integrated thermoelectric microcooler with infrared components integrated onto cooled central region (a) plane view and (b) cross-sectional view [Min G et al, 1999]

In recent years, the available air conditioners and refrigerators have become a way of life for millions of people around the world. As the standard of living increases in less developed countries, many more people will demand the convenience and comfort that they offer. At the same time, energy costs and environmental regulations regarding the manufacture and release of CFCs are also increasing. These facts are encouraging manufacturers and their customers to seek alternatives to conventional refrigeration

technology. One of the alternative refrigeration systems being used for an increasing number of these solutions is thermoelectric technology [Welling Jr T. E, 1997]. As a unique cooling device in which the electron gas serves as the working fluid, the thermoelectric module is noiseless, inherently reliable and environmentally friendly.

Actually, examples of using thermoelectric modules for refrigerators can be found as early as 1950's ~ 1960's. [Brown W.K, 1965; Boehmer A.P, 1963; Lindenblad N.E, 1954] However, the continued development on this area was slow owing to technical difficulties and the superior performance of vapour-compresion systems in term of COP. In recent years, due to the aforementioned reasons, the interests in the use of thermoelectric modules for domestic refrigerator have been revived in spite of the drawback of the low COP. Some thermoelectric modules, such as Melcor's Polar TEC™ series thermoelectric modules, was developed specifically for these low cost, high volume, commercial applications. Many improved thermoelectric refrigerators have been reported frequently. U.S Patent No. 6,003,319 entitled Thermoelectric Refrigerator with Evaporating/Condensing Heat Exchanger (shown in Figure 2-5) shows an improved heat exchanger with an evaporating surface and a condensing surface. Using this heat exchanger can increase the COP of the current thermoelectric refrigeration system. U.S. Patent No. 5,987,891 entitled Thermoelectric Refrigerator/Warmer Using no External Power shows that a refrigerator/warmer convert a natural energy such as the solar energy into electric power based on difference between the internal and external temperatures to make an external power needless as shown in Figure 2-6. U.S Patent No. 5,927,078 entitled Thermoelectric Refrigerator shows a unit, the interior of which can be always maintained at a high humidity by controlling the quantity of electric power to the thermoelectric module and to the interior fan, as shown in Figure 2-7. This refrigerator therefore can maintain the freshness of perishables, vegetables and the like for a longer time compared to a conventional refrigerator.

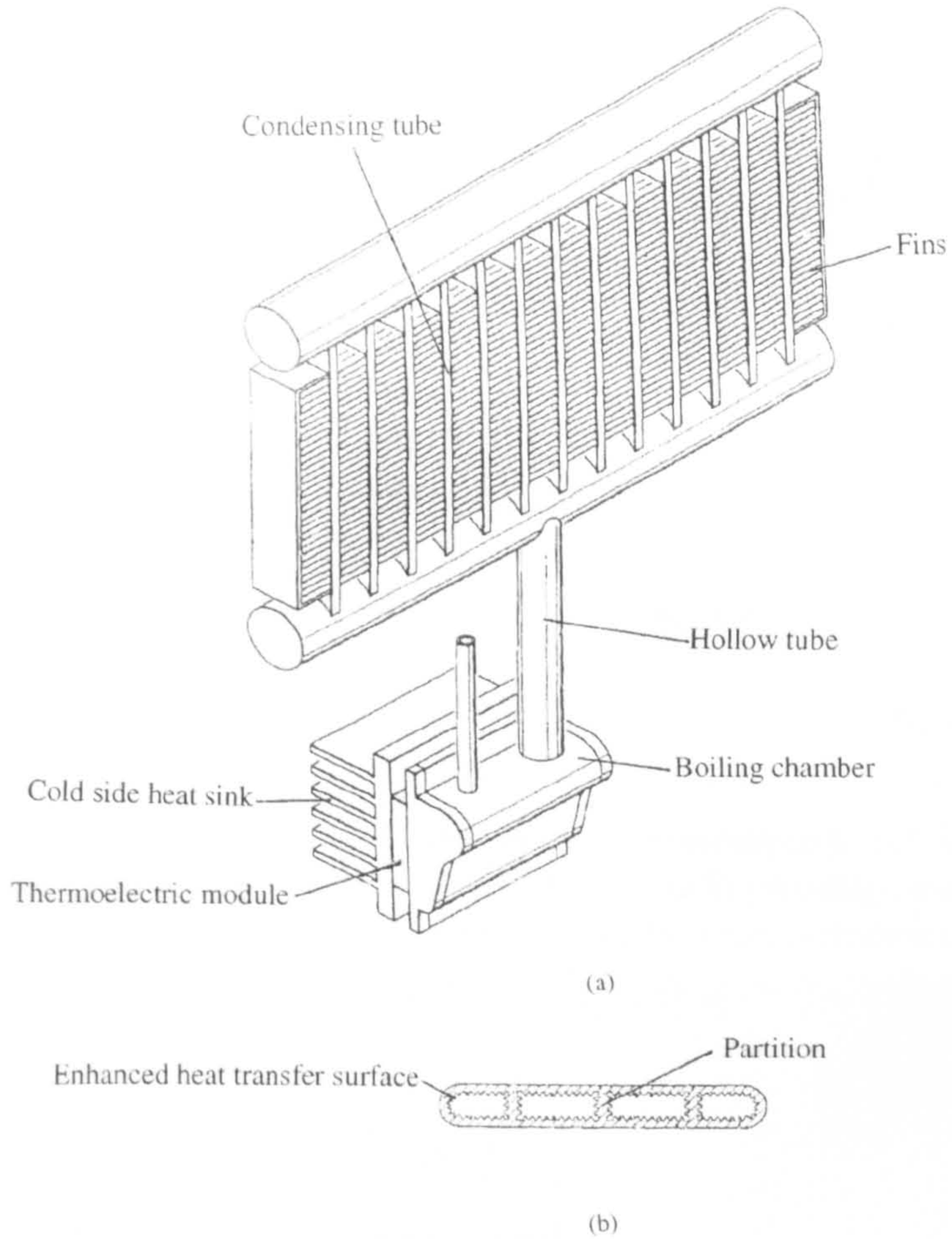

Figure 2-5. (a) Air cooled, thermosyphon reboiler-condenser assembly (b) Cross-section of the hollow condensing tube with enhanced heat transfer surface [Gilley et al, 1999]

Due to the low efficiency of present thermoelectric refrigeration systems, use of solar PV cells as the power of the thermoelectric refrigeration systems become attractive. The solar energy is clean and inexhaustible. Because the supply of the solar energy is free, efficiency of thermoelectric refrigeration system is not an overriding consideration. As solar radiation is intermittent, a means of energy storage for periods of low insolation and nighttime is essential. To achieve this, the thermoelectric refrigeration systems need to be integrated with heat storage and recovery systems. The investigation on integration of the heat storage and recovery systems with thermoelectric refrigeration systems is imperative.

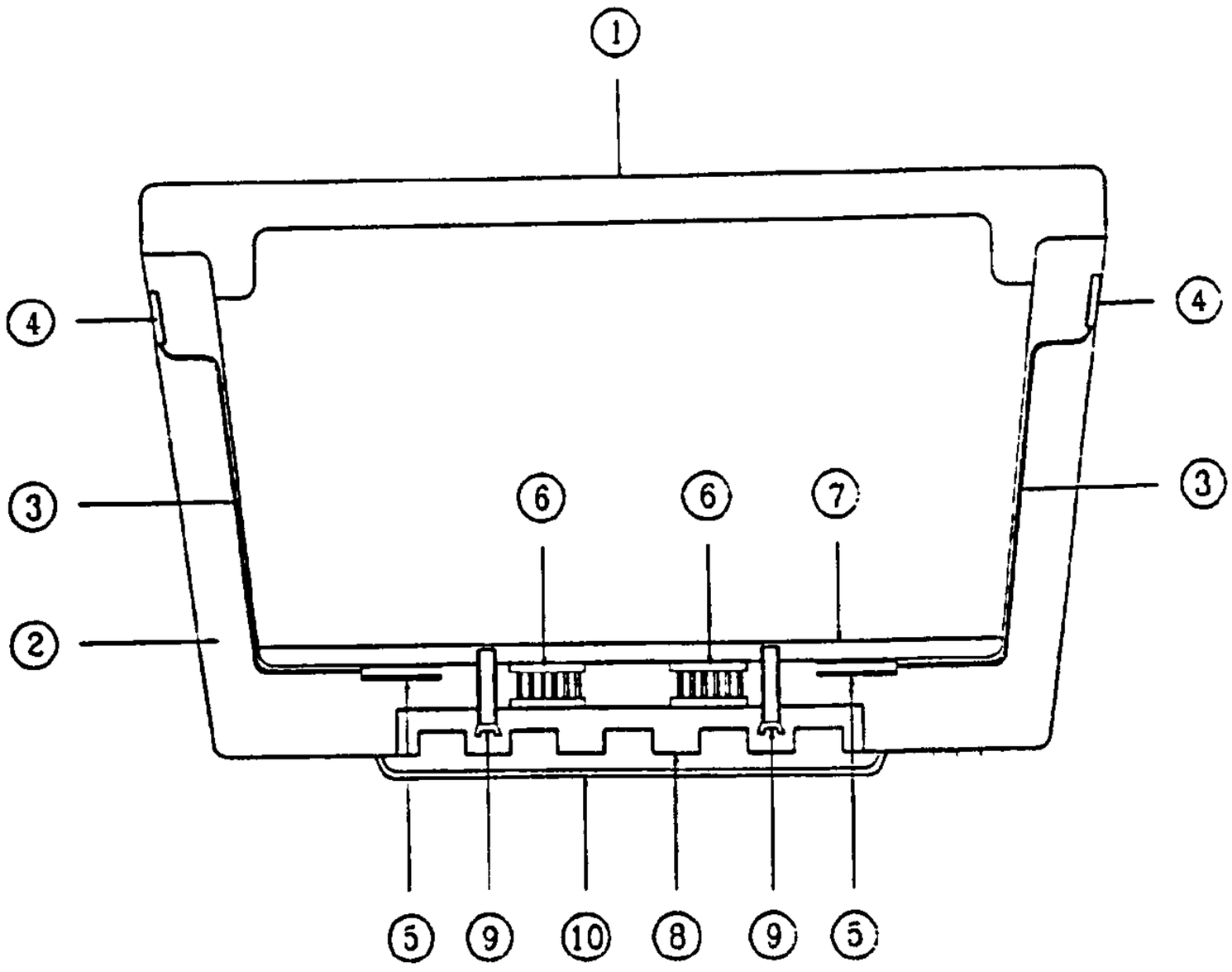

Figure 2-6. Schematic diagram of the powerless thermoelectric refrigerator/warmer. (Explanation for the Figure: 1-Lid; 2-Main body; 3-Thermoelectromotive device; 4-Out part of thermoelectric device; 5- Inner part of thermoelectromotive device; 6-Tthermoelectric module; 7-Bottom plate; 8-Radiating plate; 9-Bolts 10—Protecting net)

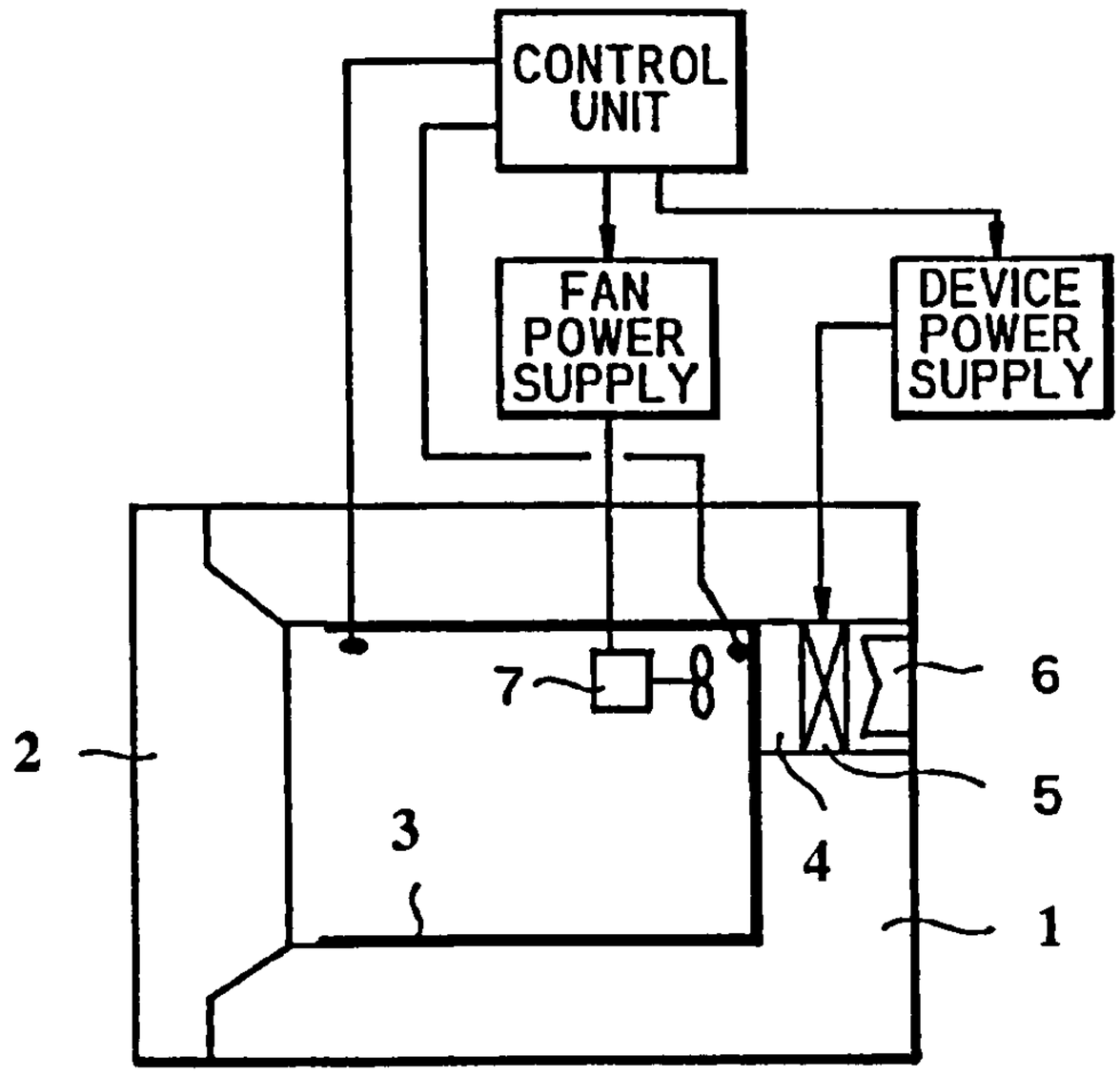

Figure 2-7. Schematic diagram of a thermoelectric refrigerator with controlling system (Explanation for the Figure: 1—Heat insulating casing; 2—Heat insulating door; 3—First thermal conductor; 4-Secondthermal conductor; 5—Thermoelectric module; 6—Circulation jacket; 7—Interior fan)

Compared to thermoelectric refrigerators, fewer thermoelectric air conditioners are reported. Reports on using thermoelectric modules for air-conditioning on different occasions can be found as early as 1960's. However, after more than 30 years, only a company supplied thermoelectric air-conditioning systems commercially [Rowe D.M,1995]. A few reports can be found in using thermoelectric air-conditioning for small scale or particular case [Bojic M,1997; Morrow R.C,2000]. Only one recent report can be found describing a thermoelectric air conditioner for cooling/heating a room space, such as living rooms, restaurants, offices, or the like [Kim C.M, 2001].

Compared to conventional gas compressed air conditioner systems, thermoelectric air conditioner systems have the following features: They can be built into a very flat unit that can be conveniently handed on walls for building air-conditioning. They can be easily switched between cooling and heating and proportionally adjusted to meet requirements for air-conditioning individually. They are environment friendly, quiet, long life span and need less maintenance. Since thermoelectric modules are low DC currents driven devices, they can accept a power supply directly from PV panel or through DC/DC conversion. These advantages make thermoelectric devices very attractive for building air-conditioning.

(c) Specific Applications and Prospects of the Development of Thermoelectric Cooling Technology

Some thermoelectric equipment for specific applications in military, aerospace, instrument, biology, medicine and industrial or commercial products have been reported. The following is some examples.

A solar cell-driven, thermoelectric cooling prototype headgear (as shown in Figure 2-8.) can be used to cool the forehead, which achieve required temperature difference between ambient and cooling temperature (4-5°C) for thermal comfort [Hara T,1998].

A prototype of thermoelectric "cryoconcentration cell" (shown in Figure 2-9) is developed for obtaining concentrated orange juice, which use Peltier effect as an

alternative to the traditional methods of cryoconcentration using the conventional refrigeration cycles based on gases such as NH_3 [Sanz-Bobi M.A, 1996].

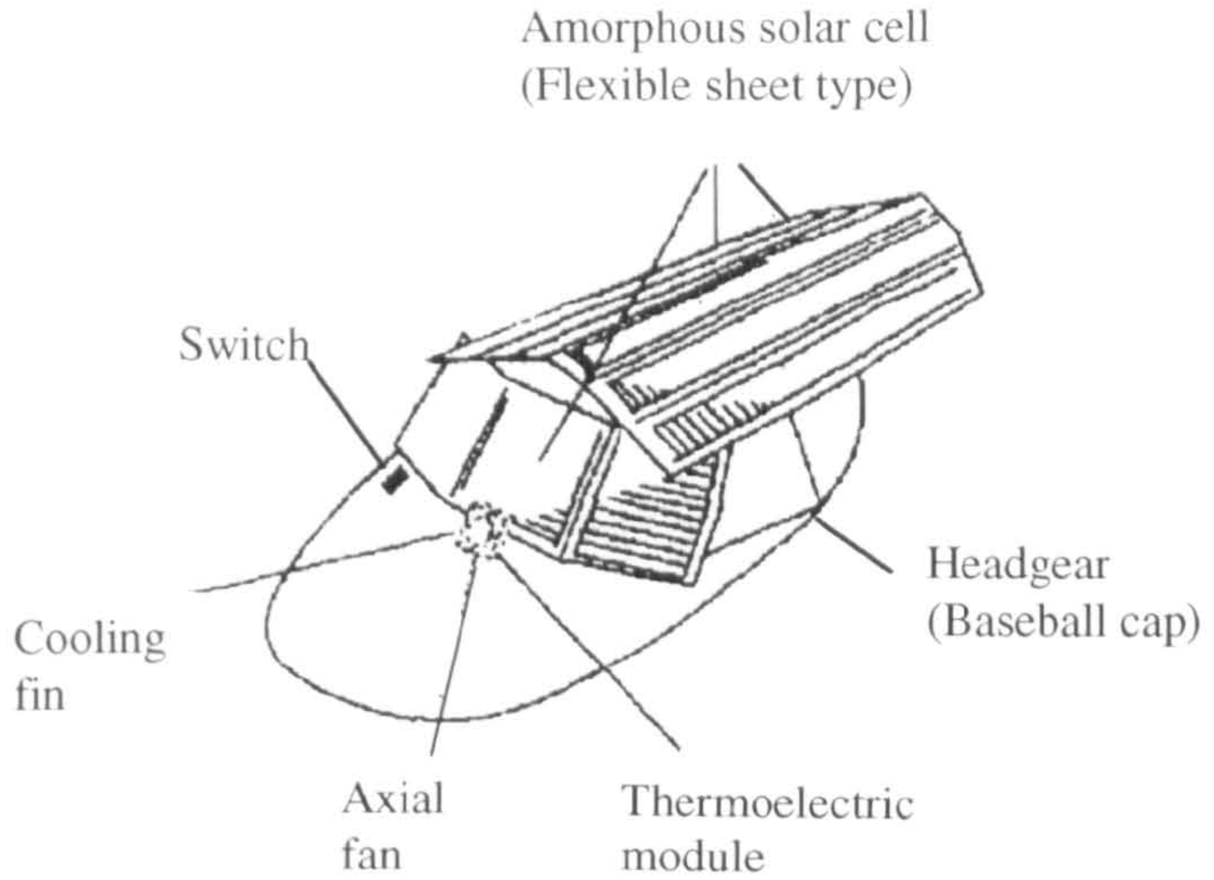

Figure 2-8. Solar cell-driven, thermoelectric cooling

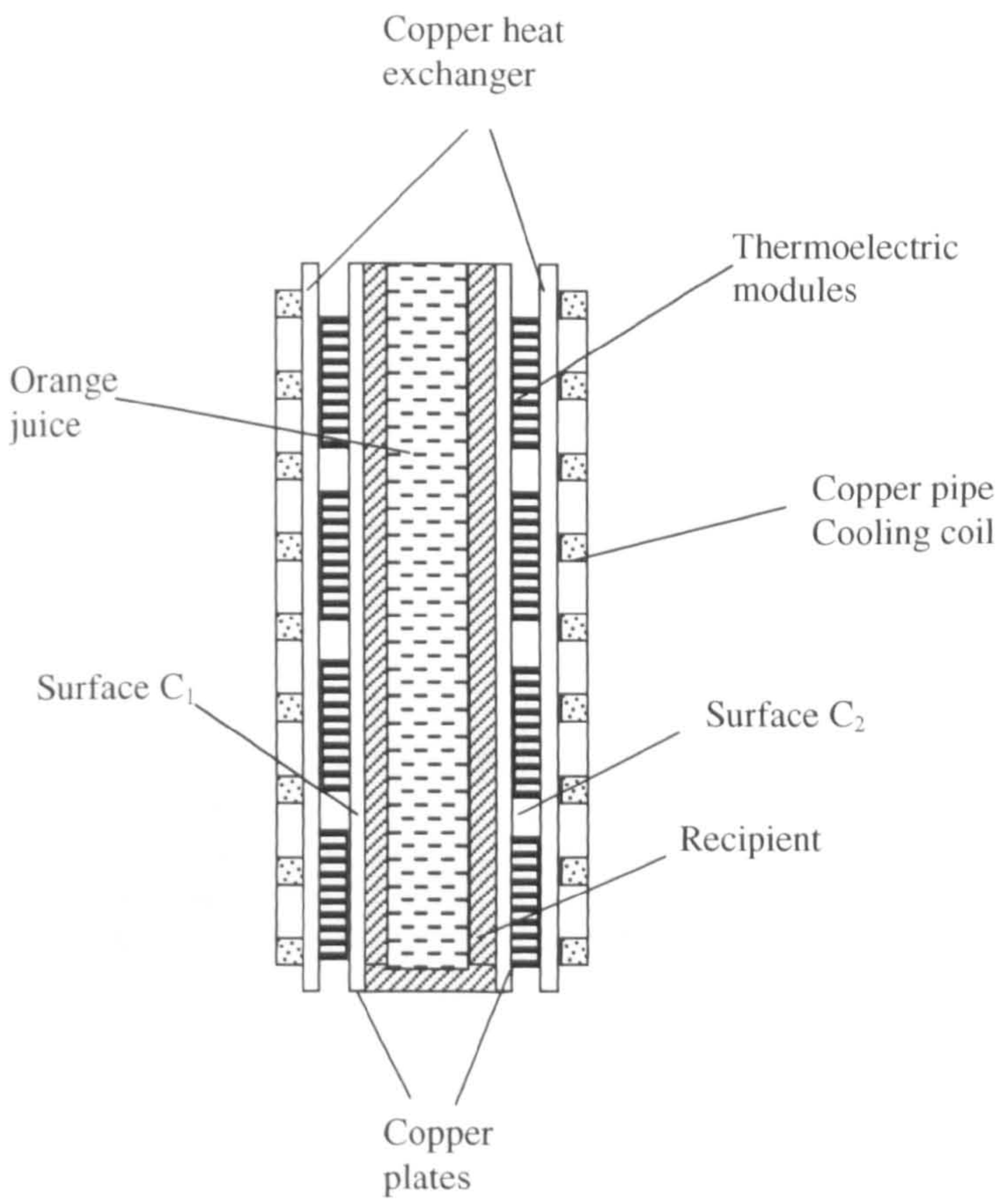

Figure 2-9. Schematic diagram of a cryoconcentration cell

An active thermoelectric intercooler is developed for heating or cooling a fluid passing through the intercooler, as shown in Figure 2-10. The intercooler may be used to cool gases from the compression stage of an engine turbocharger in order to increase engine horsepower. The intercooler could also be used to cool the oil in an engine or transmission. Alternately, the intercooler could be used to heat or cool the air provided to the passenger compartment of a vehicle [Iacullo R.S,1996].

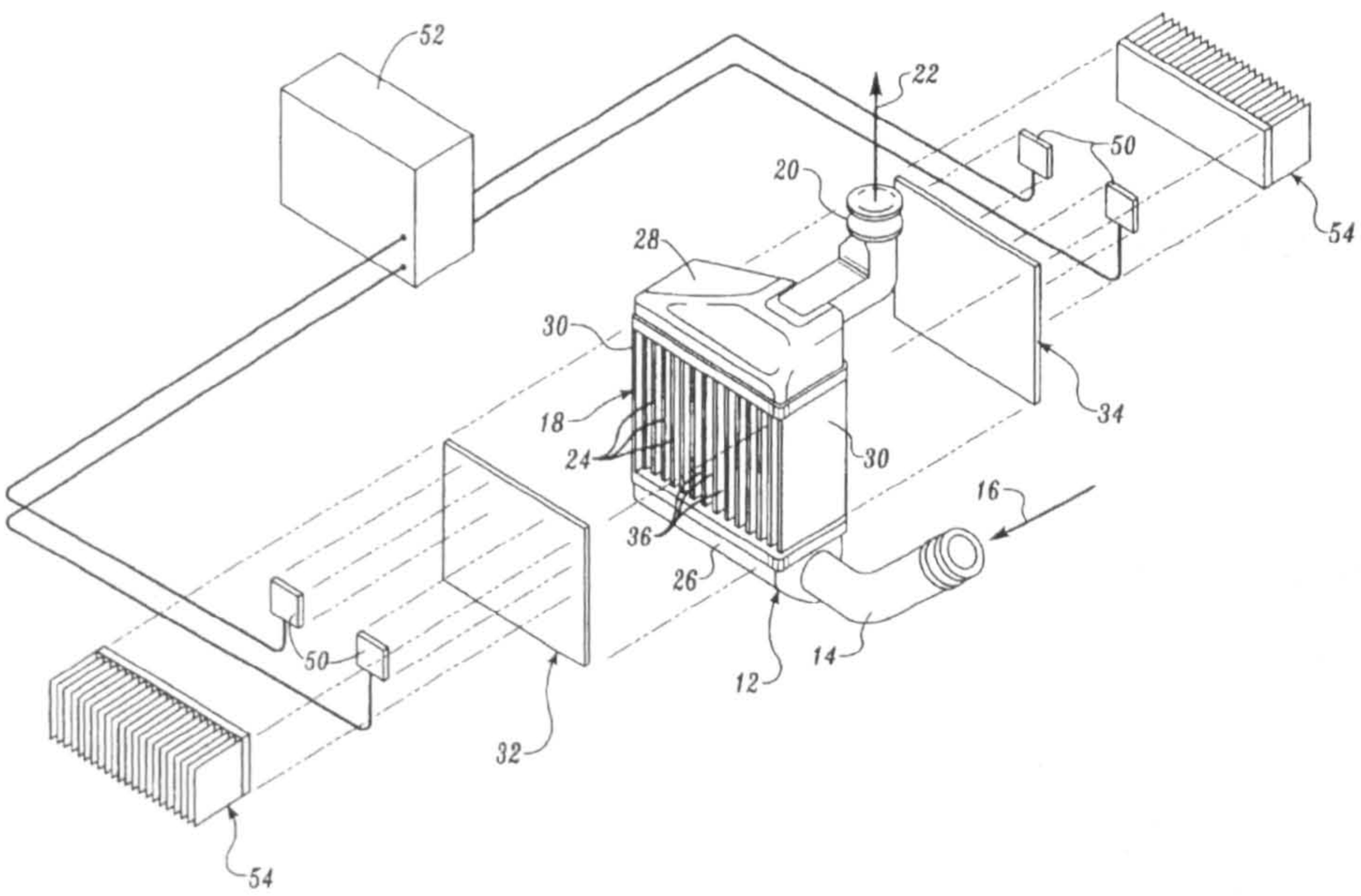

Figure 2-10. Schematic diagram of thermoelectric intercooler. *(Explanation for the Figure: 12—Chamber; 14—Inlet pipe; 16—Fluid in; 18—Body of the chamber; 20—Outlet pipe; 22—Fluid out; 24—Tubes; 26—Bottom of chamber; 28—Top of chamber; 30—Side plate; 32—Front plate; 34—Back plate; 36—Interior; 50—Thermoelectric modules; 52—Control system; 54—Conductive heat sink. * This Figure is from United States Patent, 5547019) [Iacullo R. S, 1996]*

The thermoelectric coolers have been used practically widespread fields. Thermoelectric production costs have decreased steadily and significant consumer markets of thermoelectric coolers have opened. Around 50 types of thermoelectric cooling products or assemblies are commercially available at present. There are an increasing number and variety of thermoelectric products. With each new year, the imaginations of design engineers widen with the immense possibilities of thermoelectric heating and cooling.

It is predicted [www.zts.com] that every domestic icebox could depend on thermoelectric modules. Thermoelectric domestic heat pumps and air conditioners will become competitive in the world market. This is because energy costs and demands can only increase and environmental concerns can only increase. Also the environmental treaties have banned chlorofluorocarbons. Reduced manufacturing costs of thermoelectric modules have been opening up new markets.

2.1.2 Research on Improving Coefficient of Performance of Thermoelectric Cooling Systems

The thermoelectric cooling technology has existed for about 40 years and found extensive applications. The main drawback of the thermoelectric cooling systems is low coefficient of performance (COP), particularly in larger capacity applications. The emphasis of recent research has therefore been the improvement of the COP of thermoelectric cooling systems by means of developing new materials for thermoelectric modules, optimisation of the module design and fabrication, improvement of heat exchange efficiency as well as use of multistage module.

The new thermoelectric materials with large figure of merit could make a breakthrough on improving module efficiency and the new theory of optimising the module construction could make a great improvement on module performance. These are yet to be realised in practice. Advances of research on heat exchange capacity and use of multistage module are described in the following sections.

(a) Improvement of heat exchange capacity

The COP (optimum COP) of a specific thermoelectric module is a function of module's hot and cold side temperatures respectively. Increasing the cold side temperature and decreasing the hot side temperature will improve the COP.

Figure 2-11 shows the calculated COP of a commercially available module as a function of temperature difference between the hot and cold side, at a hot side temperature of 300K, which is a typical condition for domestic refrigeration. It is shown that the COP of a thermoelectric module decreases with an increase in the temperature difference between the module's hot and cold side.

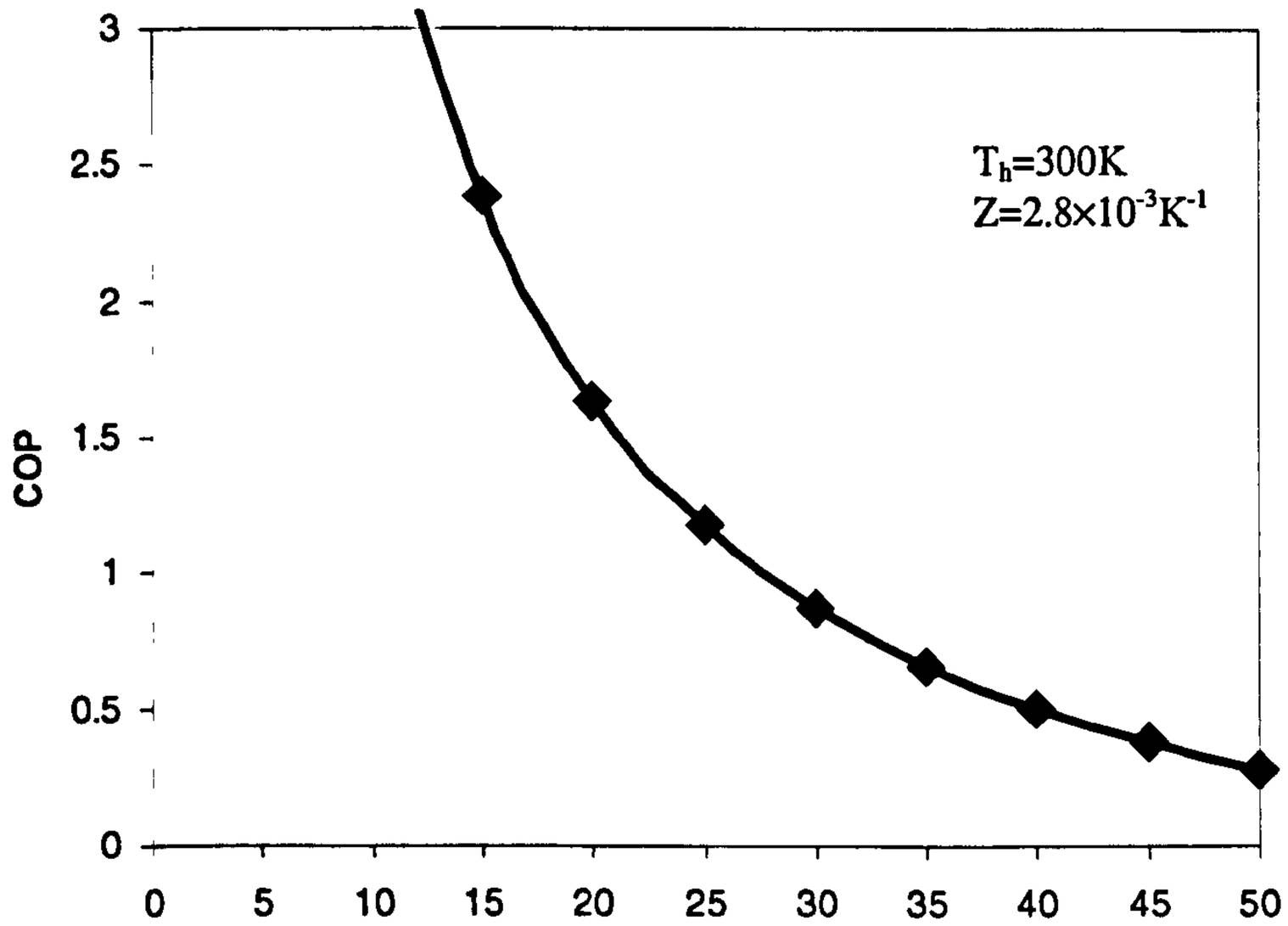

Figure 2-11. COP as a function of temperature difference across the module at hot side temperature T_h=300K [Gao M, 2000]

For a typical domestic refrigerator, a temperature difference between the ambient and the cabinet of about 25-30K at T_h=300K is usually required to achieve satisfactory cooling performance. This indicates that the maximum COP of a thermoelectric refrigerator comprised of commercially available modules is around 0.9-1.2, as shown in Figure 2-11. However, the practical COP of a thermoelectric refrigerator is much lower than this because the temperature difference between the hot and cold side of the thermoelectric modules is larger than the temperature difference between the ambient and the cabinet. In other words, the hot side temperature is higher than the ambient and the cold side temperature is lower than the cabinet temperature.

For a practical thermoelectric refrigeration system, the hot side heat exchanger rejects the heat produced on the hot side of the thermoelectric modules to the ambient and so reduces the hot side temperature. The cold side heat exchanger dissipate the heat from the cold region to the cold side of thermoelectric module and so increases the temperature of the cold side. Because the thermoelectric modules are very high heat intensity equipment, the high capacity thermoelectric heat exchangers are necessity.

The heat transfer capacity of the heat exchange system strongly influences the COP of the thermoelectric cooling system. If the heat transfer capacity of the heat exchange system is high, the temperature difference between hot and cold side of the thermoelectric cooling system may be reduced significantly, and the COP will be increased. If the heat transfer capacity of the heat exchange system is low, the temperature difference between hot and cold side will be greater, and the COP will be lower.

Heat is rejected from the hot side across a heat exchanger to the ambient. This is defined by:

$$Q_h = \frac{T_h - T_a}{R_e} \tag{2-1}$$

As shown in equation (2-1), the hot side temperature may be calculated as a function of the heat exchanger thermal resistance R_e, under specific heat flow at hot side Q_h and ambient temperature T_a. The R_e determines heat dissipating from the hot side of the thermoelectric modules by heat exchanger.

In principle, heat exchangers in thermoelectric cooling systems should be designed to minimise their thermal resistance under restrictions such as the size of the system and heat transfer method and system design method, because as the thermal resistance of the heat exchangers increases, the efficiency of thermoelectric cooling systems decreases.

Typical heat exchanger designs include natural convection, and forced convection heat exchangers for heat rejection to air, and forced convection heat exchangers for heat rejection to water flow, as shown in Figure. 2-12.

The typical heat exchanger thermal resistance for a 45 by 45mm square thermoelectric module is [Webb R L, 1998]:

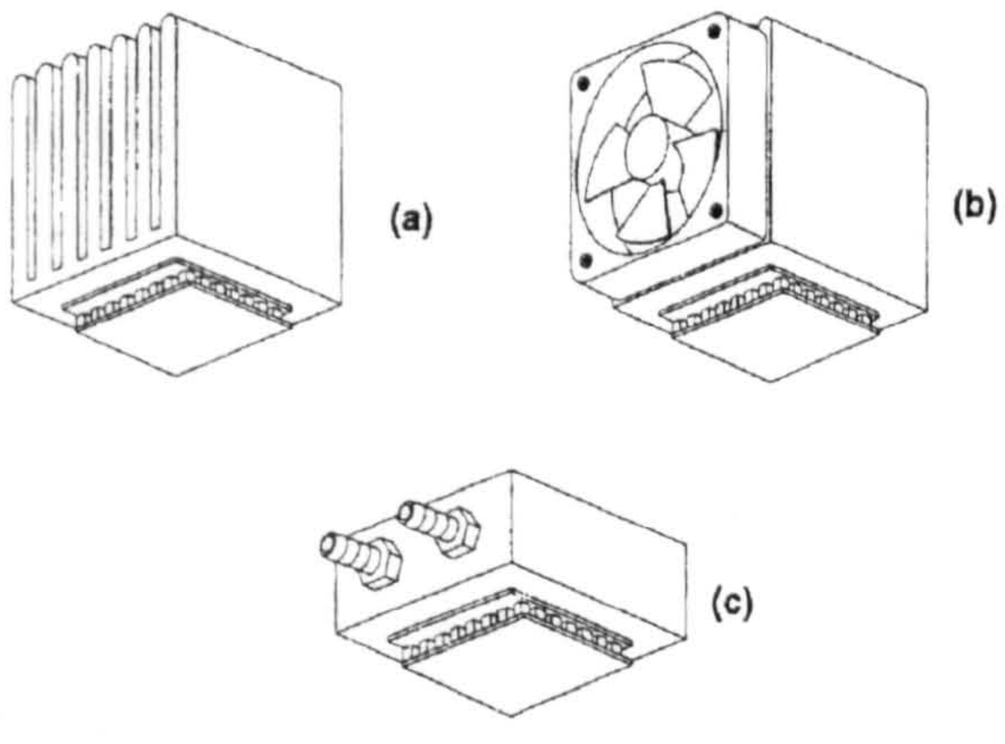

Figure 2-12. Common heat exchanger designs: (a) natural air convection; (b) forced air convection (heat sink not shown for clarity); (c) water-cooled forced convection [Webb R L. 1998]

1) Natural convection: 0.853-13.075 m^2K/kW, depending on the fin density and the ratio of the heat exchanger base plate area to the thermoelectric module area. Higher

ratios of the heat exchanger base plate area to the thermoelectric module area result in a lower thermal resistance;

2) Forced air convection: 0.531-5.759m^2K/kW, depending on the air flow rate. Larger air flow rates result in a lower thermal resistance;
3) Water-cooled exchanger: 0.348-0.737 m^2K/kW, depending on the water flow rate. Larger water flow rates result in a lower thermal resistance.

A ducted, forced-air, convection system has a higher performance than an un-ducted system.

Various types of heat pipe may be used to conduct heat from the small ceramic area to the convection surface, which is an alternate to the metal heat spreader plate. A heat pipe may also be used to assist the distribution of heat within the spreader plate. A heat pipe system must still reject heat to air or water. Hence, it must use one of the previously discussed convective heat rejection systems. Assuming a 12.7mm diameter aluminum/methanol heat pipe, and using a high performance wick structure, one can have a heat pipe resistance as low as 0.02K/W [Webb R L, 1998]. Coupling this with a liquid heat exchanger with a thermal resistance of 0.172K/W will result in a heat pipe/convection resistance of 0.132K/W [Webb R L]. Use of a heat pipe will not be of benefit for natural convection, because the dominant thermal resistance in this case is the convection resistance [Webb R L, 1998].

Water-cooled forced convection heat exchangers have excellent performance. The main drawback of a water-cooled heat exchanger is that it needs a convenient source of cooling water. Without a source of cooling water, a forced convection water heat exchanger would require a pump and radiator and associated fittings and tubing. The added resistance of the radiator would increase the overall resistance. Air-cooled systems are therefore often more desirable.

Many heat exchange systems based on the aforementioned forced air convection exchangers and the use of heat pipes have been reported.

Sofrata H (1996) reported that using a double fan in an appropriate position could significantly increase the efficiency of the forced air exchanger compared to using the single fan in a refrigerator. A long chimney for a natural-convection heat exchanger may also improve the performance of the refrigerator without the need to use fans that, of course, require the electrical power input.

A novel, air-cooled thermosyphon reboiler-condenser system has been reported [Webb-R.L, 1998], as shown in Figure 2-5, and has been used as a heat exchanger of a thermoelectric refrigerator [Gilley, 1999]. This system is capable of providing very low heat sink resistance values with air-cooling and a thermal resistance as low as 0.0194-0.0505K/W was obtained for cooling a 45mm square module. The system promises significantly higher COP for thermoelectric coolers than is possible using existing heat exchange technology. The high performance is obtained using of enhanced heat transfer surfaces.

As shown in Figure. 2-5 (a), the heat exchanger includes a boiling chamber, and a condensing chamber. The boiling surface inside the boiling chamber has a porous metal coating to enhance its heat transfer. The working fluid, which has been heated in boiling chamber to its vapour phase, can flow upwardly through the hollow tube into the condensing tube in condensing chamber. As shown in Figure. 2-5 (b), each condensing tube includes partitions, which provide the required structural strength for respective tubes and also increase the total surface area contained within each condensing tube. Enhanced heat transfer surfaces are preferably formed on the interior surface of each condensing tube. The working fluid that has been condensed into its liquid phase in the condensing chamber will flow through the hollow tube downward into the boiling chamber.

In general, thermoelectric module is very high heat intensity equipment, which need high efficiency heat exchangers to lower the hot side temperature and increase the cold side temperature in order to improve the COP. However, the optimum design and selection of the heat exchangers should be a compromise of efficiency, convenience, size and cost etc.

Use of a greater number of modules would also improve the COP of the system. Use of more modules would reduce the heat load on each module, and so lower the heat flux densities of both the hot and cold side of each module. The hot side temperature could therefore be reduced more by the heat exchange system. The main disadvantage of this is however, that the use of many modules would increase both cost and space requirements.

(b) Use of Multistage Module

The COP of thermoelectric refrigeration system decreases rapidly with increasing temperature difference but its performance can be improved by the use of multistage thermoelectric modules. To give the concept of the multistage module, the typical designs of a single-stage module and a multistage module are shown in Figure. 2-13 for comparison.

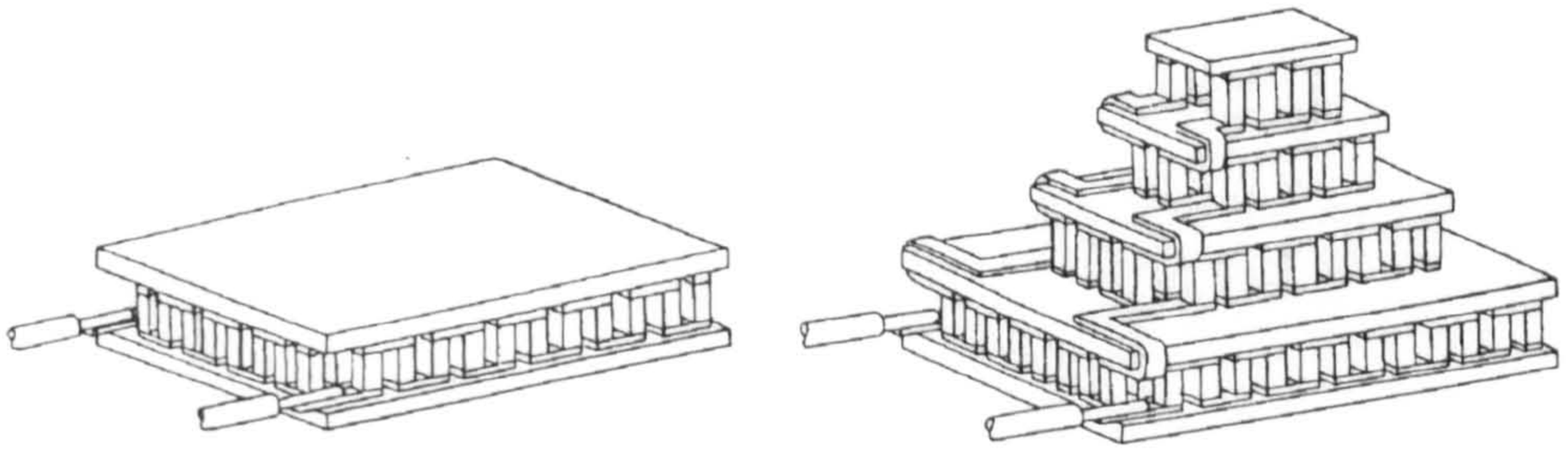

Figure 2-13. Typical thermoelectric module designs (a) single-stage module; (b) multistage module [Guyer E C, 1988]

Lindler Keith W (1998) investigated the improvement in performance that could be obtained using a multistage module. The results showed a comparison of COP as a function of hot side temperature (with a fixed cold side temperature of 20°C) for a single, commercially available CP 1.0-17-08L module, and two CP 1.0-17-08L cascaded modules. For a hot side temperature around 50°C (temperature differences of 30°C), the improvement in COP was too small to justify the added cost of a cascaded thermoelectric module. For a hot side temperature of 60°C, the single module operated at a COP of 0.670 compared to a COP of 0.719 for the cascaded module. This represents a 7.3% improvement in COP. For hot side temperature above 90°C, the improvement in

COP is significant. At a hot side temperature of 100°C, the single module COP is 0.151 compared to 0.232 for the cascaded module.[Lindler Keith W, 1998] This represents a 54% improvement in COP. This showed the multistage modules suits for the system that has large temperature difference with high hot side temperature to improve the COP. For large temperature differences (over 40°C), the improvement in COP of the cascaded system results in a much smaller heat rejection requirement, and thus, a smaller fin can be used to reject heat to ambient.[Linder Keith W, 1998]

Optimum temperature staging has been investigated to minimise entropy generation in a multi-stage cryogenic refrigeration cycle [Jeong S et al]. It was found that the best intermediate temperature distribution was to have the same high to low temperature ratio at each stage of the system. As an example, the result could be applied to the design of a cryogenic cascade thermoelectric cooling system to find the optimum size distribution of each stage.

Research on improvement of COP including several aspects as aforementioned. However, a thermoelectric module performance analysis for optimum selection (design) of the modules for a specific application has not mentioned. Optimum selection (design) of the thermoelectric module in the system design should play an important role for improving the system's performance.

2.2 Heat Pipes and Heat Pipe Thermal Performance Analysis

Heat pipes are simple heat transfer devices, having high, effective thermal conductivity and capable of transporting large amount of heat over considerable distances. Because of the simplicity of design and ease of manufacture and maintenance, these devices have found applications in a wide variety of areas, including energy conversion systems, cooling of nuclear rectors and electronic equipment, space apparatus and the solar energy system. [Abhat A., 1982; Riffat S.B. et al, 2000; Riffat S.B., 2000]

Heat pipes make use of the evaporation of a suitable working fluid, transport of the latent heat of vaporization, condensation of the vapour and back flow of the condensate to the area where evaporation takes place [Dunn and Reay, 1982]. The means of transporting the condensate from the condensation zone to the evaporation zone is the

major distinction between the different designs of heat pipes. Different forces can be utilized, e.g., capillary (surface tension) forces, gravitation, acceleration (centrifugal) forces, thermally induced pressure differences or some combination of these.

Heat pipes can be designed and constructed with various cross-sectional areas and geometries as small as 0.6mm x 0.6mm and 25 mm in length, or 2mm in diameter and 1m in length, and as large as 100m in length [Takaoka M. et al, 1985]. All heat pipes have an evaporator and condenser section where the working fluid evaporates and condenses respectively. Many heat pipes also have a transport or adiabatic section, which separates the evaporator and condenser sections by an appropriate distance intended to satisfy the heat pipe limitations and the design constraints of the application. A given heat pipe may have multiple evaporators, condensers and adiabatic sections. A working fluid usually circulates due to the influence of capillary forces in a wick. However, gravitational, centrifugal, electrostatic, and osmotic forces can also be used to return the liquid from the condenser to the evaporator.

Various types of heat pipes can be made to suit for different applications. The typical heat pipe configurations include gravity-assisted wickless heat pipe (two-phase closed thermosyphon), capillary-driven heat pipe, annular heat pipe, flat-plate heat pipe, rotating heat pipe, leading edge heat pipe, gas-loaded heat pipe, capillary pumped loop heat pipe and mono groove heat pipe. Heat pipe containers are generally circular cylinders for simplicity of design and manufacturing. However, other shapes such as rectangular (flat plate heat pipes), parallelepiped, micro/miniature, conical (rotating heat pipes), and nose-cap (leading edge heat pipes) geometries have also been investigated for special applications. Figure 2-14 and Figure 2-15 [Faghri A., 1995] shows normal gravity-assisted wickless heat pipe and normal capillary-driven heat pipe. Figure 2-16 shows a micro/miniature heat pipe.

The normal gravity assisted wickless heat pipe is without a capillary structure. It is used for operation in the earth's gravitational field. There is a certain amount of liquid in the device, forming a pool. In operation the liquid is evaporated from the pool (pool boiling) and a substantial part of the liquid is in permanent circulation: vapor flow from the

heated areas to the condensation zone, reflux of condensate to heated area. In the extreme case, the pool volume can disappear completely, so that evaporation takes place only from the heated wall surfaces, which are wetted by refluxing condensate. These devices are also called wickless heat pipes, gravity supported or, simply, gravity heat pipes. For various reasons they can also be provided, at least partly, with a capillary structure, e.g. to improve evaporation or liquid distribution or to support the pumping capacity.[Groll M et al, 1992]

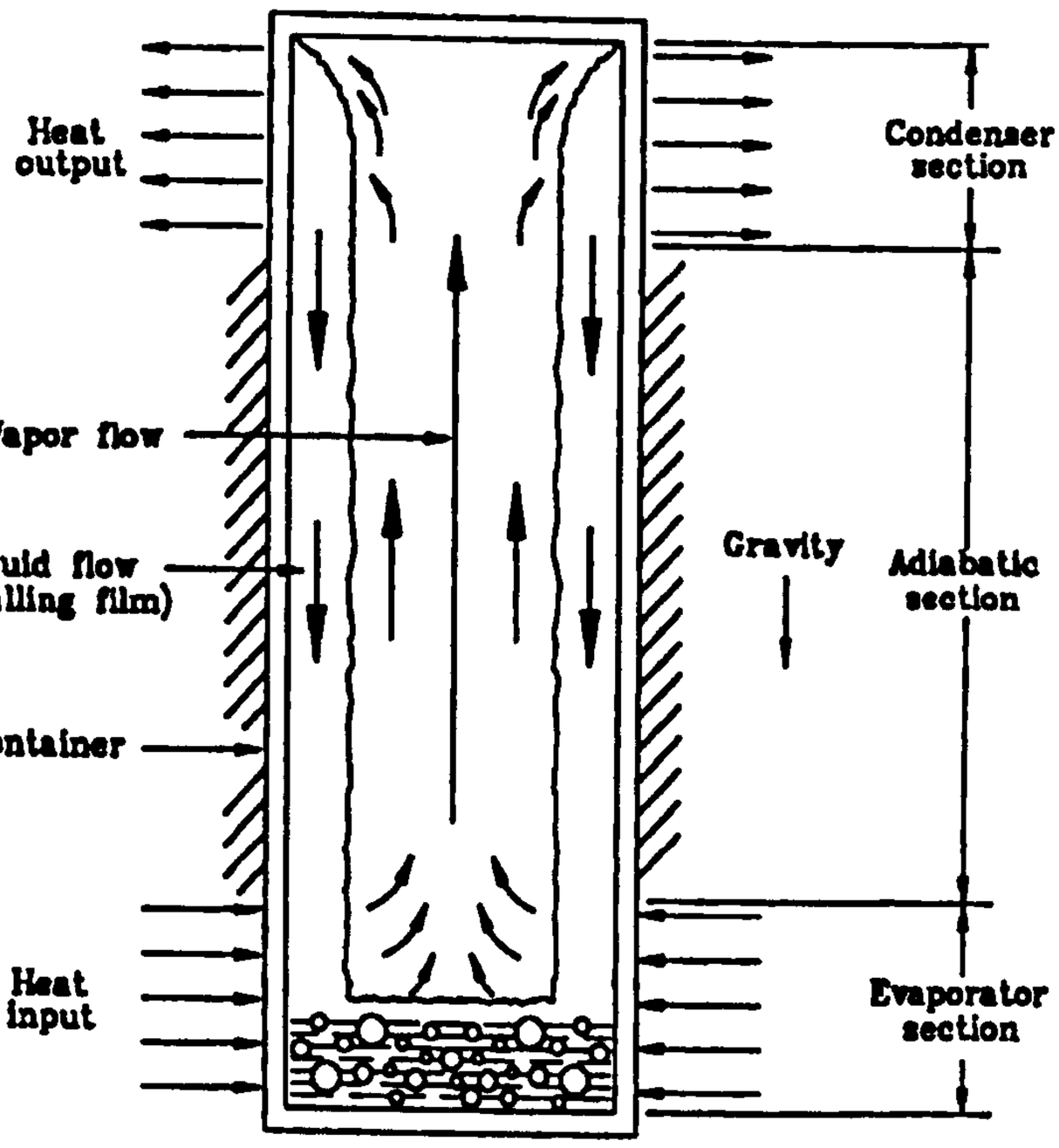

Figure 2-14. Normal gravity assisted wickless heat pipe (two-phase closed thermosyphon)

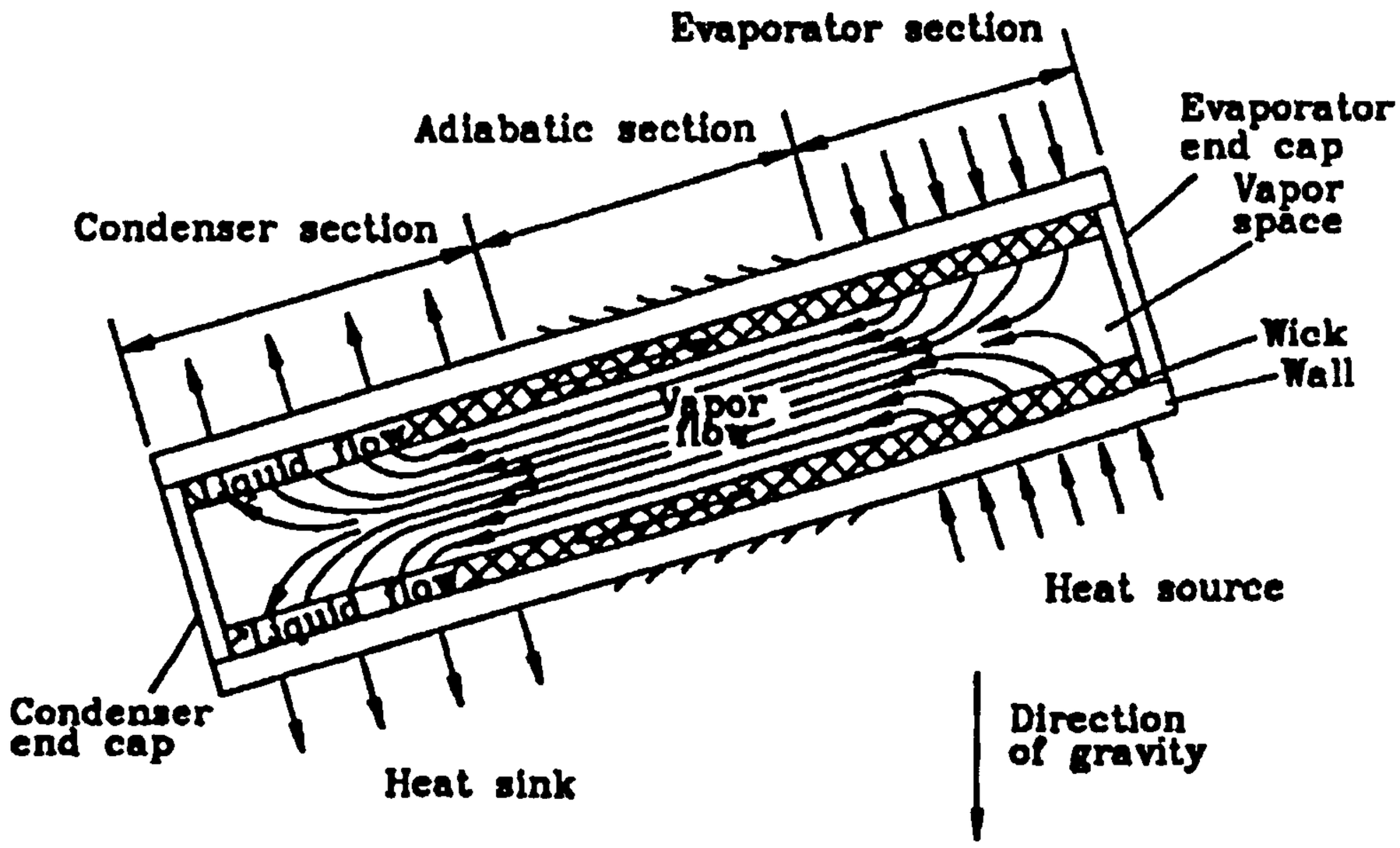

Figure 2-15. Normal capillary-driven heat pipe

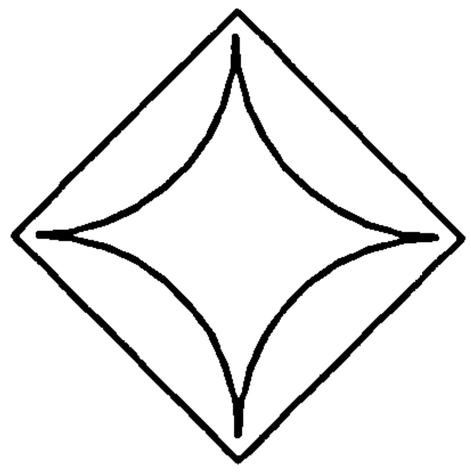

Figure 2-16. Cross section of micro/miniature heat pipe

Following the needs of industrial and scientific applications, various types of gravity heat pipes with different structure have been developed. Except for classical gravity-assisted wickless heat pipe, there are separate-type gravity heat pipe and gravity heat pipes with flow separator, as shown in Figure 2-17 and Figure 2-18 [Groll M et al, 1992]. The separate-type gravity heat pipe consist of separated evaporator and condenser tubes with one or more connecting common vapour and liquid flow lines, respectively. Since this arrangement completely decouples the evaporator and the condenser parts, two major advantages are obtained: 1) long distances between evaporator and condenser are manageable; 2) counter-current flow limitation is eliminated, since vapor and

condensate flow co-currently. These positive features are, however, accompanied by higher complexity of the system and correspondingly higher manufacturing costs. The main goal in employing flow separators is to shift the counter-current flow limitation towards higher performance. Compared to separate-type heat pipes, flow separators offer a very compact design. On the other hand, the disadvantages of separate-type heat pipes, i.e. higher complexity and cost, are also valid here.

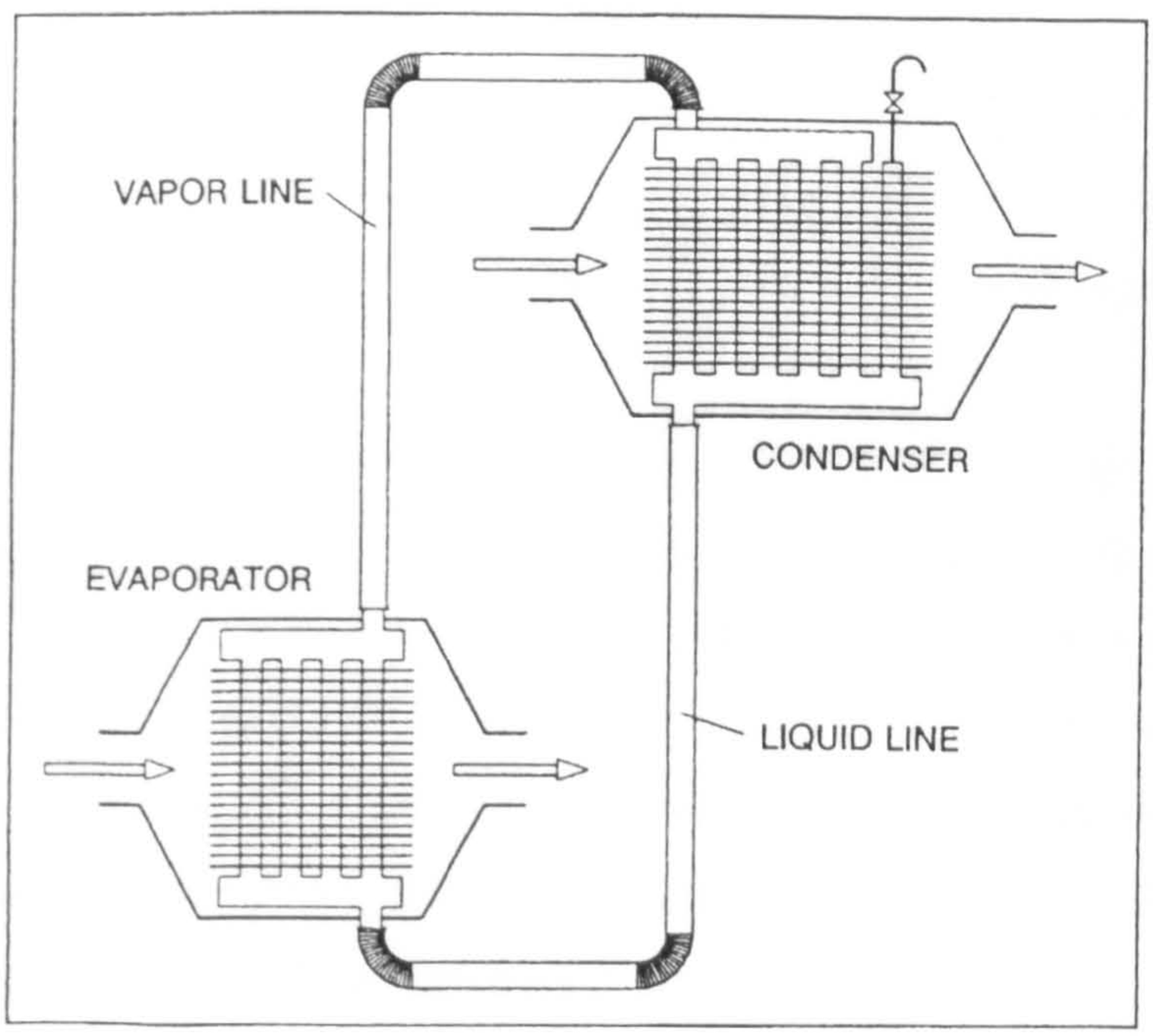

Figure 2-17. Separate-type gravity heat pipe heat exchanger

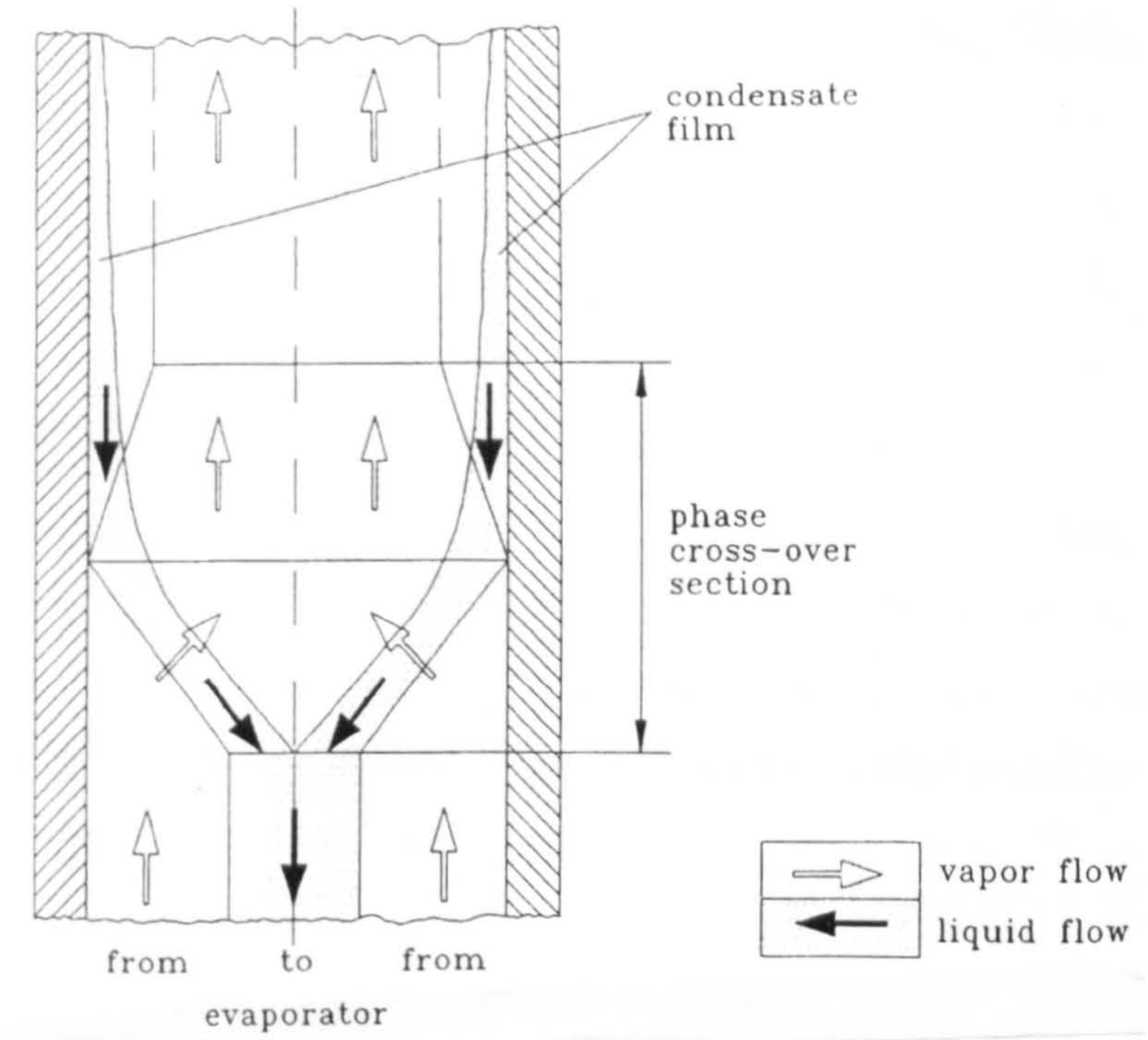

Figure 2-18. Gravity heat pipe with cross-over flow separator

For any heat pipe, the maximum heat transport capacity is governed by five limits, namely, the sonic limit, the entrainment limit, the boiling limit, the viscous limit and the capillary limits. These limits could be calculated by using the techniques presented in Dunn and Reay (1982) and Babin et al (1990), and the critical limit would be the minimum value calculated. For a gravity heat pipe, filled liquid mass also influences its heat transfer to a certain extent, representing an additional limit which could be calculated by the method presented by Zhuang J. et al(1989).

2.3 Photovoltaic Solar Cells and Their Applications

Increased global warming and deterioration of the ozone layer has stimulated interest in the use of renewable energy, in particular solar energy due to its abundance for energy provision (cooling, heating and electricity). Systems using solar energy produce no pollution, require little maintenance and provide a means of achieving a sustainable environment.

Photovoltaic (PV) cells, consisting of thin layers of semiconductor material, convert sunlight directly into electricity. PVs are solid state energy converters that have no moving parts and do not require maintenance except for cleaning of glazing to remove any deposition of dust. The first silicon solar cell was discovered, by Russell Ohl in 1940, after which the semiconductor revolution of the 1950s brought forward the first efficient solar cell (1954) and its first commercial application on spacecraft (1958). Only after the oil crises of the 1970s, the solar cell industry took root in heating/cooling system. Until recently, PV technology has been largely based on silicon wafers as semiconductor material, as used in microelectronics. At present, however, a transition seems to be in progress to a second generation of so-called thin-film PV technologies. [Zwaan Bob van der et al, 2003]

In order to describe the properties and the use of photovoltaic solar cells, it is helpful to consider the sequence of phenomena involved: from the radiation received from the sun, through the processes of absorption of this radiation, generation and transport of charge carriers in the semiconductor, separation of charge by the junction, collection of these carriers at the contacts to the device, and finally to the various types of power conditioning and storage that might be used, and the actual utilization of power generated. For example, photovoltaic generation of electricity must be coupled with an effective storage process in order to compensate for the intermittent nature of solar radiation. [Alan L. Fahrenbruch et al, 1983]

The photovoltaic solar module, usually consisting of a number of solar cells, is the main component of a photovoltaic solar energy system. Solar cells can be categorised in two main groups: wafer-type (single crystalline or multi-crystalline) and thin-film. The former is made from wafers cut from a silicon ingot. Thin-film PV cells are deposited directly onto a substrate like glass, plastic or steel. Of the 1998 commercial PV market some 85% were wafer-type, while the remaining 15% were mainly amorphous silicon (thin film) solar cells. Other thin film technologies are being developed in the laboratory, are in a pilot production phase, or start emerging as commercial technologies. Among the latter are notably CIGS (copper–indium/gallium–diselenide) and CdTe (cadmium–telluride) solar cells. It is too early to pick winners or losers among the PV technologies

available commercially or under development. Still, there seems reasonable consensus that thin-film technologies offer the best long-term prospects for low production costs, even when considerable cost reductions are to be expected for crystalline wafer technologies resulting from technological improvements and economies of scale. On the other hand, wafer-type silicon PV cells achieve today higher efficiencies (typically 12–15% for flat panels on the market) than those reached by thin-film technologies (around 6–11%). An empirical fact that might continue to hold for the longer-term future, even while efficiency improvements will probably be achieved for various technologies to some 20% in the medium term (up to 2020) and perhaps to some 30% in the long run (after 2020. Thus, it seems likely that also in the future compromises (tradeoffs) need to be made between cost and efficiency. [Zwaan Bob van der et al, 2003]

Mainly due to its high costs, PV electricity does not play a major role in global energy supply and carbon emission abatement at present. Nevertheless, from many perspectives the development potential of PV is high, PV should be a potential major electricity supply, since beyond 2020 its contribution to electricity production could become very significant, given its expected cost reductions and the general desire for reduced environmental damage and enhanced energy supply security.

A variety of photovoltaic cells suitable for stand alone and large scale pilot power generation units are now commercially available. PVs have been used for refrigeration, in pharmaceutical, medical and agricultural industries as well as vaccine refrigeration units in hospitals in remote areas. In applied PVs, 20 to 80 solar cells are connected in series (solar module) to achieve a voltage of 10-40 volts. Modules are available in sizes ranging from few watts to about 90 watts. In most of these applications, electrical batteries and control units are used which in addition to their cost, require frequent replacement due to their limited life time, and also reduce the overall energy conversion efficiency. In addition, these refrigeration systems use vapour-compression units which have moving parts such as compressors and motors which need frequent maintenance and replacement. They also employ refrigerants which could damage the earth's ozone layer and increase global warming.

As an alternative to these conventional refrigeration systems, thermoelectric refrigeration systems may be used directly in conjunction with PVs to produce cooling. The thermoelectric refrigeration systems can operate using direct current supplied from PVs. As solar radiation is intermittent, a means of energy storage for periods of low insolation and nighttime is essential. To achieve this, PVs and thermoelectric modules need to be integrated with heat storage, such as PCMs, and recovery systems. Use of PCMs to store the excess cooling allowing it to be reused in periods of low insolation and night time, so that the system can operate day and night, without the need for large electricity batteries.

2.4 Conclusion

A literature review was carried out to collect relevant information on applications, development and research of thermoelectric cooling technologies, heat pipes technology and heat pipe thermal performance analysis, and applications and development of photovoltaic solar cells. These subjects are all related to this research, as each of those is part of the areas the project involved, and therefore, better understanding of the technical progress in these areas is necessary.

In section 2.1, the basic knowledge of the thermoelectric technologies and an overview of these applications were given. The advances on the research on thermoelectric cooling system were outlined. It was shown that the thermoelectric cooling technologies have opened large markets and have vast potentialities for development. The interests in the use of thermoelectric modules for domestic refrigerator and air conditioning have been revived in spite of the drawback of the low COP. The present technologies of thermoelectric refrigerator and air conditioning were reviewed. Ideas for further development of thermoelectric refrigerator and air conditioning were given. It was pointed that the emphasis of recent research has been the improvement of COP of thermoelectric cooling systems. Several aspects that influence the COP of the thermoelectric cooling systems are analysed and improved technologies were outlined.

In section 2.2, the concepts of heat pipes were illustrated and the development of this technology was reviewed. The varieties of heat pipes used for different applications were summarised. Emphases were focused on the types of thermal diode. It would be desirable to develop a new structure for thermoelectric heat pump application. Methods used for calculating limits of heat transport capacity of normal heat pipes were listed.

In section 2.3, the concepts of PV solar cells were described, and the development of this technology as well as its applications was reviewed. It is seen that the PVs have vast potential to be power source in globe use. Use of PVs as the power supplies in thermoelectric refrigeration systems to achieve the stand-alone units can overcome the shortage of the low efficiency of thermoelectric systems.

Chapter 3. Thermoelectric Module and Heat Sink

3.1 Thermoelectric Module Performance

A thermoelectric module is a simple solid-state device that converts electrical energy into thermal energy or the reverse. A typical thermoelectric module is composed of two ceramic substrates that serve as a foundation and electrical insulation for p-type and n-type bismuth telluride thermoelements (semiconductors) that are connected electrically in series and thermally in parallel between the ceramics, as shown in Figure 1-2. Passage of a current through junctions of the dissimilar materials in the thermoelements transports heat from a low-temperature to a high-temperature reservoir. These devices can therefore be used either as coolers or heaters.

3.1.1 Thermoelectric Module Performance and Optimum Selection (Design) Model

This section provides a basic understanding of the performance of a thermoelectric module. The theory of the optimum selection (design) model for thermoelectric modules is related.

Cold-side Heat Transfer

Thermoelectric heat pumping (Peltier effect) at the cold side of a thermoelectric module is given by:

$$Q_{sb}=2N\alpha IT_c \qquad (3\text{-}1)$$

The term α is the average Seebeck coefficient of the thermoelectric material, N is the number of thermocouples, T_c is the cold side temperature of the module, and I is the DC current. It is seen from this relation that heat is pumped when current flows through the module. However, the heat pumped may include other unwanted heat sources. These heat sources are described in the following sections.

Joule Heat. Current flow generates resistive or Joule heating (Q_J) in the thermoelectric material. 50 percent of the Joule heat goes to the cold side and 50 percent goes to the hot side. The Joule heating is given by:

$$Q_J=2NI^2p/G \qquad (3\text{-}2)$$

Where, p is the resistivity of the thermoelectric material, and G is the geometry factor of the module (cross section area/length of thermoelectric element).

Conducted Heat. During operation, heat is conducted from the hot side to the cold side of the module through the thermoelectric material. The rate of heat conduction is given by:

$$Q_{cd}=2Nk(T_h-T_c)G= 2Nk\Delta TG \qquad (3\text{-}3)$$

Where, k is the thermal conductivity of thermoelectric material, and T_h is the hot side temperature.

Equation (3-3) shows that Q_{cd} increases with the temperature difference across the module. Combining Eq (3-1), (3-2), and (3-3) into the energy balance on the cold side of the module gives the following:

$$Q_c=2N(Q_{sb}-0.5Q_J-Q_{cd})= 2N[\alpha IT_c-I^2p/(2G)- k\Delta TG] \qquad (3\text{-}4)$$

Equation (3-4) is the standard equation of thermal module performance. This equation shows that a thermoelectric module no longer operates ($Q_c=0$) when the sum of one half the Joule heat ($0.5Q_J$) and the conducted heat (Q_{cd}) equals the Peltier heat (Q_{sb}).
The electrical energy consumption of the module is given by:

$$Q_E=IV=2N(I^2p/G+\alpha I\Delta T) \qquad (3\text{-}5)$$

Equation (3-5) shows that the electrical power consumption of a thermoelectric module is used to generate the Joule heat and overcome the Seebeck effect, which generates power due to the temperature difference between the two sides of the module.

The COP of the thermoelectric module for cooling is given by:

$$\varepsilon=Q_c/Q_E=\frac{aIT_c-k\Delta TG-I^2p/(2G)}{I^2p/G+aI\Delta T} \qquad (3\text{-}6)$$

It is seen from Eq(3-6) that the COP is a function of the material property coefficients and geometry factor of thermoelectric element, the temperatures of the hot side and cold side, and the current input. For specific modules and working temperatures, there exists an optimum current for maximum COP.

Solving the equation $\frac{\partial \varepsilon}{\partial I}=0$, the optimum current for the maximum COP can be given by:

$$I_{opt}=[k\Delta TG(1+(1+ZT_m)^{1/2})]/(\alpha T_m) \quad (3\text{-}7)$$

Replacing I in Eq (3-6) by I_{opt}, the maximum (optimum) COP can be given by:

$$\varepsilon_{opt}=(T_m/\Delta T)[((1+ZT_m)^{1/2}-1)/((1+ZT_m)^{1/2}+1)]-1/2 \quad (3\text{-}8)$$

where

$$T_m=1/2(T_h+T_c) \quad (3\text{-}9)$$

$$Z=\alpha^2/(pk) \quad (3\text{-}10)$$

It is seen that the maximum COP under the optimum current is a function of T_h, T_c and the figure of merit of thermoelectric material Z.

Hot-side heat transfer

An energy balance on the hot side of the thermoelectric module gives:

$$Q_h=2N(\alpha IT_h+I^2p/(2G)-k\Delta TG) \quad (3\text{-}11)$$

Q_h can also be assessed by the second thermodynamics law, i.e.,

$$Q_h=Q_c+Q_E \quad (3\text{-}12)$$

From the equation (3-4) and (3-5), we obtain the following equation:

$$Q_h=2N[\alpha IT_c-I^2p/(2G)-k\Delta TG]+2N(I^2p/G+\alpha I\Delta T)$$
$$=2N[\alpha IT_h+I^2p/(2G)-k\Delta TG] \quad (3\text{-}13)$$

It can be seen that equation (3-11) is the same as equation (3-13).

The COP of the thermoelectric module for heating is given by:

$$\eta=Q_h/Q_E=(Q_c+Q_E)/Q_E=1+Q_c/Q_E$$

i.e., $$\eta=1+\frac{\alpha IT_c-k\Delta TG-I^2p/(2G)}{I^2p/G+aI\Delta T} \quad (3\text{-}14)$$

Solving the equation $\frac{\partial \eta}{\partial I}=0$, the expression of the optimum current for the maximum COP for heating equals that for cooling, see equation (3-7).

Replacing I in Eq (3-14) by I_{opt}, the maximum (optimum) COP for heating can be given by:

$$\eta_{max}=1+(T_m/\Delta T)[((1+ZT_m)^{1/2}-1)/((1+ZT_m)^{1/2}+1)]-1/2 \quad (3\text{-}15)$$

It can be seen by the above analysis that the key point to achieve optimum (maximum) COP is to input optimum current, i.e., the operating current of the thermoelectric modules should equal to the optimum current expressed in Eq (3-7). As shown in Eq(3-4) and Eq(3-11), for a specific working temperature T_h and T_c, a specific operating current is required to obtain the required cooling/heating capacity Q_c/Q_h. By using an appropriate number of thermocouples or appropriate geometry factor, which constitutes different types of modules, the operating current can equal to the optimum current. Computer model was established to determine the optimum number of thermocouples or geometry factor of the modules required to make the operating current equal to the optimum current and to achieve maximum COP for a specific cooling/heating

requirement (known Q_c/Q_h, T_h and T_c). The flow chart of the model is shown in Figure 3-1 and computer program in C++ language is shown in attached disk (Program A).

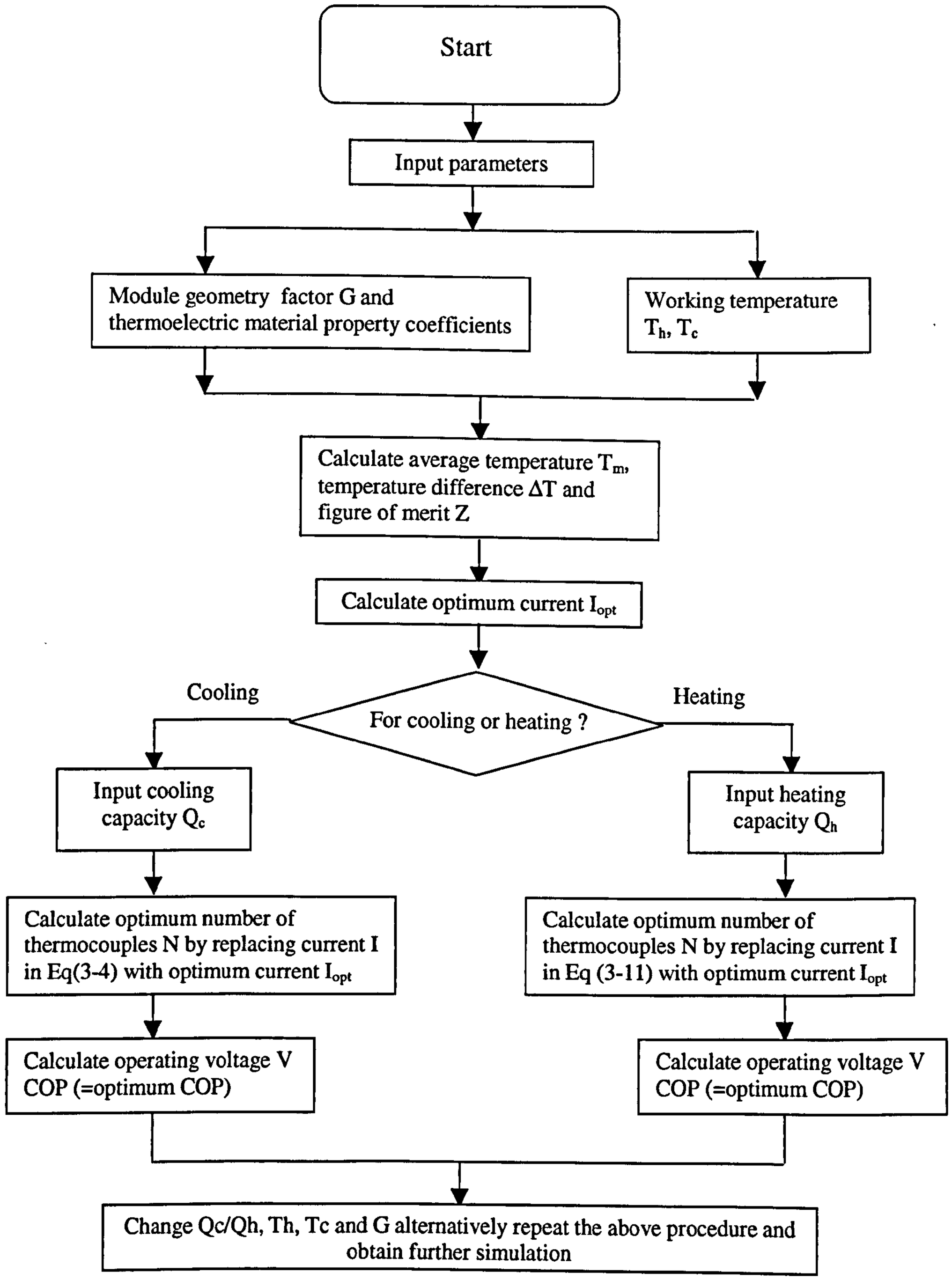

Figure 3-1. Flow chart of the optimum selection (design) model of thermoelectric modules

For this model, it is assumed all the thermocouples (thermoelectric modules) connect in series.

The thermoelectric material property coefficients applied in this model are taken from Melcor company (www.melcor.com). The parameters are shown in Appendix A:

Different module geometry factors constitute different types of modules. The module types and their geometry factors (Melcor) are shown in Appendix B, and these data were used in the modelling carried out in section 3.1.3.

3.1.2 Validation of the Optimum Selection Model

To validate the suitability and accuracy of the model used for optimum selection (design) of thermoelectric modules, comparison was carried out between the selection results using this model and the selection results using Melcor's commercially available thermoelectric cooler selection software. The Melcor's thermoelectric cooler selection software provides two options of selection, i.e, better efficiency and lower cost. Using better efficiency option we can obtain the suggested optimum thermoelectric modules (including the number and the type of the modules) and the optimum current (also operating current) for maximum COP, which suited to the specific cooling/heating requirements.

The results of the comparisons are shown in Figure 3-2 to Figure 3-5.

Figure 3-2 and Figure 3-3 show a comparison of the optimum thermoelectric parameters including optimum number of thermocouples, operating (optimum) current, optimum COP and operating voltage for various cooling capacities under fixed hot and cold side temperatures. Figure 3-4 and Figure 3-5 show a comparison of the optimum thermoelectric parameters for various hot side temperatures under fixed cooling capacity and cold side temperature. The geometry factor G used in the modelling is 0.282, which is consistent with the geometry factor of CP2-127-06 modules suggested by Melcor's thermoelectric cooler selection software. It can be seen in Figure 3-2 to Figure 3-5 that the optimum current and optimum COP obtained from the model are consistent with those from Melcor's selection software. The number of thermocouples and operating

voltages obtained from the model are very close to that from Melcor's thermoelectric cooler selection software. The reason for the existence of the small difference is the Melcor's selection software suggests the required number of the modules and the model gives the exact required number of the thermocouples. As we know, each module contains a number of thermocouples, for example, the CP2-127-06 contains 127 thermocouples. The number of the thermocouples from Melcor shown in Figure 3-2 and Figure 3-4 are the total thermocouples of the suggested modules, which can be just close to the number of thermocouples by exact calculation.

In overall, the results obtained from Melcor's selection software provide verification of the optimum selection model and indicate that the model can be used to analyses the relations between the optimum thermoelectric parameters and cooling/heating requirements, and provides the optimum thermoelectric parameters for a specific cooling/heating requirement.

Compared to Melcor's software, the model has extensive use range. Melcor's software can only be used to select Melcor's thermoelectric cooling modules, and this model can be used to select any thermoelectric cooling modules. Melcor's software can only provide information in a small range and is not convenient for analysis, and the model is convenient to be used to analyse the relations between the optimum thermoelectric parameters for a specific cooling/heating requirement.

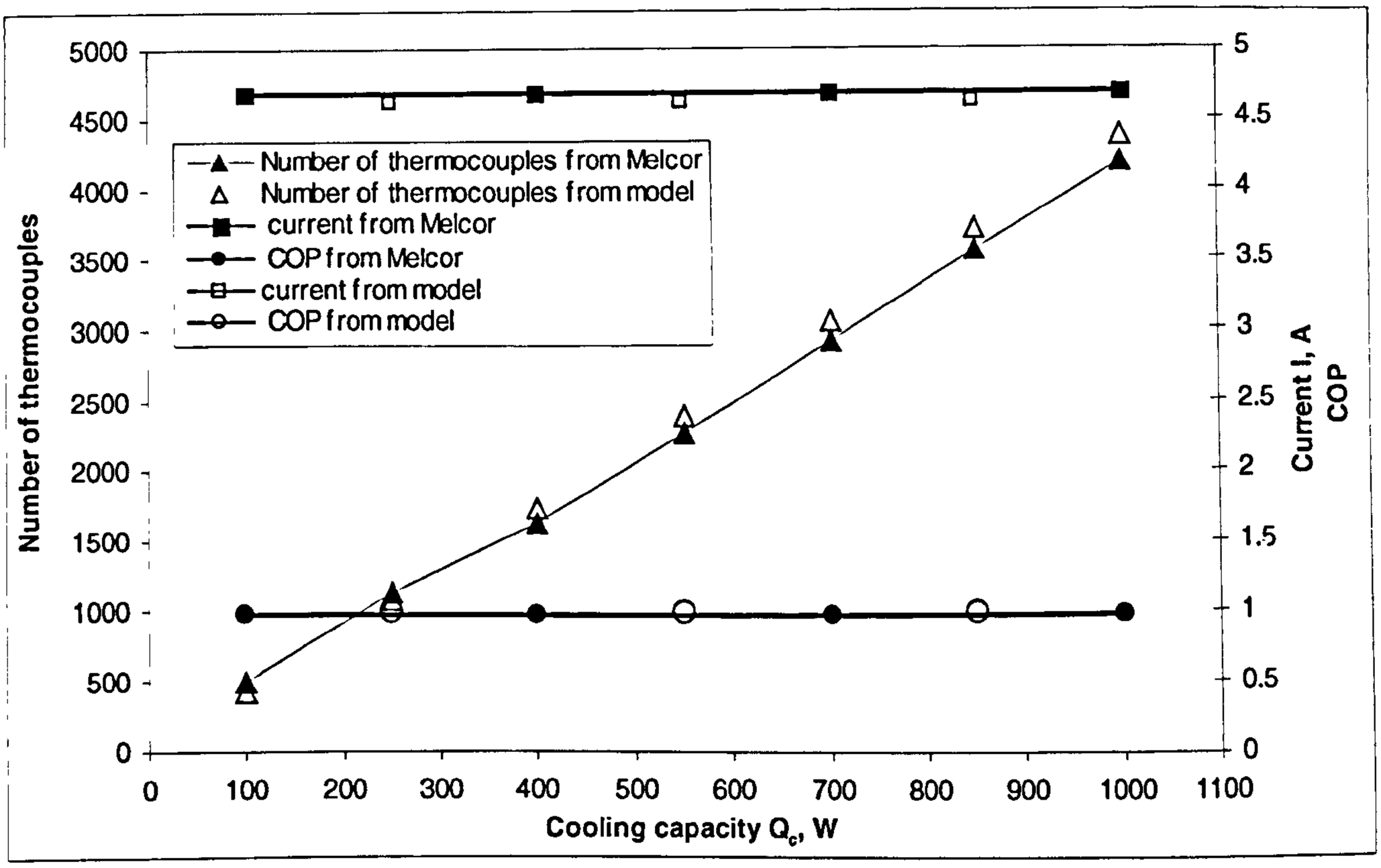

Figure 3-2. Comparison of optimum thermoelectric parameters (I, N and COP) for varied cooling capacities (T_h=45°C, T_c=17°C)

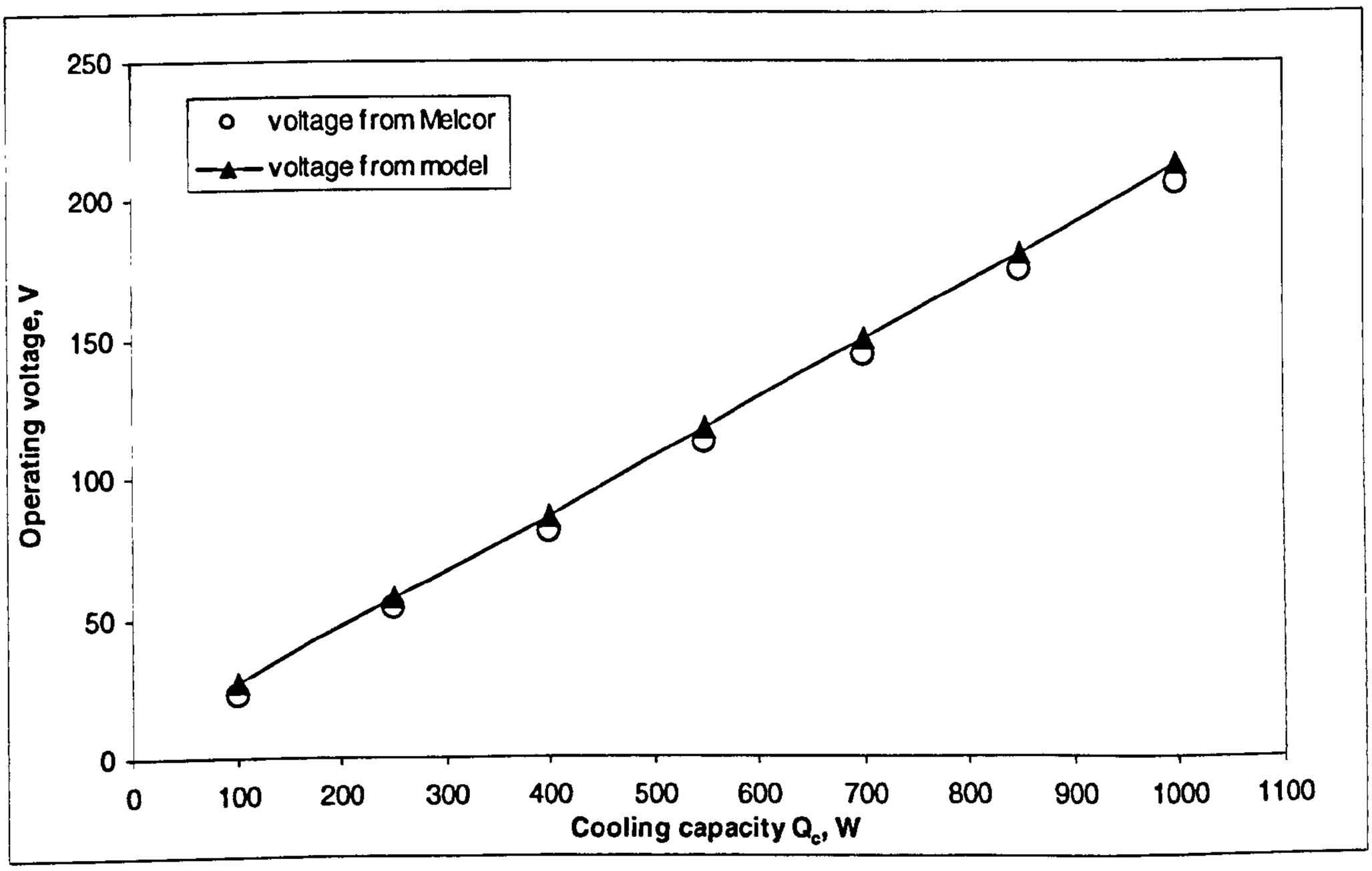

Figure 3-3. Comparison of operating voltage for varied cooling capacities (T_h=45°C, T_c=17°C)

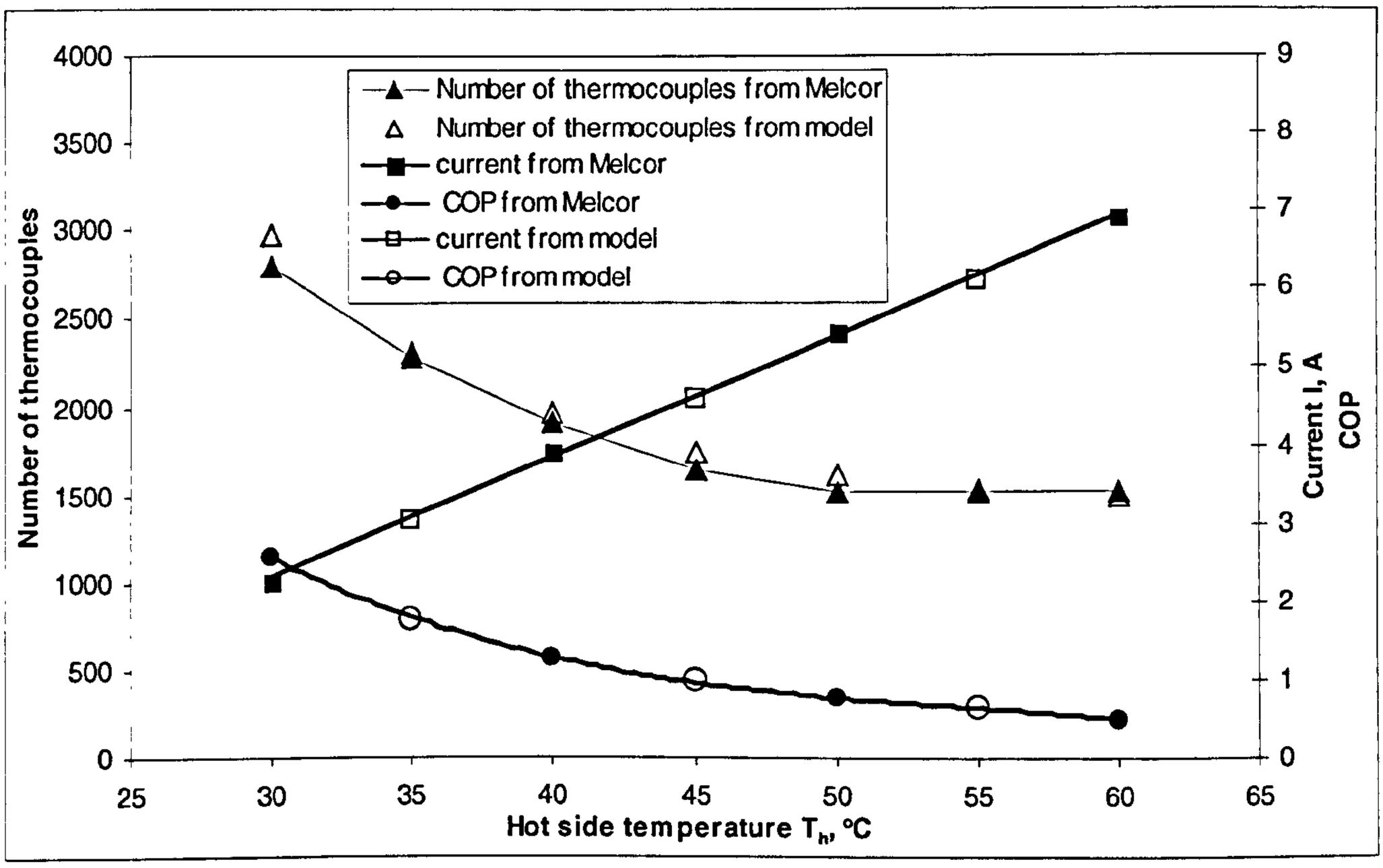

Figure 3-4.Comparison of optimum thermoelectric parameters (I, N and COP) for varied hot side temperatures (Q_c=400W, T_c=17°C)

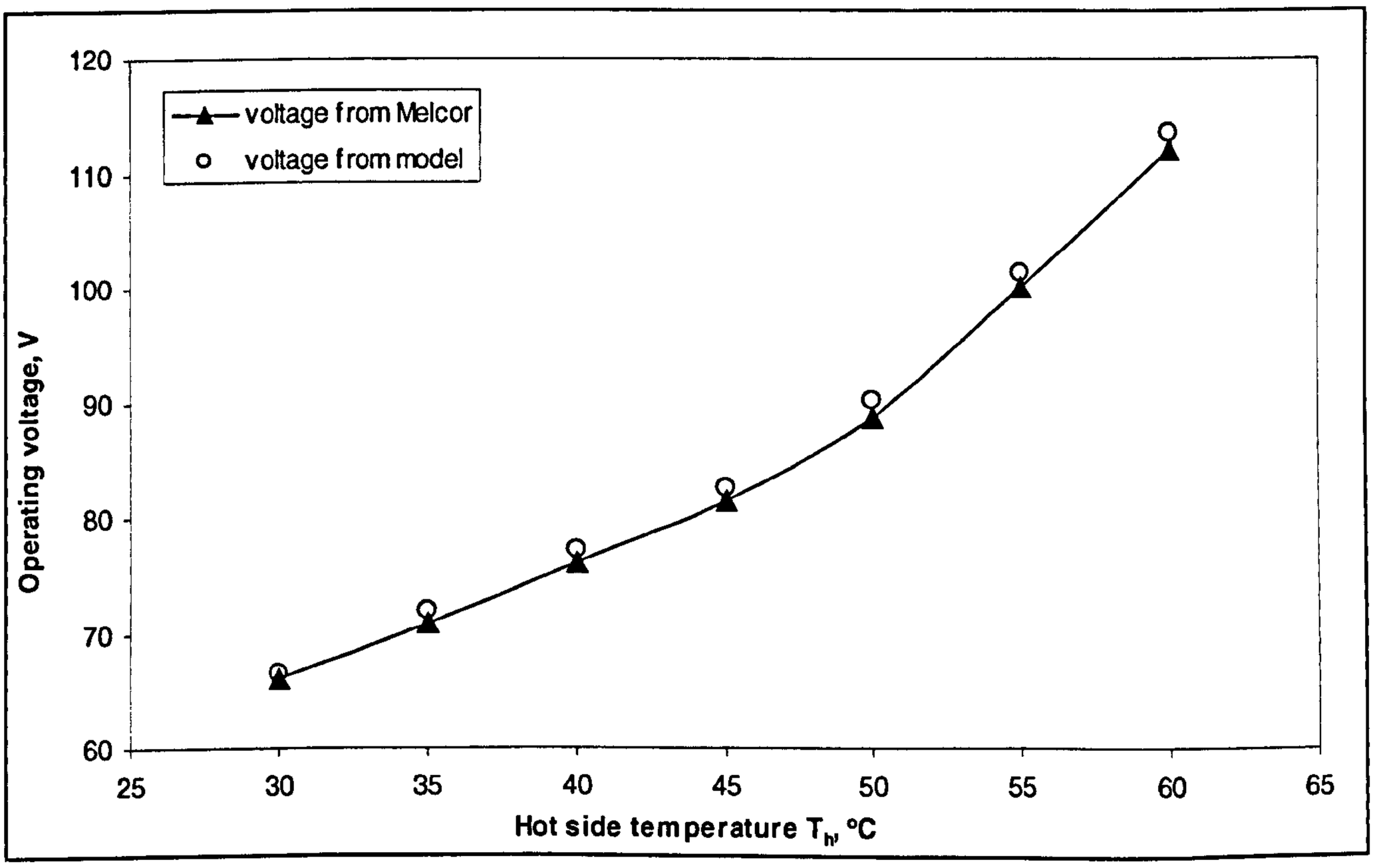

Figure 3-5. Comparison of operating voltage for varied hot side temperatures (Q_c=400W, T_c=17°C)

3.1.3 Discussion of the Modelling Results

In practice, a thermoelectric heat pump works under various conditions and therefore the cooling/heating capacity and working temperatures are variable. The cooling/heating capacity and the working temperatures (hot and cold side temperature of thermoelectric modules) used in the modelling should be the severest case, i.e., possible largest cooling/heating capacity, possible highest hot side temperature and possible lowest cold side temperature.

Cooling mode

The relation between cooling capacity (Q_c) and optimum thermoelectric parameters (N, I, V and COP) for specific working temperature (T_h, T_c) and geometry factor (G), are shown in Figure 3-6 and Figure 3-7. The simulation results show:

- The required number of thermocouples for optimum current and COP increases with the cooling capacity. This indicates that to obtain the optimum current and maximum COP, an increased cooling capacity requires an increased number of thermocouples (increased number of thermoelectric modules). An increased number of thermocouples require an increased operating voltage.
- The optimum current and optimum COP are determined by thermoelectric material property coefficients, geometry factor and working temperatures (T_h, T_c) [see Eq(3-7) and (3-8)], they have no relationship with the cooling capacity. This indicates that for the specific working temperatures, the optimum current and COP of specific modules have definite values.

The relation between hot side temperature (T_h) and optimum thermoelectric parameters (N, I, V and COP) for specific cooling capacity (Q_c), cold side temperature (T_c) and geometry factor (G), are shown in Figure 3-8 and Figure 3-9. The simulation results show:

- The required number of the thermocouples for optimum current and maximum COP decreases with the increase of hot side temperature. In other words, a higher hot side temperature requires less thermal modules to achieve optimum current and optimum COP.

- When the hot side temperature increases, the optimum current and operating voltage increases and the optimum COP decreases.
- It is seen that a lower hot side temperature has a higher optimum COP. To achieve optimum COP, more modules are required at a lower hot side temperature than at a higher hot side temperature.

The relation between geometry factor and optimum thermoelectric parameters (N, I, V and COP) for the specific cooling capacity (Q_c) and working temperatures (T_h, T_c), are shown in Figure 3-10 and Figure 3-11.

The simulation results show:

- To achieve optimum COP, the required number of thermocouples varies with the geometry factor. The larger the geometry factor, the fewer thermocouples are required.
- The optimum current increases and operating voltage decreases with the increase of the geometry factor, but the optimum COP remains the same under various geometry factors. This is because the optimum COP is determined by the working temperature T_h, T_c and the figure of merit of the material and has no relationship with the geometry factor.
- The geometry factor determines the type of thermal module. Choosing different type of modules indicates using different number of modules. Selection of the modules should consider the total area of the modules and the dimensions of the available heat sink.

Heating mode

The relation between heating capacity (Q_h) and optimum thermoelectric parameters (N, I, V, COP) for specific working temperature (T_h, T_c) and geometry factor (G), are shown in Figure 3-12 and Figure 3-13. The simulation results show:

- The required number of thermocouples for optimum current and COP increases with the heating capacity. This indicates that to obtain the optimum current and COP, an increased heating capacity requires an increased number of thermocouples (increased

number of thermoelectric modules). An increased number of thermocouples requires an increased operating voltage.

- The optimum current and optimum COP are determined by thermoelectric material property coefficients and working temperature (T_h, T_c) and have no relationship with the heating capacity. This indicates that for the specific working temperatures, the optimum current and COP have definite values.

The relation between cold side temperature (T_c) and optimum thermoelectric parameters (N, I, COP) for specific heating capacity (Q_h), hot side temperature (T_h) and geometry factor (G), are shown in Figure 3-14 and Figure 3-15. The simulation results show:

- The required number of thermocouples for optimum current and COP increases with the increase of cold side temperature. In other words, a higher cold side temperature requires a greater number of modules to achieve optimum current and optimum COP. The operating voltage increases with the required number of thermocouples.
- When the cold side temperature increases, the optimum current decreases and the optimum COP increases.
- It is seen that a higher cold side temperature results in a higher optimum COP. To achieve an optimum COP, more modules are required at higher cold side temperature than at lower cold side temperature.

The relation between geometry factor (G) and optimum thermoelectric parameters (N, I, COP) for the specific heating capacity (Q_h) and working temperatures (T_h, T_c), are shown in Figure 3-16 and Figure 3-17. The simulation results show:

- The required number of thermocouples varies with the geometry factor to achieve an optimum COP. The larger the geometry factor, the fewer thermocouples (fewer modules) are required.
- The optimum current increases and operating current decreases with the increase of the geometry factor, but the optimum COP remains the same under various geometry factors. This is because the optimum COP is determined by the working temperature T_h, T_c and the figure of merit of the material and has no relationship with the geometry factor.

- The geometry factor determines the type of thermal module. Also, selection of the modules should consider the total area of the modules and the dimensions of the available heat sink.

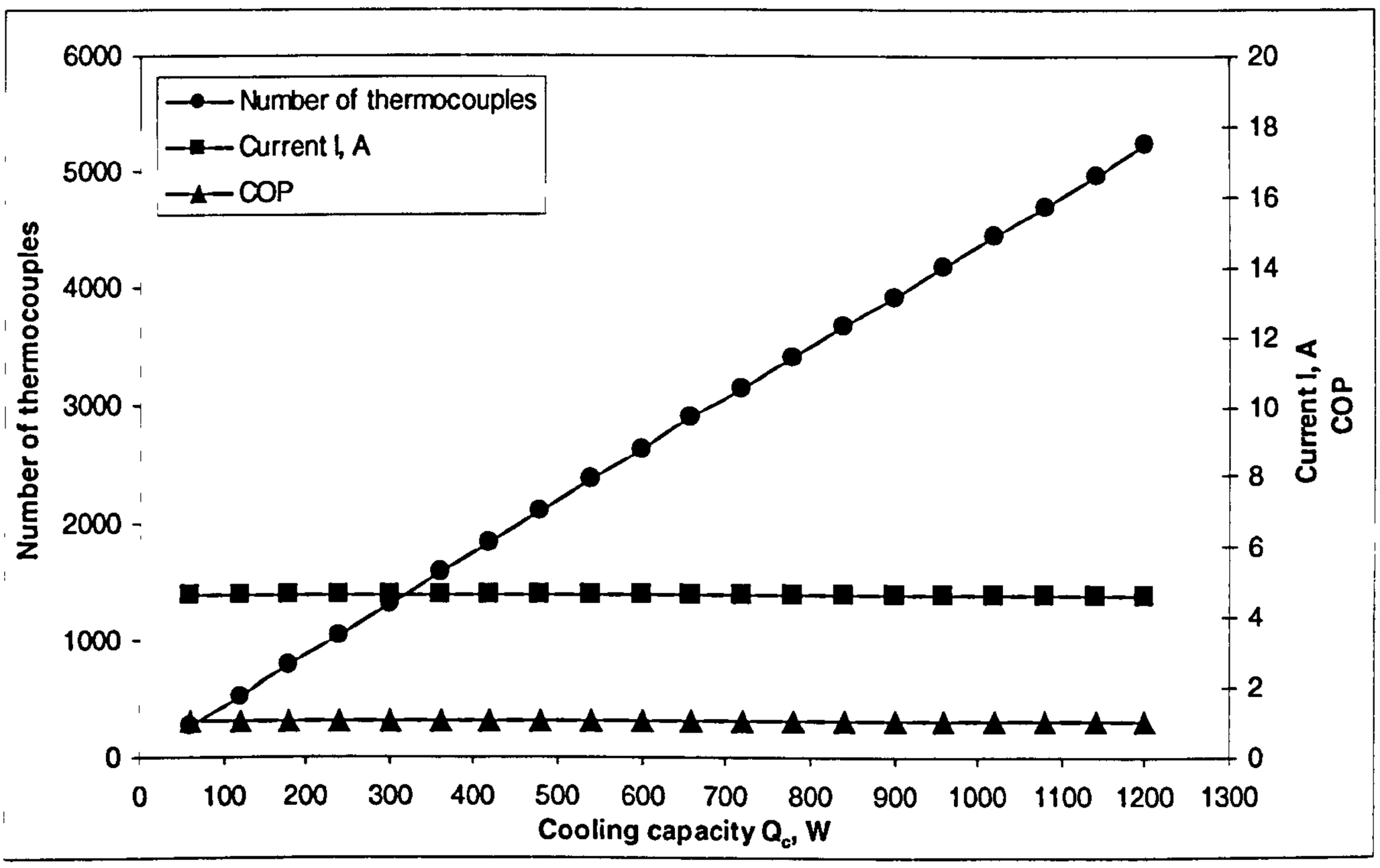

Figure 3-6. Relations between cooling capacity and optimum thermoelectric parameters (I, N and COP) for cooling mode (T_h=45°C, T_c=17°C, G=0.282)

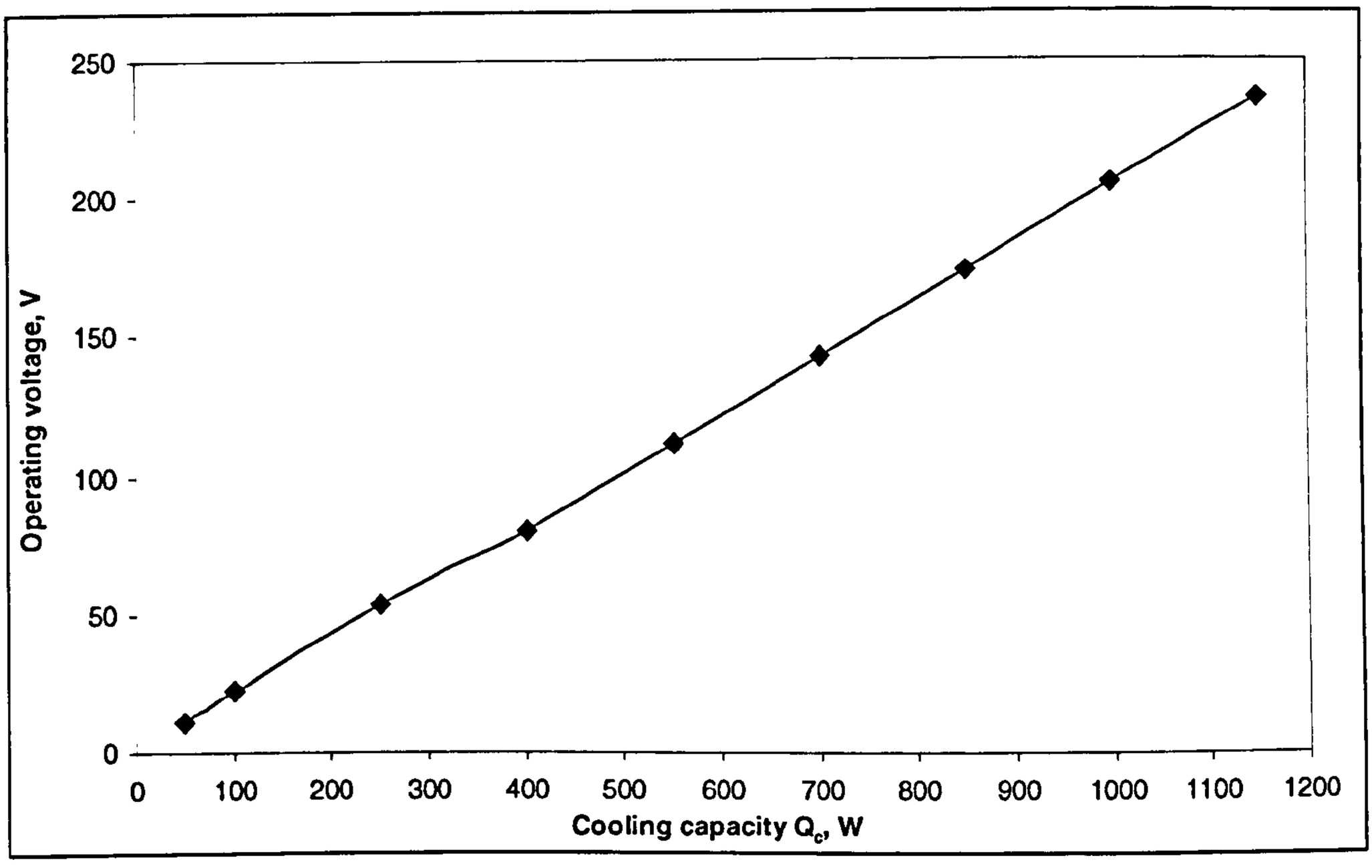

Figure 3-7. Relations between cooling capacity and operating voltage for cooling mode (T_h=45°C, T_c=17°C, G=0.282)

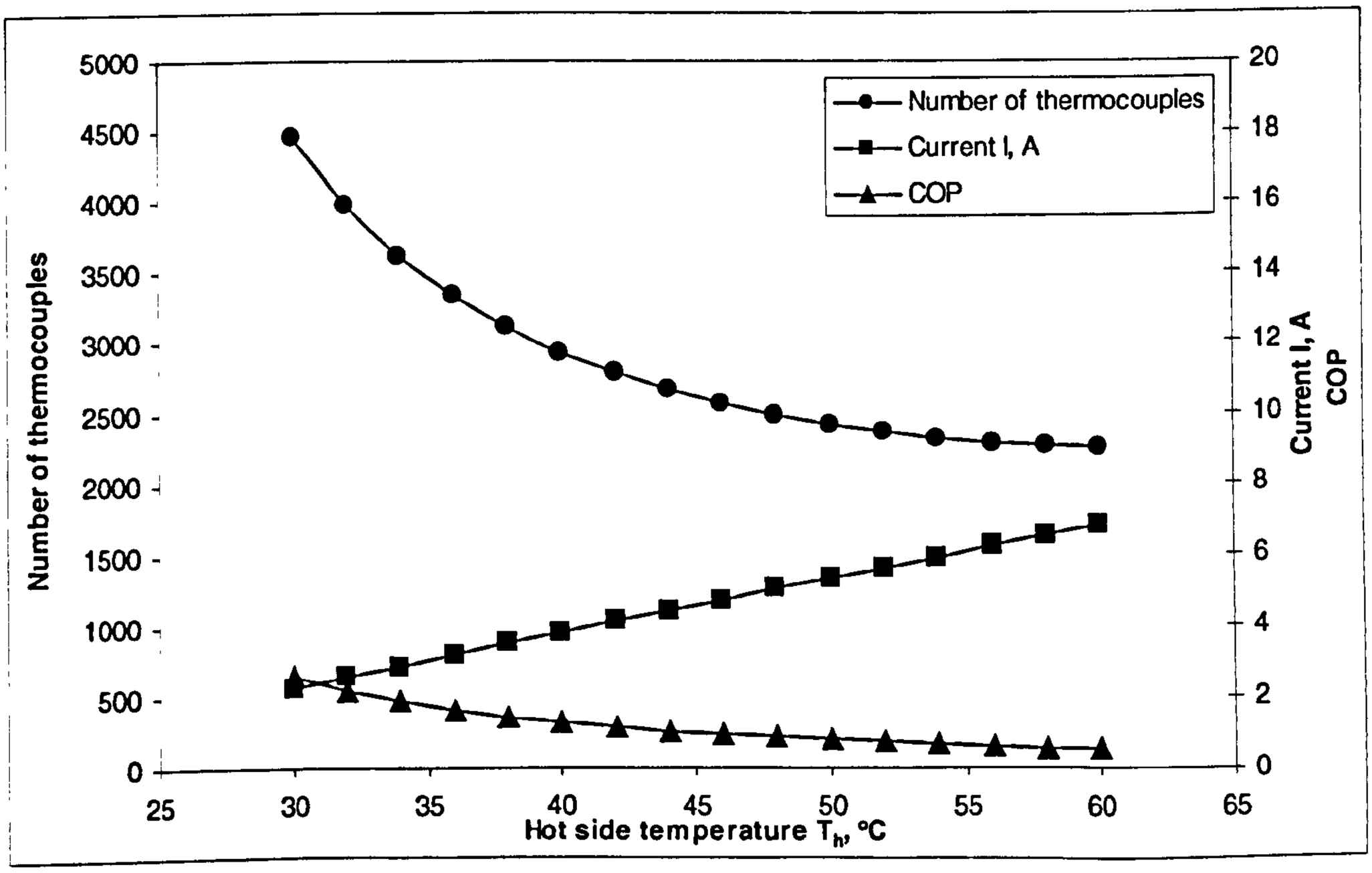

Figure 3- 8. Relation between hot side temperature and optimum thermoelectric parameters for cooling mode (Q_c=600W, T_c=17°C, G=0.282)

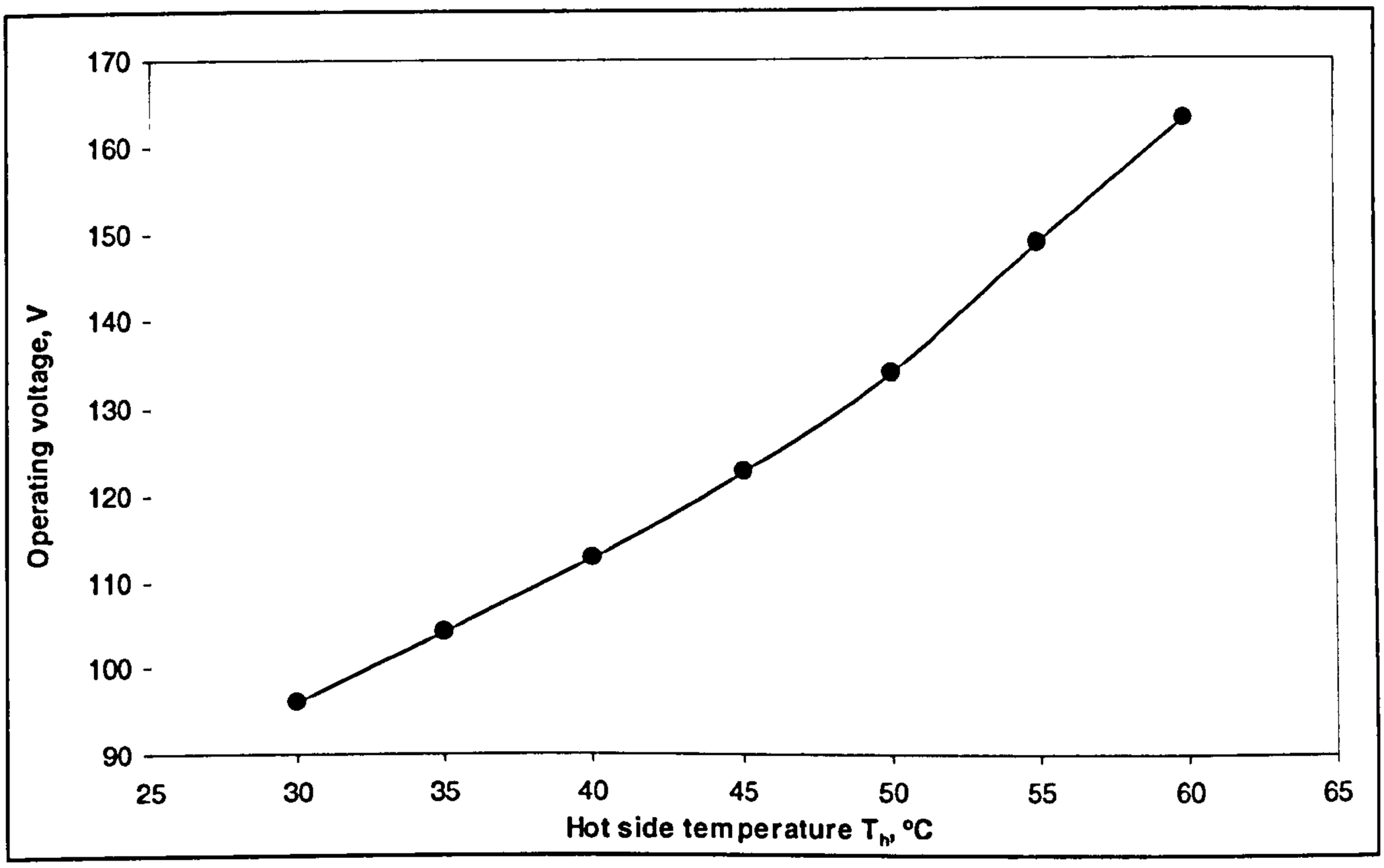

Figure 3- 9. Relation between hot side temperature and operating voltage for cooling mode (Q_c=600W, T_c=17°C, G=0.282)

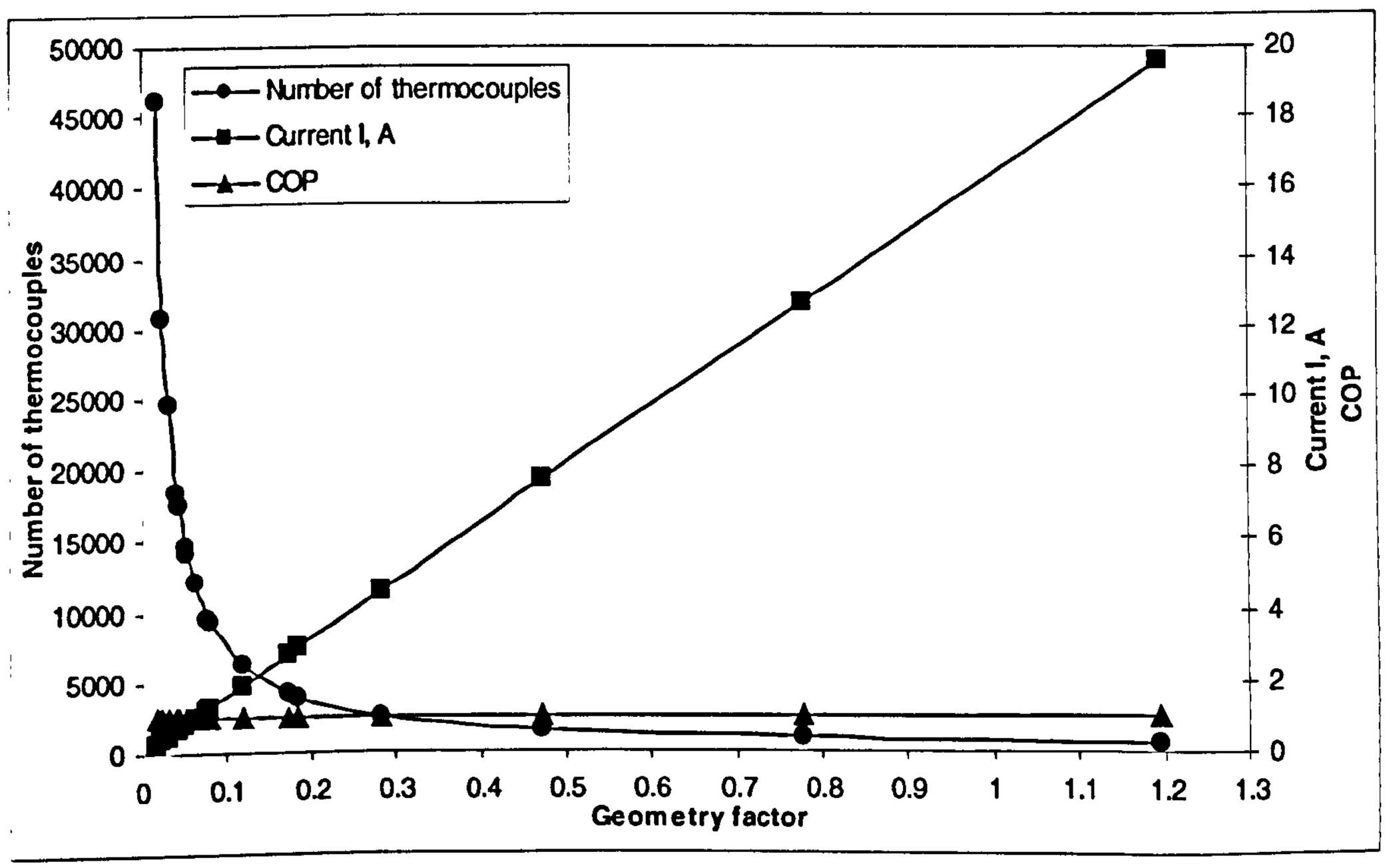

Figure 3-10. Relation between geometry factor and optimum thermoelectric parameters for cooling mode (Q_c=600W, T_h=45°C, Tc=17°C)

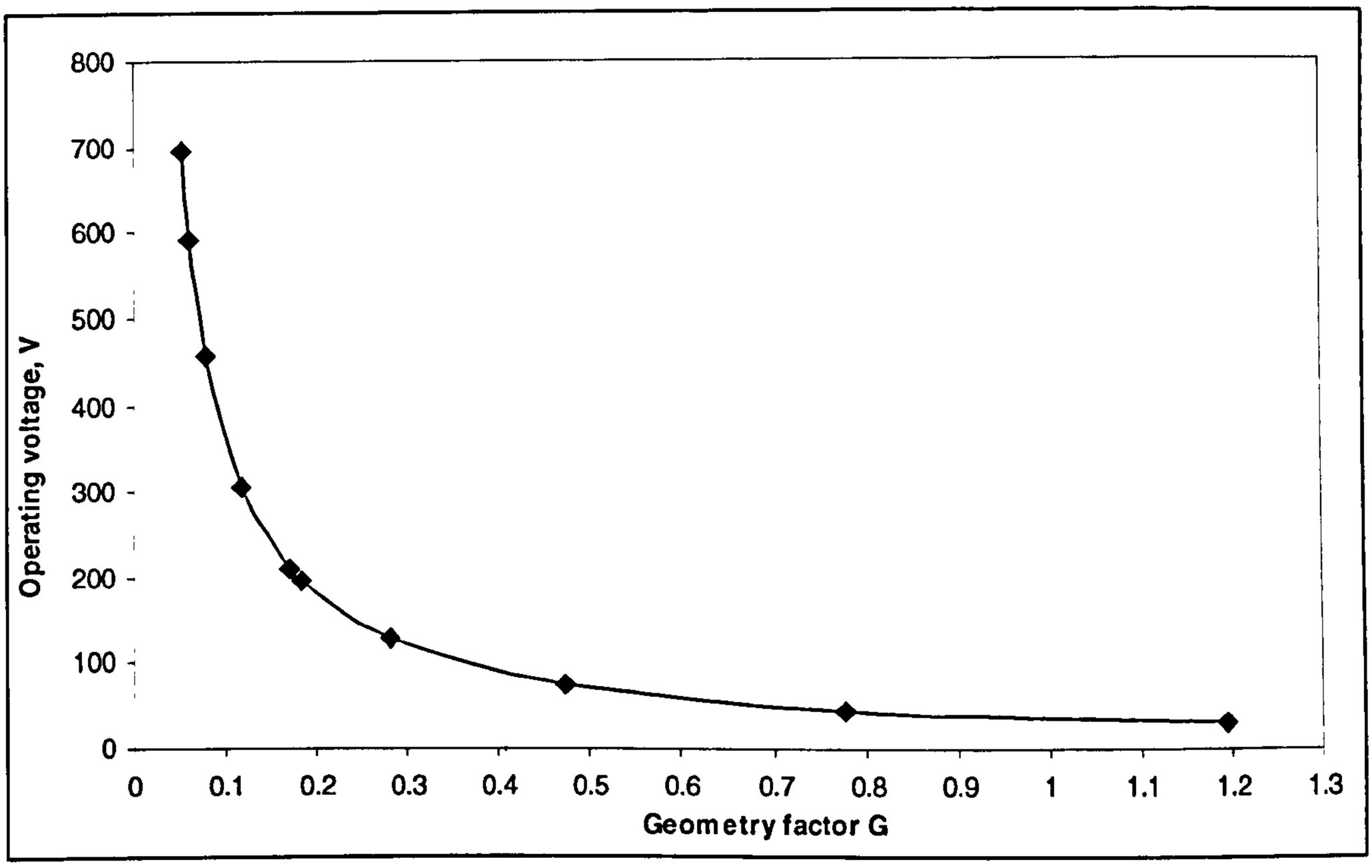

Figure 3-11. Relation between geometry factor and operating voltage for cooling mode (Q_c=600W, T_h=45°C, Tc=17°C)

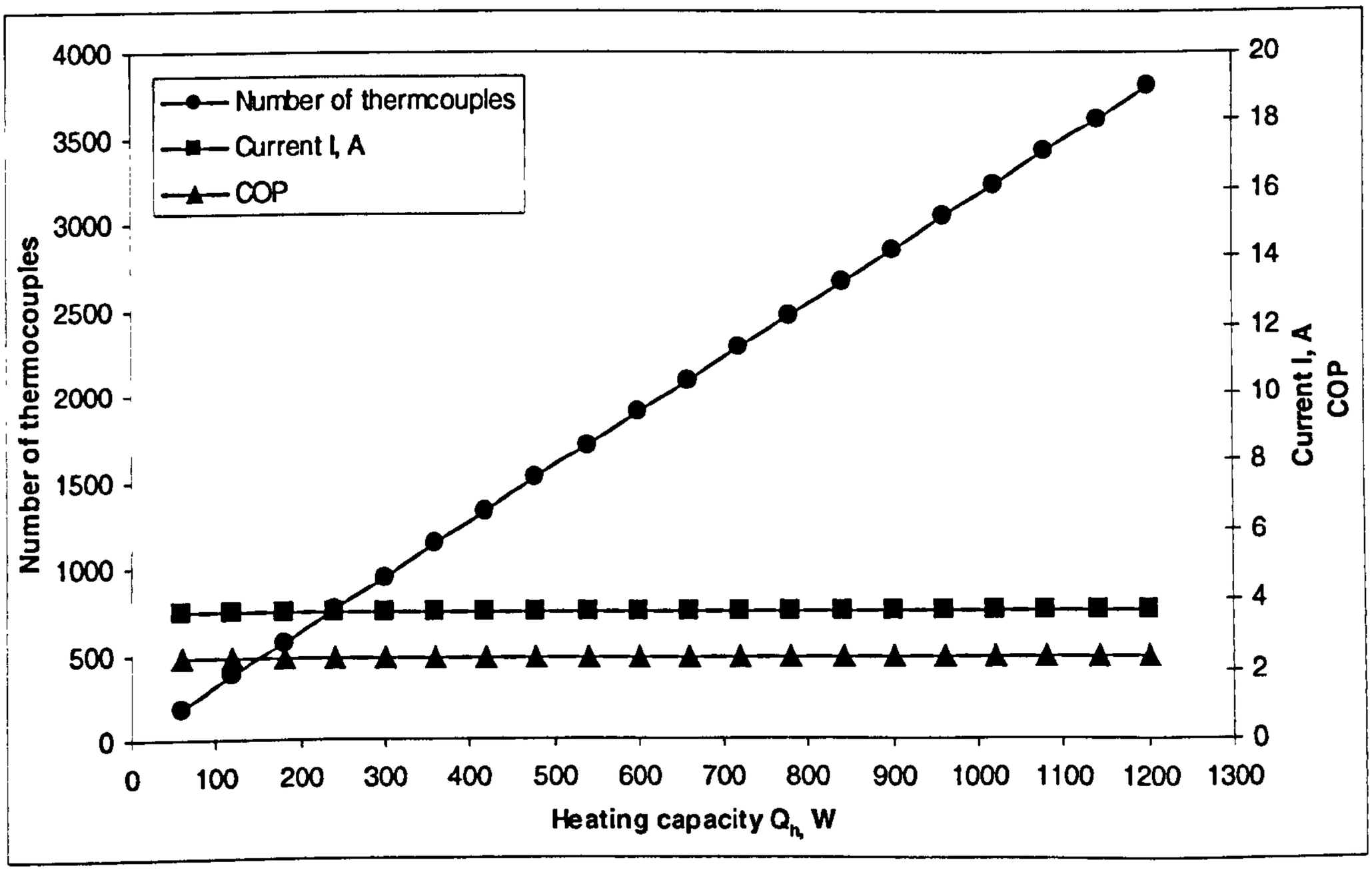

Figure 3-12. Relation between heating capacity and optimum thermoelectric parameters (I, N and COP) for heating mode (T_h=23°C, T_c=3°C, G=0.282)

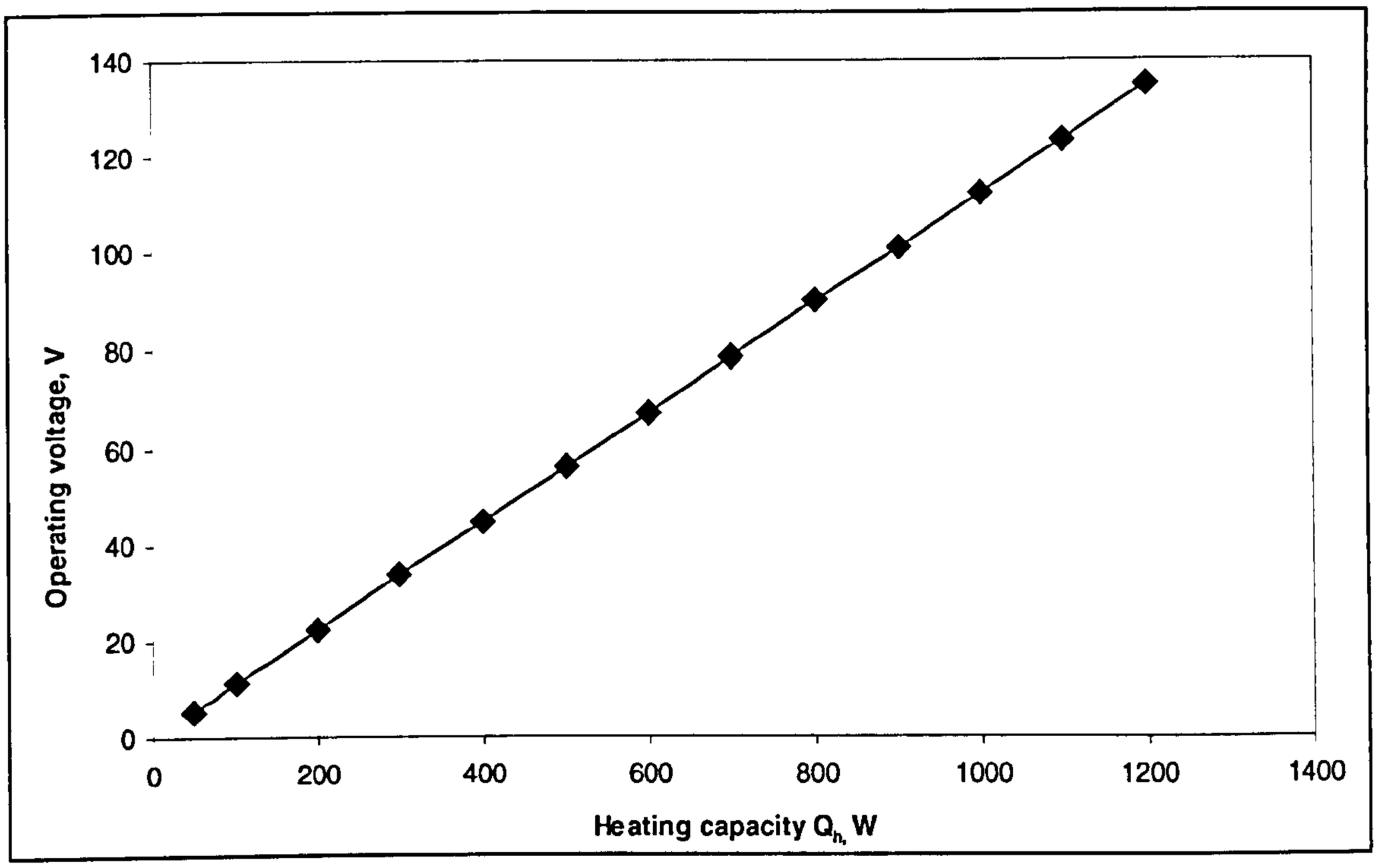

Figure 3-13. Relation between heating capacity and operating voltage for heating mode (T_h=23°C, T_c=3°C, G=0.282)

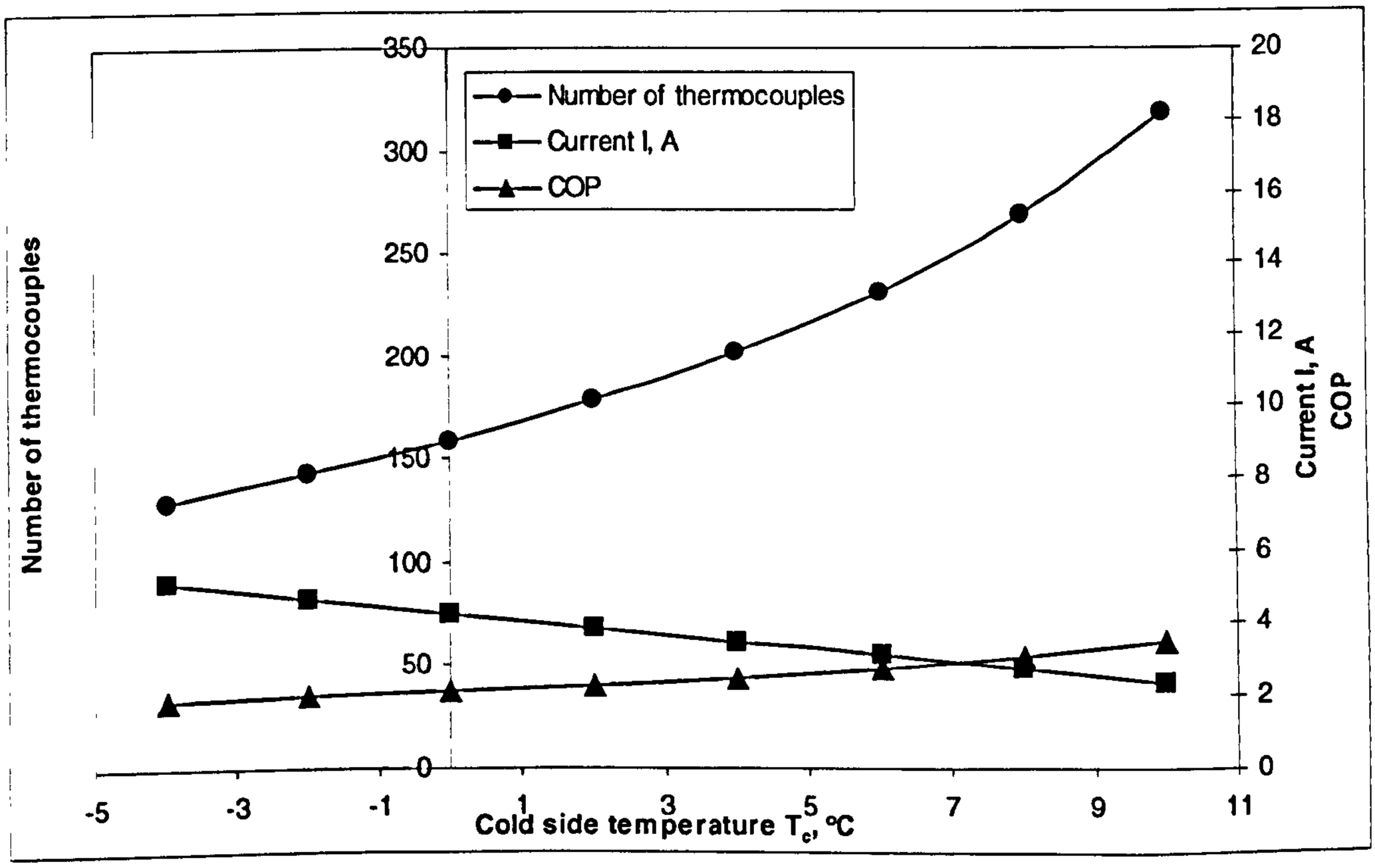

Figure 3-14. Relation between cold side temperature and optimum thermoelectric parameters for heating mode (Q_h=600W, T_h=23°C, G=0.282)

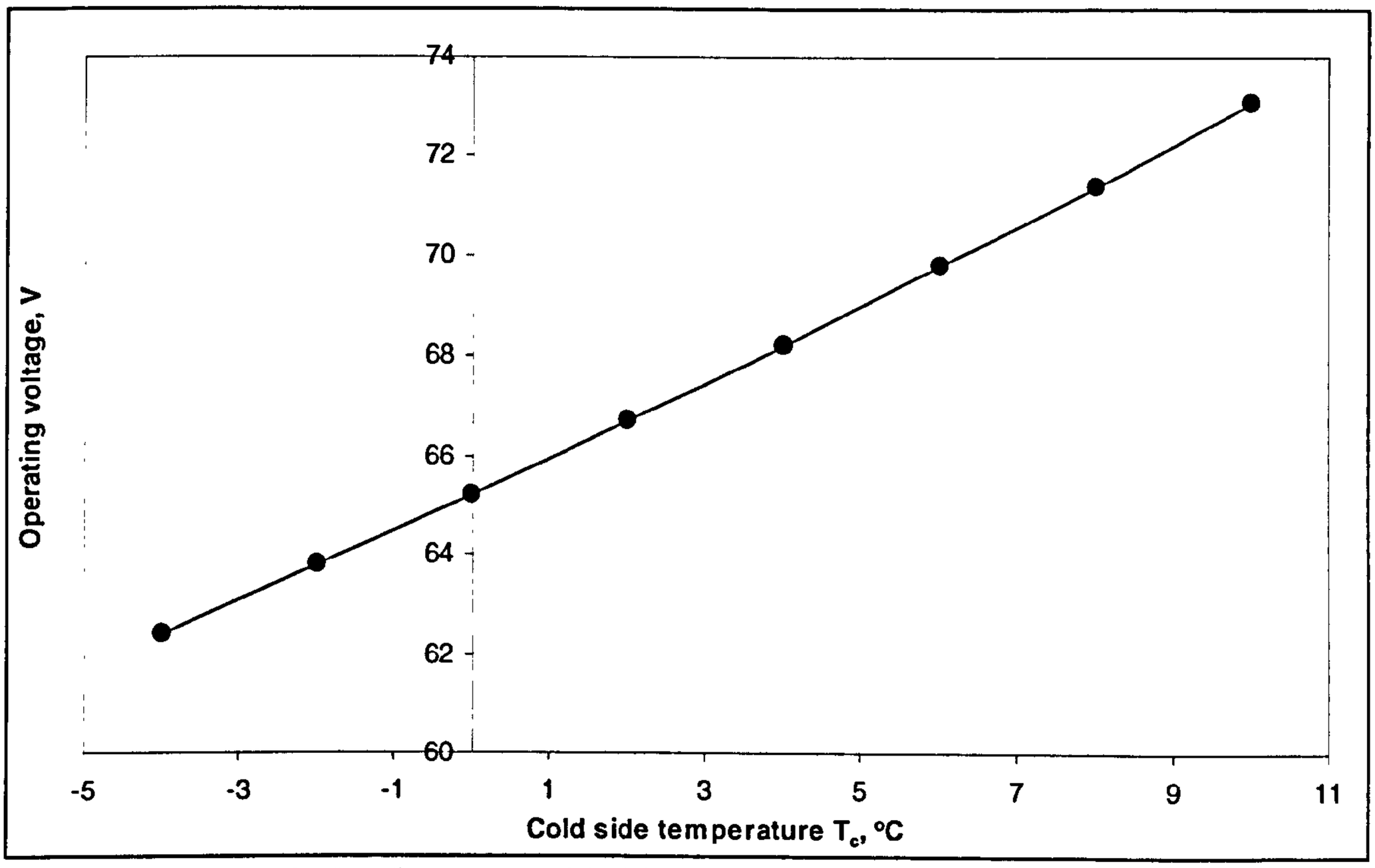

Figure 3-15. Relation between cold side temperature and operating voltage for heating mode (Q_h=600W, T_h=23°C, G=0.282)

Figure 3-16. Relation between geometry factor and optimum thermoelectric parameters for heating mode (Q_h=600W, T_h=23°C, T_c=3°C)

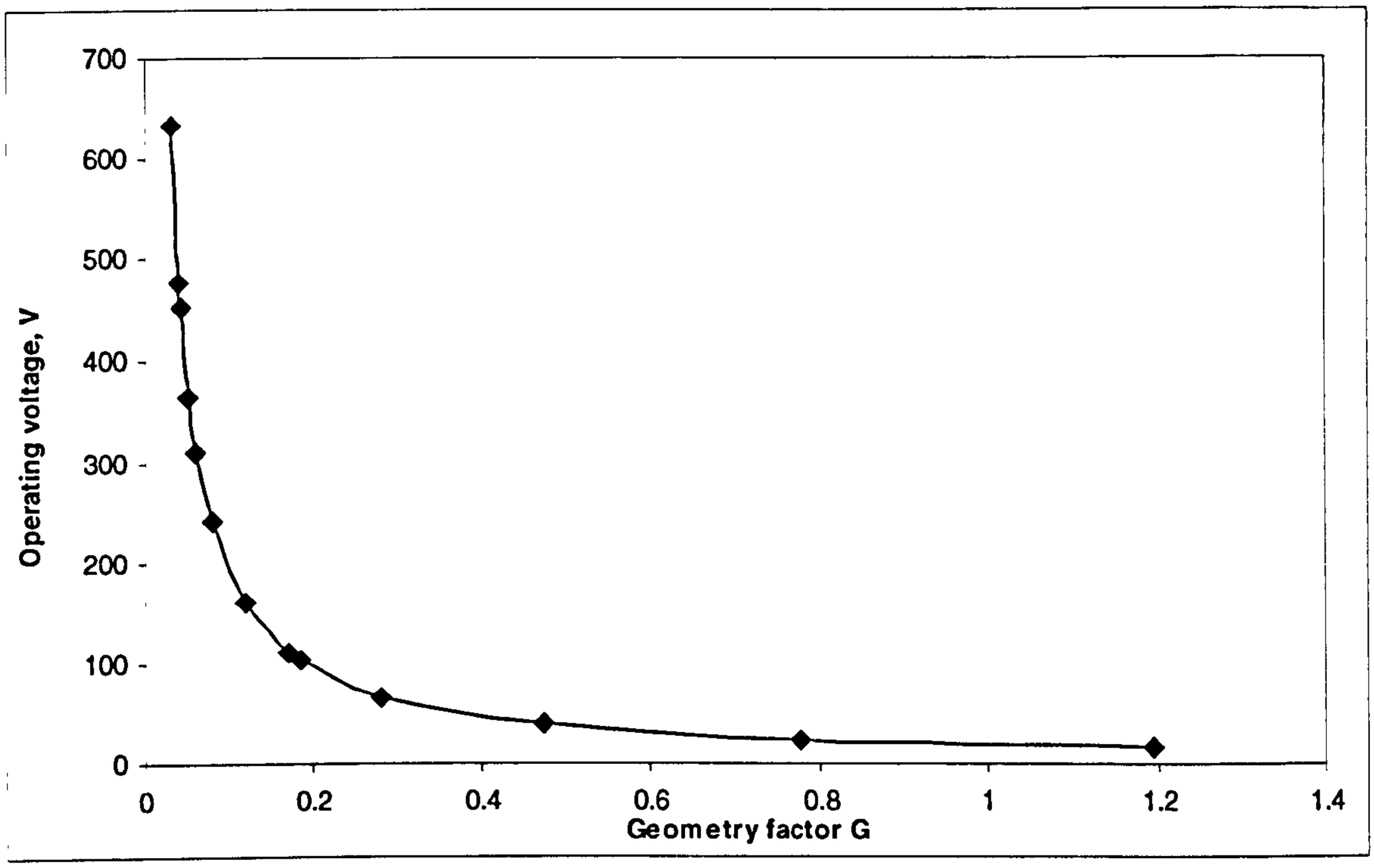

Figure 3-17. Relation between geometry factor and operating voltage for heating mode (Q_h=600W, T_h=23°C, T_c=3°C)

3.4 Finned Heat Sink Performance

Due to the high intensity heat flux, the thermoelectric modules can not work independently. They have to use heat sink to dissipate heat. Heat pipe can only conduct heat from one place to other place or distribute heat to heat sink, they can not dissipate heat efficiently. In most of the thermoelectric systems, heat sinks are essential components to keep the systems work efficiently. An analytical model of the performance of finned heat sink was set up, which shows the relation between the performance of the heat sink and its geometry parameters as well as convective coefficient. The model provides a basis for designing finned heat sink.

3.4.1 Analytical Model of the Performance of Finned Heat Sink

The analytical model was set up based on the following assumption:

- The heat sinks work under steady state conditions.

- Heat conducts across the fins in one dimension. This assumption can become reality if the fin is sufficient thin. For most practical fins the error caused by this assumption is less than 1 percent.[Lienhard John H, 2001]
- The convective heat transfer coefficient on fin surface is constant.
- There are no internal heat generations within the fin.
- The fin has a constant cross-sectional area.
- The thermal conductivity of the fin is constant.

Heat transfer from a fin, fin efficiency and thermal resistance of a fin

Analysis of the performance of a single fin is necessary in order to analyse the performance of finned heat sink.

The practical fin has the finite length and can lose heat by convection from its tip. The heat transfer from the fin with a convective tip can be expressed by:[Lienhard John H, 2001]

$$Q_f = \sqrt{hPk_f A_c}(T_r - T_s)\frac{\sinh(mL) + (\frac{h}{mk_f})\cosh(mL)}{\cosh mL + (\frac{h}{mk_f})\sinh(mL)} \qquad (3\text{-}16)$$

Where h is the convective heat transfer coefficient over the surface of the fin; P is the perimeter of the cross section of the fin; k_f is the thermal conductivity of fin material; A_c is the cross section area of the fin; L is the length of the fin; T_r is the temperature of the fin root; T_s is the temperature of the surrounding fluid over the fin;

$$m = \sqrt{\frac{hP}{k_f A_c}} \qquad (3\text{-}17)$$

The tedious equation (3-16) is not convenient for use. By using a corrected fin length in the corresponding equation for fin with insulated tip, an approximate equation can be obtained, which can replace the equation (3-16).

The corrected fin length can be calculated by:

$$L_c = L + \frac{A_c}{P} \qquad (3\text{-}18)$$

The approximate equation for calculating heat transfer from the fin with convective tip is:

$$Q_f = \sqrt{hPk_f A}_c (T_r - T_s)\tanh(mL_c) \qquad (3\text{-}19)$$

The fin efficiency is defined as the ratio of actual heat transferred from the fin to heat that would be transferred if the entire fin were $T=T_r$. Fin efficiency provides some useful information as to how well a fin is contrived. [Lienhard John H, 2001]

The fin efficiency can be expressed by:[Lienhard John H, 2001]

$$\eta_f = \frac{Q_f}{hPL_c(T_r - T_s)} = \frac{\sqrt{hPk_f A}_c (T_r - T_s)\tanh(mL_c)}{hPL_c(T_r - T_s)} = \frac{\tanh(mL_c)}{mL_c} \qquad (3\text{-}20)$$

The error caused by using the above approximate equations is less than 8 percent when

$$(\frac{h\delta}{2k_f})^{1/2} \le \frac{1}{2} \qquad (3\text{-}21)$$

Where δ is the thickness of the fin.

Changing the form of equation (3-20), the following equation can be obtained:

$$Q_f = \eta_f hPL_c(T_r - T_s) = \eta_f hA_f(T_r - T_s) \qquad (3\text{-}22)$$

Where $A_f=PL_c$ is a total surface area of a fin

Change the form of equation (3-22), the thermal resistance of a fin R_f can be expressed as follow:

$$R_f = \frac{T_r - T_s}{Q_f} = \frac{1}{\eta_f A_f h} \qquad (3\text{-}23)$$

Heat transfer from finned heat sink, finned heat sink efficiency and finned heat sink thermal resistance

The practical finned heat sink has a number of fins extruded from the base plate, as shown in Figure 3-18. The total area exposed to coolant can be calculated:

$$A_t = A_o + NA_f \tag{3-24}$$

Where A_o is total area of all the exposed regions of base plate; N is the number of the fins.

The overall heat transfer from the finned heat sink can be expressed by:

$$Q_{fs} = hA_o(T_r - T_s) + N\eta_f hA_f(T_r - T_s) \tag{3-25}$$

The first term in equation (3-25) shows the heat transfer from the exposed regions of the base plate; the second term shows the heat transfer from fins [reference to equation (3-22)].

Combining equation (3-24) and (3-25), the following equation can be obtained:

$$Q_{fs} = hA_t[1 - \frac{NA_f}{A_t}(1 - \eta_f)](T_r - T_s) \tag{3-26}$$

Compare equation (3-22) with equation (3-26), an equivalent formula for calculation of finned heat sink efficiency can be obtained, i.e.,

$$\eta_{fs} = 1 - \frac{NA_f}{A_t}(1 - \eta_f) \tag{3-27}$$

Combining equation (3-26) with equation (3-27), the following equation can be obtained:

$$Q_{fs} = hA_t\eta_{fs}(T_r - T_s) \tag{3-28}$$

Changing the form of equation (3-28), we can get the following equation:

$$R_{fa} = \frac{T_r - T_s}{Q_{fs}} = \frac{1}{\eta_{fs}hA_t} \tag{3-29}$$

Where R_{fa} is the combination of the conductive thermal resistance of the fins and the convective thermal resistance of heat sink. The finned heat sink thermal resistance should include the conductive thermal resistance of the base plate, the combination is shown as follow:

$$R_{fs} = \frac{\delta_b}{k_b A_b} + \frac{1}{\eta_{fs}hA_t} \tag{3-30}$$

Where R_{fs} is thermal resistance of finned heat sink; δ_b is the thickness of base plate; A_b is area of base plate.

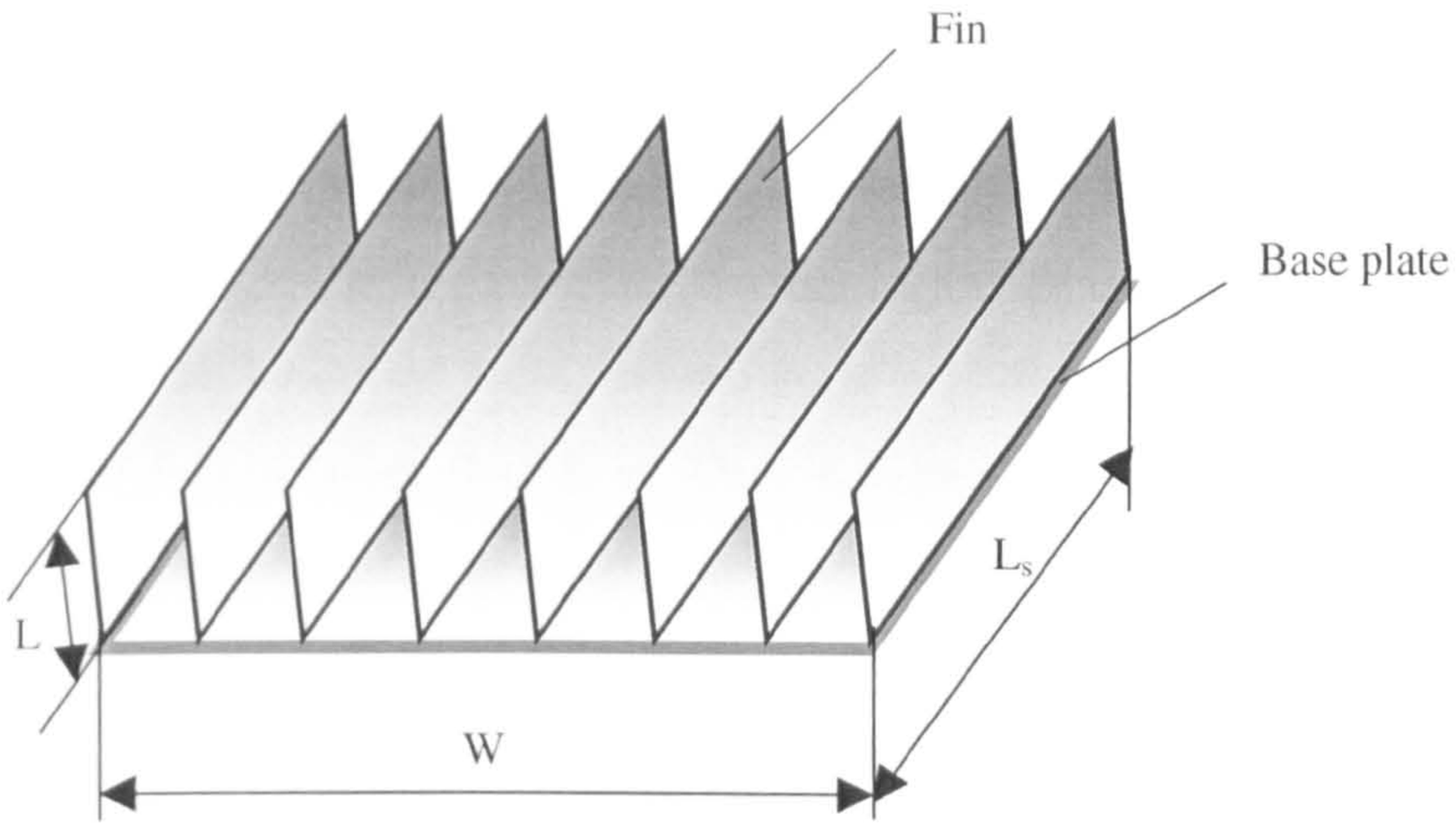

Figure 3-18. Schematic diagram of finned heat sink

Computer program in C++ language for the analytical model is shown in attached disk (Program B).

3.4.2 Modelling Results and Discussions

Computer modelling was carried out to explore the relations between finned heat sink performance (heat transfer, efficiency and thermal resistance) and length of fins, number of fins and convective coefficient. This provides a basis for optimum design of finned heat sink.

The following parameters were assumed in the modelling:

thickness of the fins----------0.5mm

width of the heat sink W (see Figure 3-9)---------- 0.35m

length of the heat sink L_s(see Figure 3-9)----------0.15m

thickness of base plate----------5mm

thermal conductivity of the finned heat sink (Al)------236W/(m.^{o}C) [Lienhard John H, 2001]

The assumed temperature difference between heat source and surrounding fluid over the finned heat sink is 15°C.

Relations between the performance of the finned heat sink and length of fins were explored by further assuming the number of the fins to be 45 and the convective coefficient to be 19.8W/m^2.°C [Fan C.Y, 1983], the results are shown in Figure 3-19 and Figure 3-20. In Figure 3-19, it is shown that the heat transfer increases quickly with the length of fins while the length of fins is within 8cm, and it does not increase obviously while the length of fins is larger than 8cm. This indicates that increase of the length of fins does not always increase the heat transfer. The efficiency decreases with the increase of the length of fins. In Figure 3-20, it is shown that the thermal resistance decreases quickly with the increase of the length of fins while the length of fins is within 8cm, and it does not decrease obviously while the length of fins is larger than 8cm. This indicates that the increase of the length of fins does not always decreases the thermal resistance. Therefore, optimum length of fins should be within an appropriate extent.

Relations between the performance of finned heat sink and the number of fins were explored by further assuming the length of the fins to be 5 cm and the convective coefficient to be 19.8 W/m^2.°C [Fan C.Y, 1983], the results are shown in Figure 3-21 and Figure 3-22. In Figure 3-21, it is shown that the heat transfer from the finned heat sink increases straight with the number of fins. The efficiency decreases with the increase of the number of fins while the number of fins is within 15, and it does not decrease obviously while the number of fins is larger than 15. In Figure 3-22, the thermal resistance decreases with the number of fins, but the decrease become slower and slower with the increase of the number of fins. Although the high density of fin indicate a good performance as above analysis, it is suggested that appropriate number of fins should be chosen considering its resistance on coolant. Higher density of fins needs more powerful equipment to produce the required flow velocity of coolant.

Relations between the performance of finned heat sink and the convective coefficient explored by further assuming the length of the fins to be 5cm and the number of the fin to be 45, the results are shown in Figure 3-23 and Figure 3-24. It is shown that the heat transfer from the finned heat sink increases quickly with the increase of the convective

coefficient and efficiency decreases with the increase of the convective coefficient. The thermal resistance decreases with the increase of the convective coefficient.

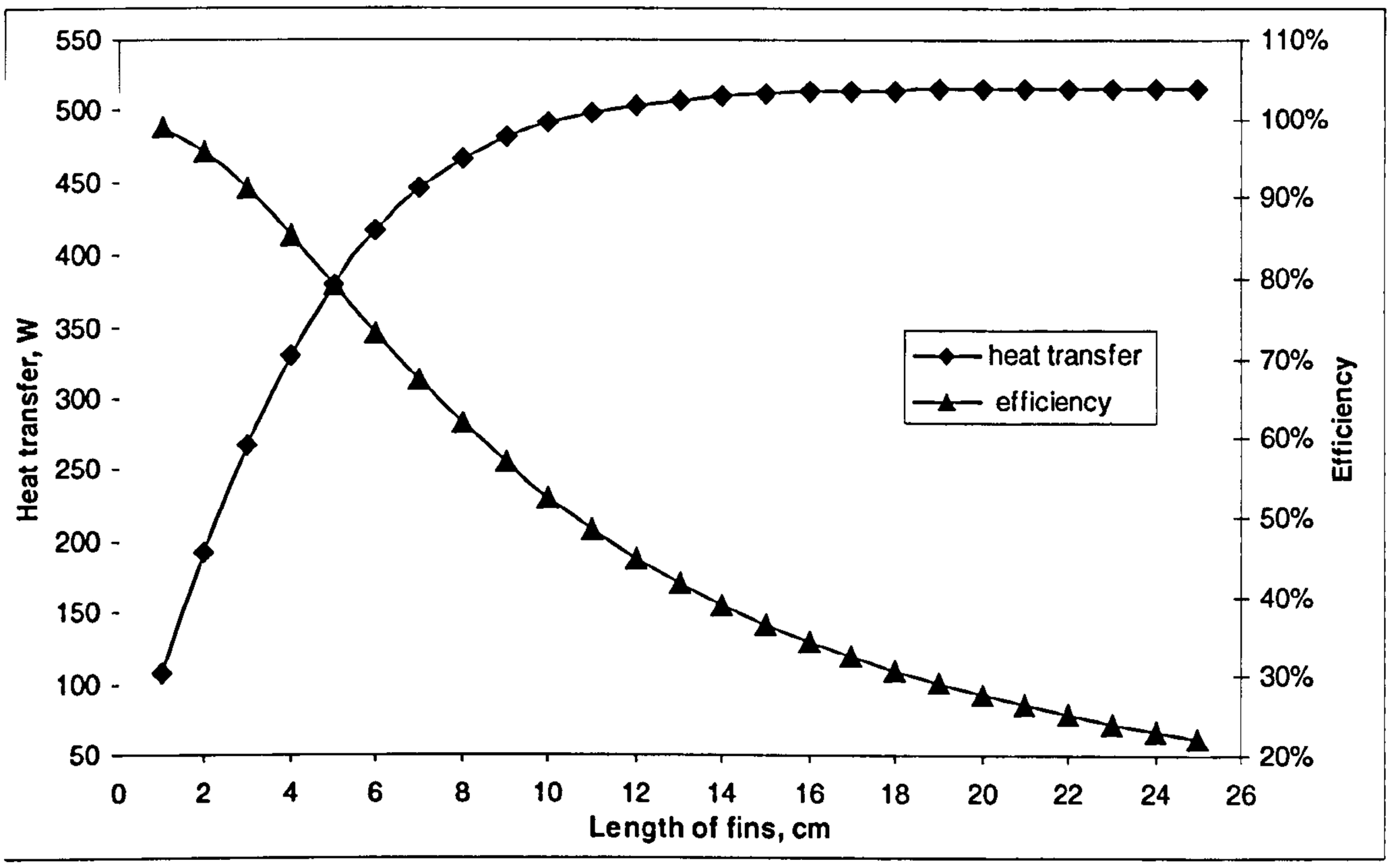

Figure 3-19. Relation between heat transfer as well as efficiency and length of fins (N=45, h=19.8W/m^2.^{o}C)

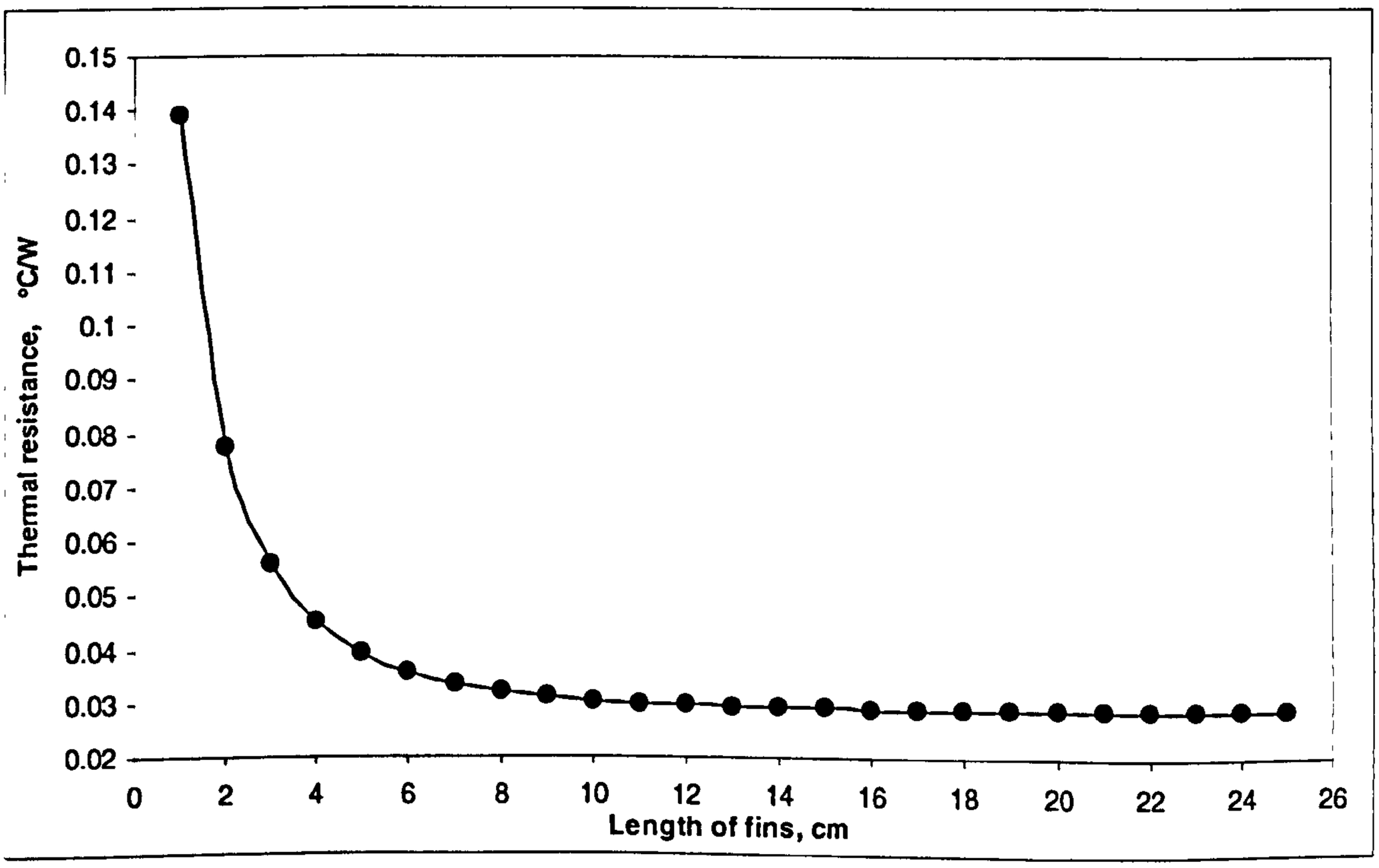

Figure 3-20. Relation between thermal resistance and length of fins (N=45, h=19.8W/m^2.^{o}C)

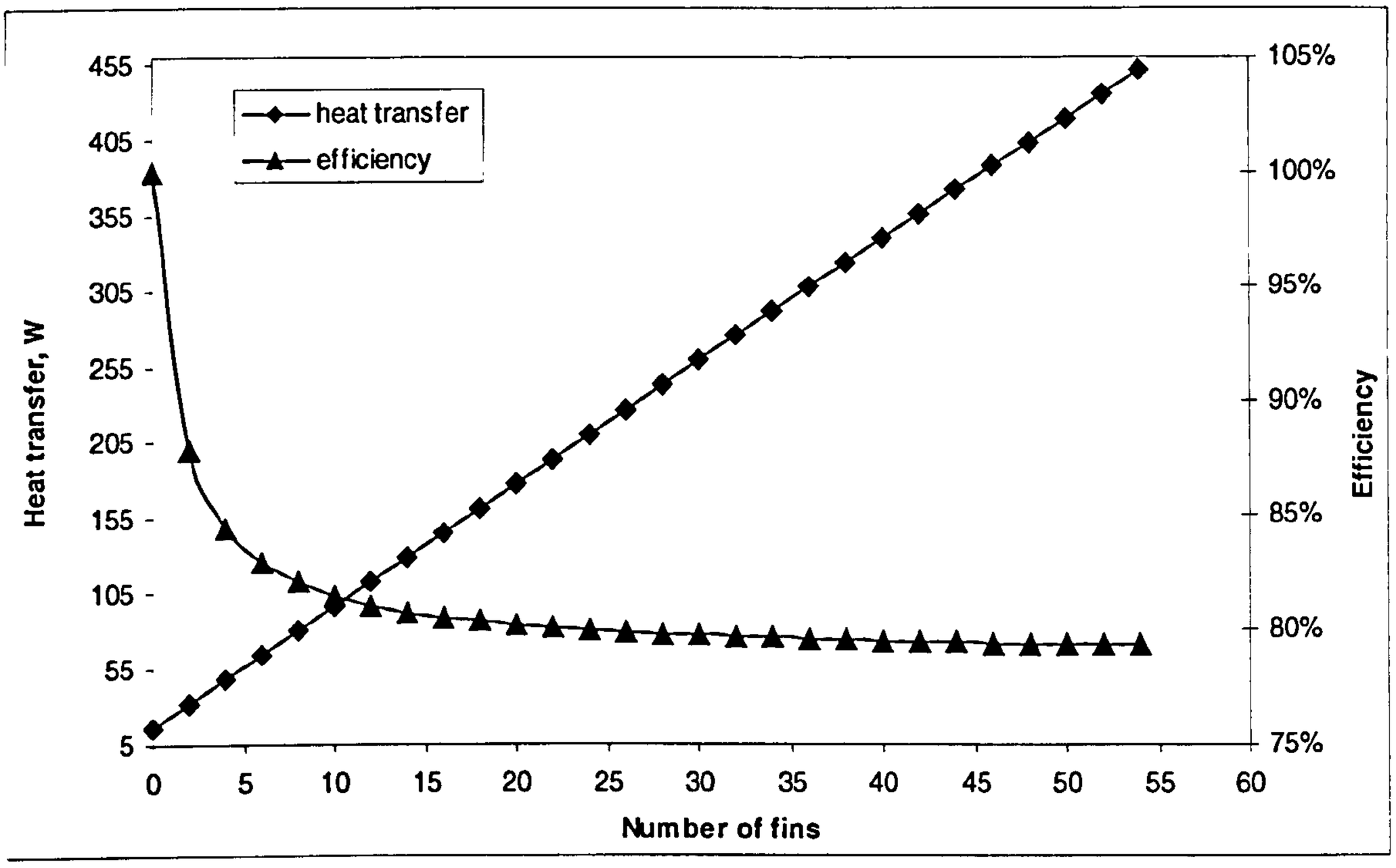

Figure 3-21. Relation between heat transfer as well as efficiency and number of fins (L_f=5cm, h=19.8W/m^2.^{o}C)

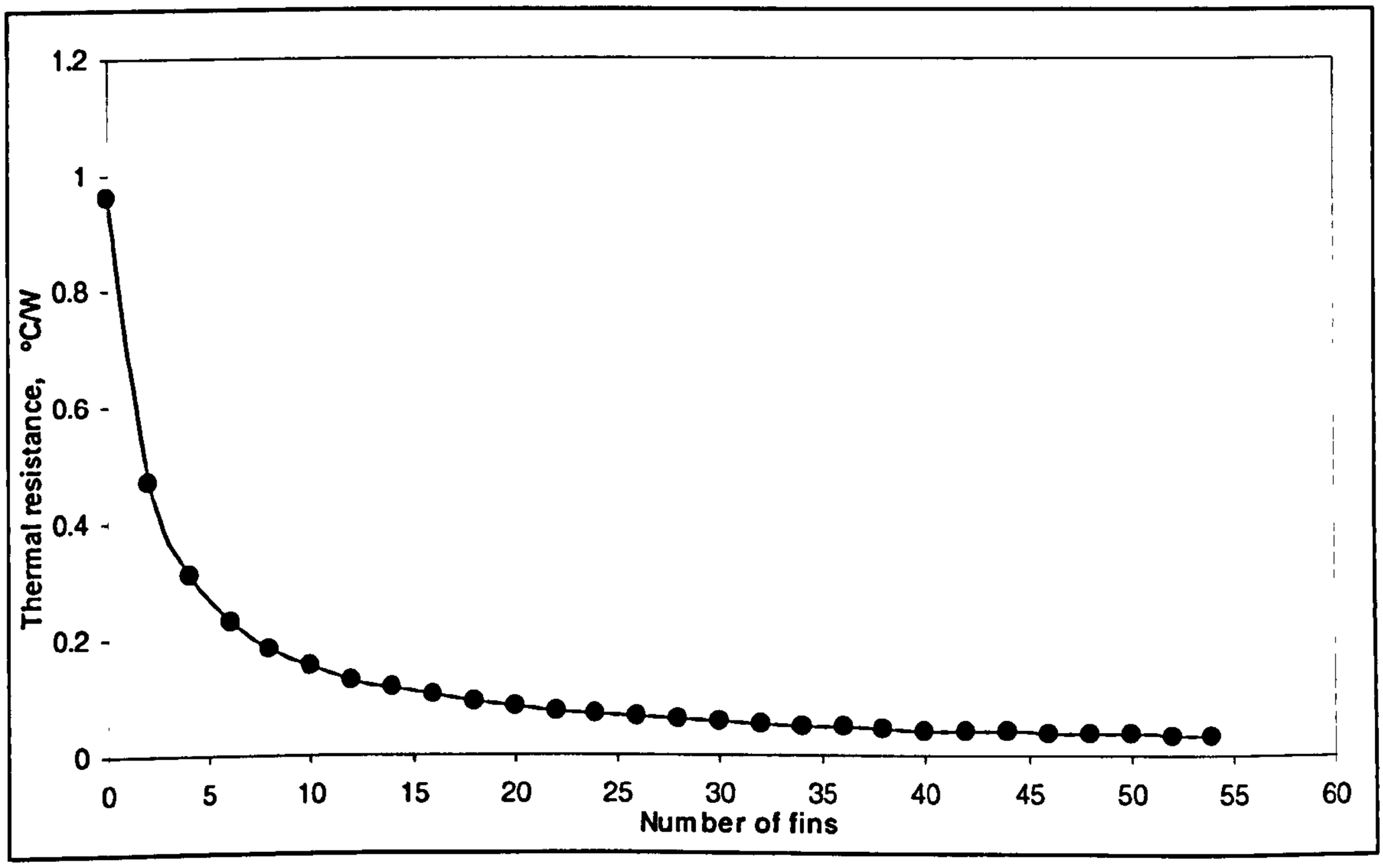

Figure 3-22. Relation between thermal resistance and number of fins (L_f=5cm, h=19.8W/m^2.^{o}C)

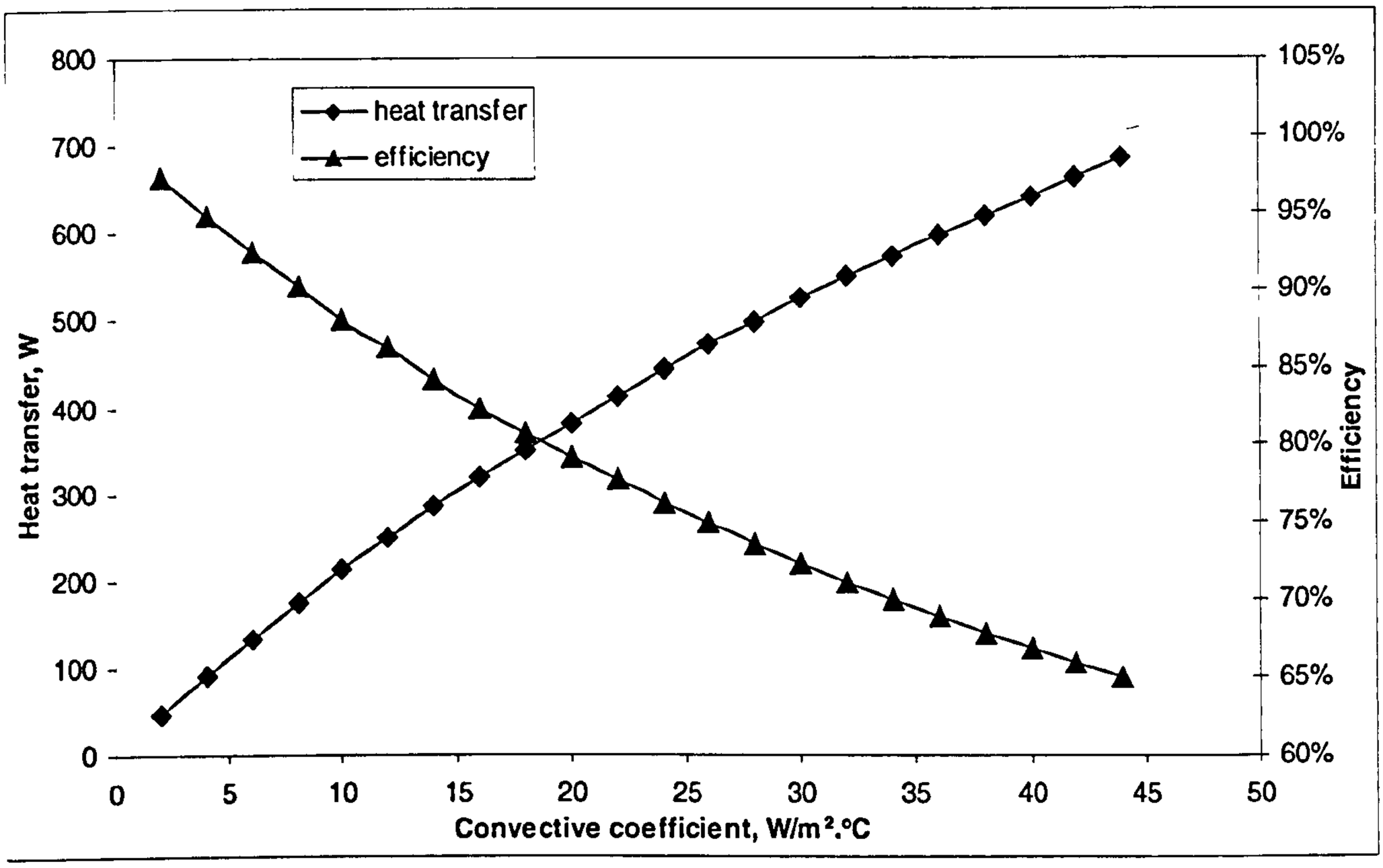

Figure 3-23.Relation between heat transfer as well as efficiency and convective coefficient (L_f=5cm, N=45)

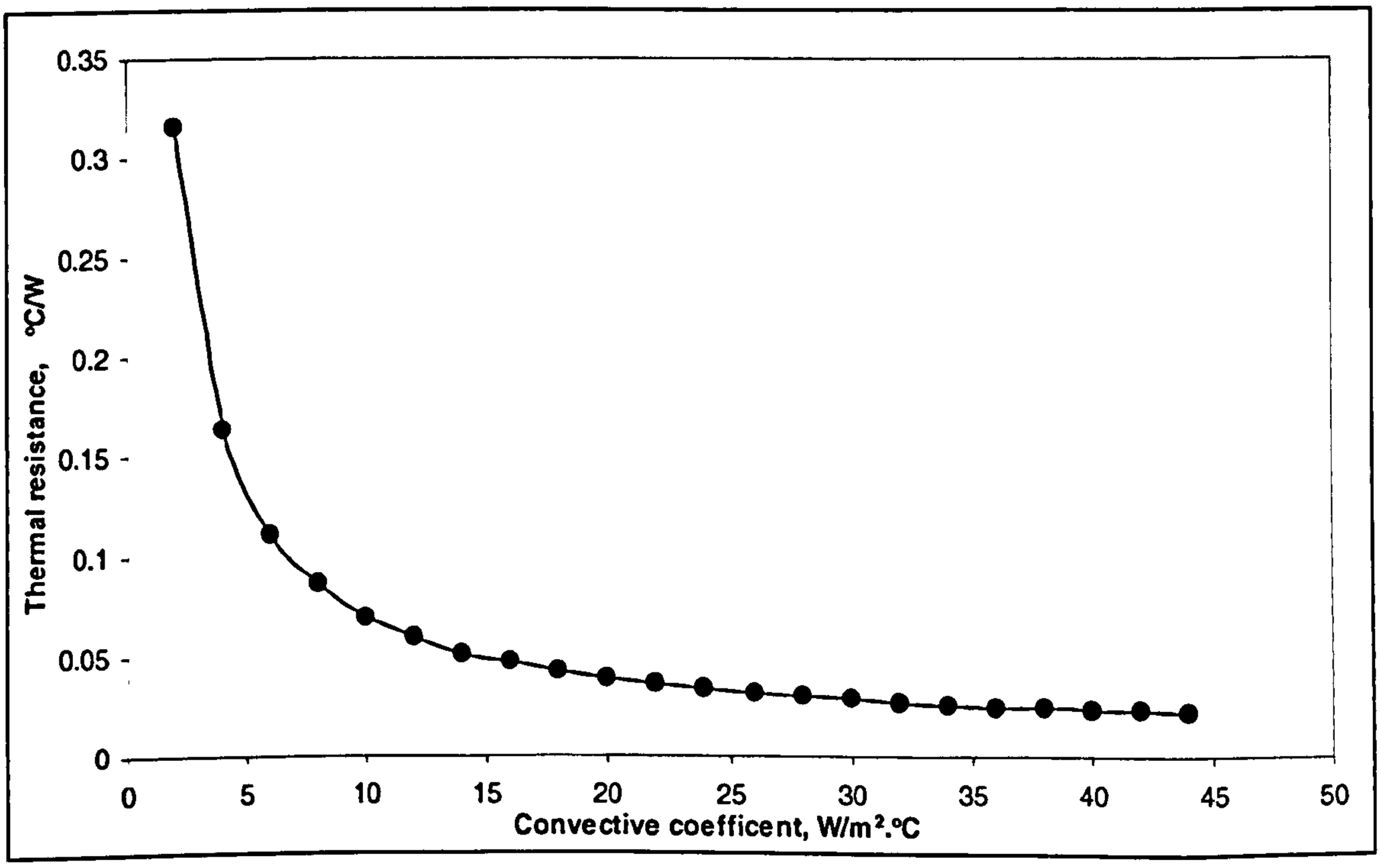

Figure 3-24. Relation between thermal resistance and convective coefficient (L_f=5cm, N=45)

3.5 Conclusion

A computer model was developed to explore the relations between the cooling/heating requirements and optimum thermoelectric parameters. It was found that optimum current should be input to obtain maximum COP. This can be done by using appropriate number of thermoelectric modules or appropriate geometry factor of the modules to make the operating current equal to the optimum current. For a specific cooling/heating requirement, the required optimum number of thermoelectric modules for optimum current and maximum COP varies with geometry factor (the type of the modules). The value of maximum COP is determined by the working temperatures and the figure of merit of the material and has no relationship with the cooling/heating capacity and the geometry factor.

A computer model was developed to explore the relations between the performance of the finned heat sink and its geometry parameters as well as convective coefficient. Modelling results showed that the heat transfer from the finned heat sink increases and thermal resistance decreases with the increase of the length of fins in some extent, number of fins and convective coefficient. However, the efficiency decreases with the increase of these factors. The modelling provides a basis for optimum design of a finned heat sink.

Chapter 4. Heat Pipes and Heat Pipe Thermal Performance Analysis

4.1 Conventional Heat Pipes and a New Type Heat Pipe

Conventional heat pipes have simple column containers with straight single channels. If the cross section diameters or equivalent diameters are larger than 2mm, the channel geometry are usually circular or rectangular. The inner surface of these heat pipes may be fitted with wicks, which are used to produce capillary force to aid the operation of the heat pipes; but some are wickless, which are operated by gravitational force, called thermal diode. The above heat pipes are called normal heat pipes. If the cross section diameters is within 0.1mm-2mm, the channel geometry is usually a concave trapezoid with tapered triangular channels in each of four corners [Babin et al, 1989], as shown in Figure 2-16. This kind of heat pipes is called micro/miniature heat pipe. Micro/miniature heat pipes are wickless heat pipes. Capillary action produced by the sharp corners of the channel plays a major role for the operation of this kind of heat pipe. For any heat pipe, the geometrical shape of the cross section is a critical factor affecting its performance.

To meet different applications, various heat pipes can be derived based on the concept of the aforementioned conventional heat pipes. For this PhD work, a new type heat pipe (thermal diode) was required, as shown in Figure 1-1. The evaporator and condenser of the thermal diode are flat panels with circular holes inside the panels. This structure can withstand a higher pressure and therefore keeps the surface of the panels flat, which is essential for this work. The holes connect each other at the end to keep the working fluid inside the thermal diode at the same level. The adiabatic section is a circular tube. The angle between the flat panel and the adiabatic section is 120^{o}, which incurs less resistance to fluid flow than an angle of 90^{o}. The flat panels and the adiabatic section are connected with headers.

During operation of this new type heat pipe, liquid evaporates on the internal surface of the evaporator, the vapour enters the condenser via the adiabatic section and condenses on the internal surface of the condenser. For a thermal diode with a single tube, the condensate then returns to the evaporator via the adiabatic section by gravity and distributes on the internal surface of the evaporator. Heat applied to the evaporator section by an external source then vaporizes the working fluid on the internal surface of

evaporator. The heat pipe can therefore continuously transport the latent heat of vaporization from the evaporator to the condenser section. For this new type thermal diode heat pipe, the condensate from the adiabatic section cannot flow along all the holes of the evaporator, it can only flow along one or two holes. Therefore, it can not distribute the condensate to the internal surface of other holes to form liquid film. This causes that the thermal diode cannot work efficiently.

To solve this problem, two methods are suggested. One is to use more liquid in the thermal diode. The liquid fill level should be 100% evaporator length, which of course can always keep internal surfaces of all the holes of the evaporator wet. Another method is to use capillary wick in the internal surface of evaporator. The capillary wick will drive the liquid from the bottom of the evaporator to the whole internal surface of evaporator and distribute the liquid evenly on the surface. Unlike the conventional normal heat pipe, the action of the wick in this case is not to return the condensate from the condenser to evaporator; it is to distribute liquid from the bottom of the evaporator to its whole internal surface.

Investigation of the conventional heat pipe can provide a basis for investigation of any types of heat pipes. Based on the investigation of the conventional heat pipes, the new type thermal diode was investigated for the above two cases, i.e., using more liquid and using wick in the evaporator.

4.2 Analytical Model Set-up—Limits of Heat Transport Capacity

Limits of maximum heat transport capacity

For any heat pipe, the maximum heat transport capacity is governed by six limits [Dunn and Reay, 1982]; namely, the sonic limit, the entrainment limit, viscous limit, boiling limit, capillary limits and liquid fill limits.

1) ***Sonic limit***: When the vapour velocity approaches sonic speed, the mass flow of the fluid achieves its critical limit, this is also called "choke". Further increase of pressure drop does not produce further increase of the mass flow rate and heat transport capacity. This maximum heat transport capacity is called the sonic limit.

2) ***Entrainment limit***: Owing to the reverse flow between liquid and vapour, a shear force exists at the interface of the liquid-vapour phase. If the velocity of the vapour increases to a high value, some small liquid blocks in the interface will be split and carried forward by vapour flow from the evaporation section to condensation section. This will result in ineffective heat transfer. We call the heat transfer under the critical flow state the entrainment limit.

3) ***Viscous limit***: The flow of both vapour and liquid will cause pressure reduction due to the viscous effect. This will limit mass flow rate and heat transportation. The limit is called viscous limit.

4) ***Boiling limit***: When radial heat flow rate increases to a certain value, the liquid near the inner wall will be superheated and bubbling will occur. This will produce an unacceptable high temperature in local parts of the evaporation section. This critical heat transport volume is called the boiling limit.

5) ***Capillary limit***: With increasing of heat flow rate, the liquid evaporation rate will also increase. However, if the capillary forces produced in the heat pipe are not able to draw enough liquid back to the evaporation section, the wall of lower part of the evaporation section will dry out. This critical heat transfer is called the capillary limit.

6) **Liquid fill limit:** For gravity assisted two-phase thermosyphon (thermal diode) heat pipes, the filled liquid volume is also a critical condition for heat pipe operation. For a certain radial heat flow rate, if only a small volume of liquid is used within the heat pipe, the liquid film on the wall of lower part of evaporation section would be broken due to excessive evaporation. Furthermore, the liquid deposited at the bottom of the heat pipe also evaporates gradually until dried out. In order to prevent this, a minimum filled liquid volume is required corresponding to a given heat input. In other word, a given filled volume allows a limited radial heat flow rate, which is called dry-out limit.

Mathematics model

The formulae for limits of heat transport capacity for conventional heat pipes with or without wick were developed. On the basis of these formulae the calculation of maximum heat transport capacity of the new type heat pipe was also presented.

Consider each hole in the new type thermal diode as a single thermal diode. All the single thermal diodes have the same adiabatic section. The cross section area of the adiabatic section is equal to the total cross sectional area of all the single thermal diodes. The new type thermal diode can then be taken as numerous single thermal diodes parallel in width. Firstly, we will consider a single thermal diode as a simulation object and determine its optimum sizes and working conditions. This concept will then be developed to simulate the whole thermal diode.

Due to all the single holes connecting each other, a natural circulation flow is created in the evaporator of the new type thermal diode, gravity does not play a role in promoting fluid flow in the evaporator. This will be considered in the calculation of the capillary limit.

Using the techniques presented in Dunn and Reay (1982) and Babin B.R. et al (1990), the above five limits may be expressed as:

Sonic Limit

$$q_{s,m} = k_s A_v \rho_v h_{fg} (\gamma R_{vc} T_v / (2(\gamma+1))^{1/2} \qquad (4\text{-}1)$$

Where, k_s is the shape factor of the heat pipe channel geometry (circle---1; regular hexagon---0.964; square ---0.883; micro/miniature---no report, a value similar to square pipe, such as 0.85, could be applied)

Entrainment Limit

$$q_{e,m} = k_s A_v h_{fg} (\sigma \rho_v / (2r_{h,w}))^{1/2} \qquad (4\text{-}2)$$

Boiling Limit

$$q_{b,m} = \frac{2\pi d_{eff} k_{eff} T_v}{h_{fg} \rho_v \ln(r_i / r_v)} (\frac{2\sigma}{r_n} - \Delta p_{c,m}) k_s \tag{4-3}$$

Viscous Limit:

$$q_{v,m} = \frac{k_s r_v^2 h_{fg} \rho_v p_v A_v}{16 \mu_v l_{eff}} \tag{4-4}$$

Capillary Limit

$$\Delta p_{cl} \geq \Delta p_{rg} + \Delta p_{ag} + \Delta p_l + \Delta p_v \tag{4-5}$$

Due to the influence of gravity on the heat pipes investigated, the heat transport capacity is also governed by the filled liquid mass. Zhuang (1989) expressed this parameter as follows:

$$G_f = (0.8 l_c + 0.8 l_e + l_a)(\frac{3\mu_1 \rho_1 \pi^2 d_i^2}{k_l h_{fg} g})^{1/3} q_c^{1/3} \tag{4-6}$$

For wickless heat pipes including conventional normal wickless pipes and the new type pipe without wick, there are no capillary pressure differences along the pipe length, i.e., $\Delta p_{cl}=0$. In addition, the entrainment limit may be expressed in a different way, as shown below (Zhuang, 1989)

$$q_{e,m} = k_s f_1(\phi) C_w^2 \frac{\pi d_i^{2.5}}{4} \frac{h_{fg} \sqrt{g \rho_v (\rho_l - \rho_v)}}{[1 + (\rho_v / \rho_l)^{0.25}]^2} \tag{4-7}$$

$C_w=0.725$

$$f_1(\phi) = (\frac{\phi}{180} + \sqrt{\sin 2\phi})^{0.65} \tag{4-8}$$

For conventional micro/miniature gravitational heat pipes or the wicked normal heat pipe, the net capillary pressure difference Δp_{cl} is calculated by using LaPlace-Young equation and assuming that during steady state operation the capillary radius of the curvature in the condenser section approaches infinity. This assumption allows the capillary pressure difference, Δp_{cl}, to be defined as a function of the surface tension σ,

the wetting angle θ, and the radius of curvature of the liquid-vapour interface in the evaporator, r_{ce}.

$$\Delta p_{cl} = (2\sigma / r_{ce})\cos\theta \tag{4-9}$$

The corner regions of the micro/miniature heat pipe may be approximated to a triangle, and hence the capillary radius may be found as:

$$r_{ce} = w/\cos(\alpha+\theta) \tag{4-10}$$

Where, w is half the groove width and is dependent on the position along the pipe length and the fluid properties; α is equal to half the included angle of the geometry.

For the new type thermal diode with wick, Δp_{cl} is to drive the liquid from the bottom of evaporator to the whole internal surface of the evaporator. Due to the single channel connecting each other to create a natural circulation flow in the evaporator, gravity does not play a role in promoting fluid flow in the evaporator. This case is similar to the wicked conventional normal pipes located horizontally, the net capillary pressure difference Δp_{cl} is expressed as:

$$\Delta p_{cl} = 2\sigma / r_{ce} \tag{4-11}$$

For any wicked heat pipes, the capillary radius may be expressed in different ways, depending on wick structure, the following expression is capillary radius of mesh as wick:

$$r_{ce} = (w+d)/2 \tag{4-12}$$

Where, w is the distance between adjacent wires; d is the diameter of the mesh wire;

For any kind of heat pipe, the radial and axial hydrostatic pressure drops Δp_{rg}, Δp_{ag} are the result of the gravitational forces and may be expressed as:

$$\Delta p_{rg} = -\rho_l g d_v \cos\phi \tag{4-13}$$

$$\Delta p_{ag} = -\rho_l g l_p \sin\phi \tag{4-14}$$

Where l_p is the length of liquid column in the heat pipe;

For conventional heat pipes, l_p is calculated as:

$$l_p = l_e + l_c + l_a - h_f \tag{4-15}$$

For the new type thermal diode, as a natural circulation flow is created in the evaporator, gravity forces does not play a role on hydrostatic pressure drops, l_p should not include the length of liquid column in evaporator, the l_p therefore should be calculated as:

$$l_p = l_c + l_a \sin\psi \tag{4-16}$$

Where ψ is the angle between the adiabatic section and the horizontal surface;

The liquid pressure drop, Δp_l, may be found by evaluating the shear forces at the liquid-solid and liquid-vapour interfaces. These forces inhibit the return of the liquid through the wall areas and may be computed by integrating the pressure gradient over the length of the heat pipe. For constant heat addition and heat rejection, this yields:

$$\Delta p_l = -(\frac{\mu_l}{KA_l h_{fg} \rho_l}) l_{eff} q_c \tag{4-17}$$

For the pipe with wick

$$K = r_{hl}^2 / 8 \tag{4-18}$$

For the pipe without wick

$$K = 1 \tag{4-19}$$

$$l_{eff} = 0.5 l_e + l_a + 0.5 l_c \tag{4-20}$$

Due to the compressibility of the vapour phase and the mass addition and removal in the evaporation and the condensation section, determination of the vapour pressure drop, Δp_v, in the heat pipes is complicated. Because of the large difference in the density between the liquid and vapour phases, the velocity of the vapour phase must be significantly higher than the velocity of the liquid phase. Hence, the pressure gradient

due to variation in the dynamic pressure, which is due to velocity and density changes, must also be considered when evaluating the vapour pressure drop. The following is the expression for the vapour pressure drop:

$$\Delta p_v = \left(\frac{C(f_v \mathrm{Re}_v)\mu_v}{2(r_{hv})^2 A_v \rho_v h_{fg}}\right) l_{eff} q_c \tag{4-21}$$

In addition, this pressure gradient also partly results from the frictional drag in the heat pipes.

The friction factor, f_v, and the constant, C, can be determined once the local axial Reynolds number and Mach number are defined. These expressions are given below.

$$\mathrm{Re}_v = \frac{2(r_{hv})q_c}{A_v \mu_v h_{fg}} \tag{4-22}$$

$$M_v = \frac{q_c}{A_v \rho_v h_{fg} (R_{vc} T_v \gamma)^{0.5}} \tag{4-23}$$

Kraus and Bar-Cohen (1983) gave the expressions for f_v and C, for different sets of conditions, as follows:

$$\mathrm{Re}_v \le 2300, \quad M_v \le 0.2 \tag{4-24}$$

$$(f_v \mathrm{Re}_v) = 16, \quad \mathrm{C}=1.00$$

$$\mathrm{Re}_v \le 2300, \quad M_v \succ 0.2 \tag{4-25}$$

$$(f_v \mathrm{Re}_v) = 16$$

$$C = C_1 = \left(1 + \left(\frac{\gamma - 1}{2}\right) {M_v}^2\right)^{0.5}$$

$$\mathrm{Re}_v > 2300, \quad \mathrm{M}_v \le 0.2, \tag{4-26}$$

$$(f_v \mathrm{Re}_v) = 0.038$$

$$C = C_2 = \left(\frac{2\gamma_{hv} q_c}{A_v h_{fg} \mu_v}\right)^{0.75}$$

$$Re_v>2300, \qquad M_v>0.2 \tag{4-27}$$

$$(f_vRe_v)=0.038$$

$$C=C_1C_2$$

The flow chart for this analytical model is shown in Figure 4-1 and computer program in FORTRAN language is shown in attached disk (program C).

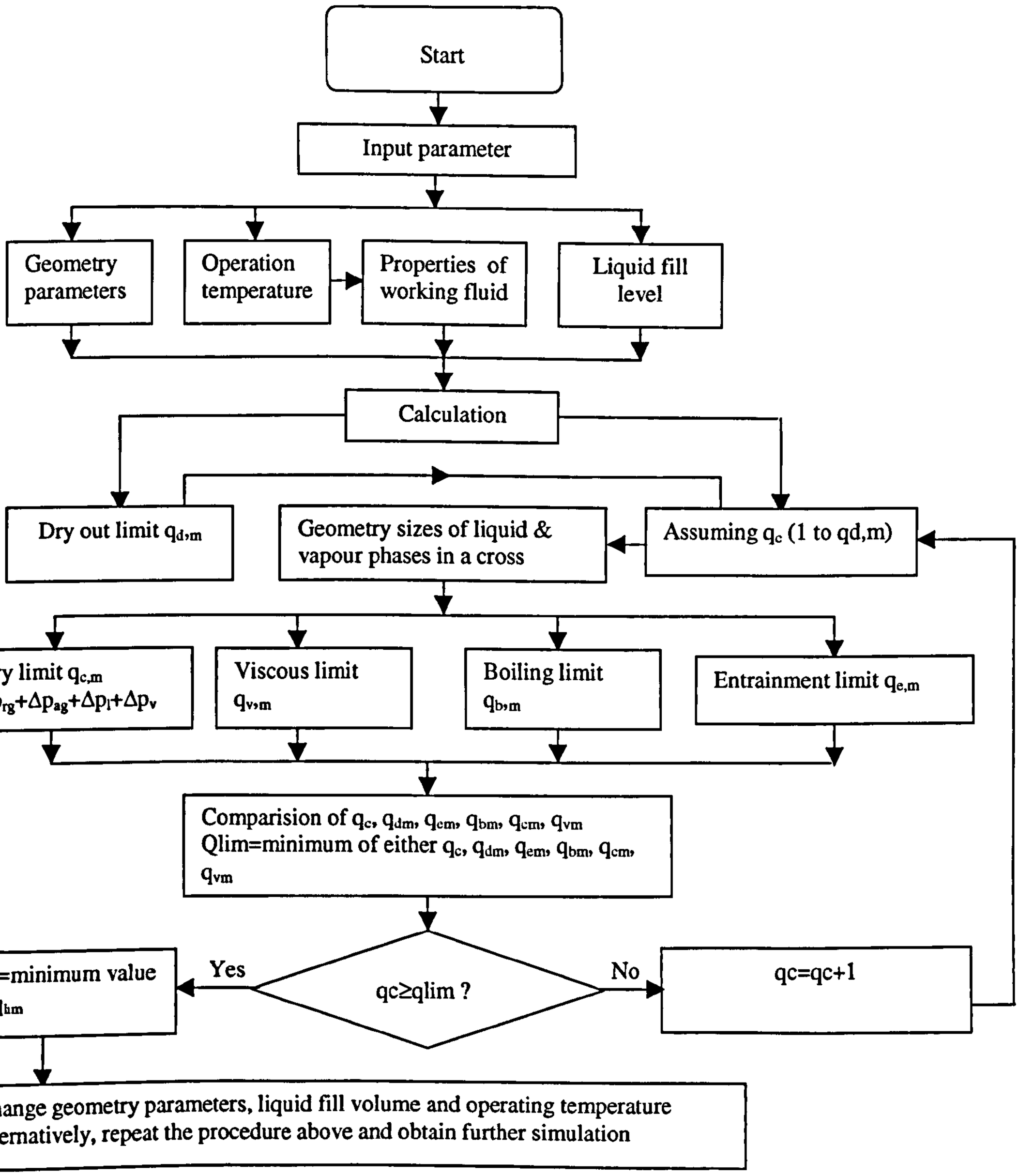

Figure 4-1. Flow chart of limits of heat transport capacity model

4.3 Validation of the Analytical Model

It is difficult to test the maximum heat transport capacities of heat pipes in common laboratories, and the reports relevant to the test data of the maximum heat transport capacities of heat pipes are rare. Only a report can be found to be available to validate the suitability and accuracy of the model [Babin B.R, 1990]. Comparison was carried out between the modelling results and the published experimental data for a conventional micro heat pipe.

Two test pipes were constructed [Babin B. R, 1990], one made of silver and the other copper. They were both charged with 0.032g of distilled, deionized water and were evacuated. In addition, two uncharged test pipes, one each of copper and silver, were tested to determine the amount of heat conducted through the wall to establish a baseline for evaluating the improvement in performance due to the vaporization and condensation of the working fluid.

Figure 4-2 illustrates the geometry of the heat pipes investigated. The shape factors and the sizes of the heat pipe are indicated in Tables 4-1. The limits of heat transport capacity, including capillary, sonic, entrainment, viscous limits and boiling limit, were calculated using the model, and the results were illustrated in Figure 4-3. The simulation results of capillary pressure, liquid pressure and vapour pressure are shown in Figure 4-4.

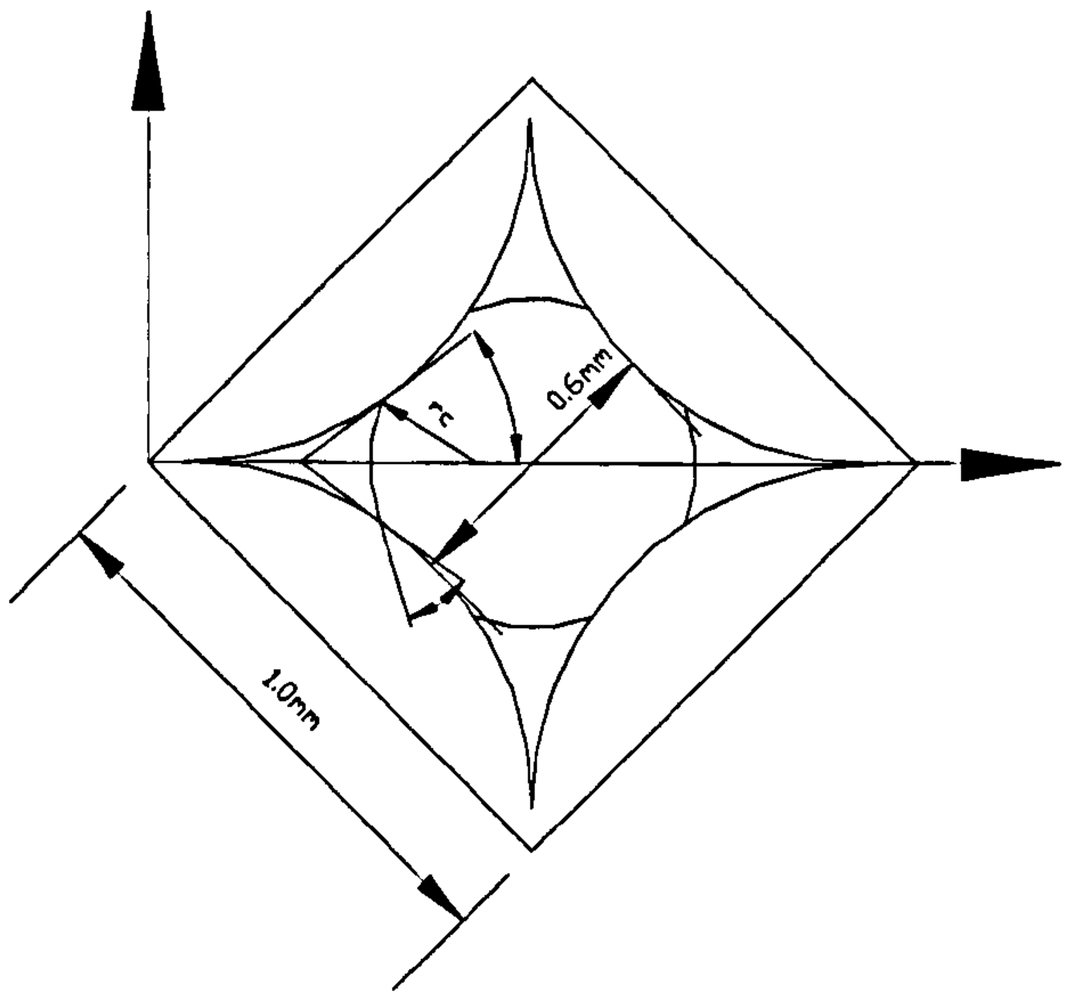

Figure 4-2.Cross-sectional dimensions of the micro heat pipe

Table 4-1. Micro heat pipe dimensions

Length, m	0.05
Length of condenser, m	0.0127
Length of evaporator, m	0.0127
Half of the width of the liquid-vapour interface, m	0.000133
Half of the angle of the sharp corner, rad	0.5854
Thermal conductivity of liquid K_l, w/m.°C	0.6
Thermal conductivity of vapour K_v, w/m.°C	0.975

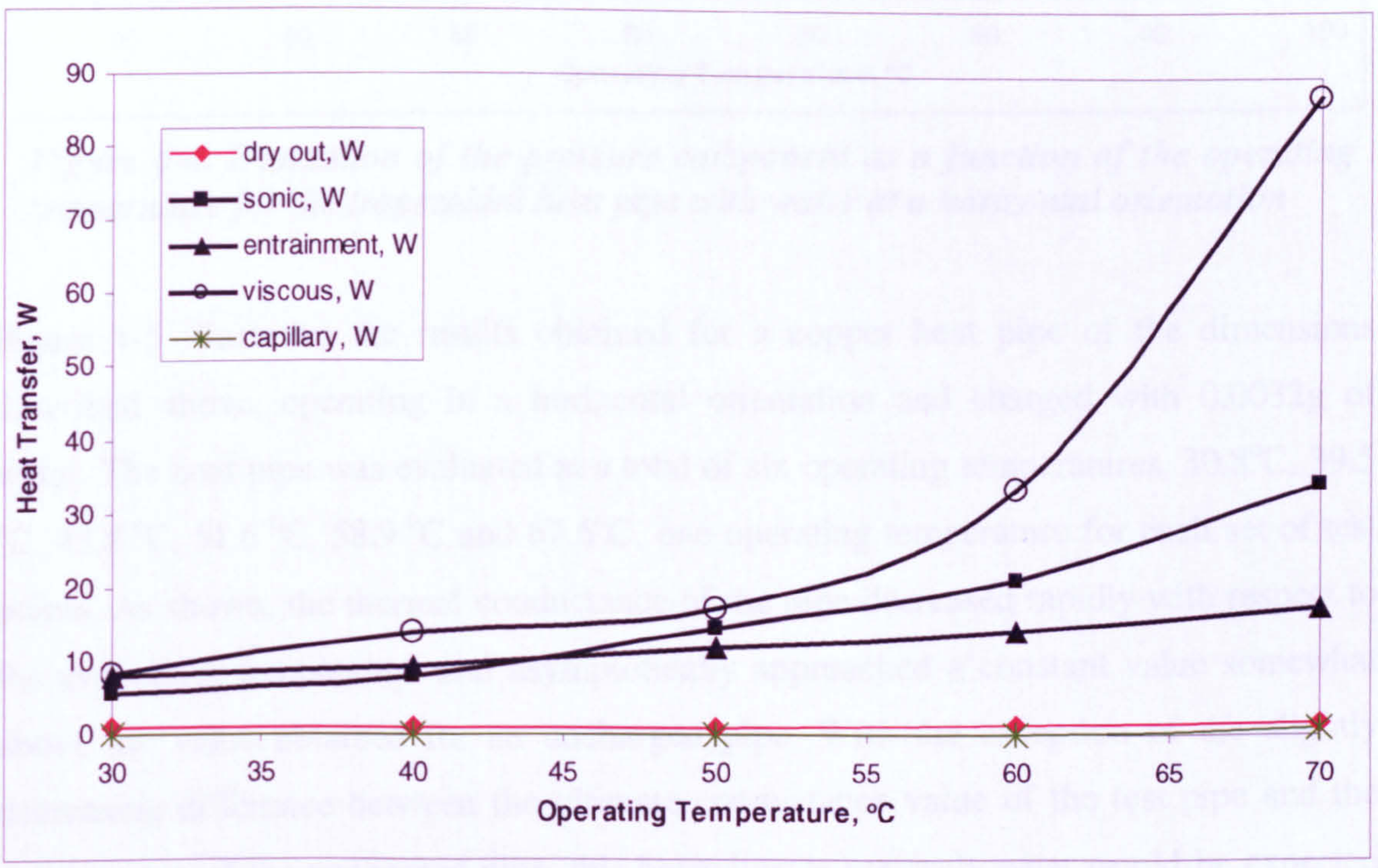

Figure 4-3. Limits of heat transport capacity of a trapezoidal micro heat pipe with water at a horizontal orientation

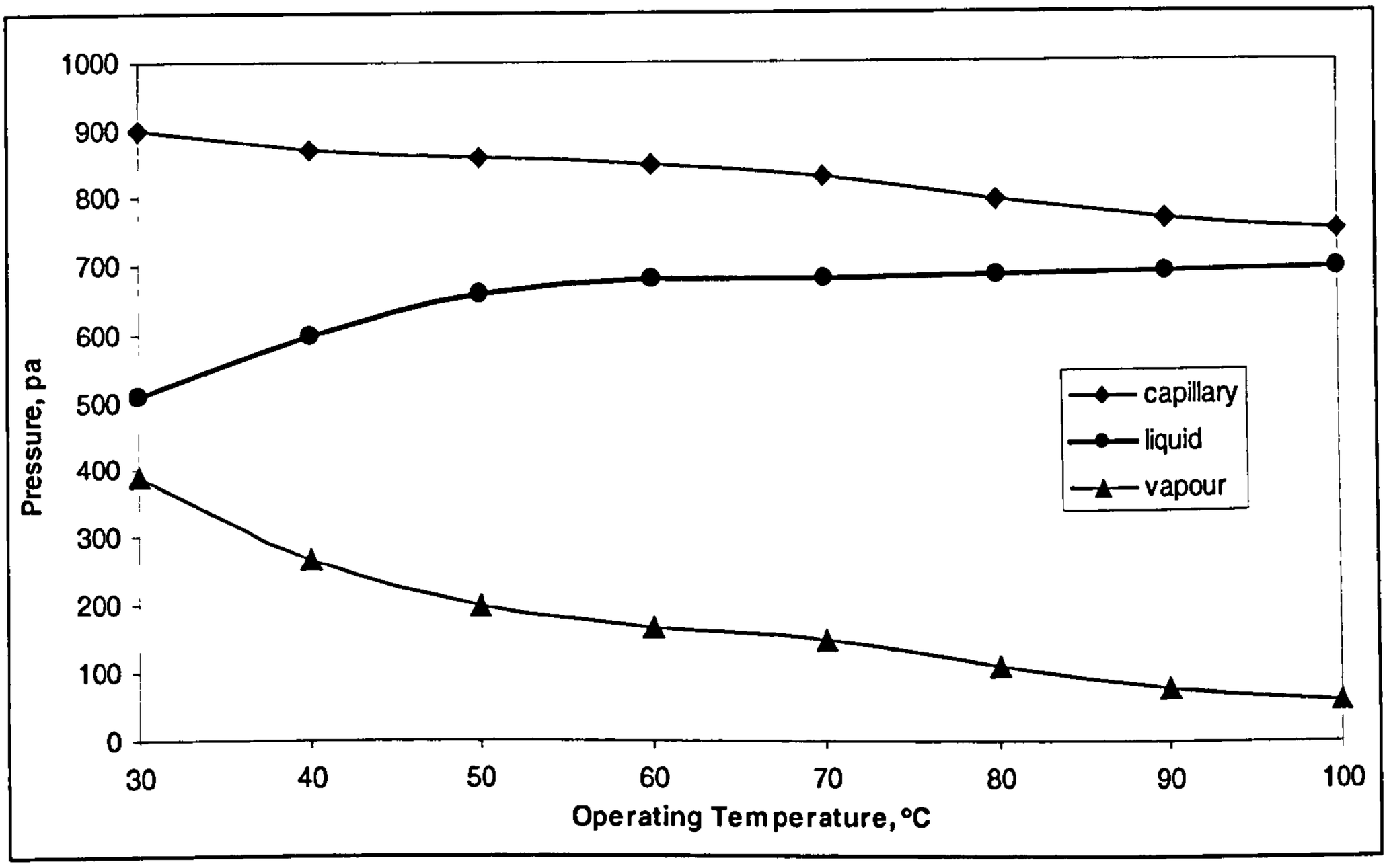

Figure 4-4. Evaluation of the pressure component as a function of the operating temperature for the trapezoidal heat pipe with water at a horizontal orientation

Figure 4-5 illustrates the results obtained for a copper heat pipe of the dimensions described above, operating in a horizontal orientation and charged with 0.0032g of water. The heat pipe was evaluated at a total of six operating temperatures, 30.8°C, 39.5 °C, 43.8 °C, 51.6 °C, 58.9 °C and 67.6°C, one operating temperature for each set of test points. As shown, the thermal conductance of the pipe decreased rapidly with respect to the evaporator temperature and asymptotically approached a constant value somewhat above the value obtained for an uncharged pipe. With the exception of the slightly decreasing difference between the ultimate conductance value of the test pipe and the conductance of the uncharged pipe, this behaviour is precisely what would be expected for a heat pipe in which the evaporator is slowly drying out. Increases in the input power initially caused the liquid meniscus to recede into the liquid channels located in the corners of the heat pipe. This resulted in a decrease in the radius of curvature of the liquid-vapour meniscus, a corresponding decrease in the cross-sectional area of the liquid, and hence, a slight increases in the evaporator temperature. The receding of the meniscus continued with increasing power, until dry-out of the evaporator occurs.

The slightly decreasing difference between the ultimate conductance value of the test pipe and the conductance of the uncharged pipe resulted from an increase in the effective size of the evaporator. Prior to dry-out, all the vaporisation occurs in the evaporator region. Once dry out begins, the temperature of the heat pipe wall in the adiabatic section increases and a small part of the adiabatic section began to act as an evaporator. As the power continued to increase, the dry-out in the evaporator spread and the portion of the adiabatic section that behaved as an evaporator expanded. In the extreme case where complete dry-out of the evaporator section occurs, a large portion of the adiabatic section may behave as an evaporator and may even begin to dry out at the end farthest from the condenser.

Figure 4-6 illustrated the results for the various test points obtained for a silver heat pipe of the same dimensions, charged with 0.0032 g of water. The test conditions were similar; however the operating temperature at which the silver heat pipe was evaluated were 31.8°C, 32.3°C, 42.0°C, 52.5°C, and 62.8°C. As shown, the trends and tendencies were all similar to those of the copper pipe tested.

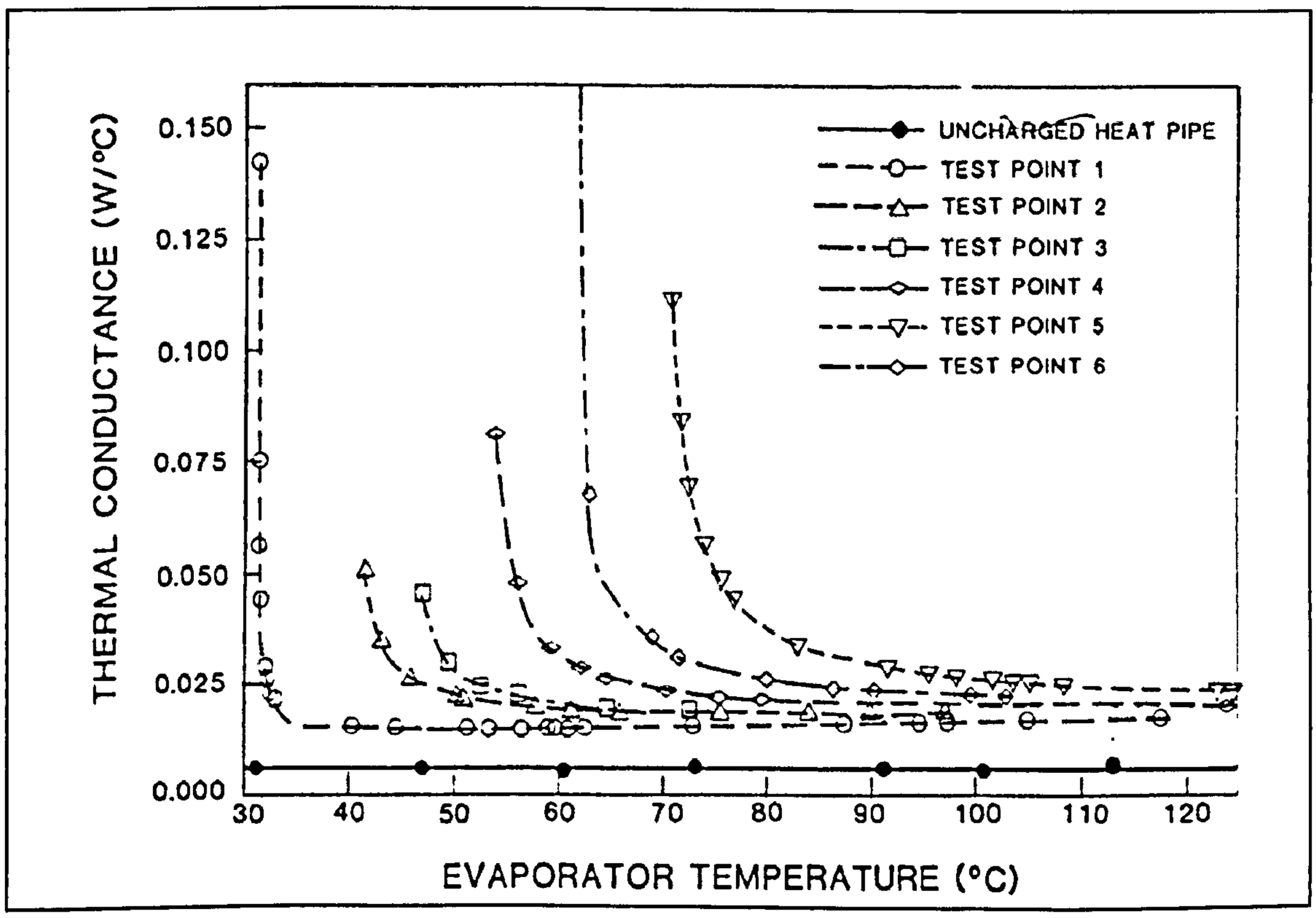

Figure 4-5. Measured thermal conductance of a trapezoidal micro heat pipe as a function of the evaporator temperature (copper, 0.032 g charge)[Babin B.R, 1990]

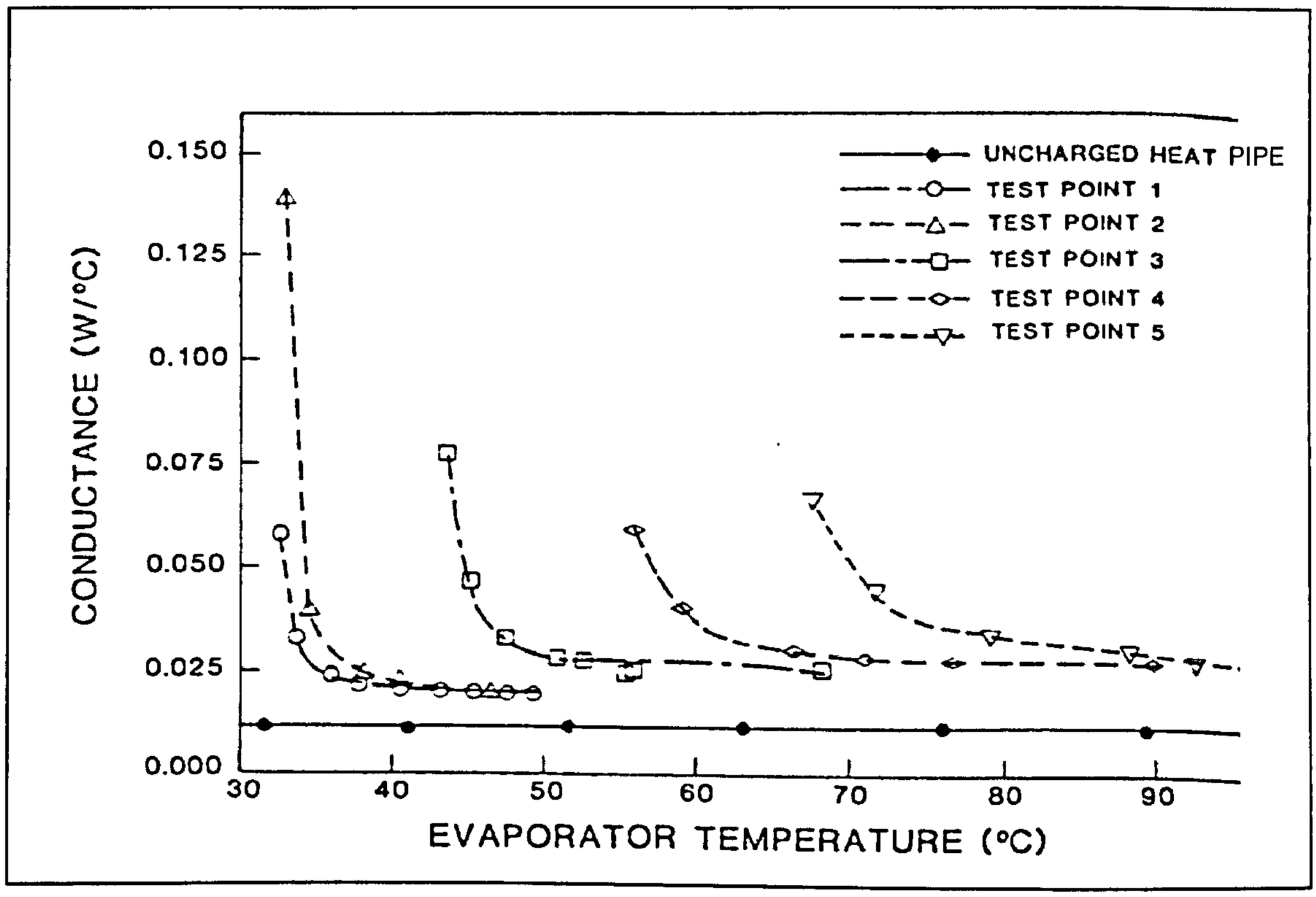

Figure 4-6. Measured thermal conductance of a trapezoidal micro heat pipe as a function of the evaporator temperature (silver, 0.032 g charge)[Babin B R, 1990]

In order to compare the experimental results with those predicted by the analytical model, it was necessary to develop a method for determining the point at which dry-out begins. The experimental data presented in Figures 4-5 and 4-6 clearly display a change in the operation of the two test pipes as the operation temperature and power levels were increased. After reviewing the experimental data, an attempt was made to identify and quantify better the onset of dry-out. Because, as discussed previously, there was no clear cut division between the evaporator and condenser, this proved to be quite difficult.

Several strategies were completed, including development of a mathematical method for determining the maximum curvature for each operating temperature. The final approach used was to select a region on both sides of the point of maximum curvature, which is a range around the point at which the most rapid change of the conductance occurs with respect to evaporator temperature. This range was assumed to be the region over which dry-out occurred. The initial point, which will be referred to as the onset of dry-out, was identified as that point where the slope of a line tangent to the curve was 60 deg. The termination of dry-out was assumed to occur at that point where slope of the tangent line

was 30 deg. Although this would appear to be a large range, in reality it is probably reasonably close to the actual behaviour, since dry-out is a gradual process and unlike the sonic or boiling limit, develops quite slowly.

Figures 4-7 and 4-8 illustrate the results of this process and compare the measured input power to the heat pipe evaporator, with the maximum heat transfer capacity predicted by the model for the copper and silver test pipes, respectively. As shown, at low operating temperatures, this model over-predicts the experimentally determined maximum heat transport capacity by approximately 15 percent for both the copper and silver test pipes. Between operating temperatures of 40 and 60, the model predicts dry-out with a reasonable degree of accuracy, and above 60 the model slightly under-predicts dry-out.

In overall, the steady-state experimental results provide experimental verification of the trapezoidal micro heat pipe concept and indicate that the analytical model can be used to predict accurately the level of performance. Since variations in the way the dry-out phenomenon is defined can significantly increase or decrease the experimentally determined values, the discrepancy between the measured and predicted values may in part be due to the technique used to define dry-out. As a result, the perceived accuracy of the models is strongly dependent upon the way dry-out is defined. To resolve this problem, it is necessary to understand the dry-out phenomenon better and define more clearly when it begins and how it proceeds.

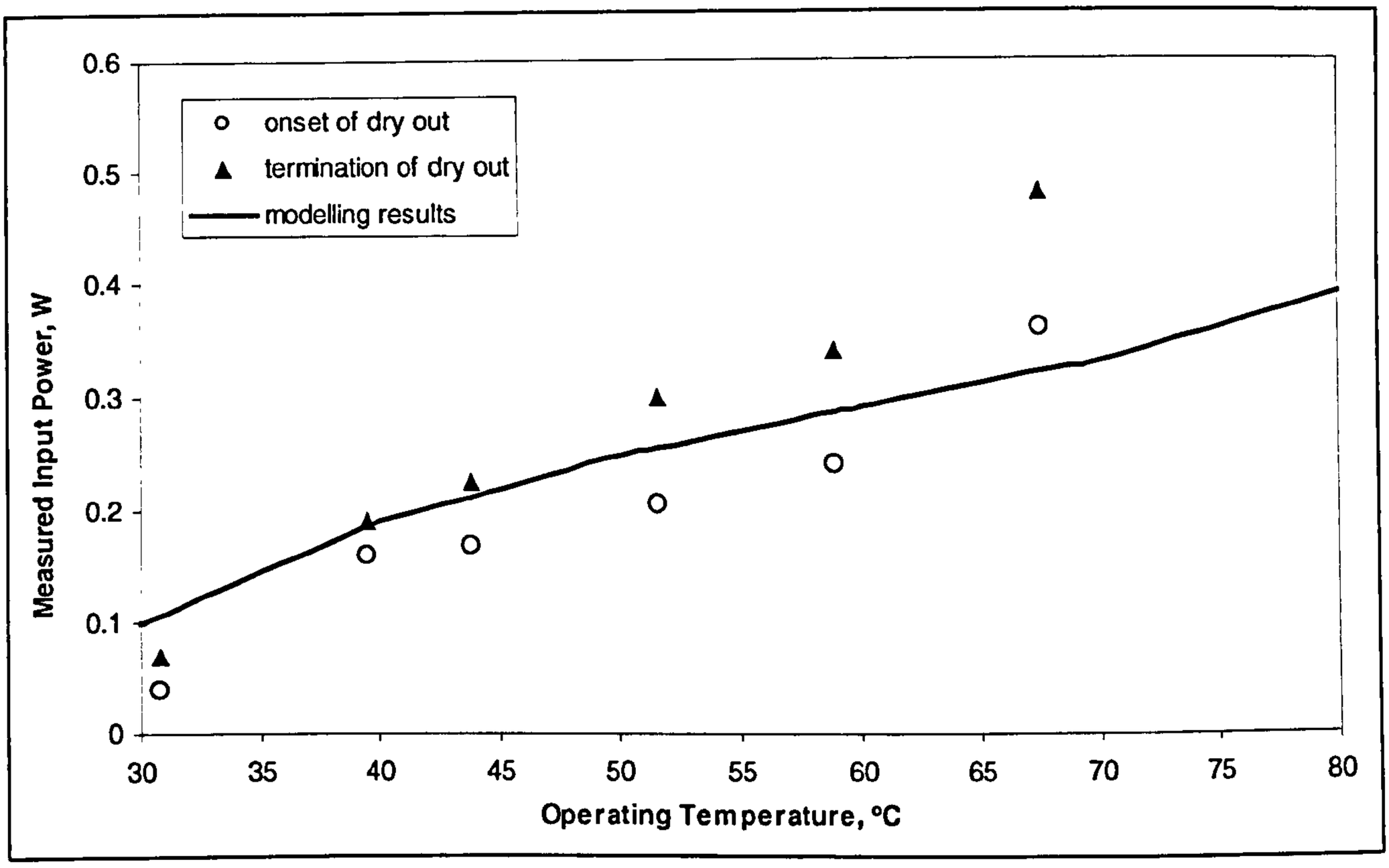

Figure 4-7. Comparison of the maximum heat transport capacity of a trapezoidal micro heat pipe as a function of the operating temperature (copper, 0.0032 g charge)

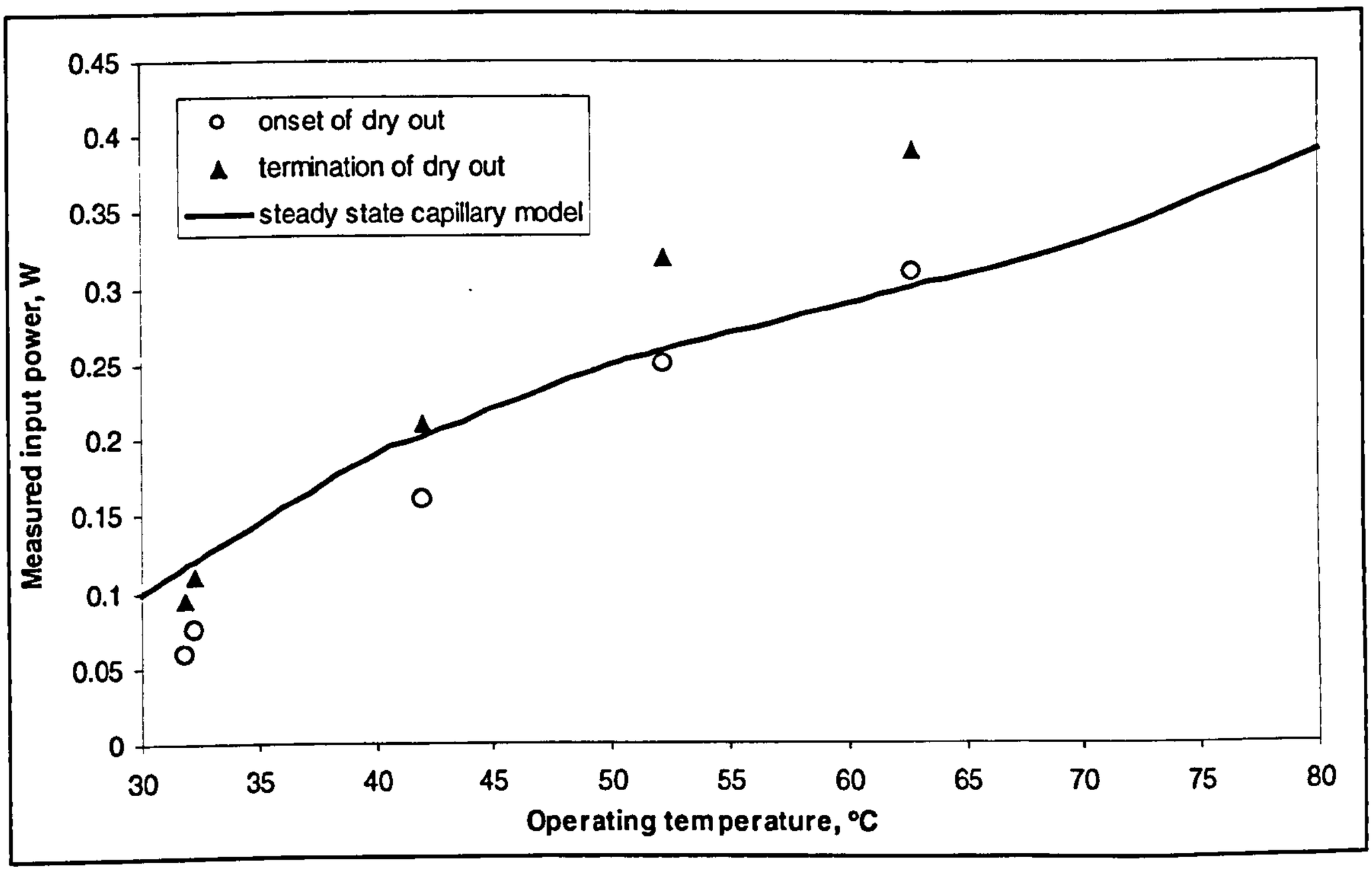

Figure 4-8. Comparison of the maximum heat transport capacity of a trapezoidal micro heat pipe as a function of the operation temperature (silver, 0.032 g charge)

4.4 Modelling of the Heat Transfer of the New Type Heat Pipe and Discussion

For the purpose of optimum designing the new type thermal diode, the modelling of the heat transfer of the new type thermal diode was carried out. Consider this new type thermal diode will work in two modes, i.e, cooling mode (in summer) and heating mode winter (in winter), a larger working temperature range is required. The working fluids n-pentane (working temperature range is -20°C~120°C) and HFE-7100 (working temperature range is -20°C~70°C) are suitable for this application and are used as working fluids in the modelling.

As mentioned in section 4.1, due to the particular structure of the new type thermal diode, it could be constructed for two cases: one uses wick to distribute liquid in the evaporator; another fills more liquid to keep the internal surface of the evaporator wet. The thermal performance of the two cases were investigated and compared. These related to the relations of the maximum heat transport capacity with liquid fill level, working temperature and thermal diode geometry dimension.

The analytical model was used to determine maximum heat transport capacity. The invariable parameters in the modelling are assumed, i.e., for both thermal diodes with and without wick, the lengths of the evaporator and condenser are 0.32m respectively, the lengths of the adiabatic section is 0.15m. For the thermal diode with wick, three layers of woven wire mesh (mesh count: 200) wick was assumed. These assumptions were in consistent with the testing condition of the thermal diode operation in the thermoelectric heat pump.

Relation between maximum heat transport capacity and working temperature

Figure 4-9 and Figure 4-10 show the relations between maximum heat transport capacity and working temperature for the thermal diodes with and without wick. These results were obtained by further assuming the cross section diameter to be 0.01m and the liquid fill level to be 0.08m.

The simulation results indicates that for the same values of the working temperature, the maximum heat transport capacities of the thermal diodes without wick (dominated by entrainment limts) are much greater than those with wick (dominated by capillary

limits), and increase obviously with the working temperature. For the maximum heat transport capacities, n-pentane is superior to HFE-7100.

Relation between maximum heat transport capacity and liquid fill level

Figure 4-11 and Figure 4-12 show the relations between maximum heat transport capacity and liquid fill level for the thermal diodes with and without wick. The results were obtained by further assuming the cross section diameter to be 0.01m and working temperature to be 45°C.

The simulation results indicates that the maximum heat transport capacities of the thermal diode with wick (dominated by capillary limits) increase with liquid fill level. When the liquid fill level is greater than 0.22m, the increase is significant. However, to use the wick in the new type thermal diode is intending not to use higher liquid fill level, the role of the wick is to distribute liquid from bottom of evaporator to the whole internal surface of the evaporator. Normally a liquid fill level of 1/3-1/4 of the evaporator length is suggested in a heat pipe [Dunn and Reay, 1982], in which cases, the maximum heat transport capacities of thermal diode with wick are only 18-19W for n-pentane pipe, 11-12W for HFE-7100 pipe.

The maximum heat transport capacities of the thermal diodes without wick remain constant and are much more than that with wick, if the liquid fill level is greater than 0.04m, for this condition the maximum heat transport capacities are dominated by entrainment limit. If the liquid fill level is less than 0.04m, the maximum heat transport capacities are dominated by dry out limit, which increases with the liquid fill level. The investigation suggests that the liquid fill level does not influence the maximum heat transport capacities if it is over 0.04m.

Relation between maximum heat transport capacity and cross section diameter

Figure 4-13 and Figure 4-14 show the relations between the maximum heat transport capacity and cross section diameter for the thermal diodes with and without wick. The results were obtained by further assuming the working temperature to be 45°C and liquid fill level to be 0.1m.

The heat transport capacities of the thermal diodes with and without wick increase obviously with the increase of the cross-section diameters.

For the same values of cross section diameter, the heat transport capacities of the thermal diodes without wick (dominated by entrainment limit) are much greater than those of the pipes with wick (dominated by capillary limit).

An analysis

The maximum heat transport capacities of the thermal diodes without wick, dominated by entrainment limit, are much greater than those of with wick under the various working temperatures, liquid fill levels and cross section diameters, while n-pentane and HFE-7100 are used as working fluids.

The maximum heat transport capacities of the thermal diode with wick, dominated by capillary limit, are much less because viscous pressure drop Δp_l [see Eq(4-17)] occurring in the liquid phase is greater. The reason for causing greater viscous pressure drop is smaller coefficient for liquid phase resistance calculation K and less latent heat of vaporisation of n-pentane and HFE-7100.

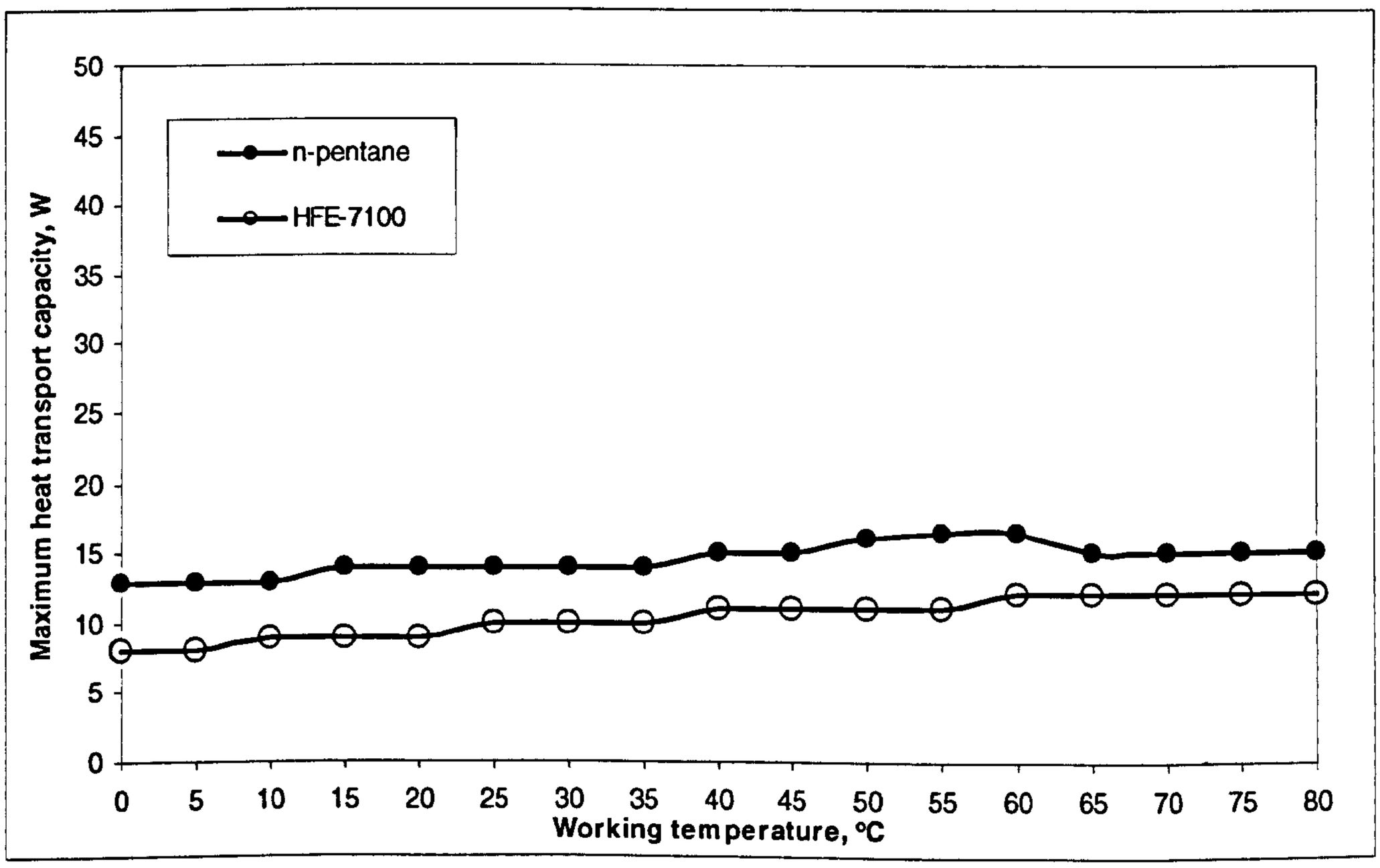

Figure 4-9. Relation between heat transport capacity and working temperature for pipe with wick

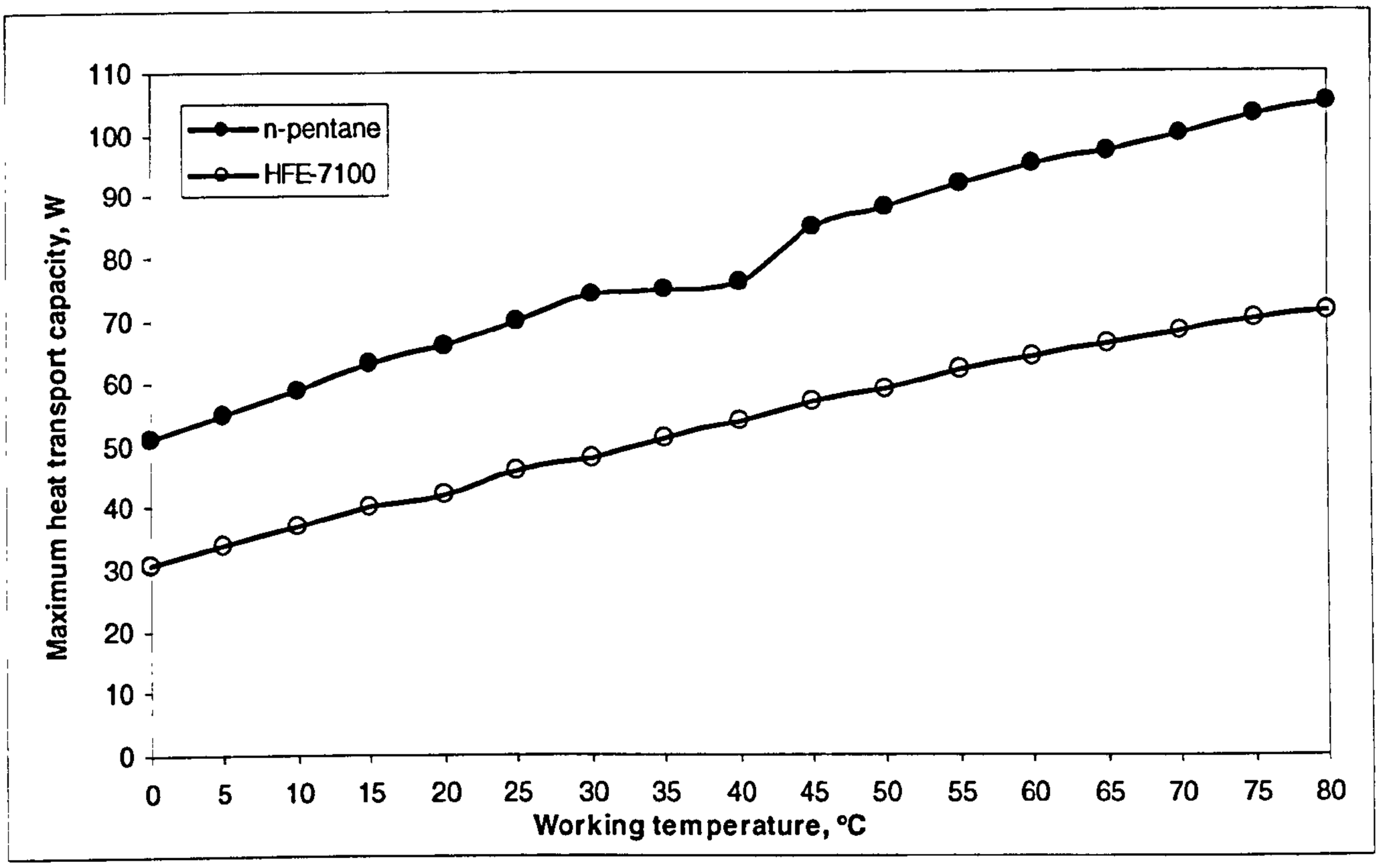

Figure 4-10. Relation between heat transport capacity and working temperature for the pipe without wick

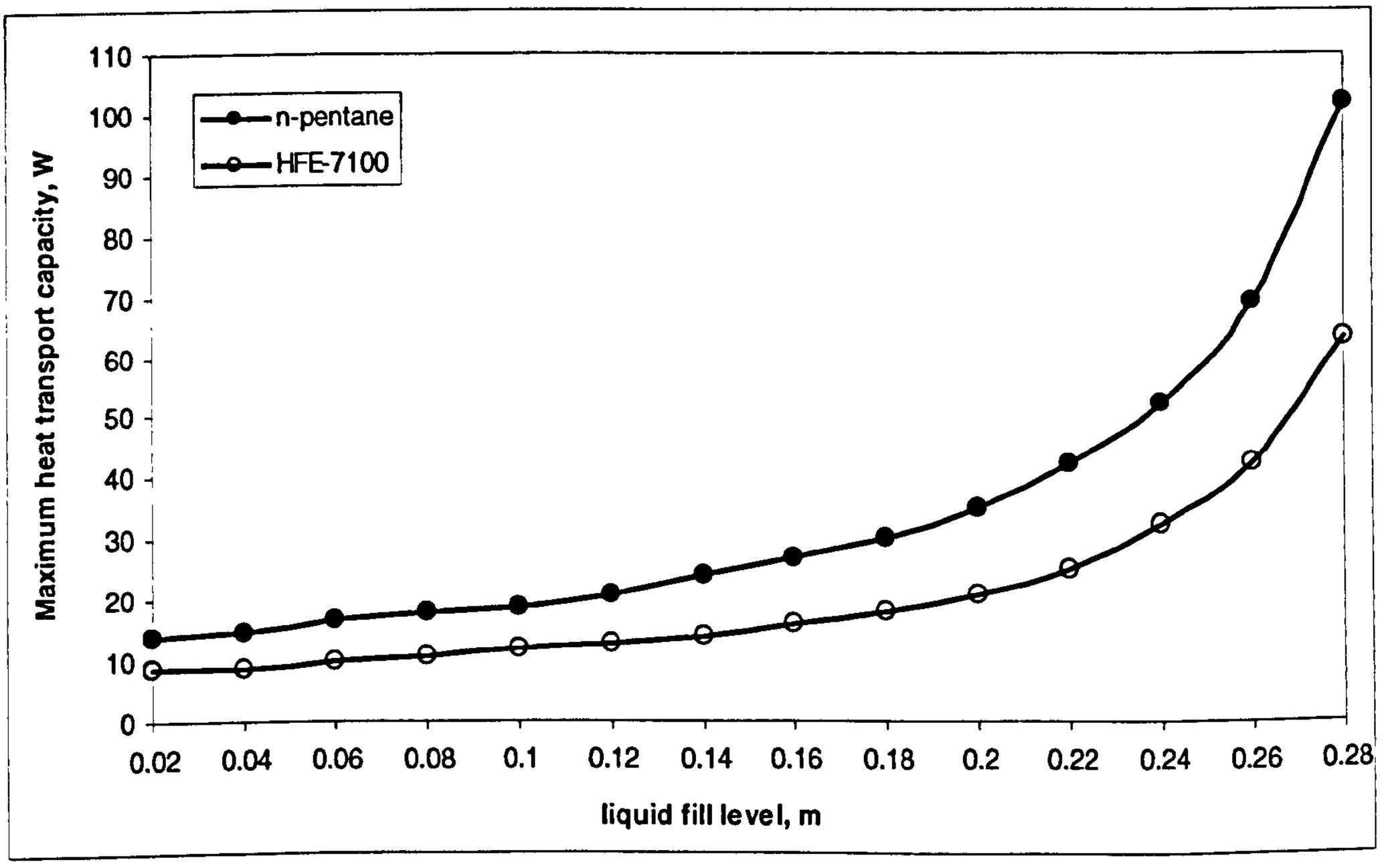

Figure 4-11. Relation between maximum heat transport capacity and liquid fill level for the pipe with wick

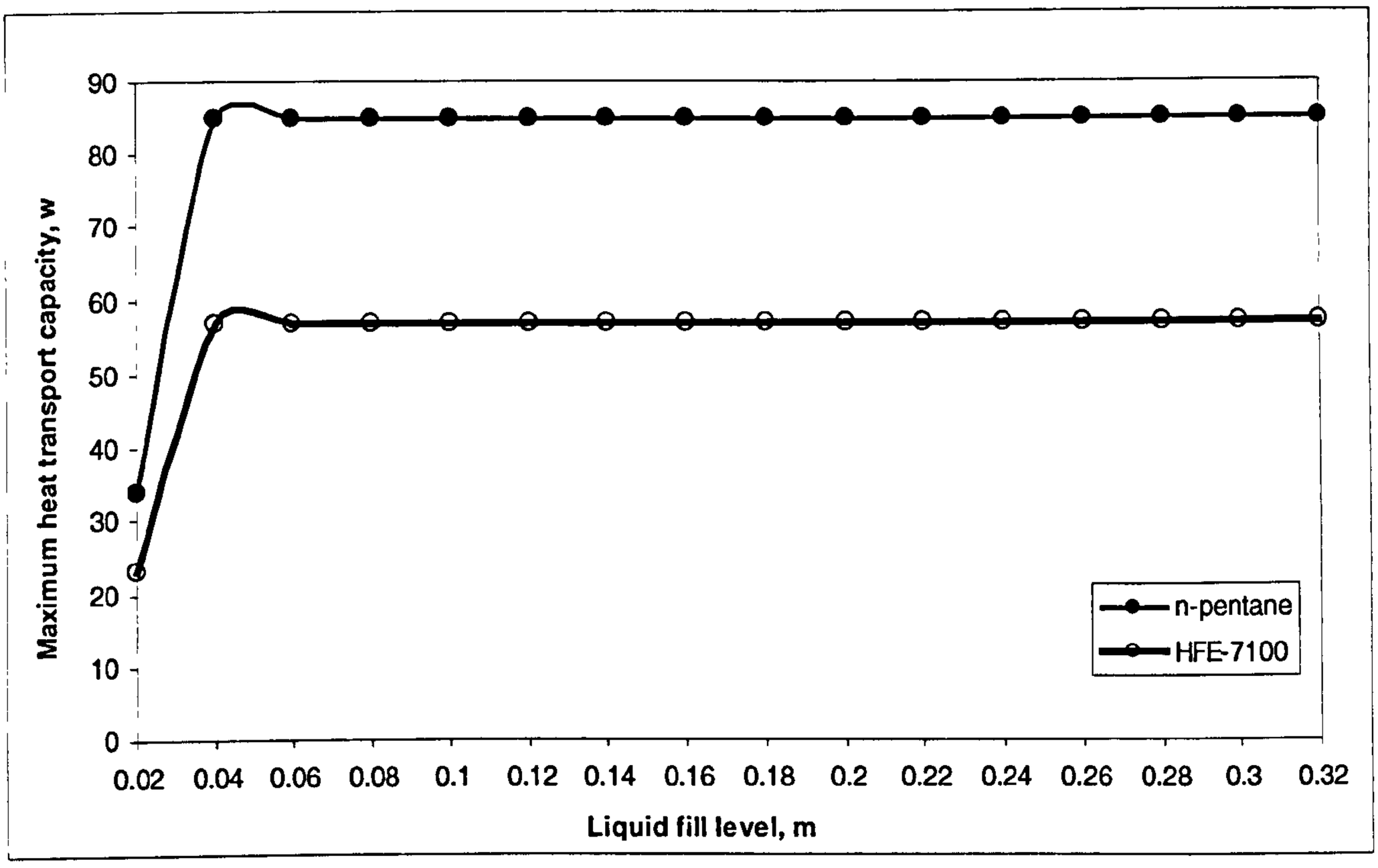

Figure 4-12. Relation between heat transport capacity and liquid fill level for the pipe without wick

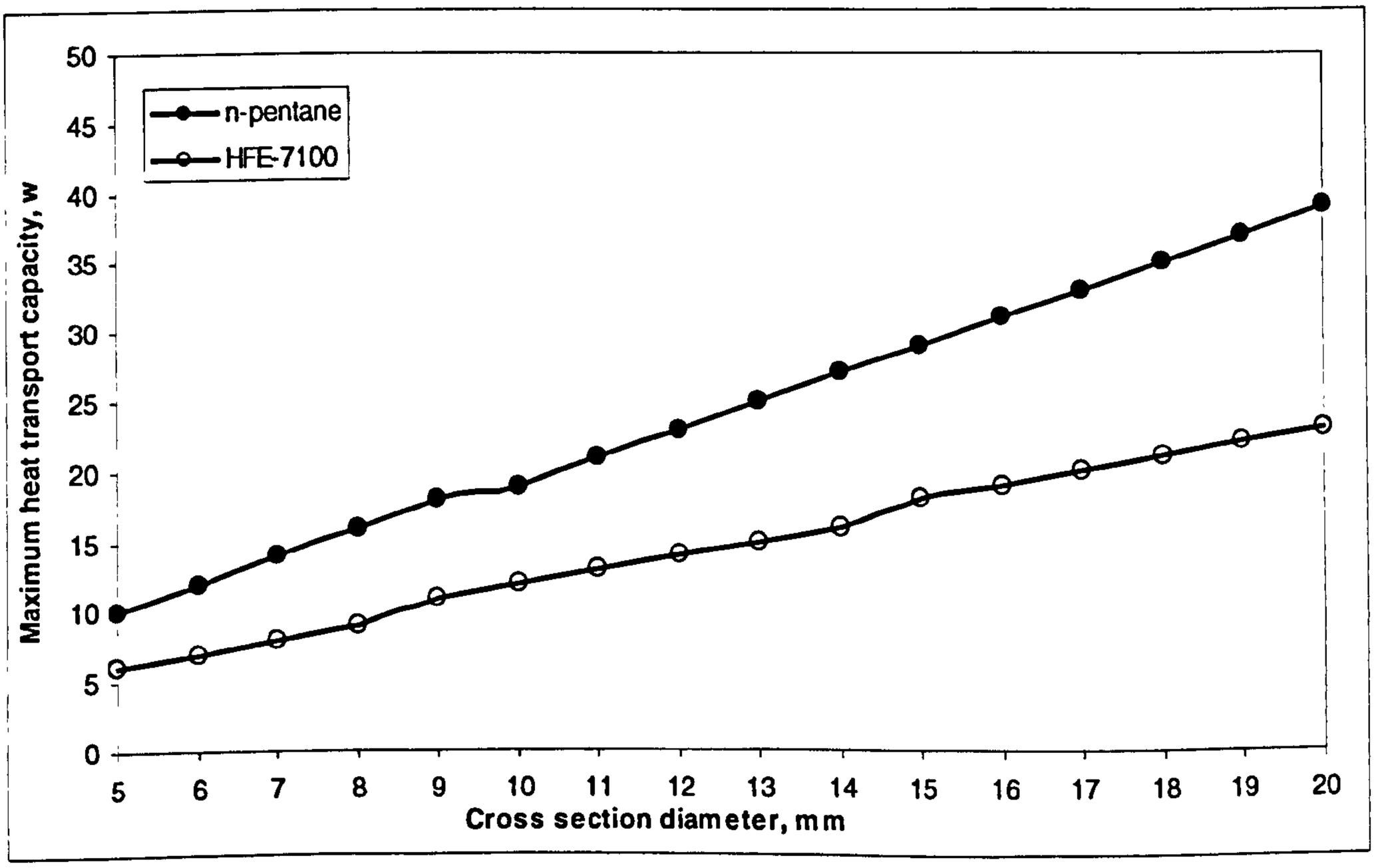

Figure 4-13. Relation between heat transport capacity and cross section diameter for the pipe with wick

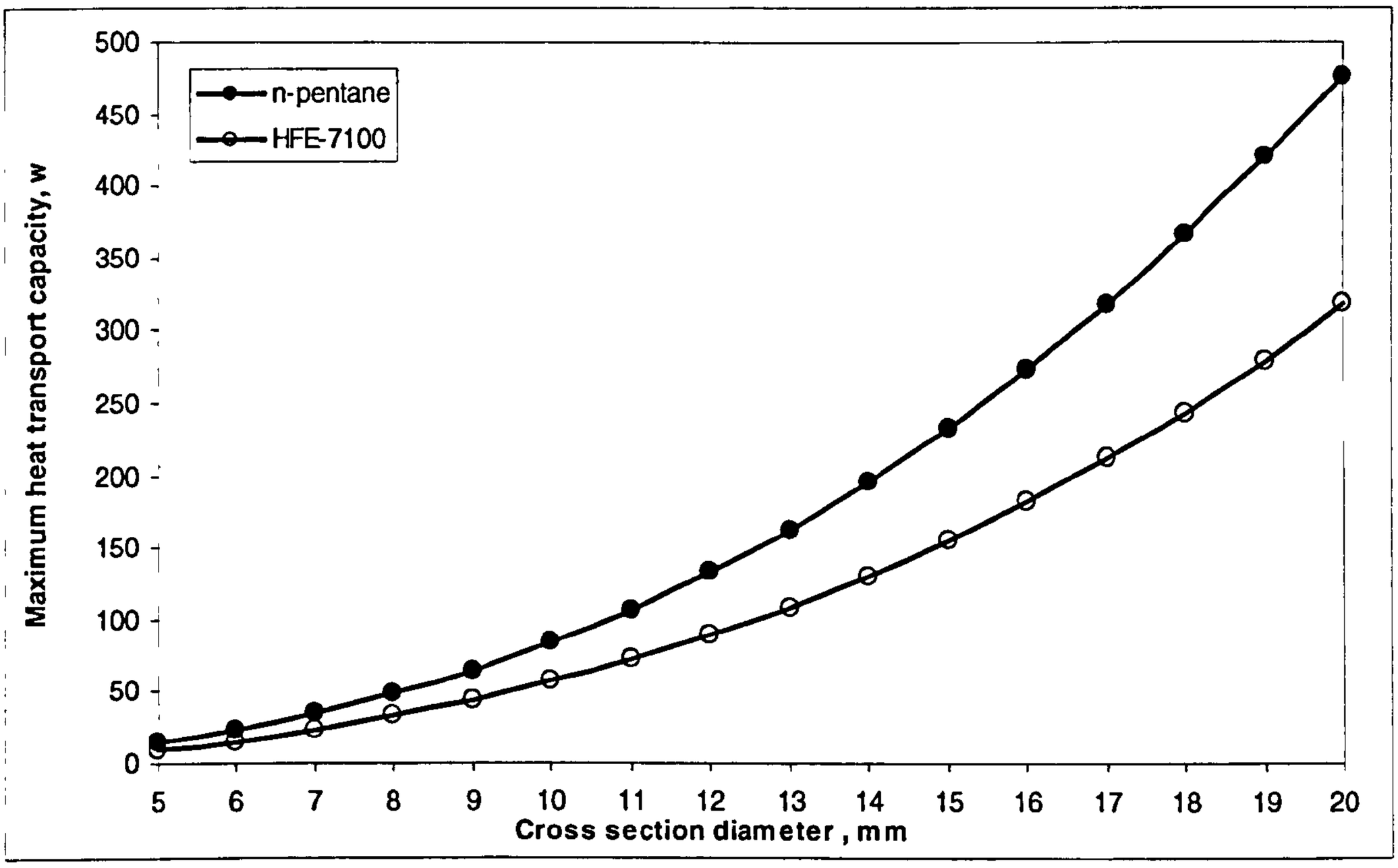

Figure 4-14. Relation between heat transport capacity and cross section diameter for the pipe without wick

4.5 Conclusion

The conventional heat pipes including normal heat pipes, micro/miniature heat pipes and a new type thermal diode, with/without wick, were illustrated in this chapter. The investigation of the conventional heat pipes provided the basis for investigation of a new type heat pipe.

An analytical model was developed to evaluate the thermal performance of all above heat pipes. The maximum heat transport capacity is taken as the index evaluating heat transfer capability of a heat pipe, which is governed by six limits, i.e., the sonic limit, the entrainment limit, the boiling limit, the viscous limit, the capillary limit and the filled liquid mass limit. The physical phenomena and mathematical theory involved with the process were indicated, and a computer program was developed based on the above analysis.

The modelling was carried out to analyse the thermal performance of the new type thermal diode that is intending to be used as the components of the novel thermoelectric heat pump. It was found that:

- The maximum heat transport capacities of the new type thermal diode without wick, dominated by entrainment limit, are much greater than that of with wick under the various working temperatures, liquid fill levels and cross section diameters, while n-pentane and HFE-7100 are used as working fluids.
- The maximum heat transport capacities of the new type thermal diode with wick, dominated by capillary limit, are much less because viscous pressure drop Δp_l [see Eq(4-17)] occurring in the liquid phase is greater. The reason that cause greater viscous pressure drop is smaller coefficient for liquid phase resistance calculation K and less latent heat of vaporisation of n-pentane and HFE-7100.
- The maximum heat transport capacities of the new type thermal diode without wick, dominated by entrainment limit, are greater and they increase with the increase of working temperature and cross section diameter, and remain constant for various liquid fill levels greater than 0.04m.
- For the maximum heat transport capacities of both thermal diodes with and without wick, n-pentane is superior to HFE-7100.

Chapter 5. Thermoelectric Heat Pump System

5.1 Design of the Thermoelectric Heat Pump Prototype System

A small-scale thermoelectric heat pump prototype system was designed to work in two modes, i.e., cooling mode and heating mode. It comprised of a new type thermal diode, eight thermoelectric modules and three heat sink units and two cooling fans, as shown in Figure 5-1. The system is mounted on one of the walls of a large box (1.22m×1.22m×1.22m), which was insulted on the inside by a 70mm thick polystyrene plate, held in place by wood plate of thickness 20mm. This box simulated a room for the experiment.

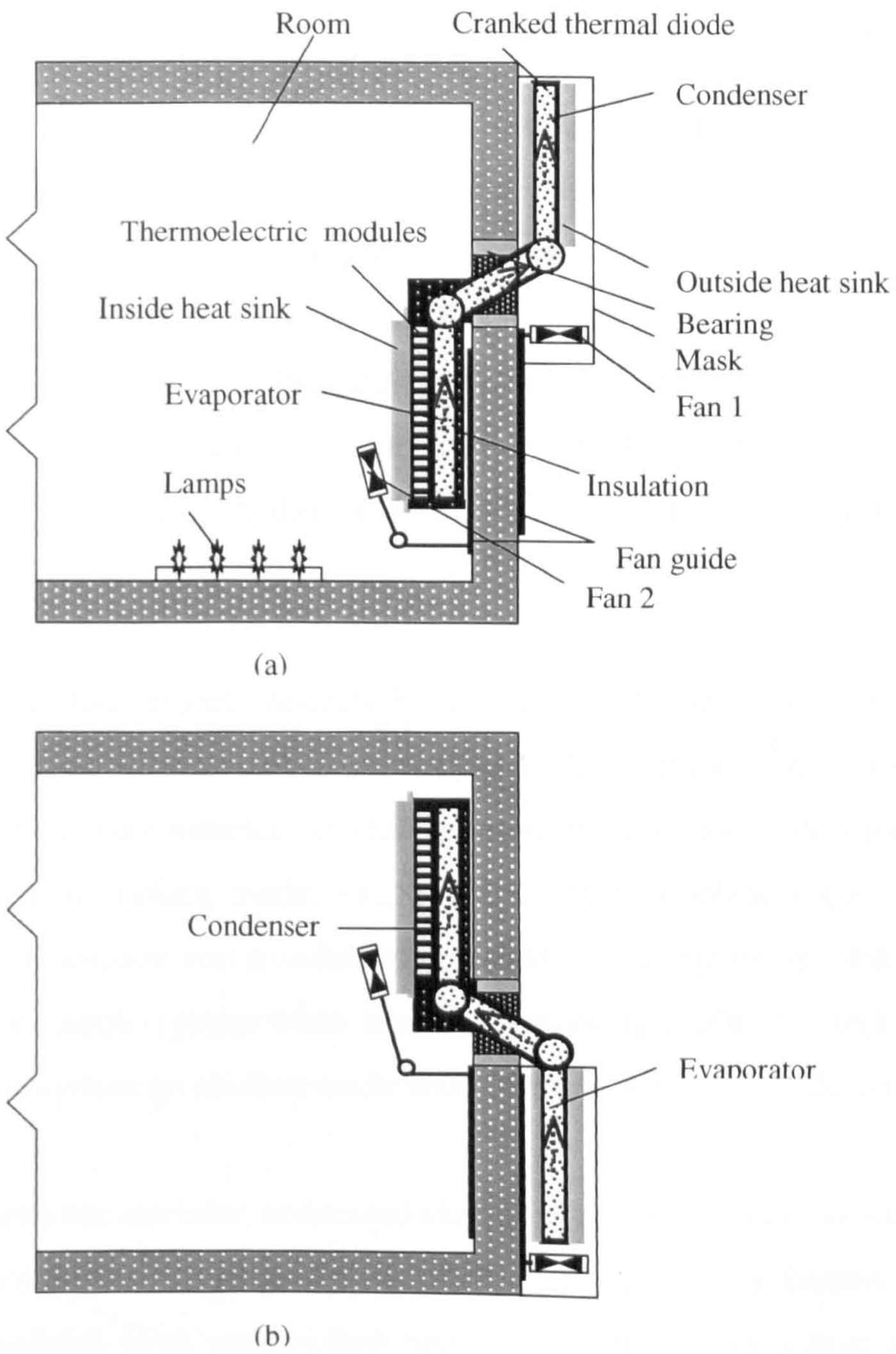

Figure 5-1. Schematic diagram of the thermoelectric heat pump (a) cooling mode (b) heating mode

Calculations have been carried out using the analytical model described in Chapter 4 to estimate the performance of the new type thermal diode that were used in this heat pump system. Since the new type thermal diode without wick has much higher heat transport capacity than that with wick, it was decided to use the new type thermal diode without wick for this application. The thermal diode was designed taking into account its suitable size to fit the total area of the thermoelectric modules, maximum heat transfer capacity and economy in manufacturing. The structure of the thermal diode is shown in Figure.1-1. The evaporator and condenser of the thermal diode are flat panels, which sizes are 320mm×150mm×15mm respectively. Each panel contains 11 circular holes of Ø10mm inside. The holes connect each other at the end to keep the working fluid inside the thermal diode at the same level. The adiabatic section is a circular tube with the length of 120mm. The angle between the flat panel and the adiabatic section is 120°, which incurs less resistance to fluid than an angle of 90°. A bearing is used to switch the thermal diode from cooling to heating mode, or the reverse. The flat panels and the adiabatic section are connected with headers. The adiabatic section and the headers are tubes with internal diameter of 50mm. The working fluid in this thermal diode is n-pentane, which has a work range of –20°C~120°C. The liquid fill level of the thermal diode is 0.3m. The maximum heat transport capacities of the thermal diode are 940W at a working temperature of 45°C (cooling mode), and 630W at a working temperature of 5°C (heating mode).

The optimum selection model described in Chapter 3 was used to select the thermoelectric modules used in this system. The eight thermoelectric modules (type CP2-127-06, Melcor) were selected to obtain optimum COP under designed severest working conditions in cooling mode, i.e., possible largest cooling capacity, possible highest hot side temperature and possible lowest cold side temperature. Due to the low COP of the thermoelectric system when working in cooling mode, the improvement of performance of the system on cooling mode was a main concern in this design.

The eight thermoelectric modules, connected electrically in series, were mounted side by side on the surface of one flat panel (located inside the box) of the thermal diode. The thermoelectric modules were sandwiched between the panel and a heat sink (called inside heat sink). Two heat sink units (called outside heat sink) were mounted on both

sides of another panel (located outside the box) of the thermal diode, as shown in Figure 5-1. The thermal contacts between all contacting surfaces were improved by applying a thin film of thermal grease. The panel with the mounted thermoelectric modules performed as an evaporator in the cooling mode, and a condenser in the heating mode, while the other panel located at outside the box performed as a condenser in the cooling mode, and an evaporator in the heating mode.

The heat sinks were designed being capable to dissipate the heat absorbed on the cold side and heat produced on the hot side. The inside heat sink was designed to have the thermal resistance of 0.133655 $^{o}CW^{-1}$ (when the air velocity is 1m/s; convective coefficient is13.97W/$m^{2o}C$). The outside heat sink was designed to have the thermal resistance of 0.123681 $^{o}CW^{-1}$ (when the air velocity is 2m/s; convective coefficient is 19.8W/$m^{2o}C$). Calculations have been carried out using the analytical method of the performance of finned heat sink described in Chapter 3 to determine dimensions and the number of fins of the heat sinks used in this heat pump system. The fins of the heat sinks were positioned vertically. Two cooling fans were used to provide air flow toward inside heat sink and outside heat sink respectively in the tests. The fan 1 is only used in the prototype system for laboratory test. For the real system mounted on the building, the fan 1 is not needed because the nature wind would provide the required airflow.

The heat pump system will work in two modes. In cooling mode, shown in Figure 5-1 (a), heat from the building is extracted by the thermoelectric modules. The heat causes the working fluid inside the thermal diode to boil and vaporise. As the vapour flows to the condenser section (situated outside the building) it condenses and releases heat to the ambient. Heat sinks and fans are used to help dissipating heat. The thermal diode is able to prevent reverse heat flow in the event of power failure. Four lamps (25W, 40W, 60W, 100W) were used in the prototype system to simulate heat sources in the testing.

In heating mode, the thermal diode will be rotated along the axis of the bearing to reverse the functions of the evaporator and condenser sections and also the direction of the DC power will be changed, as shown in Figure.5-1(b). A small fan (not shown in the figure) was mounted on the wall of the box to produce heat losses. Heat provided by the system to heat the interior of the box comes from two sources: one is electrical power;

and the other is the ambient air. Ambient heat extracted by the evaporator section of the thermal diode causes the working fluid to vaporise. As the vapour flows to the condenser section of the thermal diode, it condenses and releases heat to the thermoelectric modules. These upgrade the heat to a more useful temperature that can then be used for space heating in the box (room).

5.2 Analytical Model Set-up

An analytical model has been developed to simulate the performance of the novel thermoelectric heat pump system under various operating and weather conditions.

A number of heat processes exist in various areas of the thermoelectric heat pump. The processes would proceed until balance states are achieved and would be inter-linked by developing the analytical model.

Formulas

The following formulas show relations for the various parameters in the system, and are useful for setting up the analytical model.

Heat balance equation across the inside heat sink:

$$T_c=T_{in}-Q_cR_c \qquad \text{(for cooling mode)} \qquad (5\text{-}1c)$$

$$T_h=Q_hR_c+T_{in} \qquad \text{(for heating mode)} \qquad (5\text{-}1h)$$

Average temperature of the hot and cold side of the thermoelectric modules:

$$Tm=(T_h+T_c)/2 \qquad (5\text{-}2)$$

Temperature difference between the hot and cold side of the thermoelectric modules:

$$\Delta T=T_h-T_c \qquad (5\text{-}3)$$

Heat balance equation across the thermal diode and outside heat sink*:

$$Q_h=(T_h-T_a)/(R_h+R_{hp}) \qquad \text{(for cooling mode)} \qquad (5\text{-}4c)$$

$$Q_c=(T_a-T_c)/(R_h+R_{hp}) \qquad \text{(for heating mode)} \qquad (5\text{-}4h)$$

Power consumption:

$$P_e=Q_h-Q_c \qquad (5\text{-}5)$$

Calculation of COP by its definition:

$$COP=COP_1=Q_c/P_e \quad \text{(for cooling mode)} \tag{5-6c}$$

$$COP=COP_1=1+Q_c/P_e \quad \text{(for heating mode)} \tag{5-6h}$$

Operating current:

$$I=(2NaT_c-\sqrt{(2NaT_c)^2-4Np(Q_c+2Nk\Delta TG)/G})/(2Np/G) \tag{5-7}$$

Calculation of COP by formulae of thermoelectric module performance analysis:

$$COP=COP_2=[\alpha ITc-k\Delta TG-I^2p/(2G)]/(I^2p/G+\alpha I\Delta T) \quad \text{(for cooling mode)} \tag{5-8c}$$

$$COP=COP_2=1+[\alpha ITc-k\Delta TG-I^2p/(2G)]/(I^2p/G+\alpha I\Delta T) \quad \text{(for heating mode)} \tag{5-8h}$$

The material property coefficients α, p and k are shown in Appendix A.

* ***Calculation of thermal resistances of the thermal diode***

Eq(5-4c) and Eq(5-4h) require values of the thermal resistance of the thermal diode, which can be calculated by a subroutine. The calculation of this thermal resistance is detailed below.

The heat extracted by the evaporator on the hot side will be transported to the outside heat sink (in cooling mode) or cold side of the thermoelectric modules (in heating mode) through evaporation and condensation of the working fluid in the heat pipes. There are several heat resistances in this process, namely, the evaporator wall resistance, the equivalent resistance of the working fluid in the evaporator, the vapour flow resistance, the equivalent resistance of the working fluid in the condenser, and condenser wall resistance. These resistances may be expressed as follows [Dunn P.D. and Reay D.A.,1982]:

Evaporator wall resistance:

$$R_{p,e}=\frac{r_0^{\,2}\ln(r_0/r_{ie})}{2l_ek_p} \tag{5-9}$$

Evaporator saturated wick (liquid film for heat pipe without wick) resistance:

$$R_{w,e}=\frac{r_0^{\,2}\ln(r_{ie}/r_v)}{2l_ek_e} \tag{5-10}$$

Vapour flow resistance:

$$R_{v,p} = \frac{\pi r_0^{\,2} f_v T_v (l_e/6 + l_a + l_c/6)}{\rho_v \lambda J} \tag{5-11}$$

Condenser saturated wick (liquid film for heat pipe without wick) resistance:

$$R_w = \frac{r_0^{\,2} \ln(r_{i,c}/r_{v,c})}{2 l_c k_e} \tag{5-12}$$

Condenser wall resistance:

$$R_{p,c} = \frac{r_0^{\,2} \ln(r_{0,c}/r_{i,c})}{2 l_c k_p} \tag{5-13}$$

Total resistance:

$$R_{hp} = R_{p,e} + R_{w,e} + R_{v,p} + R_w + R_{p,c} \tag{5-14}$$

Structure of the Model

For an existing system, the known parameters for a simulation are cooling capacity Q_c (cooling mode) or heating capacity Q_h (heating mode), and the inside room T_{in} and ambient temperature T_a. These parameters are insufficient to calculate operating current and COP by using the above formulas directly. An analytical model with a loop block is required to solve this problem. The flow chart of the model is shown in Figure 5-2. The program in C++ language is shown in attached disk (program D).

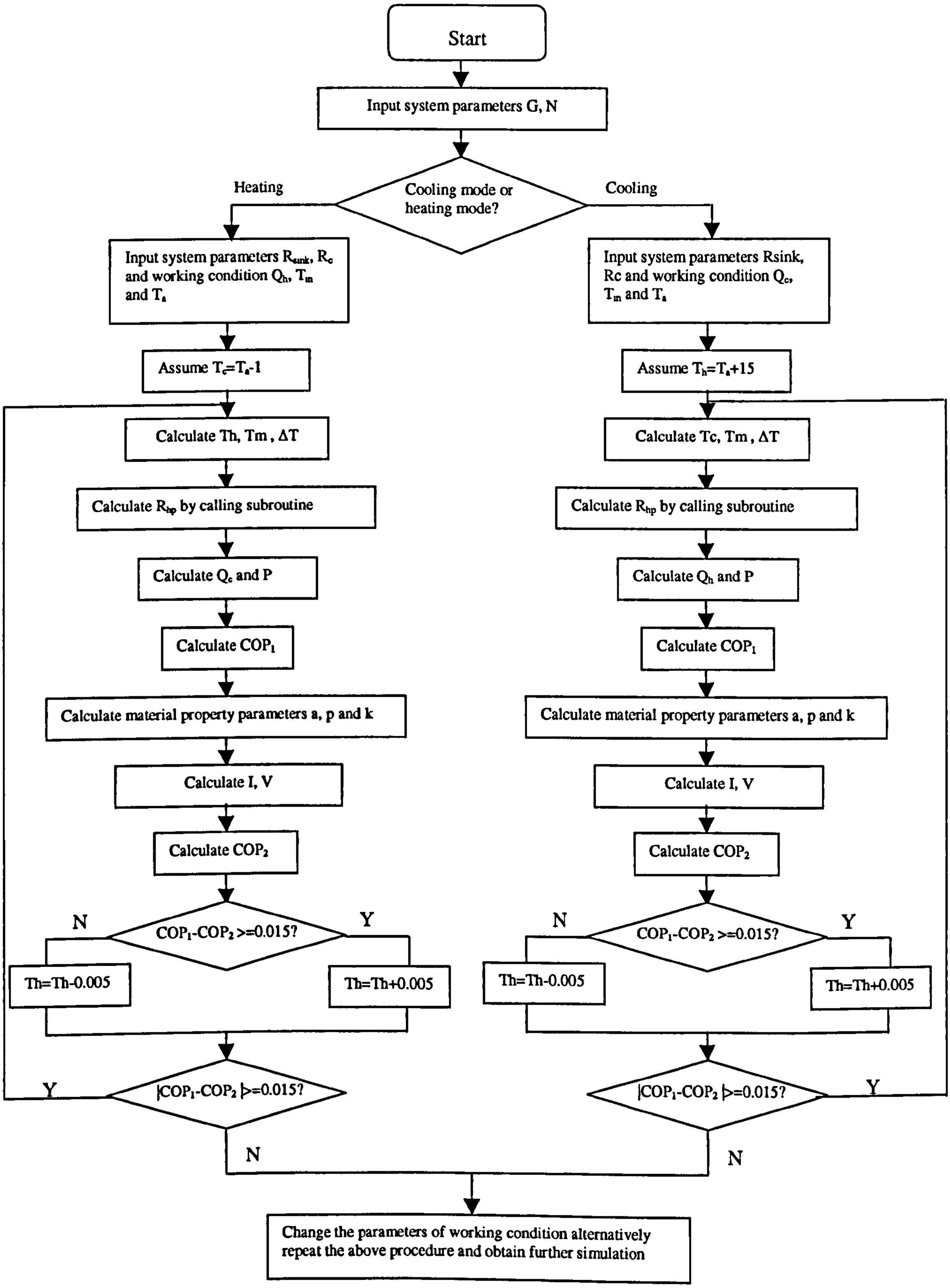

Figure 5-2. Flow chart of the system simulation model

5.3 Modelling of the Performance of the Heat Pump Prototype System and Discussion

The analytical model was used to simulate the performance of the heat pump prototype system. The simulation results were obtained for various operating and weather conditions, for both cooling mode and heating mode. The required operating currents under these conditions were also shown. For the fixed system, the operating voltage is a function of operating current I, hot and cold side temperature T_h, T_c. This relation can be seen in Eq(3-5).

5.3.1 Modelling of Cooling Mode

The simulation was carried out for various cooling capacities by assuming the temperature inside room to be 21°C when the heat balance is achieved and the ambient temperature to be 24°C. The results are shown in Figure 5-3. It can be seen that the COP decreases and the operating current increases with the increase of the cooling capacity. Due to more heat to be conducted, which requires larger temperature difference across the inside heat sink, the cold side temperature will therefore decrease when the inside room temperature is fixed. Furthermore, the increasing cooling capacity and power consumption leads to more heat to be conducted by the thermal diode and the outside heat sink, which requires larger temperature difference across the two components, the hot side temperature will therefore increase when the ambient temperature is fixed. Figure 5-4 shows the variation of the hot and cold side temperatures of the thermoelectric modules with cooling capacity, which was obtained by the modelling. The increasing temperature difference between hot and cold side will decrease the COP of the thermoelectric modules, and therefore further increase the required operating current, this relation can be seen in Eq(5-7) and Eq(5-8c).

The simulation was also carried out for various ambient temperatures by assuming the temperature inside room to be 21°C when the heat balance is achieved and no heat sources inside the room. The results are shown in Figure 5-5. It is seen that the operating current increases and the COP decreases with the increase of the ambient temperature. This is because increasing ambient temperature requires increasing hot side temperature to keep the required temperature difference across the thermal diode and outside heat sink. Furthermore, due to the increase of the ambient temperature, the heat transfer from

the environment to the interior of the room increases, therefore, more heat needs to be conducted out to keep the temperature inside the room to be 21°C and more power consumption is required. This requires increasing temperature difference across the inside heat sink, which therefore leads to the cold side temperature to decrease. The variation of the hot and cold side temperatures of the thermoelectric modules with ambient temperature is shown in Figure 5-6. The increasing temperature difference between hot and cold side of thermoelectric modules decreases the COP and further increases the power consumption.

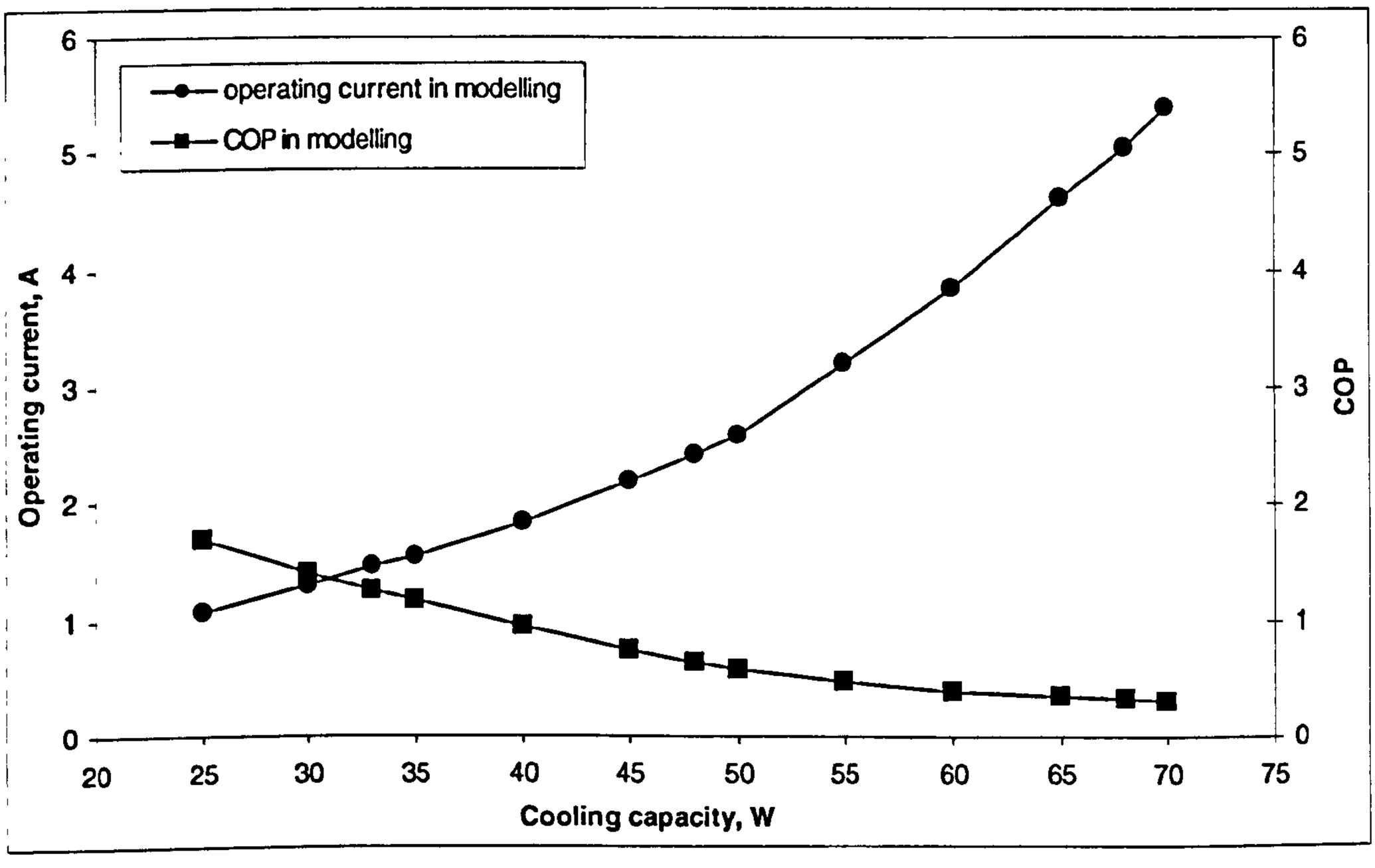

Figure 5-3. Variation of operating current and COP with cooling capacity in modelling [$V=-1.4I^2+17.6I-4.4(V)$]

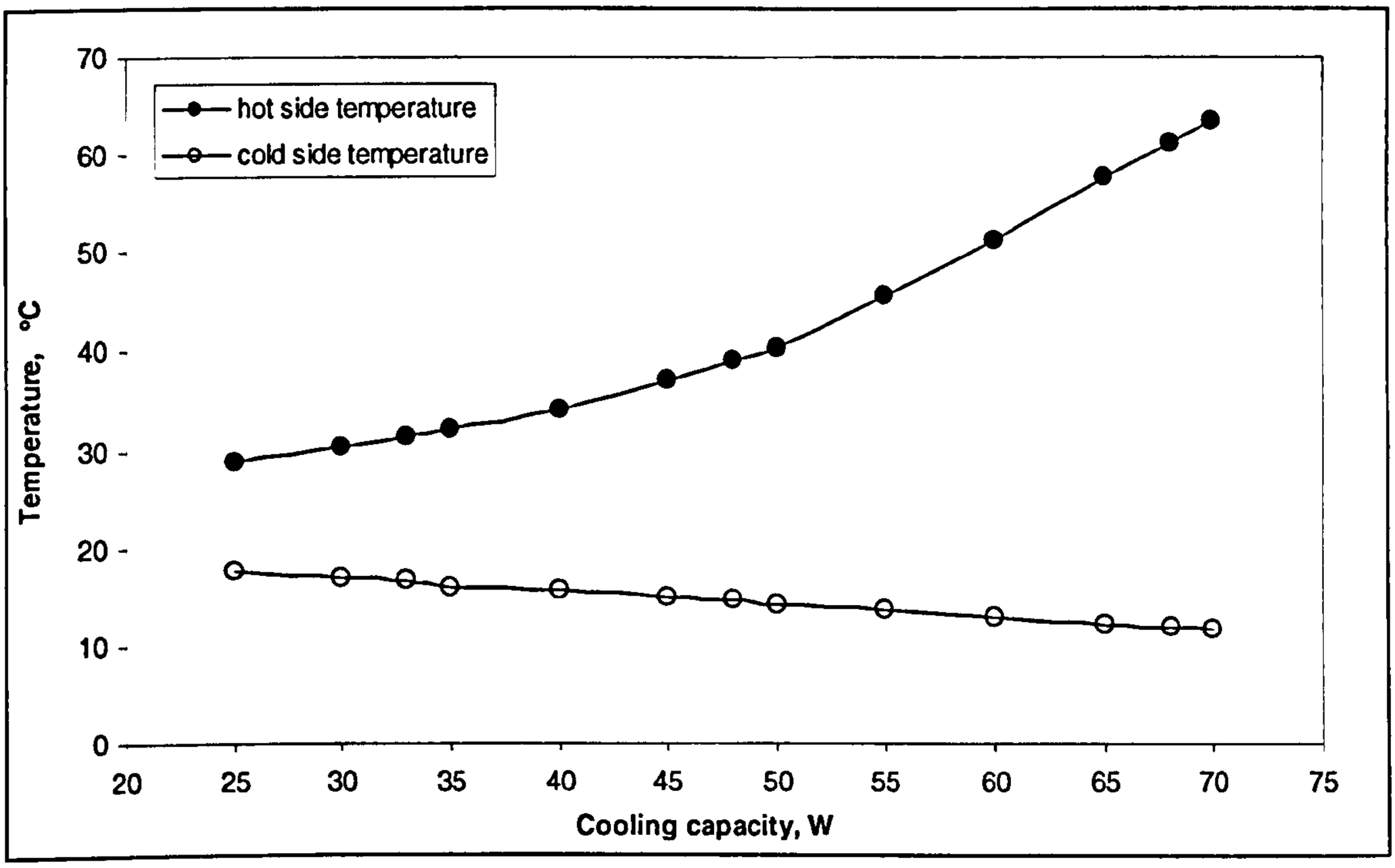

Figure 5-4 Variation of hot side and cold side temperatures of thermoelectric modules with cooling capacity in modelling

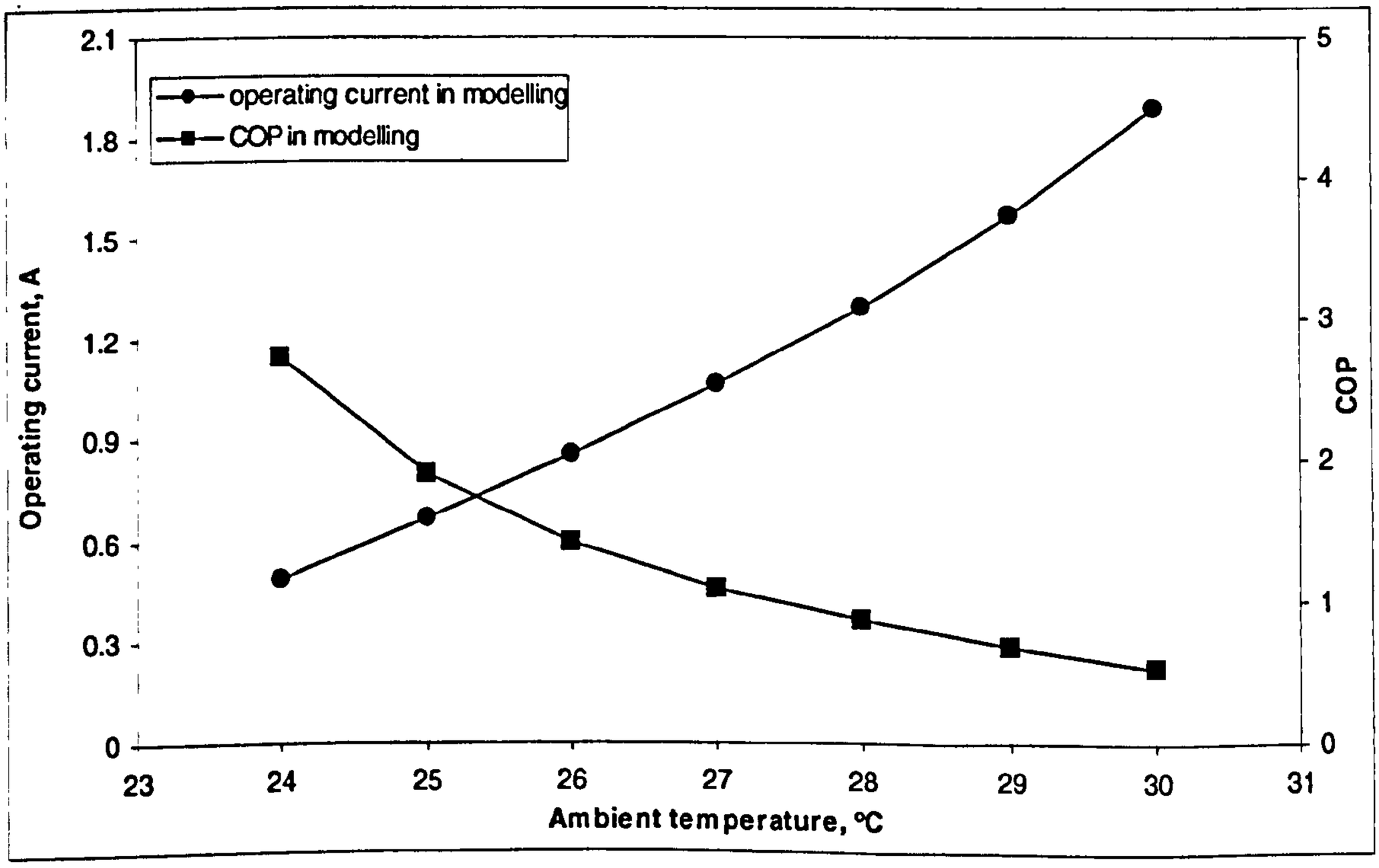

Figure 5-5 Variation of operating current and COP with ambient temperature in cooling mode in modelling[$V=0.14I^2+12.7I-0.11(V)$]

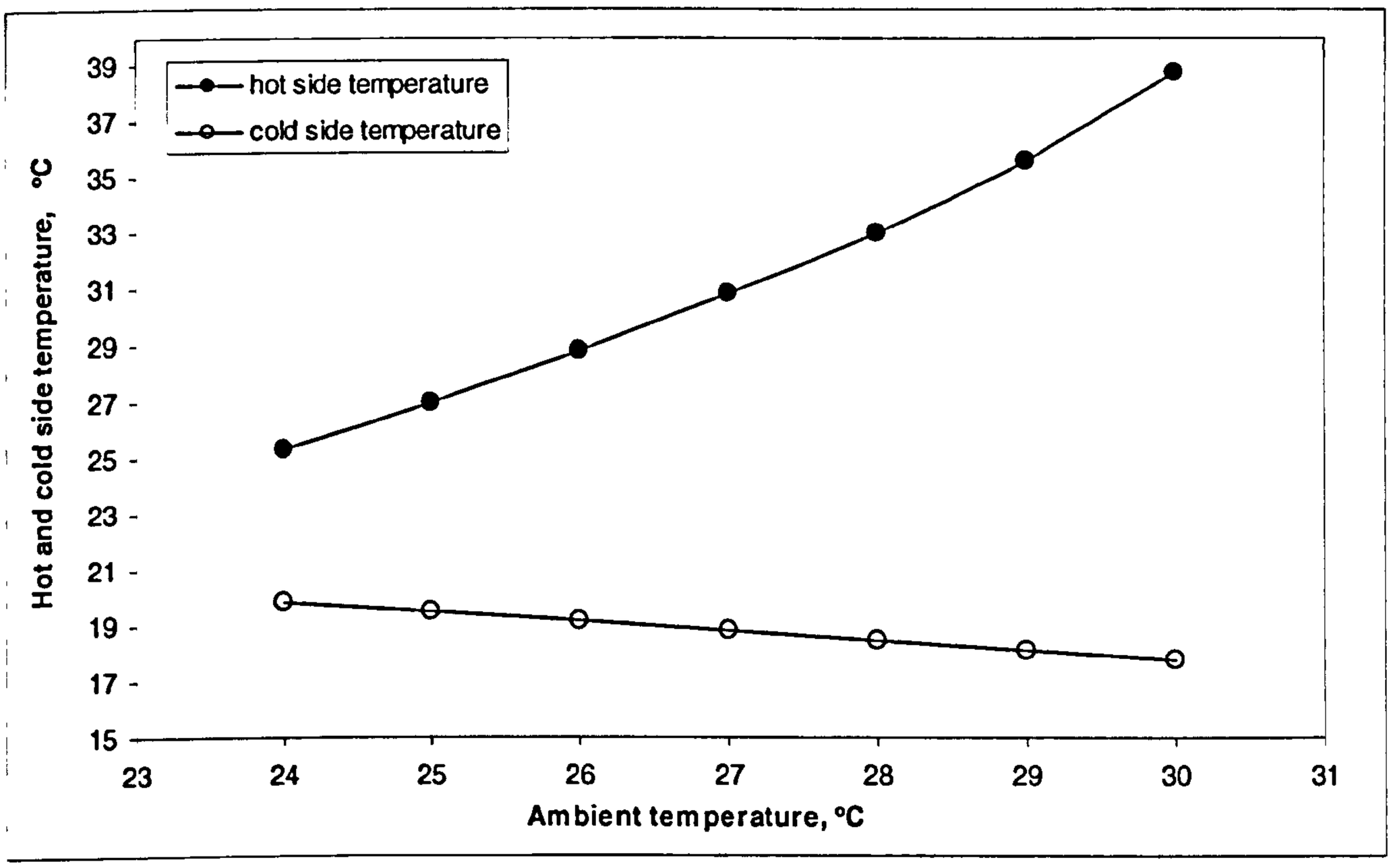

Figure 5-6. Variation of hot side and cold side temperatures of thermoelectric modules with ambient temperature in cooling mode in modelling

5.3.2 Modelling of Heating Mode

The simulation was carried out for various heating capacity by assuming temperature inside room to be 18°C when the heat balance is achieved and the ambient temperature to be 5°C. The results are shown in Figure 5-7. It is seen that the operating current increases and the COP decreases with the increase of the heating capacity. Due to more heat to be conducted to the inside room, which requires larger temperature difference across the inside heat sink, the hot side temperature will increase when the inside room temperature is fixed. Due to more heat is conducted from the ambient to the cold side of the modules, which requires larger temperature difference across the thermal diode and the outside heat sink, the cold side temperature will decrease when the ambient temperature is fixed. Furthermore, larger heating capacity requires more power consumption in the system, this is further increasing operating current and temperature difference between the hot and cold side. Figure 5-8 shows the variation of the hot and cold side temperatures of the thermoelectric modules with heating capacity obtained by modelling. The increasing temperature difference between hot and cold side of

thermoelectric modules decreases the COP, and therefore further increase the required operating current, this relation can be seen in Eq(5-7) and Eq(5-8h).

The simulation was also carried out for various ambient temperatures by assuming the temperature inside room to be 18°C when the heat balance is achieved. The results are shown in Figure 5-9. It is seen that the operating current decreases and the COP increases with the increase of the ambient temperature. Due to the increase of the ambient temperature, the heat loss from the inside the room to ambient decreases, therefore, less heat requires to be conducted by the system to keep the temperature inside the room to be 18°C. This requires less temperature difference across the inside heat sink, which leads to the hot side temperature to decrease. Furthermore, the more important reason for the cold side temperature to increase is the increasing ambient temperature itself. The increase of the ambient temperature increases the working temperature of the thermal diode. This causes the cold side temperature increase. Decrease of the heat transfer by the thermoelectric modules requires less electric power to be consumed in the system, this is why the operating current is decreased. Figure 5-10 shows the variation of the hot and cold side temperatures of the thermoelectric modules with ambient temperature in heating mode, obtained by modelling. The decrease of the temperature difference between hot and cold side of thermoelectric modules increases the COP.

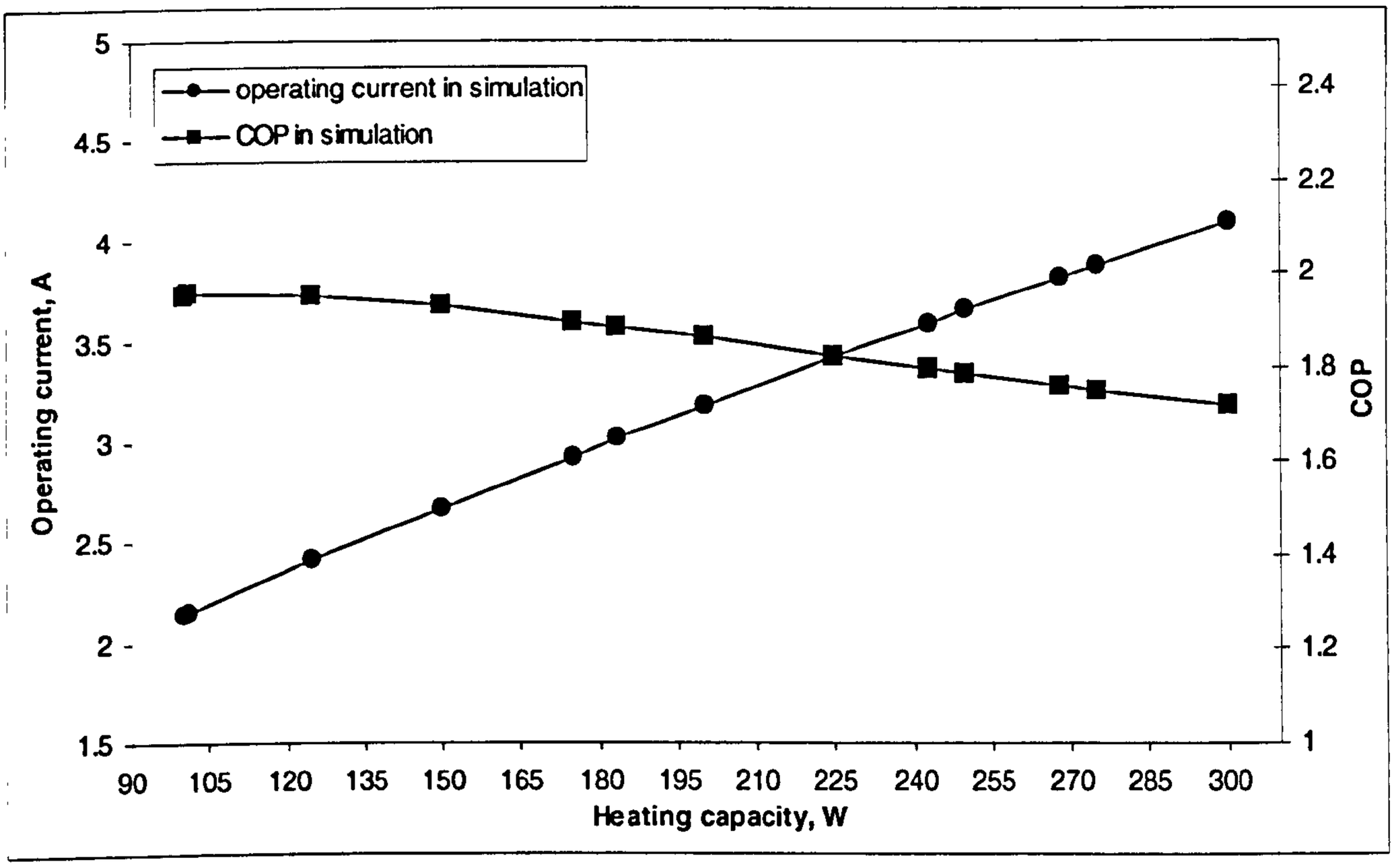

Figure 5-7 Variation of operating current and COP with heating capacity in modelling [$V=-2.5I^2+24.9I-19(V)$]

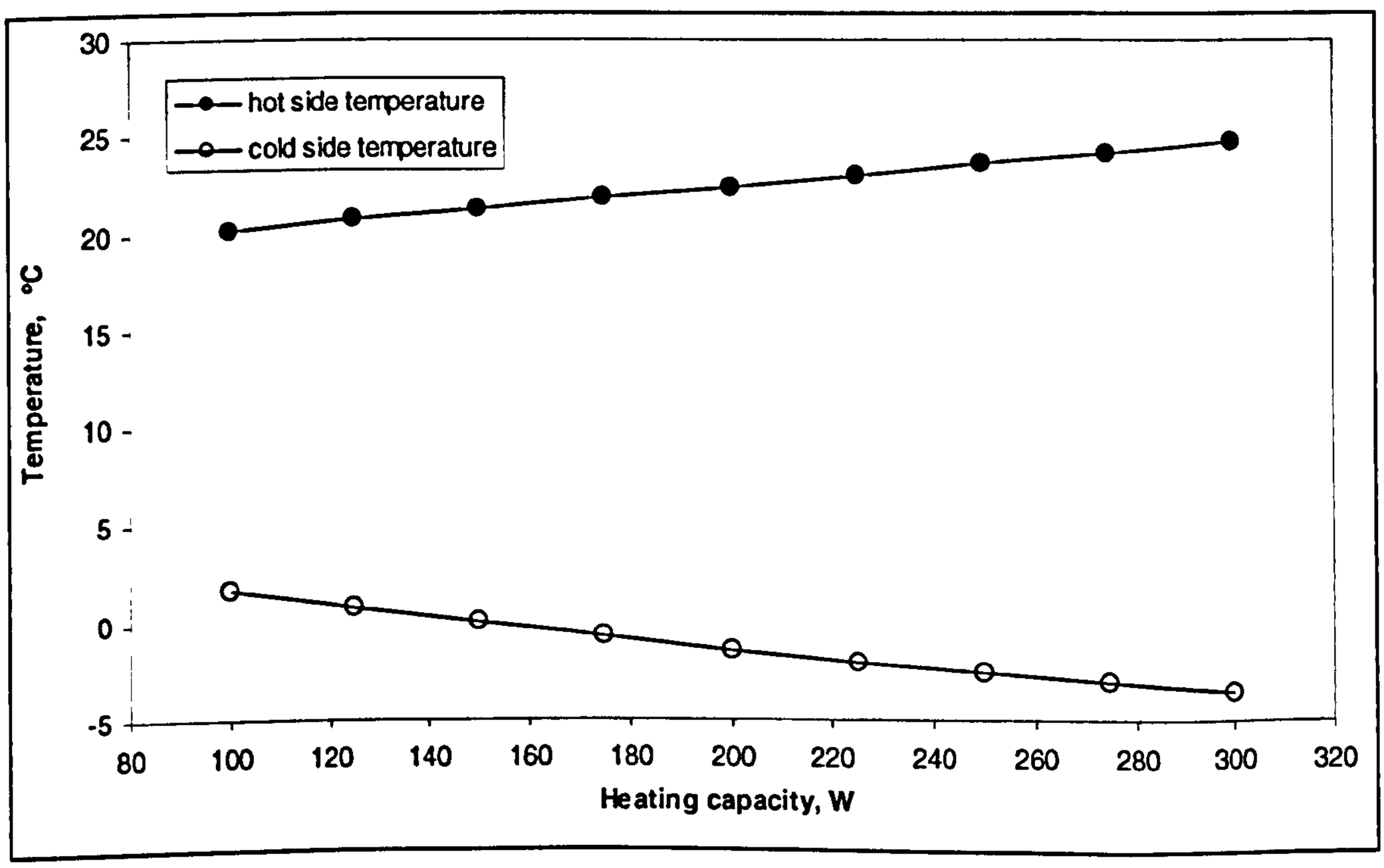

Figure 5-8 Variation of hot side and cold side temperatures of thermoelectric modules with heating capacity in modelling

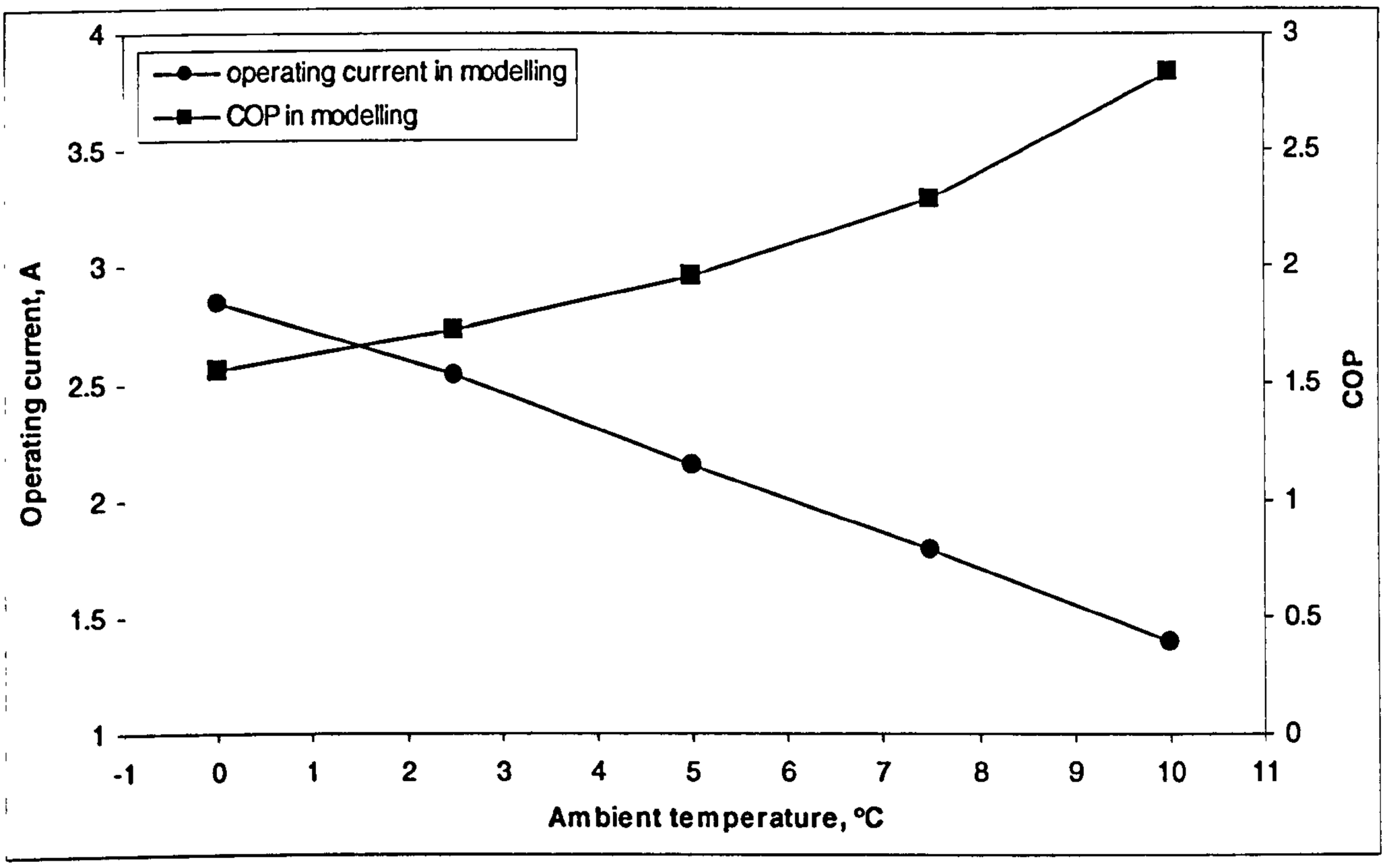

Figure 5-9. Variation of operating current and COP with ambient temperature in heating mode in modelling[$V=0.2I^2+10I+1.1(V)$]

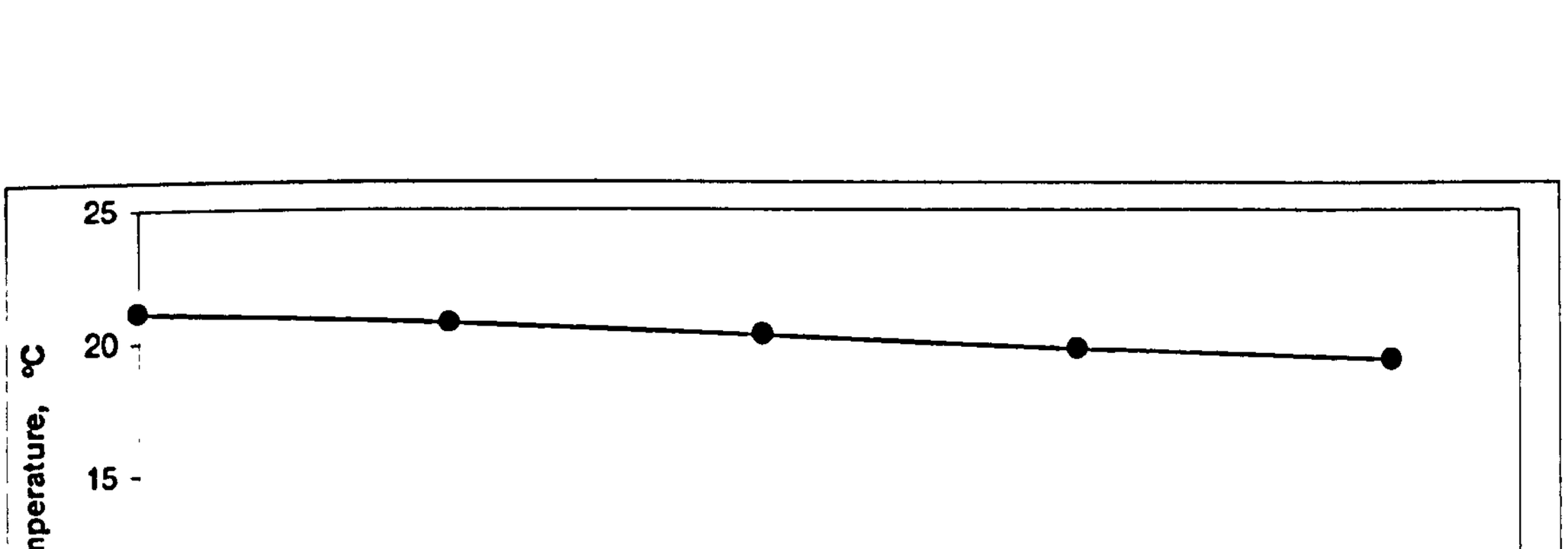

Figure 5-10. Variation of hot side and cold side temperatures of thermoelectric modules with ambient temperature in heating mode in modelling

5.4 Experimental Testing

The heat pump prototype was fabricated and tested at laboratory of School of the Built Environment, University of Nottingham. Photograph of the new type thermal diode is shown in Figure 5-11. Photographs of the heat pump are shown in Figure.5-12(a) and Figure.5-12(b). In Figure 5-12(b), the heat sink is taken off and the mounted thermoelectric modules are shown. As mentioned in section 5.1, the thermoelectric heat pump prototype was mounted on a larger box that simulates a room. The larger box was located in an environment chamber in the laboratory. A control system for the test process was located at outdoors of the environment chamber. The photograph of the test control system is shown in Figure 5-13. /The test control system included an environmental chamber temperature controller, a computer and an adjustable DC power supply. By adjusting the environmental temperature controller, the environment chamber provided various ambient temperatures for the large box. The computer that connected to a data taker was used to monitor the heat transfer process and collect data. The adjustable DC power supply was used to provide various DC currents for different tests and adjustable DC current to fit the required power in a test. The tests were carried out by cooling (in cooling mode) and heating (in heating mode) the interior of the large box at various operating conditions and ambient temperatures. The photographs of the test system are shown in Figure 5-14 (a) and Figure 5-14 (b). Figure 5-14 (a) shows the layout of the test system. The two small fans were used to produce air flow toward the inside and outside heat sink respectively (the big blue fan is just used to heat up the interior of the box quickly when a test is finished and not belongs to this system). Figure 5-14 (b) shows the system in operating. A duct covering the outside heat sink and fan made the wind produced by the fan to be used effectively. The temperatures were measured at various positions, including cold and hot side of the thermoelectric modules (TECs), evaporator and condenser of the heat pipe, the interior of the box and the environment. T-type thermocouples (Figure 5-15) were used to measure the temperatures. The measured data was acquired by the Datataker DT 500 (Figure 5-16) and transferred to the computer.

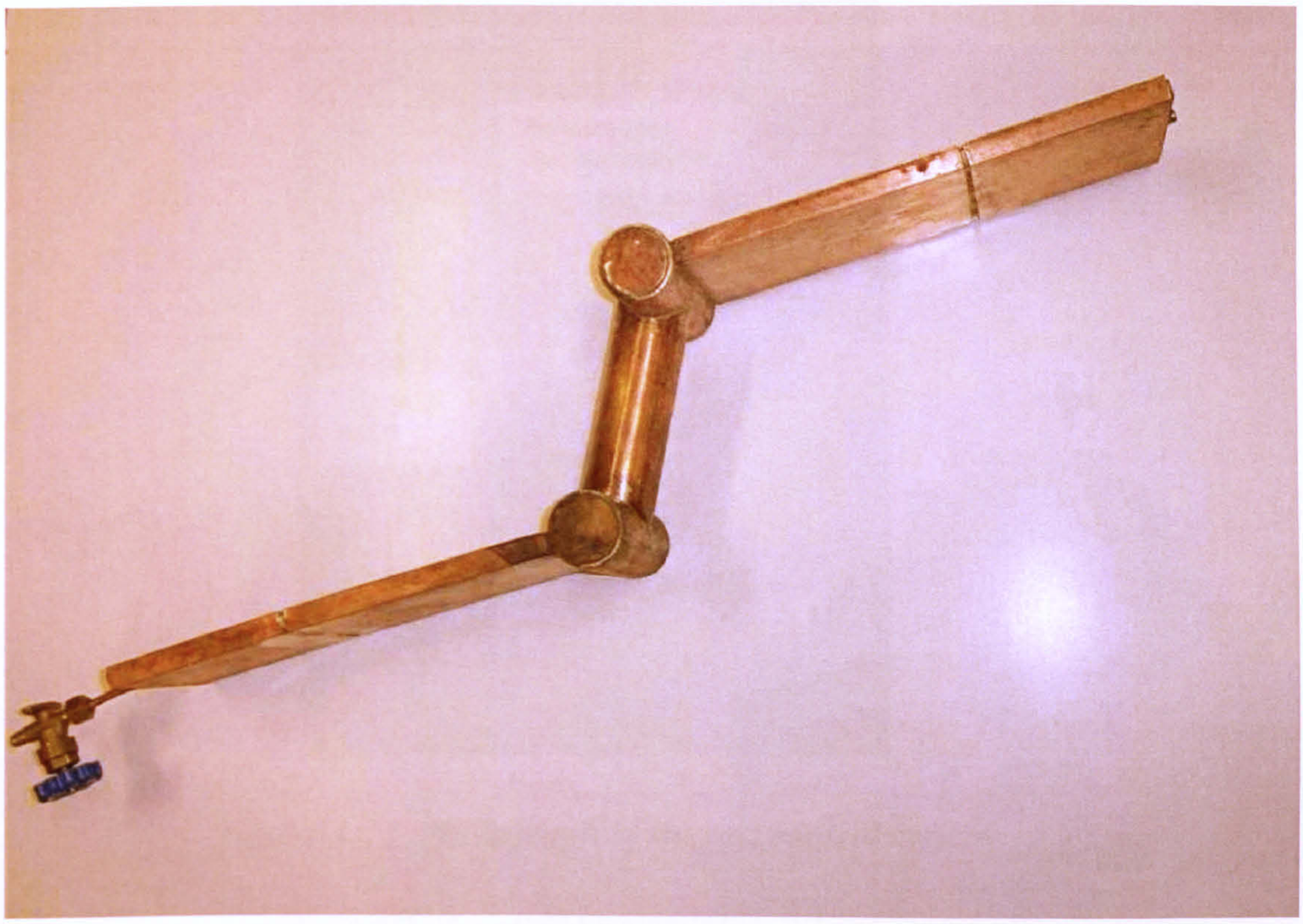

Figure 5-11. Photograph of the new type thermal diode

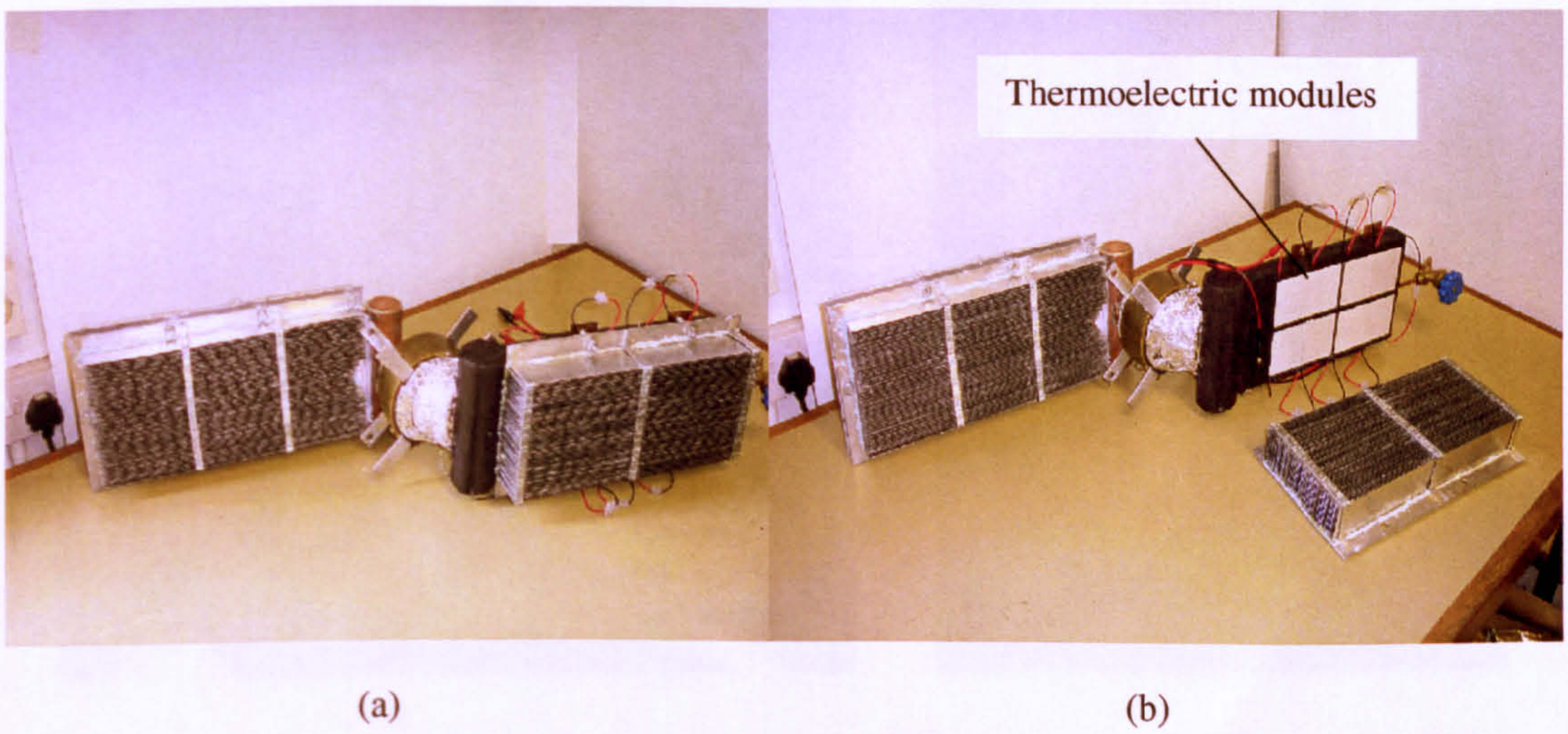

(a) (b)

Figure 5-12. Photographs of the heat pump (a) mounted heat pump (b) thermoelectric modules mounted in the heat pump

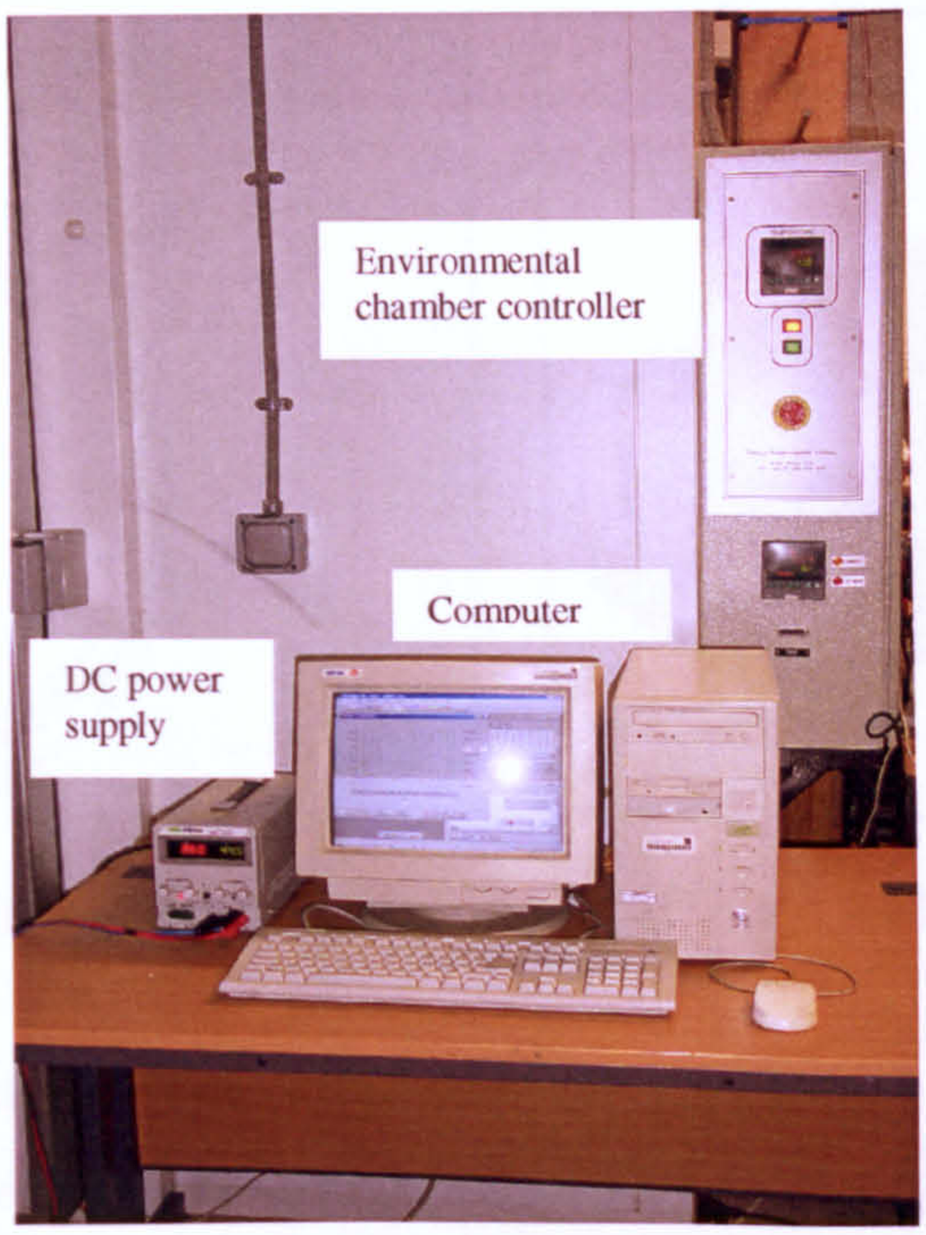

Figure 5-13. Photograph of the test control system

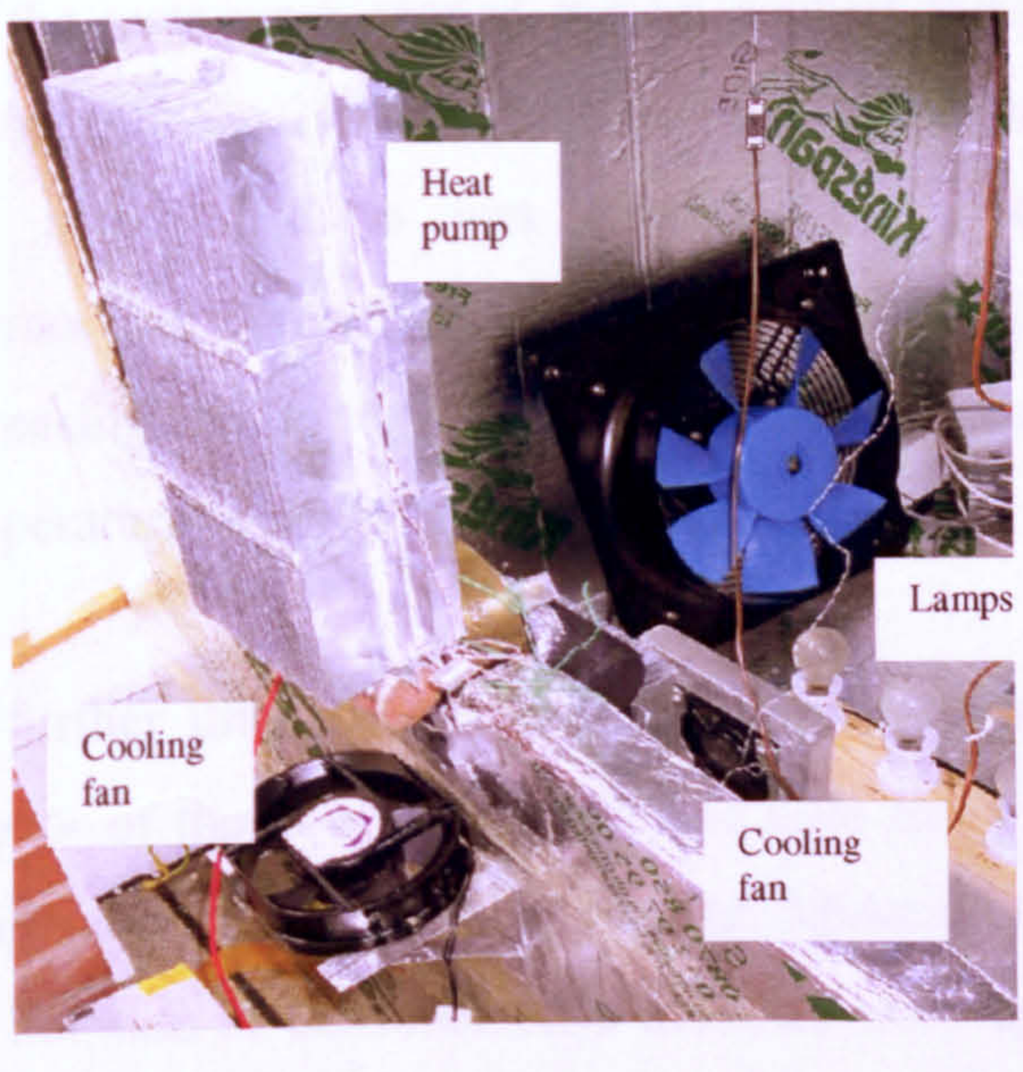

(a) (b)

Figure 5-14. Photographs of the test system (a) layout of the test system (half wall was taken off to show all the equipment) (b) system in operating

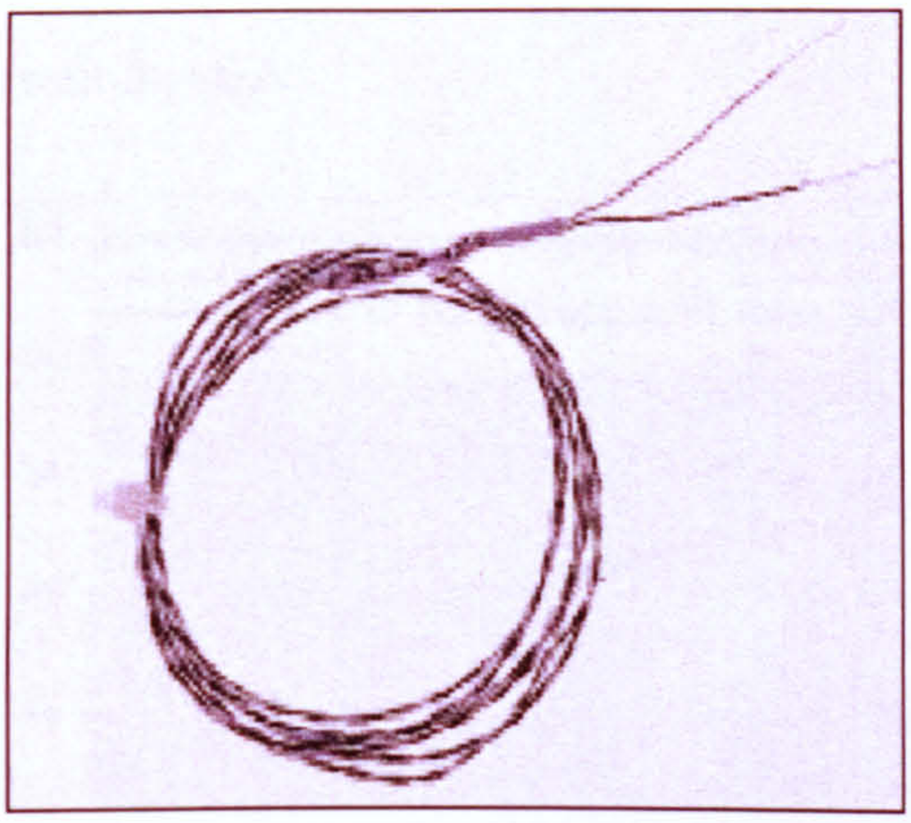

Figure 5-15. T-type thermocouples

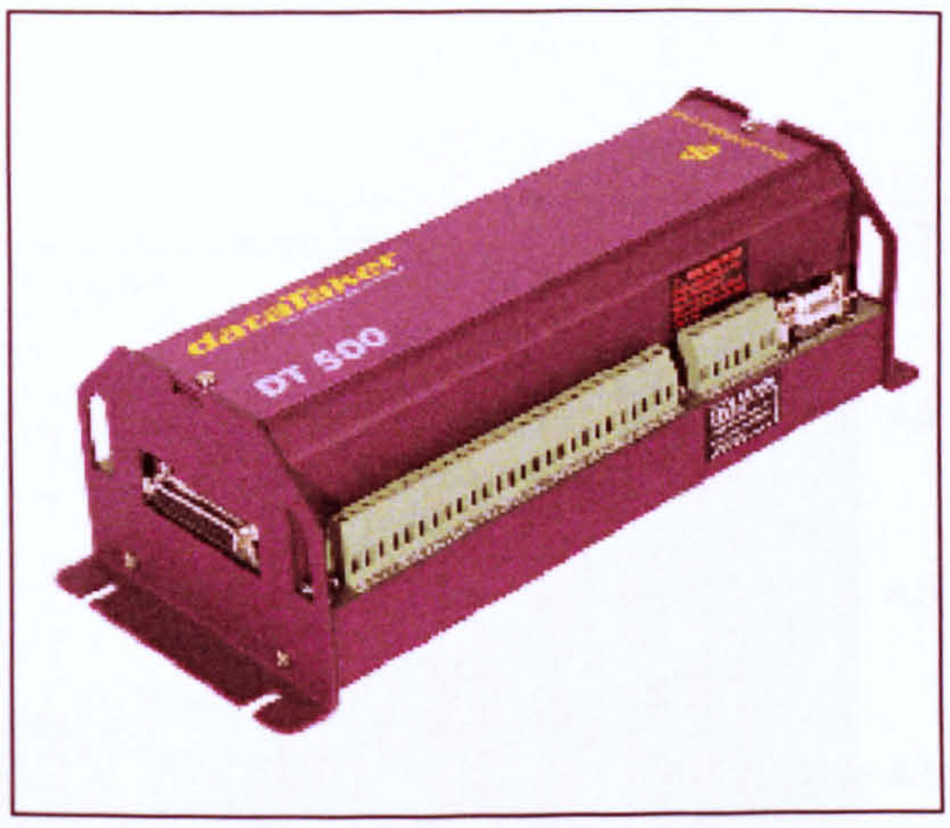

Figure 5-16. Datataker DT 500

5.4.1 Testing of Cooling Mode

Tests in the cooling mode include two parts: one was carried out for various heat loads, which were produced by opening different lamps, at ambient temperature of 24°C; another was carried out for various ambient temperatures without heat source inside the box.

All the tests were carried out by cooling the interior of the box from a temperature around 30°C to 21°C (a comfortable temperature in summer), at which the heat balance was achieved. This was achieved by controlling the DC current through the thermoelectric modules, i.e., providing less DC current at the beginning and then increasing the current step by step until a heat balance was achieved at interior box temperature of approximately 21°C.

To further illustrate the test process, one of the tests is shown in Figure 5-17. The interior of the box was intended to cool from around 30°C to around 21°C at ambient temperature 30°C. At the beginning, 3.6Amp DC current was given. The temperature of the hot side of thermoelectric modules went up continuously and that of the cold side went down continuously. When the temperature of both the hot and cold side of thermoelectric modules did not change significantly, the heat balance nearly achieved, and the temperature of interior of the box had been cooled to 24°C. To further reduce interior of the box temperature, more current should be given. This was done step by step, ie, 3.6A, 3.8A, 4.0A, 4.2A, 4.4A, 4.6A, each step achieved a new heat balance until

the heat balance achieved at interior of the box temperature around 21°C while the current is 4.6A.

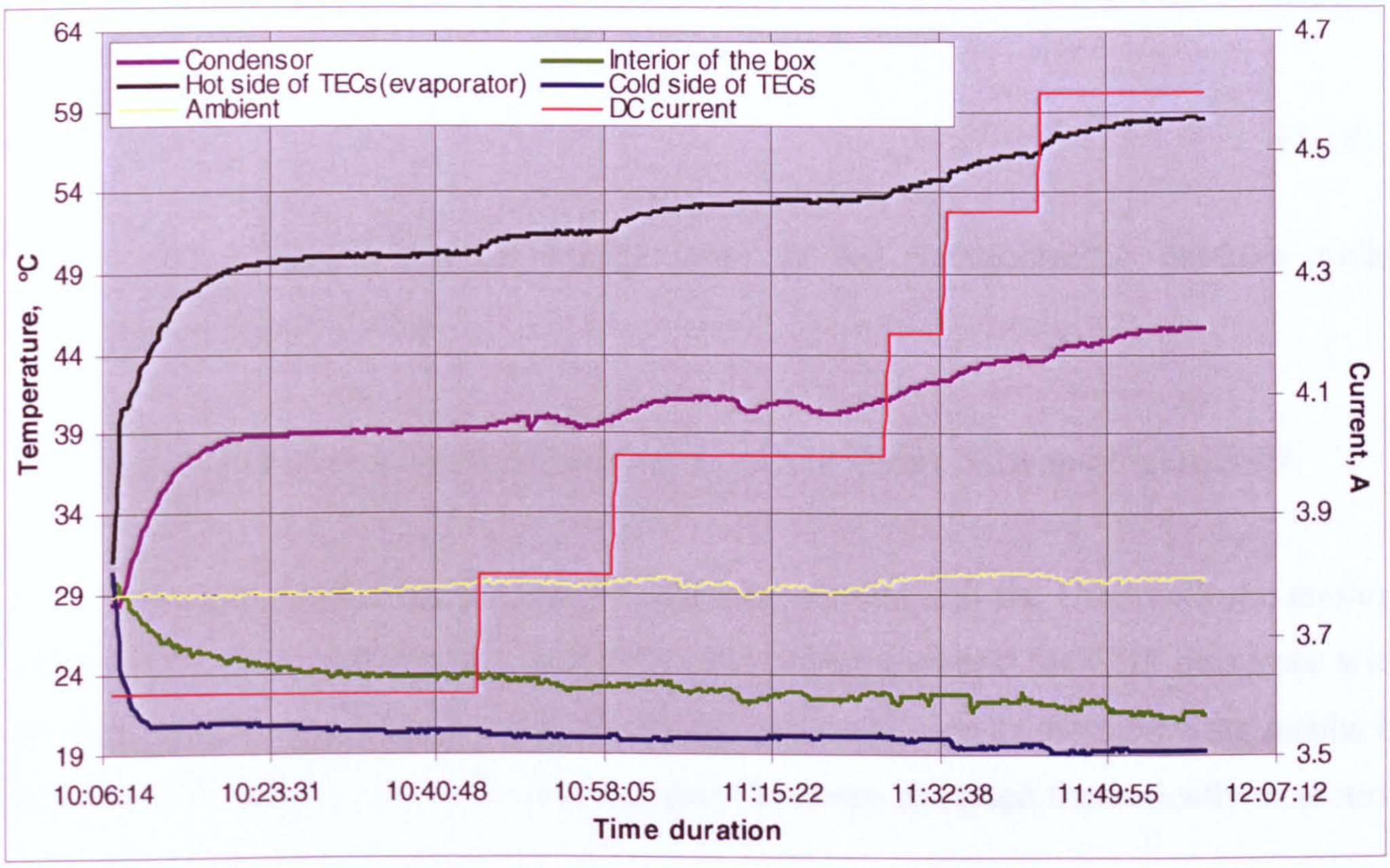

Figure 5-17. Variation of the temperatures and DC current with time in the test [V=19.2I-20.407(V)]

Performance in the cooling mode was evaluated by calculating the cooling energy dissipated inside the box and the electrical energy input to the thermoelectric modules. For the system in heat balance, the cooling energy produced by the system is equivalent to the sum of heat load and the heat transfer from ambient to the interior of the box through the wall:

$$Q_{cooling} = Q_{load} + Q_{wall} \tag{5-15}$$

Where Q_{load} is the heat load provided by the lamps, Q_{wall} is heat transfer from the ambient to the interior of the box.

$$Q_{wall} = U_w A_{wall} (T_a - T_{in}) \tag{5-16}$$

Where U_w is the coefficient of the heat transfer of the box

$$U_w = \frac{1}{1/h_{in} + R_{wall} + 1/h_{out}} \tag{5-17}$$

A_{wall} is the total area of the box.

The COP of the heat pump system in cooling mode was calculated using the following equation:

$$COP = Q_{cooling} / Q_{input} \tag{5-18}$$

Where Q_{input} is the electrical energy input to the thermoelectric modules under conditions of heat balance.

The results of the tests in cooling mode are shown in Figure 5-18 and Figure 5-19.

Figure 5-18 shows the variation of the operating current and the COP with the cooling capacity. It can be seen that the operating current increases and the COP decreases with the increase of the heat load, which shows the same tendency as the modelling results in section 5.3.1, and the reason for this tendency has been analysed theoretically in section 5.3.1.

Figure 5-19 shows the variation of the operating current and the COP with the ambient temperature. It can be seen that the operating current increases and the COP decreases with the increase of the ambient temperature, which shows the same tendency as the modelling results in section 5.3.1, and the reason for this has been analysed theoretically in section 5.3.1. The comparison of the modelling and test results is illustrated in section 5.5.

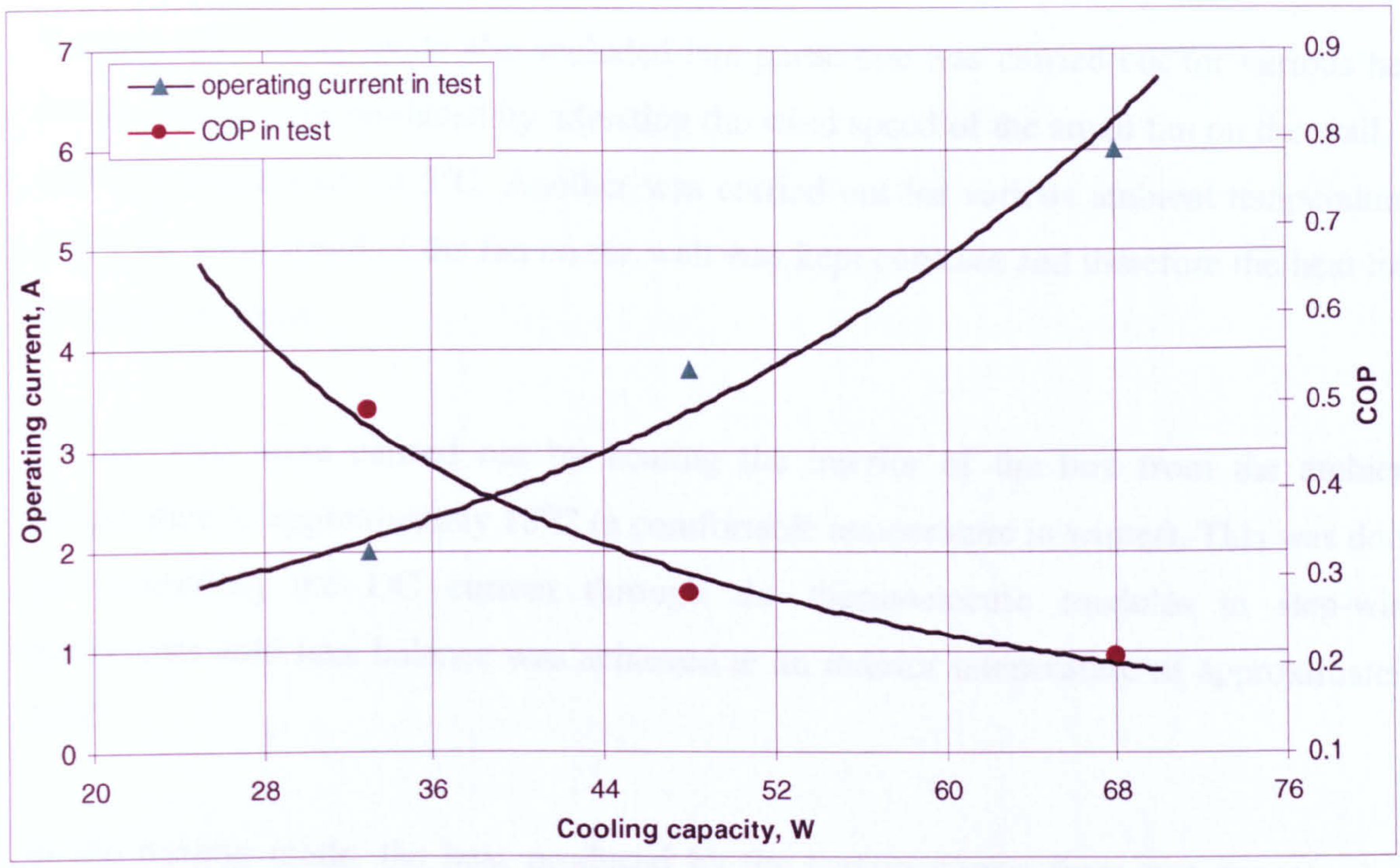

Figure 5-18.Variation of the operating current and the COP with cooling capacity in cooling mode in the test [V=12.5I-1.97(V)]

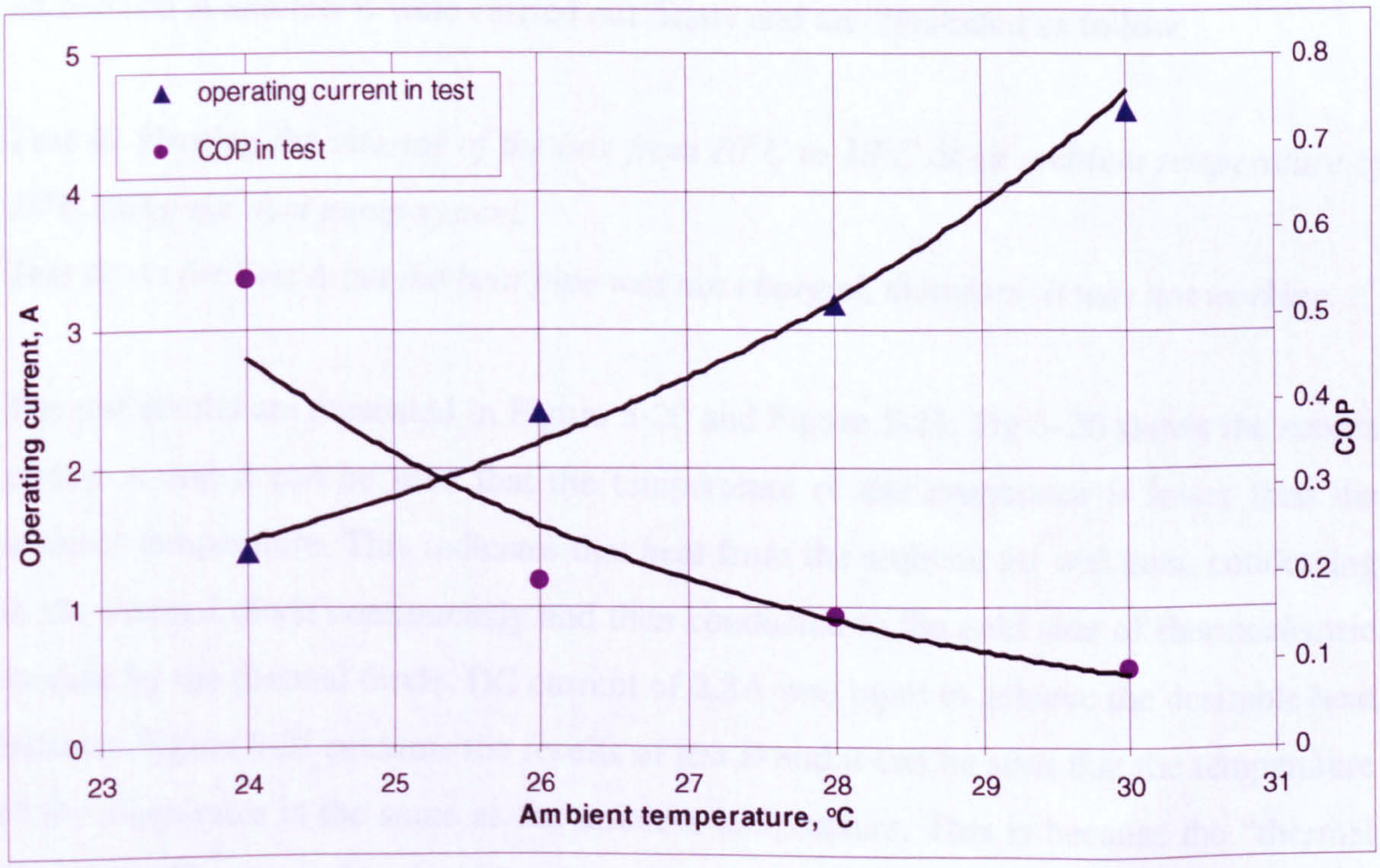

Figure 5-19. Variation of the operating current and the COP with ambient temperature in cooling mode in the test [V=14I-5.72(V)]

5.4.2 Testing of Heating Mode

Tests in the heating mode also included two parts: one was carried out for various heat losses, which were produced by adjusting the wind speed of the small fan on the wall, at ambient temperature of 5°C. Another was carried out for various ambient temperatures while the wind speed of the fan on the wall was kept constant and therefore the heat loss was kept constant.

All the tests were carried out by heating the interior of the box from the ambient temperature to approximately 18°C (a comfortable temperature in winter). This was done by controlling the DC current through the thermoelectric modules in step-wise increments until heat balance was achieved at an interior temperature of approximately 18°C.

In the heating mode, the heat produced by the system comes from two sources, i.e., electrical power and the ambient. Heat from the ambient is conducted by thermal diode to the cold side of the thermoelectric modules, and then conducted by the thermoelectric modules from the cold side to hot side to heat the interior of the box. To investigate the effect of the thermal diode in conducting heat from the ambient air, the additional tests named test A and test B were carried out firstly and are illustrated as follow:

Test A: *Heating the interior of the box from 10°C to 18°C at an ambient temperature of 10°C using the heat pump system.*
Test B: *As for Test A but the heat pipe was not charged, therefore, it was not working.*

The test results are presented in Figure 5-20 and Figure 5-21. Fig 5-20 shows the results of test A and it can be seen that the temperature of the evaporator is lower than the ambient temperature. This indicates that heat from the ambient air was been conducting to the thermal diode continuously and then conducted to the cold side of thermoelectric module by the thermal diode. DC current of 2.8A was input to achieve the desirable heat balance. Figure 5-21 presents the results of test B and it can be seen that the temperature of the evaporator is the same as the ambient temperature. This is because the "thermal diode" could not conduct heat from the evaporator to condenser and therefore did not absorb heat from the ambient. As the thermal diode absorbed heat from the ambient in

test A, the cold side temperature was higher than that in test B, and also less power was required to achieve the desirable heat balance. DC current of 2.8A was input in this test, as shown in Figure 5-20. The cold side temperature in test B was much lower and more power was required to achieve the desirable heat balance. As shown in Figure 5-21, at the beginning the DC current of 2.8A was input and that could not achieve the desirable heat balance. The desirable heat balance was achieved while the DC current increased to 3.6A.

Performance in the heating mode was evaluated by calculating the heating energy dissipated inside the box and the electrical energy input to the thermoelectric modules. For heat balance, the heating energy produced by the system is equivalent to the sum of heat loss through the fan on the wall and the heat transfer through the wall.

$$Q_{heating} = Q_{loss} + Q_{wall} \tag{5-19}$$

Where Q_{loss} is the heat loss produced by the fan on the wall; Q_{wall} is heat transfer from the interior of the box to the ambient [see eq(5-19)].

$$Q_{loss} = C_p \rho V_a S_a (T_{in} - T_a) \times 1000 \tag{5- 20}$$

The COP of the heating system was calculated using the following equation:

$$COP = Q_{heating} / Q_{input} \tag{5-21}$$

Where Q_{input} is the electrical energy input to the thermoelectric modules when heat balance is achieved at interior of box temperature of approximately 18°C.

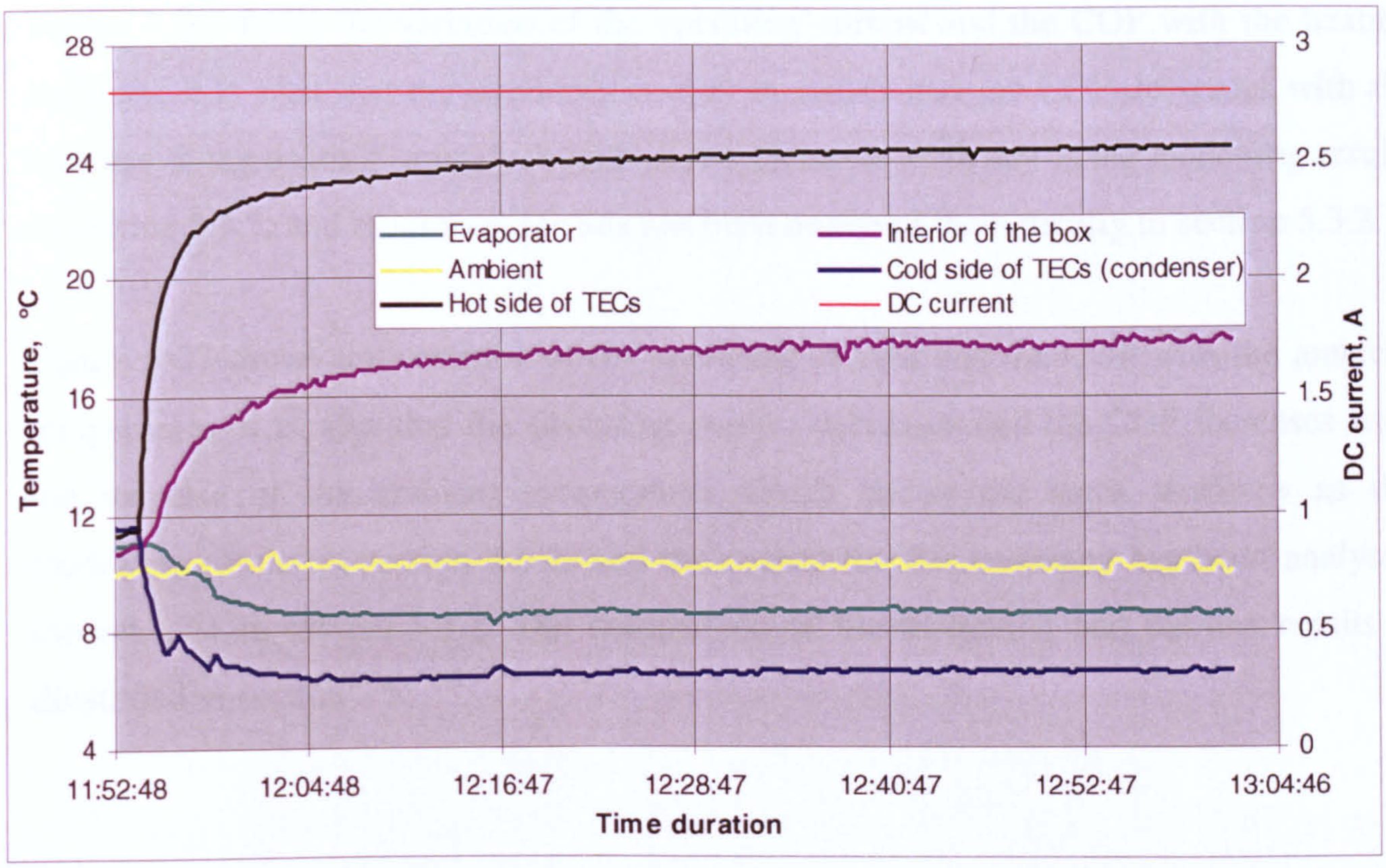

Figure 5-20. Variation of temperatures and DC current with time in test A (V=26.5V)

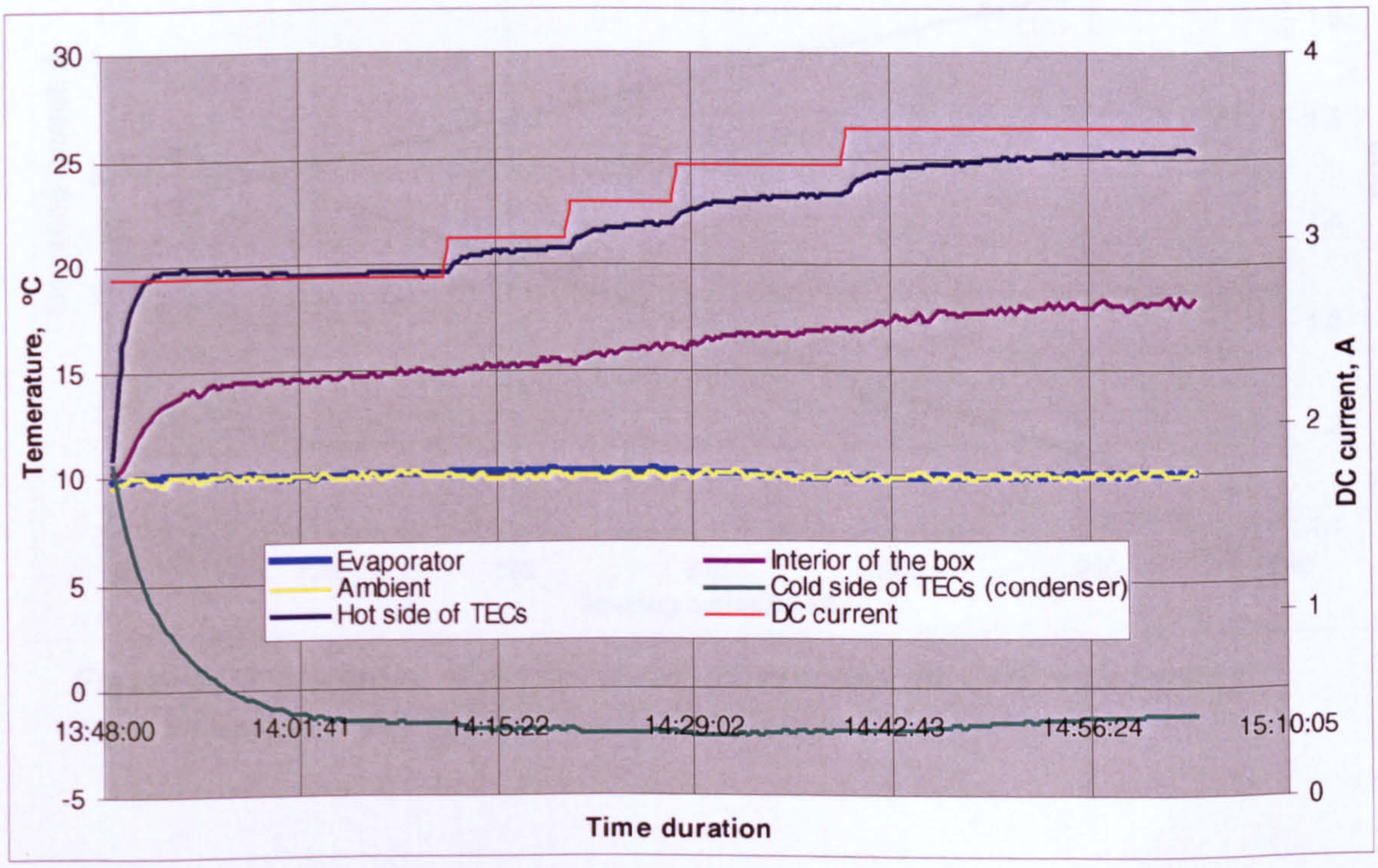

Figure 5-21. Variation of temperatures and DC current with time [V=16.6I-18.2(V)]

Figure 5-22 shows the variation of the operating current and the COP with the heating capacity. It is seen that the operating current increases and the COP decreases with the increase of the heating capacity, which shows the same tendency as the modelling results in section 5.3.2, and the reason for this has been analysed theoretically in section 5.3.2.

Figure 5-23 shows the variation of the operating current and the COP with the ambient temperature. It is seen that the operating current decreases and the COP increases with the increase of the ambient temperature, which shows the same tendency as the modelling results in section 5.3.2, and the reason for this tendency has been analysed theoretically in section 5.3.2. The comparison of the modelling and the test results is illustrated in section 5.5

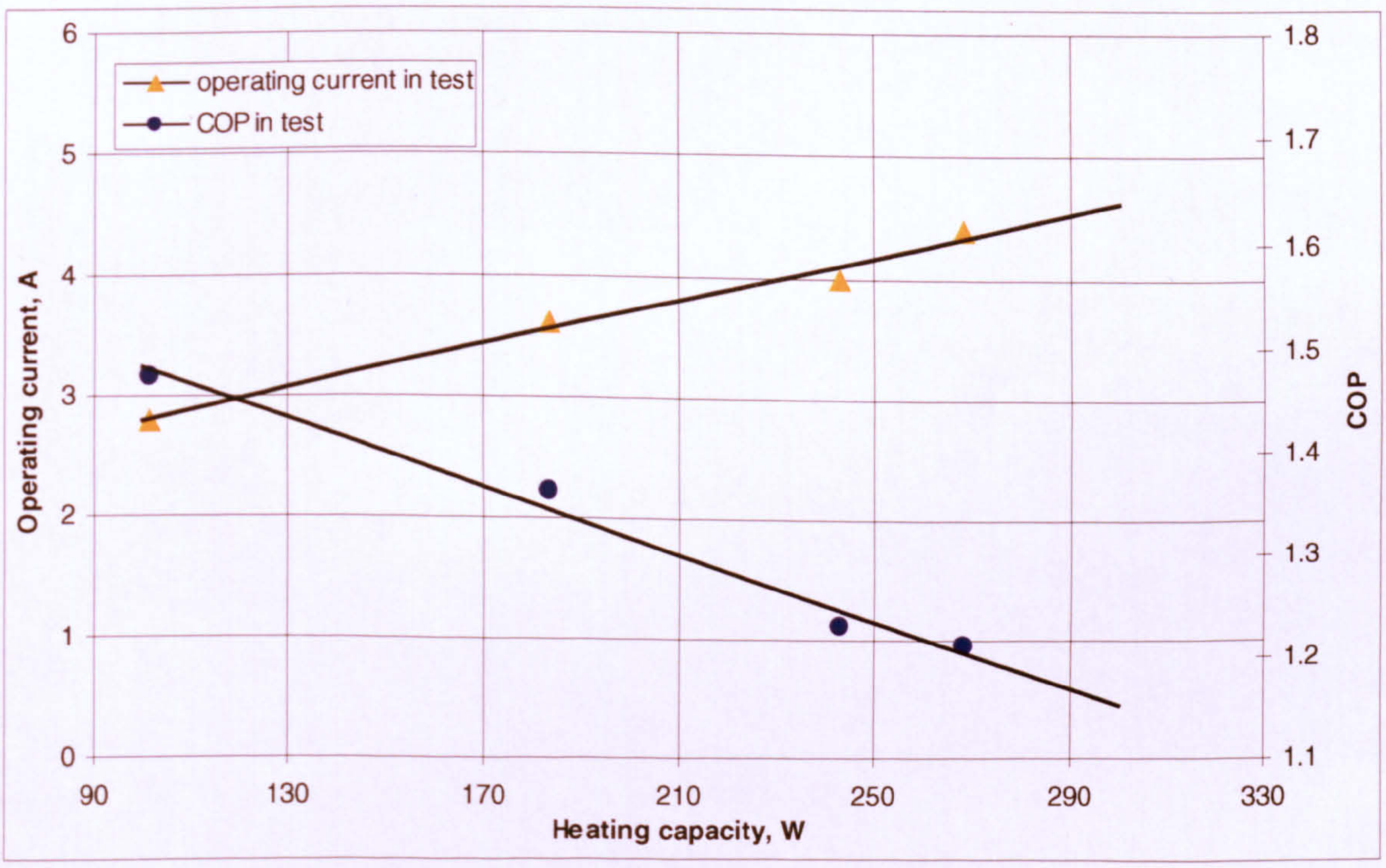

Figure 5-22. Variation of the operating current and the COP with heating capacity in heat mode in test [V=11.1I+0.45(V)]

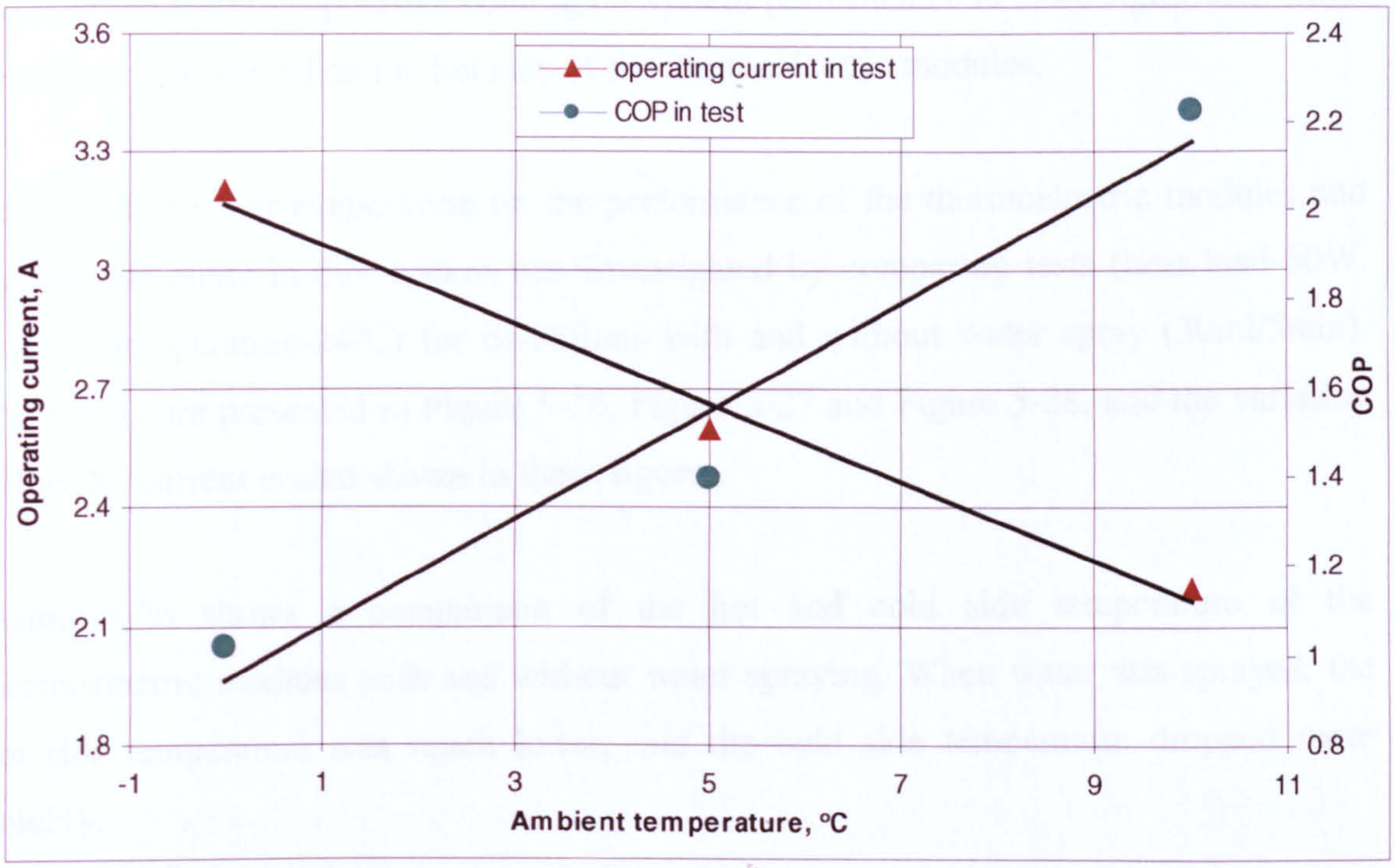

Figure 5-23. Variation of the operating current and COP with ambient temperature in heating mode in test [V=10.5I+2.2(V)]

5.4.3 Testing of Improving Coefficient of Performance in Cooling Mode by Using Evaporation of Water

As aforementioned, the COP of the thermoelectric system can be improved by reducing the hot side temperature of the thermoelectric modules. In the cooling mode of this system, this can be done by removing heat more efficiently from the condenser of the thermal diode to the ambient. As we know, water has large latent heat of evaporation. To investigate the effect of cooling due to evaporation of water on system performance, more tests in cooling mode were carried out for the condition of spray water evenly on the outside heat sink. The test results were compared with those in section 5.4.1 (without spray water) and are shown in Figure 5-24 and Figure 5-25.

Figure 5-24 shows a comparison of COP at various cooling capacities for the tests with and without water spraying. Figure 5-25 shows a comparison of COP at various ambient temperatures for the tests with and without water spraying. It is seen that providing cooling of the outside heat sink by spraying water (30ml/min) onto it for subsequent evaporation, results in a 78%~233% improvement of the COP. As water has a high

latent heat of evaporation, this method provided an effective means of cooling. The effect of the water evaporative cooling on system performance is more significant when more heat is produced on the hot side of the thermoelectric modules.

The effect of water evaporation on the performance of the thermoelectric modules and the thermal diode in this system was investigated by comparing tests (heat load-60W, ambient temperature-24°C) for conditions with and without water spray (30ml/5min). The results are presented in Figure 5-26, Figure 5-27 and Figure 5-28, and the variation of the DC current is also shown in these figures.

Figure 5-26 shows a comparison of the hot and cold side temperature of the thermoelectric modules with and without water spraying. When water was sprayed, the hot side temperature was much lower, and the cold side temperature dropped more quickly.

As less power was required when water was sprayed, the achieved temperature difference between the hot and cold side was much lower, as shown in Figure 5-27. The temperature difference, of course, increased with DC power step by step.

Figure 5-28 shows the comparison of the temperature difference between the evaporator and the condenser sections of the thermal diode with and without water spray. With water spray, the temperature difference between the evaporator and condensor of thermal diode was much less and increased more slowly than without water spray. This indicates that the performance of the thermal diode increases when the condenser is cooled.

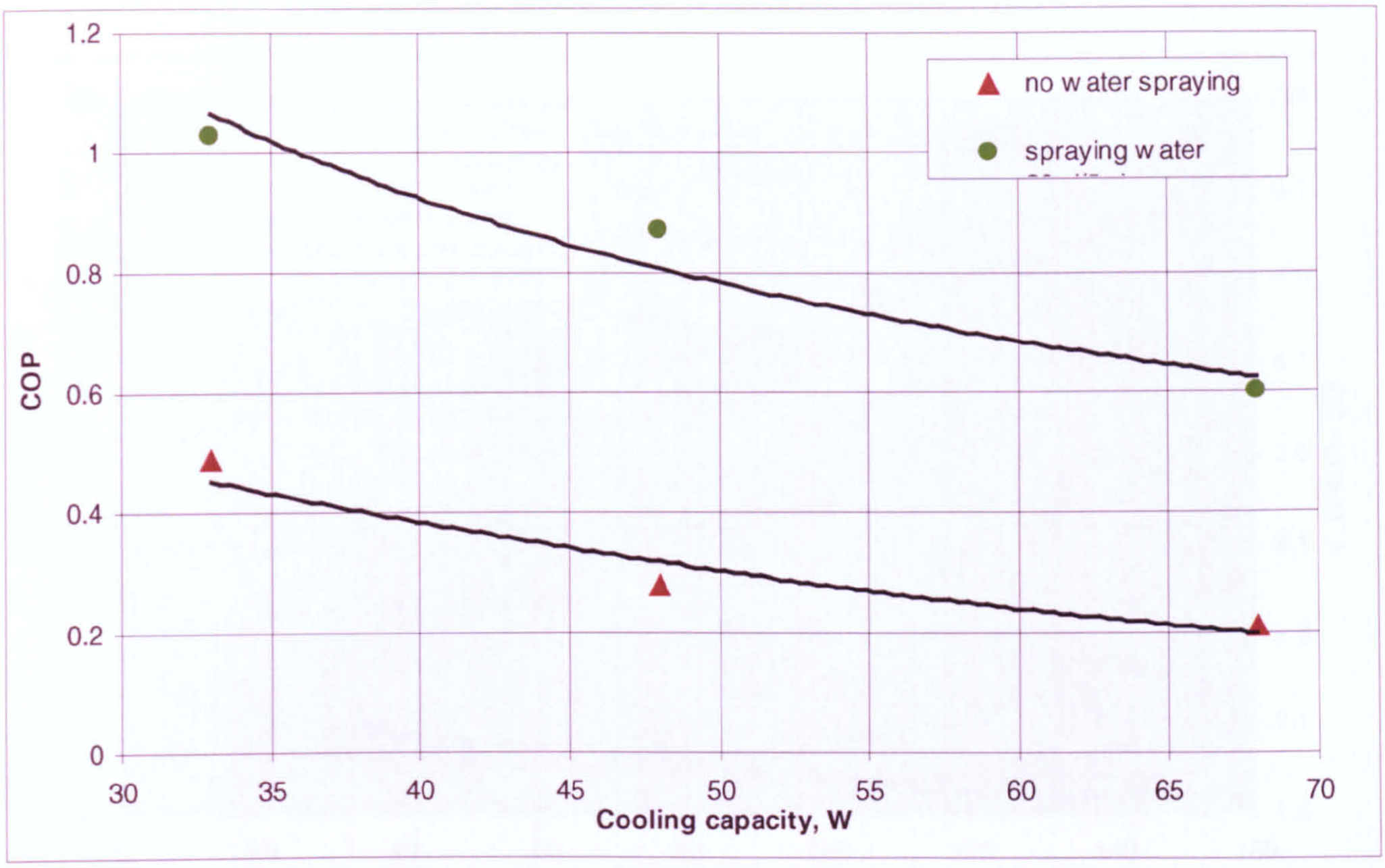

Figure 5-24. Comparison of COP at various cooling capacity for the tests with and without water spraying

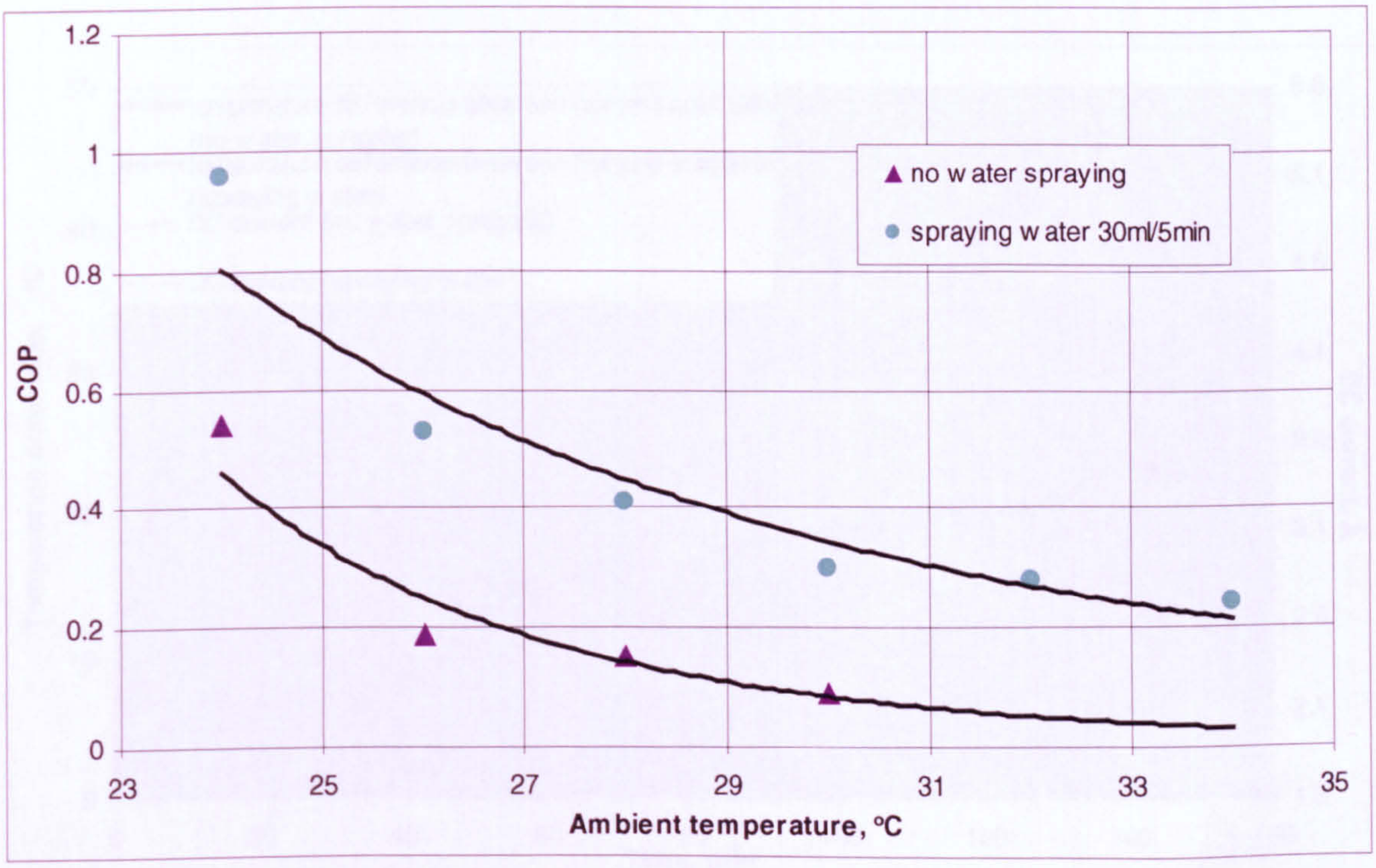

Figure 5-25. Comparison of COP at various ambient temperatures for the tests with and without water spraying

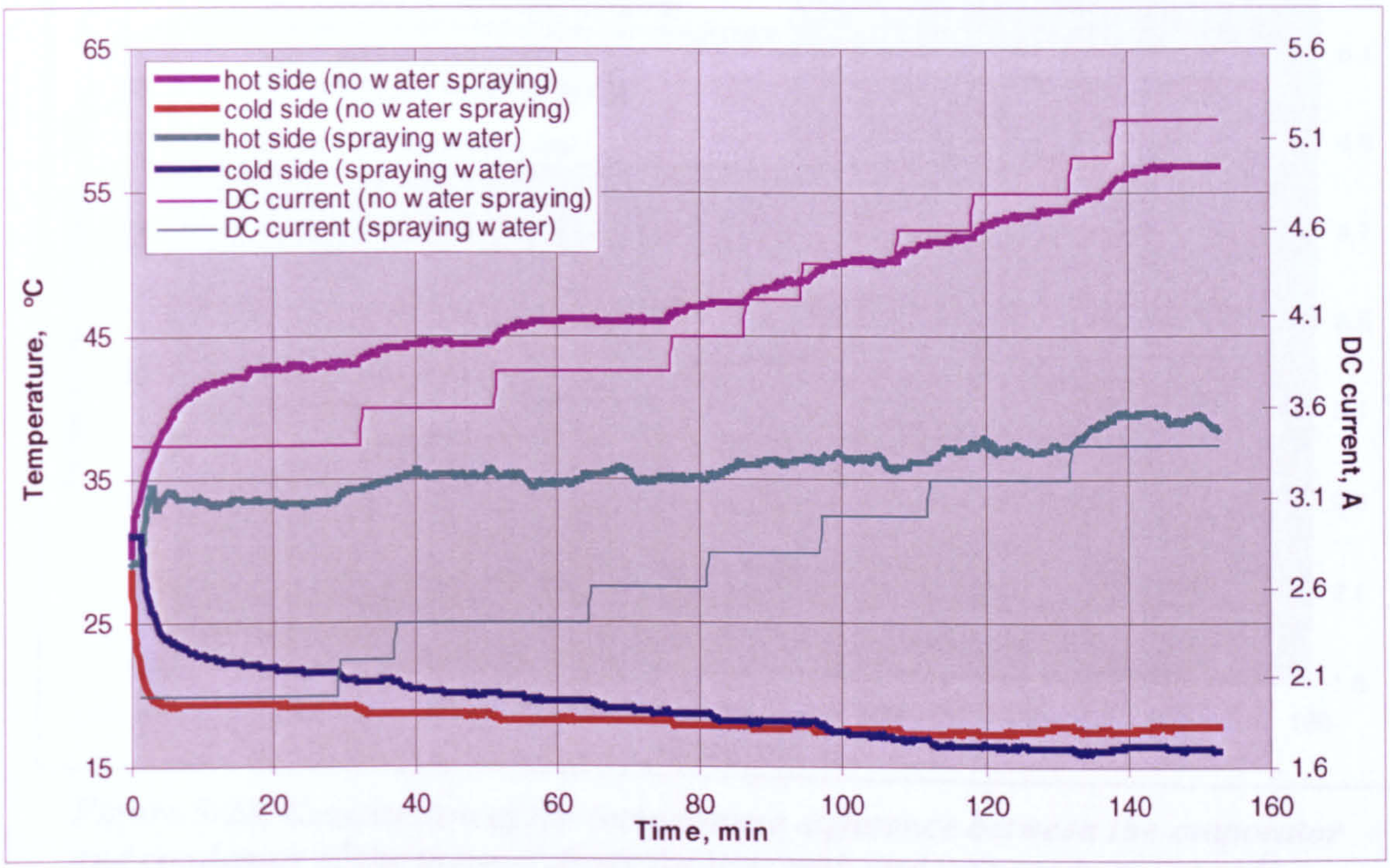

Figure 5-26. Comparison of the hot/cold side temperatures of thermoelectric modules for the tests with and without water spraying

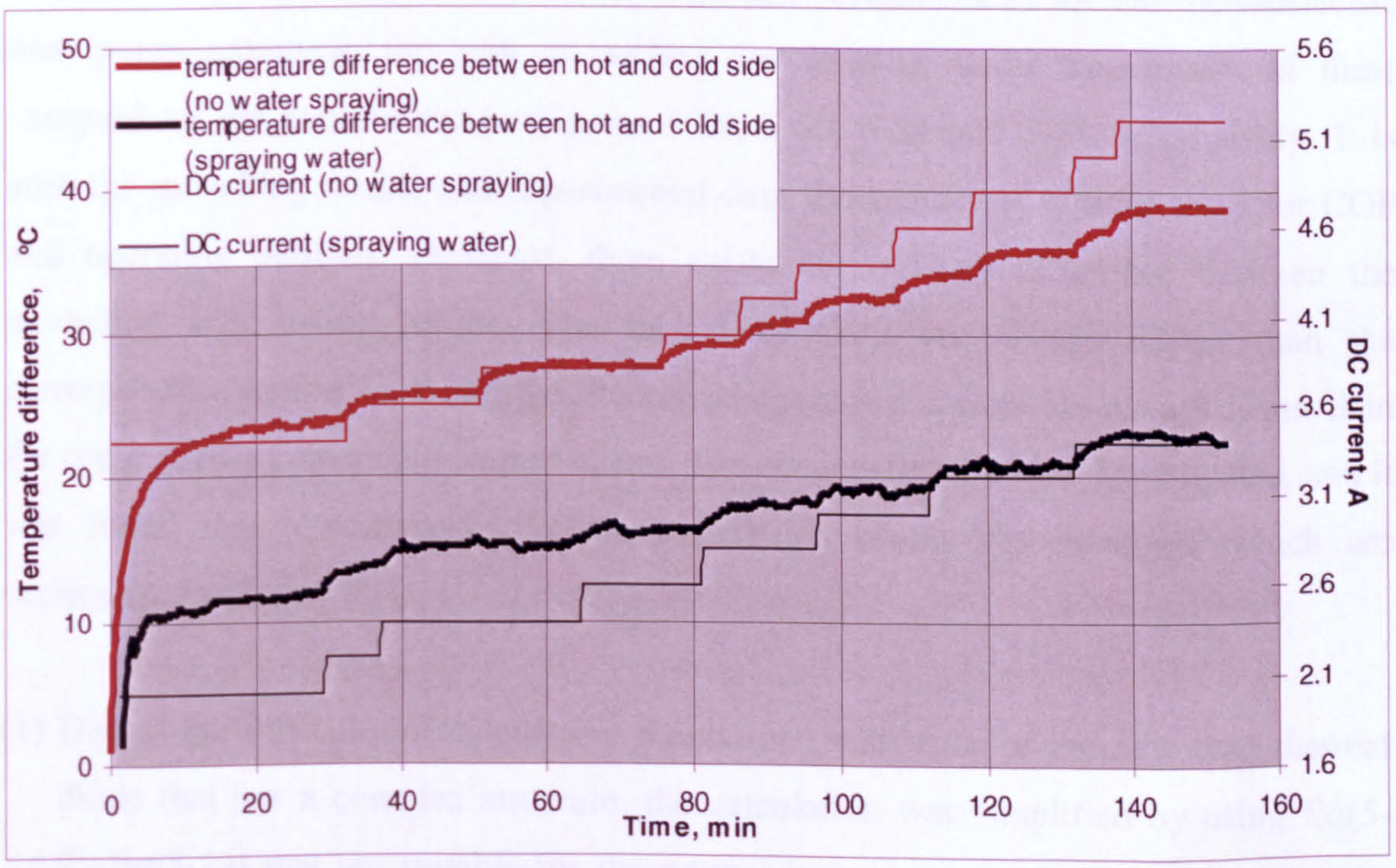

Figure 5-27. Comparison of temperature difference between the hot and cold sides for tests with and without water spraying

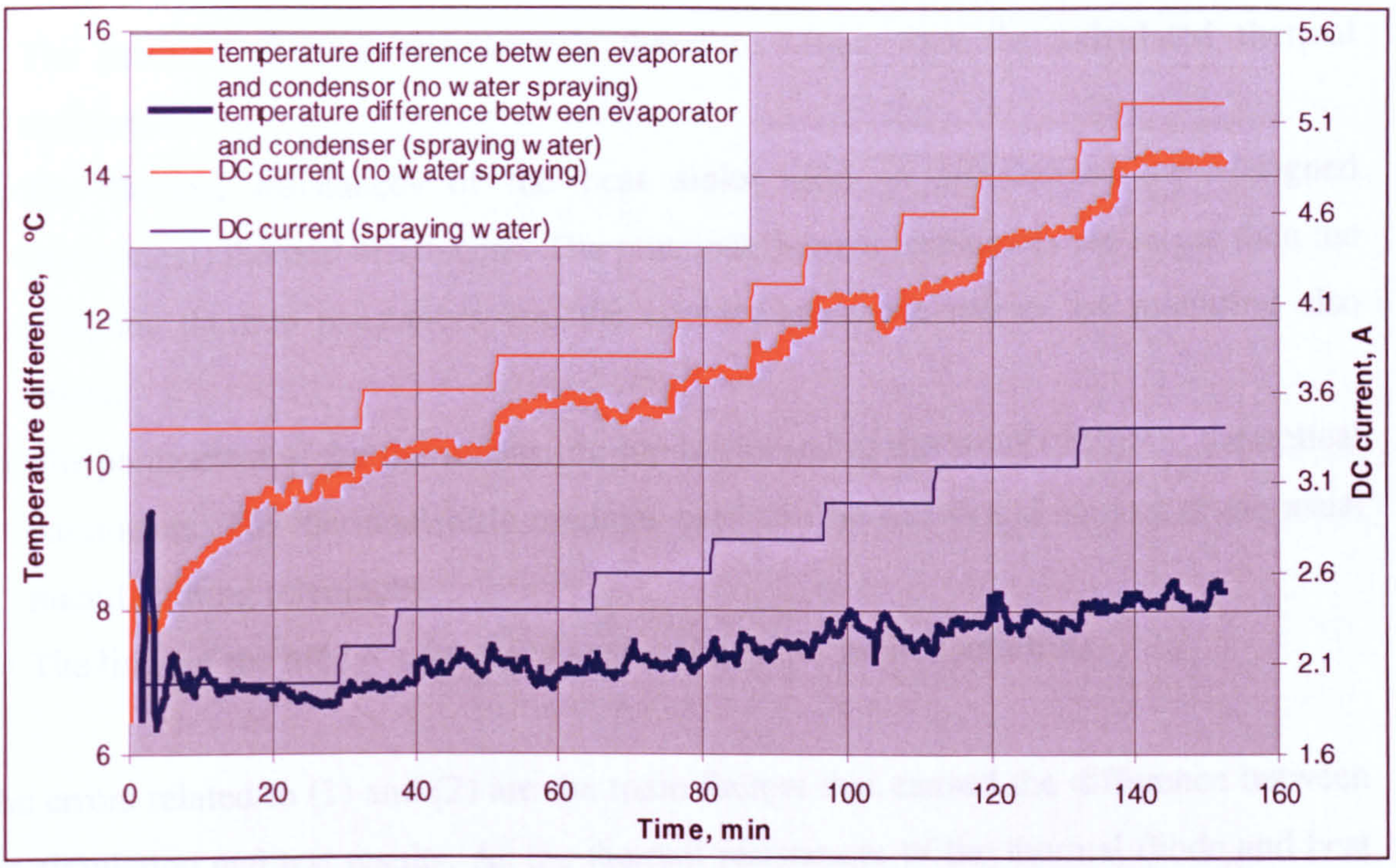

Figure 5-28. Comparison of the temperature difference between the evaporator and condenser of the thermal diode for tests with and without water spraying

5.5 Comparison of the Modelling and Testing Results

Comparison was carried out between the modelling results (shown in section 5.3) and experimental results (shown in section 5.4.1 and section 5.4.2) for the thermoelectric heat pump prototype, for both of cooling and heating mode. The results of these comparisons are summarised in Figures 5-29, 5-30, 5-31 and 5-32, respectively. It is seen the modelling results and experimental data showed a very similar trend for COP and operating currents. However, there exists the obvious difference between the modelling and testing results. The theoretical COP are always higher than the corresponding testing COP and the theoretical operating current are always lower than the corresponding operating current in test. The reasons for this were investigated, and it was found that a number of factors contributed to the discrepancies, which are summarised as follow:

(1) Due to the difficulty of calculating the thermal resistance of the new type thermal diode that has a complex structure, the calculation was simplified by using Eq(5-9)~Eq(5-14) that are suitable for the normal heat pipes, i.e., the new type thermal diode was treated as 11 normal thermal diodes each having the diameter of 10mm.

The practical thermal resistance is therefore larger than the calculated thermal resistance.

(2) The thermal resistances of the heat sinks used in simulations are designed (theoretical) thermal resistances. The practical thermal resistances are larger than the designed thermal resistances and the contact resistance caused by mounting also exists.

(3) The parameters of the thermoelectric modules used in the simulations are theoretical parameters. The thermoelectric modules used for the test would subject to the usual manufacturing tolerances.

(4) The limit of the model's accuracy causes the errors in the modelling.

The errors related to (1) and (2) are the main factors that caused the difference between the simulation and test results. As the thermal resistances of the thermal diode and heat sinks in the modelling are smaller than that in practice, the hot side temperatures of the thermoelectric modules in the modelling are smaller than that in practice, and the cold side temperatures in the modelling are higher than those in practice. This indicates the temperature differences between the hot and cold side in the modelling are smaller than those in the test. This cause the COP obtained in the modelling to be greater than found in the testing and the operating currents in modelling to be less than those in the test. The errors related to (3) and (4), cause uncertain errors. It contributed minor discrepancies between the modelling results and testing results.

The main error factors related to (1) and (2) contributed to the discrepancies of the hot and cold side temperatures between the modelling and the testing directly. Therefore, they can be corrected by comparing the hot and cold side temperatures in modelling with those in tests, and give the correction factors. The correction factors were determined by dividing the experimental hot and cold side temperatures by the modelling hot and cold side temperatures respectively. Figure 5-33 and Figure 5-34 shows the correction factors of hot and cold side temperatures respectively.

The more accurate hot and cold side temperatures can be obtained by using the correction factors in the modelling. The more accurate COP and operating currents can then be calculated by using the modified hot and cold side temperatures in equations (5-

7), (5-8c) and (5-8h). The computer program of modelling can complete this correction process by adding the correction function to it. Figure 5-35 to Figure 5-38 shows the comparisons of the modified modelling results and the testing results. It is shown that the modified results are much more close to the testing results, the difference between the COP in modelling and the COP in testing is within 0.2.

This correlation would be applied to any circumstance for this type of thermoelectric heat pump, and expected to improve the accuracy of the modelling predictions to a substantial extent.

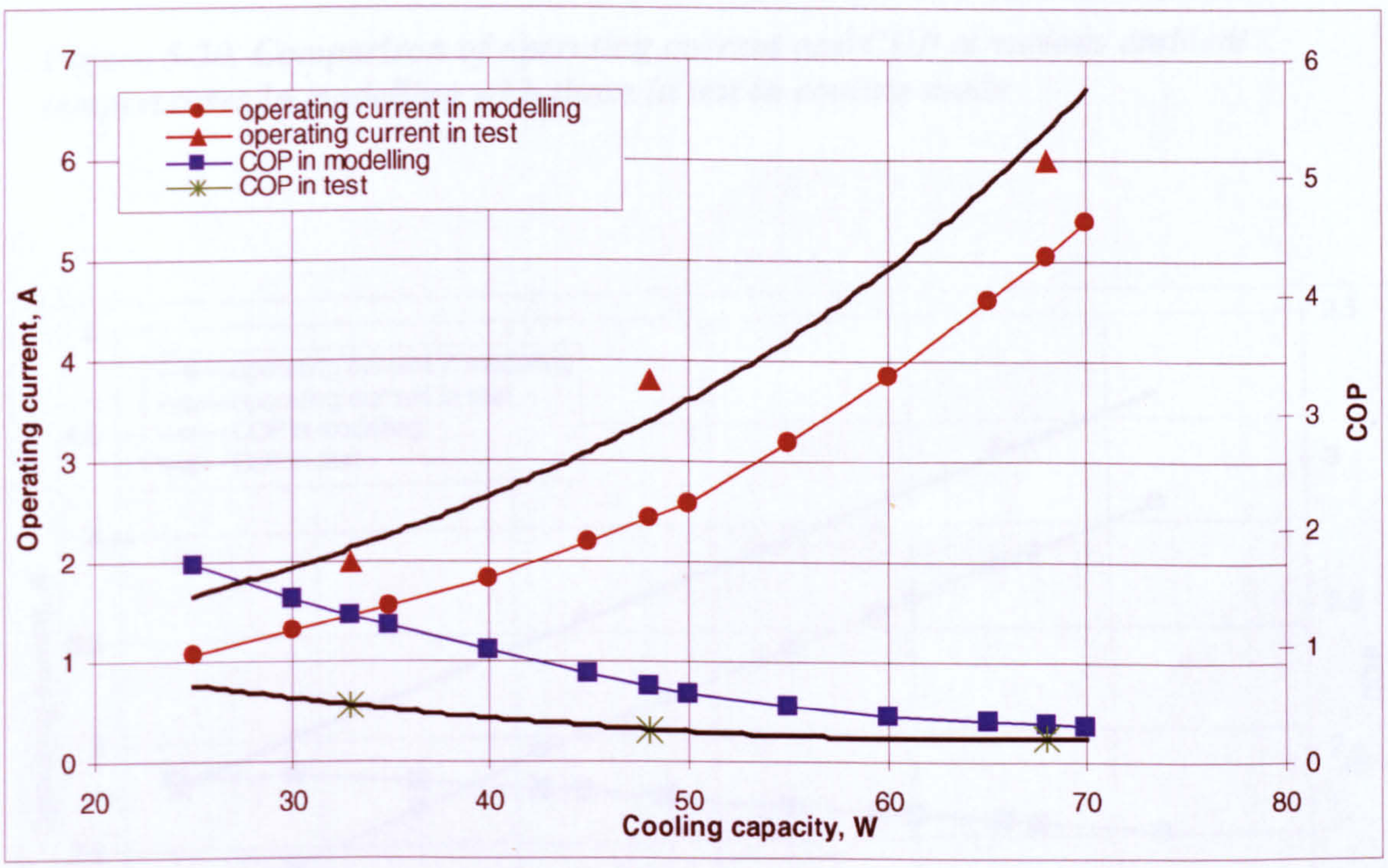

Figure 5-29. Comparison of operating current and COP at various cooling capacities in modelling with those in test in cooling mode

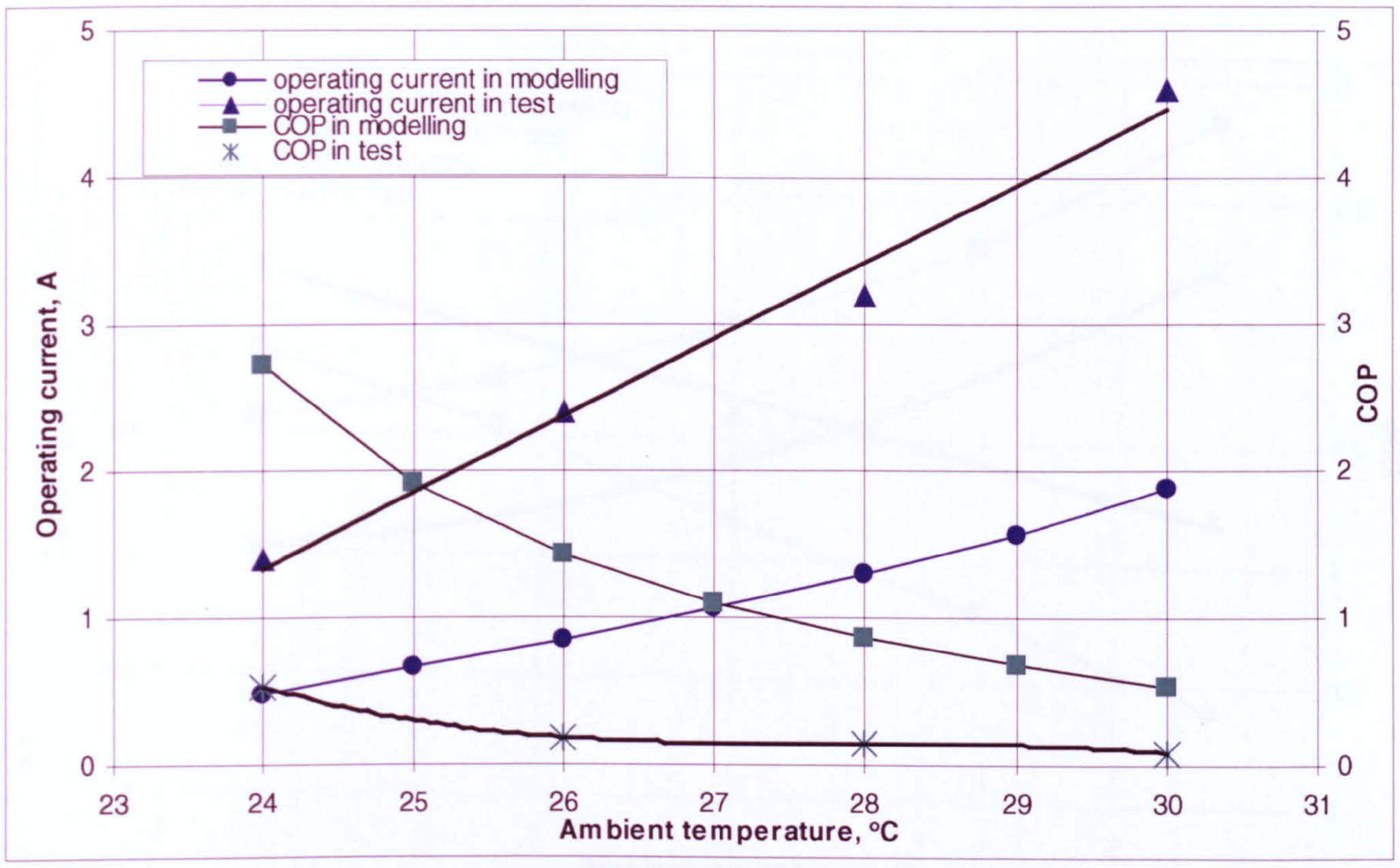

Figure 5-30. Comparison of operating current and COP at various ambient temperatures in modelling with those in test in cooling mode

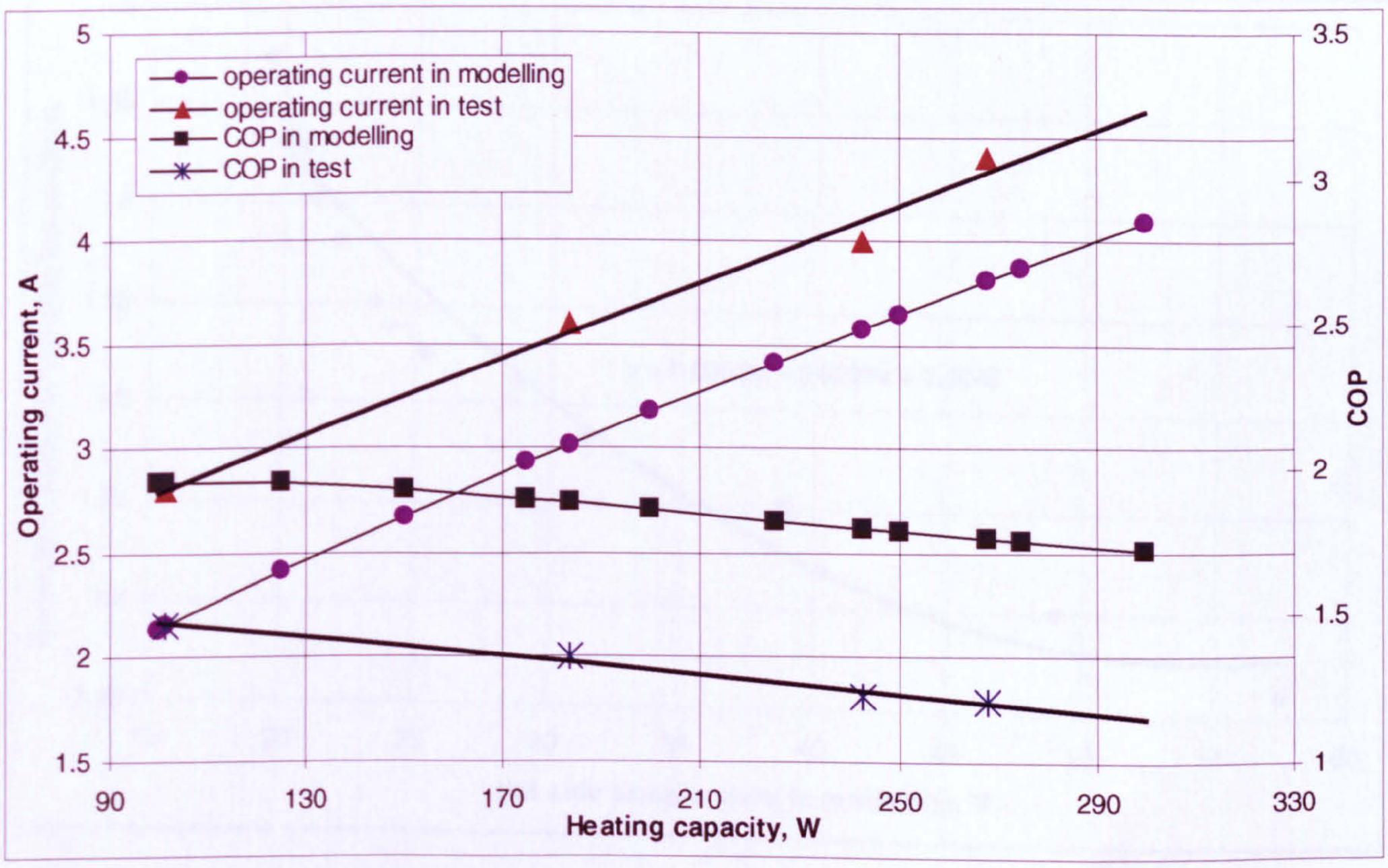

Figure 5-31.Comparison of operating current and COP at various heating capacities in modelling with those in test in heating mode

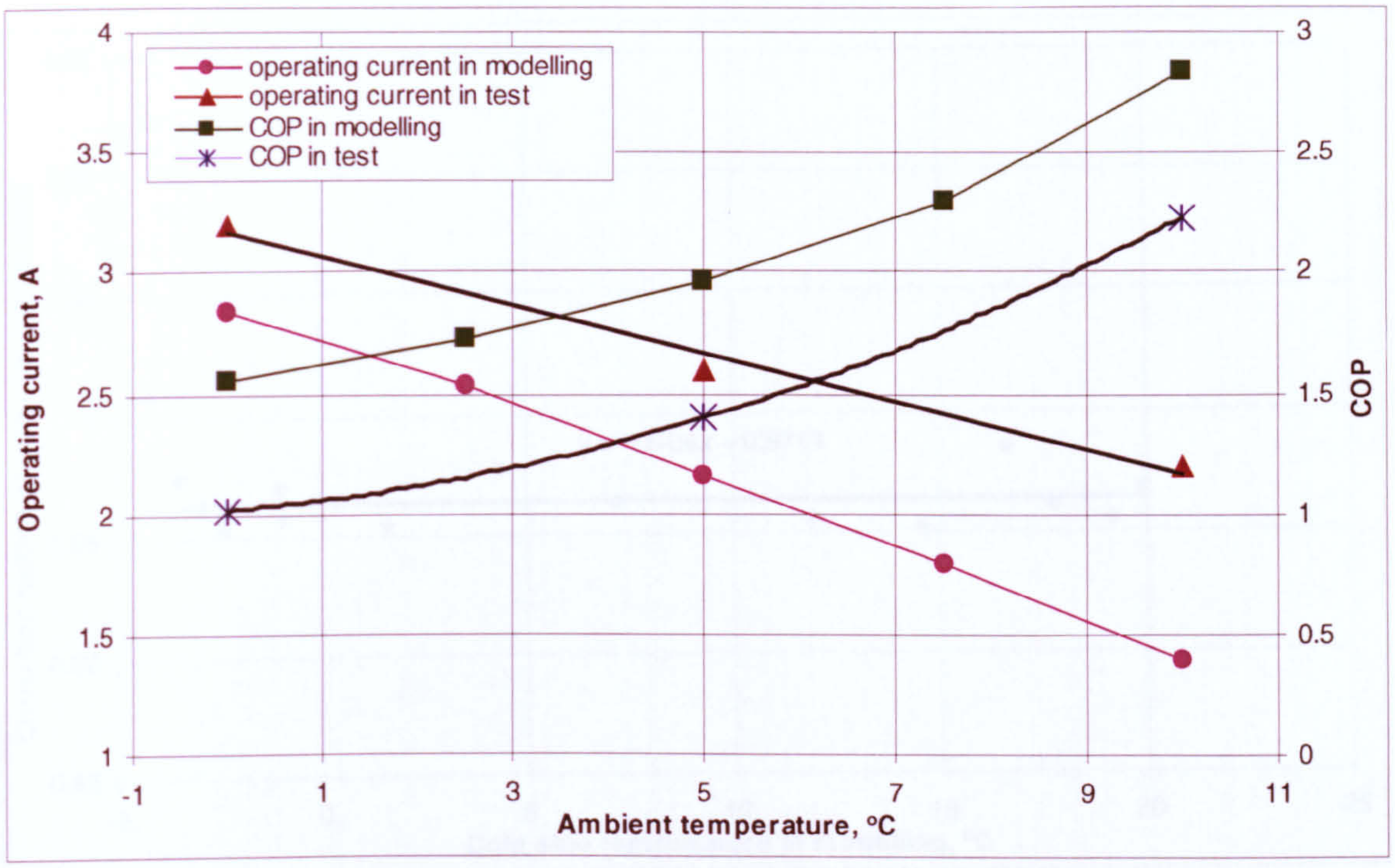

Figure 5-32. Comparison of operating current and COP at various ambient temperatures in modelling with those in test in heating mode

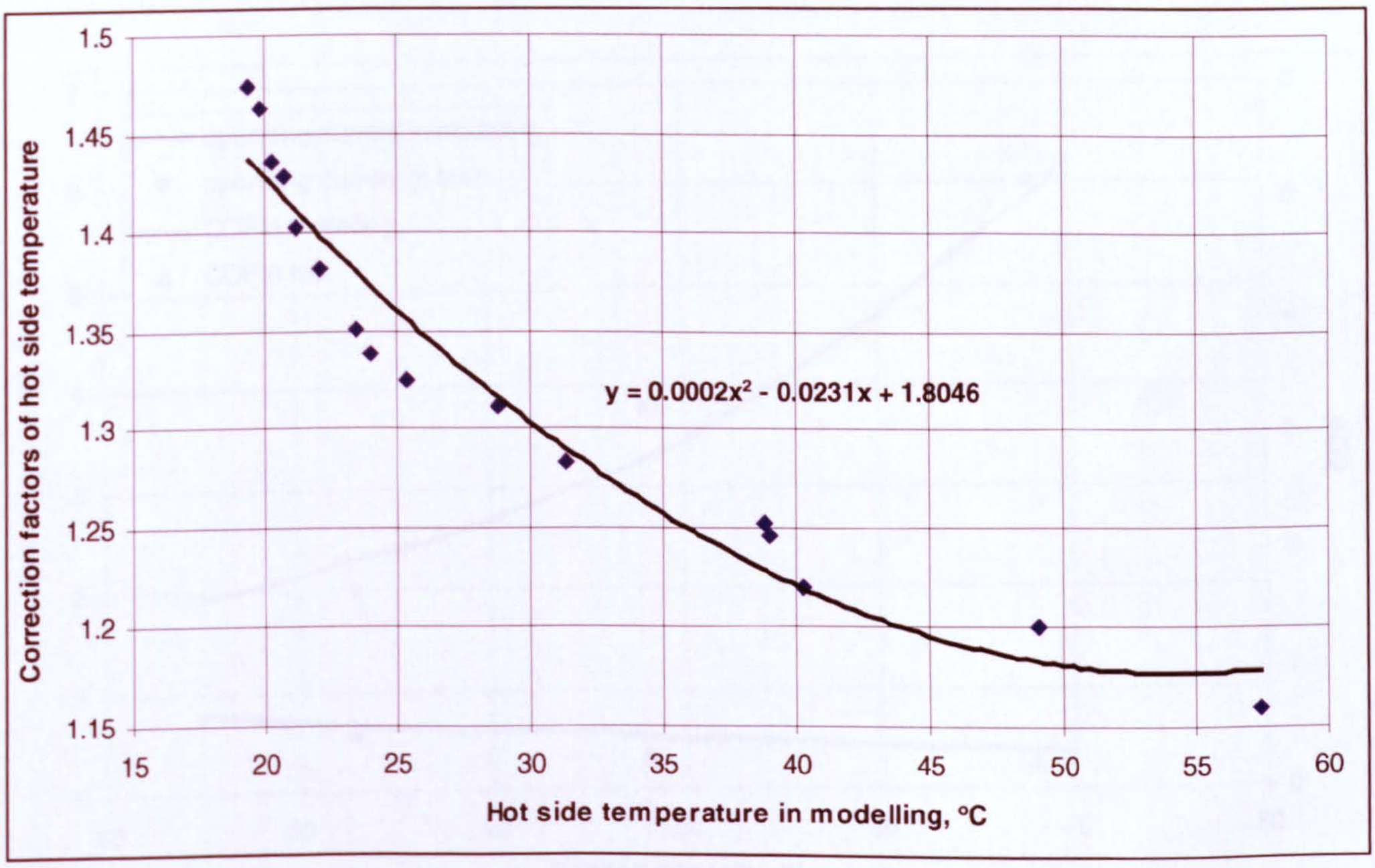

Figure 5-33. Correction factors of hot side temperature

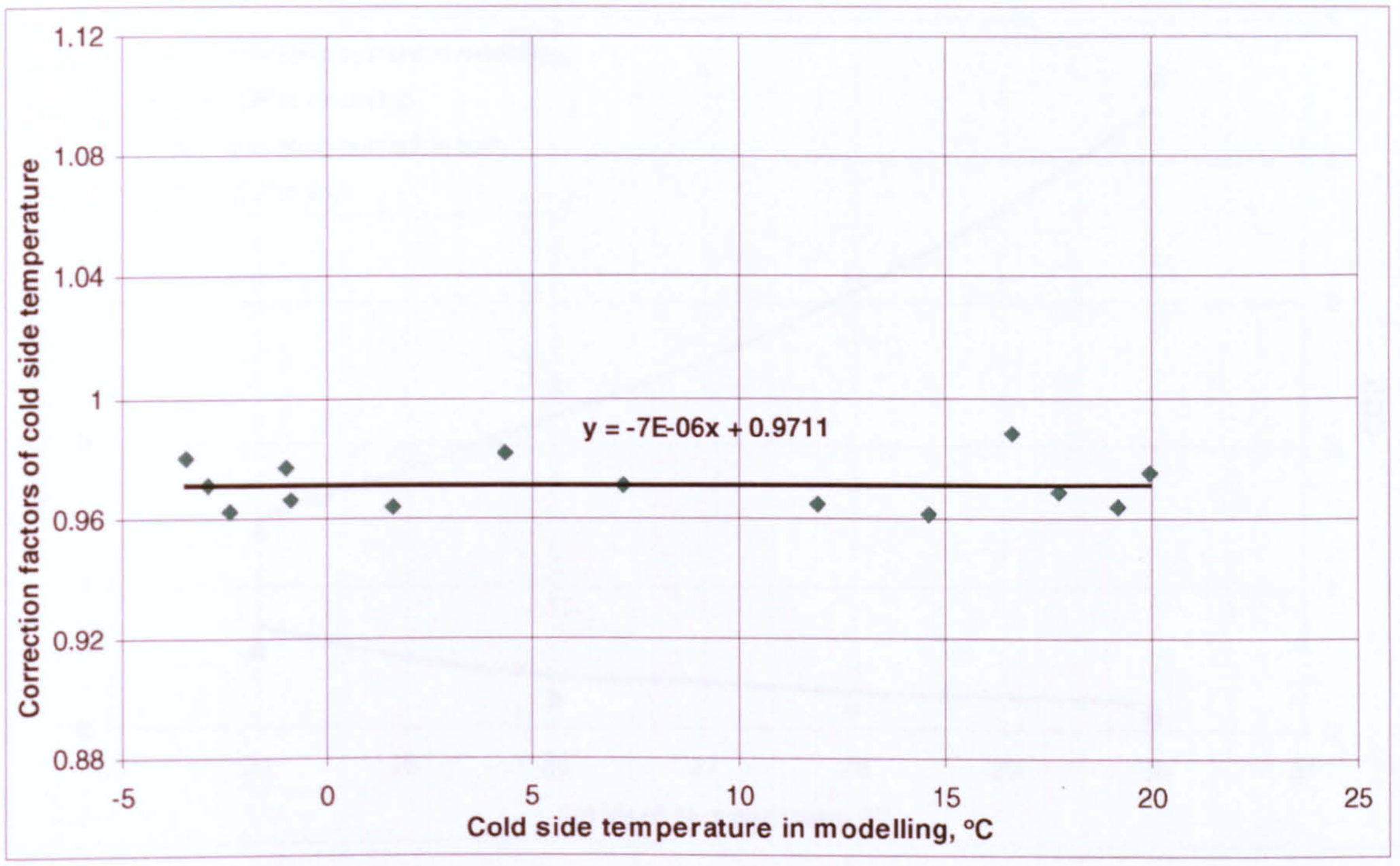

Figure 5-34. Correction factors of cold side temperature

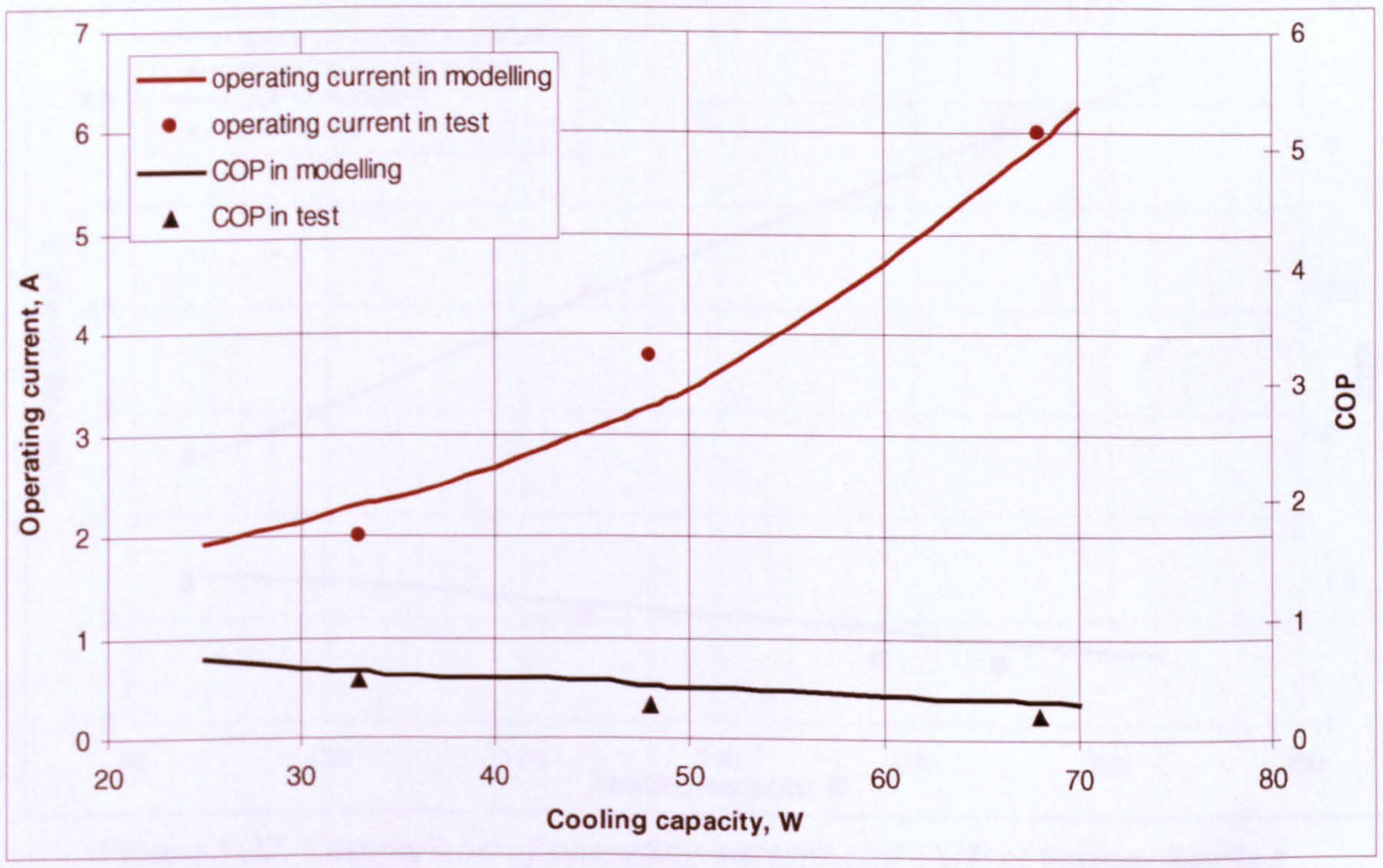

Figure 5-35. Comparison of operating current and COP at various cooling capacities in modified modelling with those in test in cooling mode

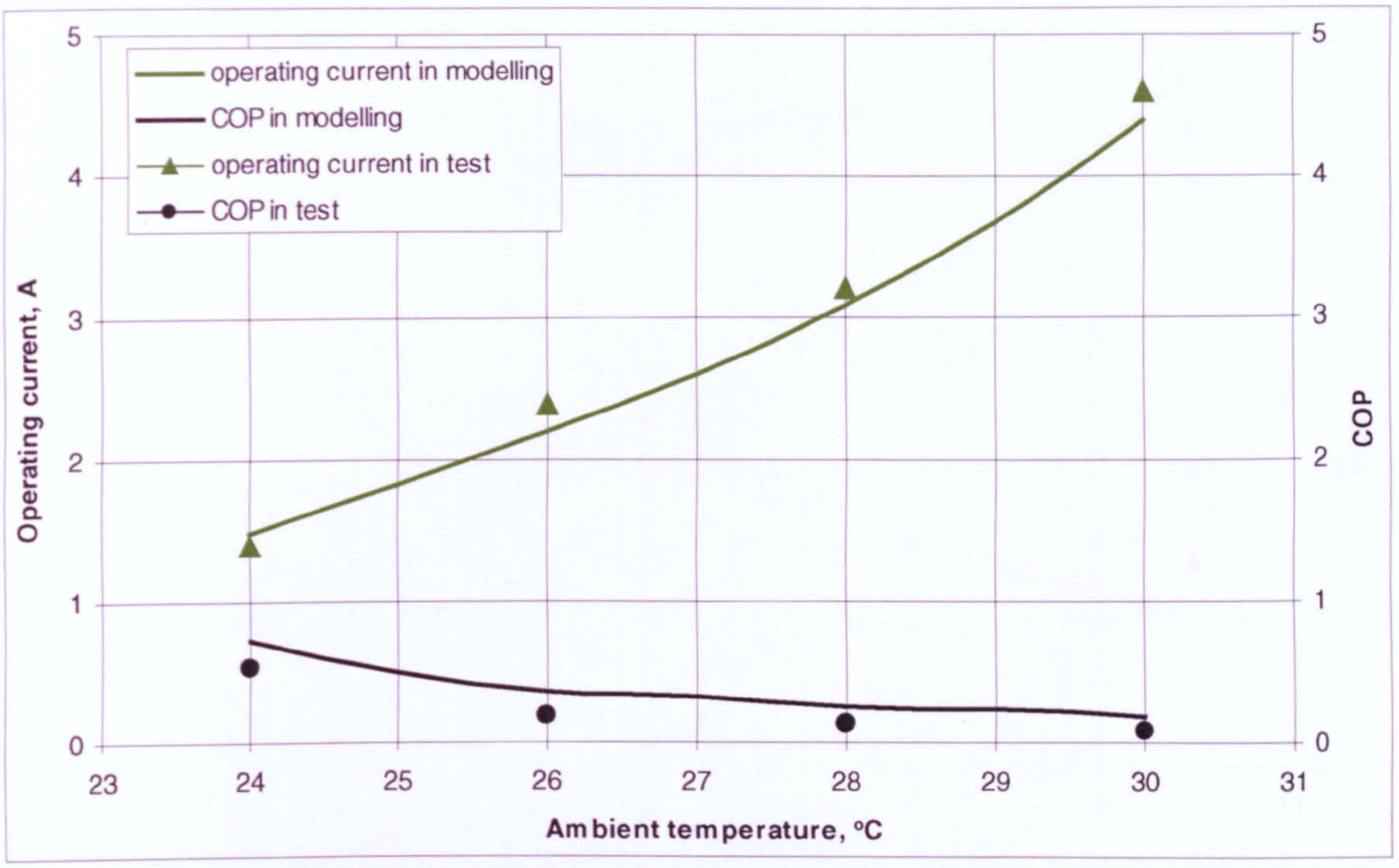

Figure 5-36. Comparison of operating current and COP at various ambient temperatures in modified modelling with those in test in cooling mode

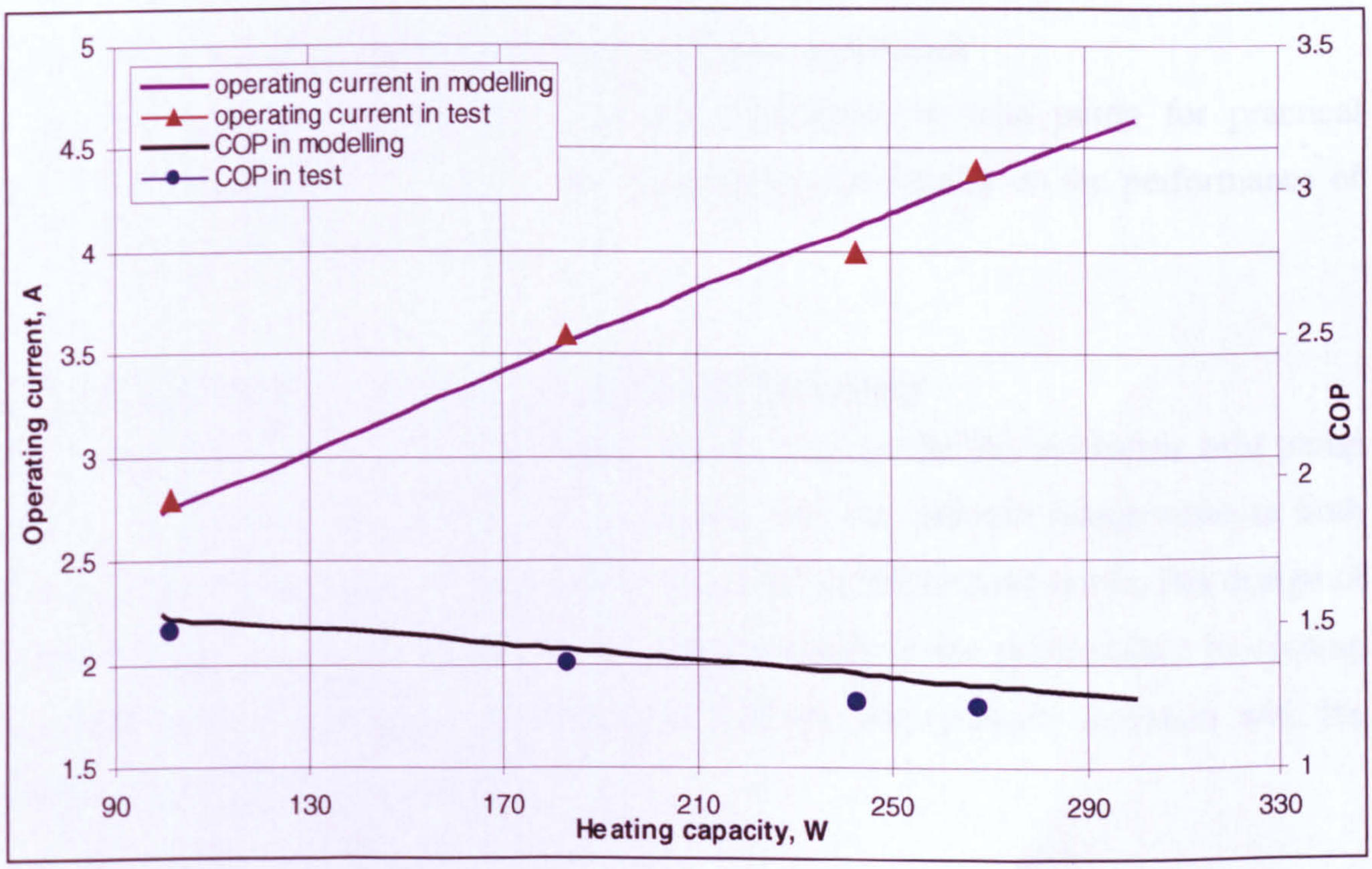

Figure 5-37. Comparison of operating current and COP at various heating capacities in modelling with those in test in heating mode

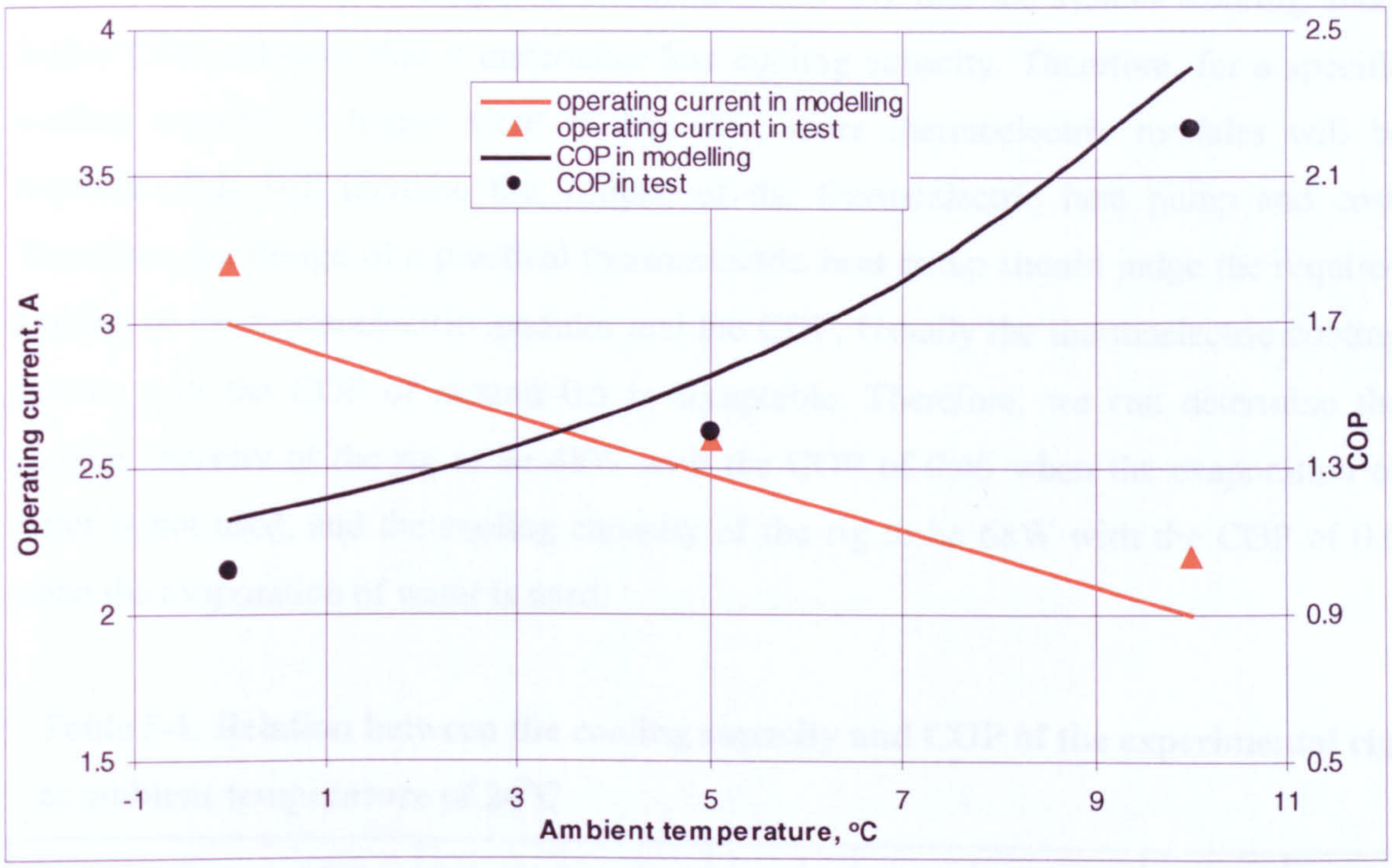

Figure 5-38. Comparison of operating current and COP at various ambient temperatures in modified modelling with those in test in heating mode

5.6 Estimation of the required scale for building application

An estimation of the required scale of the thermoelectric heat pump for practical application in building was carried out. The estimation is based on the performance of aforementioned heat pump prototype.

Determination of the COP of the thermoelectric heat pump

The modelling and testing results showed that the COP of the thermoelectric heat pump system varies with the cooling/heating capacity and the ambient temperature in both cooling and heating modes. Due to relative low COP of the cooling mode, this design of the heat pump was mainly based on the considerations of the performance in cooling mode. For a fixed ambient temperature, the COP in cooling mode decreases with the increase of the cooling capacity.

Table 5-1 shows the cooling capacity and the corresponding COP of the experimental rig at ambient temperature 24°C (the temperature of the inside box is 21°C). The system

using evaporation of the water on the outside heat sink in cooling mode was also considered in this estimation. It is shown in Table 5-1 that the system working under higher COP indicates that it undertakes less cooling capacity. Therefore, for a specific cooling capacity if higher COP is desirable, more thermoelectric modules will be required. This will increase the volume of the thermoelectric heat pump and cost. Therefore, the design of a practical thermoelectric heat pump should judge the required number of the thermoelectric modules and the COP. Usually the thermoelectric cooling system with the COP of around 0.5 is acceptable. Therefore, we can determine the cooling capacity of the rig to be 48W with the COP of 0.46 when the evaporation of water is not used, and the cooling capacity of the rig to be 68W with the COP of 0.6 when the evaporation of water is used.

Table 5-1. Relation between the cooling capacity and COP of the experimental rig at ambient temperature of 24°C

Cooling capacity, W		25	33	40	48	55	68	80
COP	No spray water	0.69	0.57	0.51	0.46	0.41	0.34	0.26
	Spray water		1.03		0.87		0.6	
Type of the modules: CP-2-127-06 (Melcor)								

Required scale of the thermoelectric heat pump for an office

The estimation of the required scale of the thermoelectric heat pump was carried out for an office in a building in Scotland (Zhao, 2002). The design conditions and parameters of the office are shown in Table 5-2.

Table 5-2. Design conditions and parameters of an office

Area, m^2	Cooling/heating capacity, W/m^2		Environmental temperature, °C	
15	Summer	Winter	Summer	Winter
	60	40	24	-4
Temperature inside the room: 21°C				

The total cooling capacity of the office is $15m^2 \times 60W/m^2 = 900W$. The required thermoelectric modules should be the total cooling capacity /determined cooling capacity of the rig × number of the thermoelectric modules of the rig.

The total heating capacity of the office is $15m^2 \times 40W/m^2 = 600W$. The COP in heating mode can be obtained by modelling based on the above-determined scale of the heat pump.

The results of the estimated scale for the office are shown in Table 5-3, which gave the required number of the thermoelectric modules and the performance of the heat pump system. Of course, the thermal diode and the heat sink system should be designed to fit this scale.

Table 5-3. Required number and total area of thermoelectric modules and the performance of the system for an office

	Number of modules	Total area, m^2	COP		Power required, W	
			Cooling mode	Heating mode	Cooling mode	Heating Mode
No spray water in cooling mode	150	0.54	0.46	1.13	1957	531
Spray water in cooling mode	106	0.38	0.6	1.12	1500	536

5.7 Environmental and Potential Economical Effects

Conventional vapour-compression air conditioners have the advantages of high COP and low purchase price. However, most working fluids employed in conventional vapour-compression air conditioners are damaging to the environment and as vapour-compression systems contain moving parts, they have the further disadvantages of being noisy and requiring regular maintenance. Concern over global warming and depletion of ozone layer has simulated research to develop cooling methods which do not employ environmentally damaging working fluids such as CFCs and HCFCs. One of the methods is to employ thermoelectric cooling systems. Thermoelectric cooling systems use Peltier effect to produce cooling, they don't contain moving parts (except for cooling

fan) and have long life span. They are environmental friendly, as they are solid state heat pump and don't use environmentally damaging working fluids.

Compared to the conventional vapour-compression air conditioner, the thermoelectric cooling systems have the disadvantages of low COP and high cost. The COPs of the vapour-compression air conditioners are around 2.2~3, while the COP of the thermoelectric heat pump system in this research is 0.5 in cooling mode. Current commercially available thermoelectric air conditioners have the COP of 0.38~0.45 in cooling mode. A 2600W vapour-compression air conditioner costs just £318, while a 320W thermoelectric air conditioner costs £880 [Riffat S.B, 2004]. It is seen that on the basis of performance and cost, the thermoelectric cooling systems are not competitive to the conventional vapour-compression systems.

However, it is predicted that thermoelectric domestic heat pumps and air conditioners will become competitive in the world market. This is because energy costs and demands can only increase and environmental concerns can only increase. Also the environmental treaties have banned chlorofluorocarbons. [www.zts.com]

Furthermore, the new thermoelectric materials with large figure of merit ZT could make a breakthrough on applications of the thermoelectric modules in various fields. Currently, bismuth telluride (Bi_2Te_3), which is the best low temperature thermoelectric material and is widely employed in thermoelectric generators and coolers. Bi_2Te_3 possess a maximum value of ZT~1. If the ZT could be raised to 2 or 3, the thermoelectric cooling system would be competitive with vapour compression cooling systems. Recent advances have indicated the possibility of overcoming classical limitations and increasing the figure of merit of the thermoelectric materials significantly. The investigations include the following aspects: tailoring the microstructure of a material to increase phonon scattering in order to decrease thermal conductivity; reducing the dimensionality of the material so that quantum size-effects alter the ratio between the electrical and thermal conductivity; use of quasicrystals as potential thermoelectric materials; use of inhomogeneous materials (with functional gradients) and development of thin-film thermoelectric materials which has achieved a figure of merit of approximate 2.4 [Venkatasubramanian R, 2001].

In addition, investigations have demonstrated the effect of size of the thermoelements on the COP and heat pumping capacity of the thermoelectric module. A relatively long thermoelement is required to obtain a large COP, while a relatively short thermoelement is desirable for achieving maximum heat pumping capacity. The optimum module design will be a compromise between the requirements of COP and heat pumping capacity. The investigations also showed that reducing the contact resistances, is an essential requirement to achieve a further improvement in both COP and heat pumping capacity of a thermoelectric module [Gao M, 2000].

Moreover, thermoelectric cooling systems can directly employs solar PV cells as power source, by which the low COP would not be a main drawback. Although PVs are expensive at present, it is anticipated the development of the technology particularly regarding preparation methods, and market growth will bring about a fall in prices. The development of the manufacturing technology of the semiconductor material will also reduce the prices of the thermoelectric modules. Combining PVs with thermoelectric refrigeration system will produce an attractive system that are stand alone, no moving part and noise, environment friendly.

In a word, the thermoelectric cooling system would become competitive in both economical and environmental aspects in the future.

5.8 Conclusion

- A thermoelectric heat pump prototype were designed and constructed to work in two modes, i.e., cooling mode and heating mode. The heat pump incorporated a number of innovative ideas in structure design to produce a compact unit. Analytical models were used to optimise the design (selection) of all the components with the aim of improving the COP of the system.

- A theoretical model was developed to estimate the thermal performance of the heat pump system for various operating and weather conditions. The heat processes in different areas of the heat pump were investigated, and these were then corresponding linked together by a set of heat balance equations.

- The thermal performance of the heat pump system was investigated using the computer model developed. Given the structure of the heat pump, the COP and the required DC current varies with cooling capacities (in cooling mode), heating capacities (in heating mode) and ambient temperature. In cooling mode, the COP decrease and the DC current increase with the increase of cooling capacity and environmental temperature. In heating mode, the COP decrease and the DC current increase with the increasing heating capacity, the COP increase and the DC current decrease with the increasing ambient temperature.

- Laboratory tests were carried out to provide experimental results on the performance of the heat pump prototype. The tests were carried out in the environmental chamber in School of the Built Environment, University of Nottingham. Test results were obtained for different cooling (heating) capacities and ambient temperatures. Experimental COP in cooling mode decreases with the increase of the cooling capacity and ambient temperature. Experimental COP in heating mode decreases with the increase of heating capacity and increases with the increase of ambient temperature. Further tests in cooling mode were carried out to investigate the effect of cooling due to evaporation of water on system performance. It was found that providing cooling of the outside heat sink by spraying water (30ml/min) onto it for subsequent evaporation, resulted in a 78%~233% improvement of COP.

- Modelling and experimental results were compared for the heat pump prototype. It was found that the modelling results and experimental data showed a very similar trend for COP and operating currents, however, distinct differences exists between the values of the modelling and test results, the experimental COP are lower and required currents are larger than the values predicted by modelling. One reason for this is the calculation of the thermal resistance of thermal diode in modelling was simplified due to the existing difficulty of calculating the thermal resistance of the new type thermal diode with a complex structure. Another reason for this is the difference between the designed heat sinks and the practical heat sinks. These cause the larger difference between the hot side and cold side temperatures shown in modelling and those in tests. The reasons for the difference between modelling and experimental results also include the limit of the model's accuracy as well as the

manufacturing tolerances of the thermoelectric modules. These treatments were not taken into account in modelling development and processing.

- Correction factors were determined by dividing the hot and cold side temperatures obtained in tests by the hot and cold side temperatures obtained in modelling respectively. By correcting the hot side and cold side temperatures more accurate modelling results were obtained. This correlation would be applied to any circumstance for this type of thermoelectric heat pump, and expected to improve the accuracy of the modelling predictions to a substantial extent.

- The required scale for an office in a building in Scotland was estimated. The estimation was carried out for the system both using evaporation of water and not using evaporation in cooling mode. An acceptable COP of around 0.5 in cooling mode is determined. The estimated scale for the office is 150 pieces of CP2-127-06 thermoelectric modules with the area of 0.54m^2 while not using the evaporation of water in cooling mode, and 106 pieces of CP2-127-06 thermoelectric modules with the area of 0.38m^2.

- The environmental and potential effects were analysed and investigated. Although on the basis of performance and cost, the thermoelectric cooling systems are not competitive to the conventional vapour-compression systems presently, the thermoelectric heat pumps have the potential large market due to the environmental concerns. Furthermore, the investigations on the thermoelectric material for high ZT could improve the COP greatly. The development of the manufacturing technology of semiconductor material could reduce the prices of thermoelectric modules and PVs. Therefore, combining PVs with thermoelectric refrigeration system will produce an attractive system that are stand alone, no moving part and noise, environment friendly. The thermoelectric cooling system would become competitive in both economical and environmental aspects.

Chapter 6. Experimental Investigation of Thermoelectric Refrigerator Using Phase Change Material

6.1 Aim of the Experimental Investigation

As aforementioned, combining PVs with thermoelectric refrigeration system will produce an attractive system that are stand alone, no moving part and noise, environment friendly. As solar radiation is intermittent, a means of energy storage for periods of low insolation and night time is essential. To achieve this, the system needs to be integrated with heat storage and recovery systems. The work described in this chapter was to investigate the use of phase change materials in a refrigerator to store the excess cooling, allowing it to be reused in periods of low insolation and nighttime. The system can then operate day and night, without the need for large electricity batteries.

6.2 Scheme of the Experimental Investigation

The work involved the design, fabrication and testing of a small thermoelectric refrigeration prototype. The experimental investigation was carried out in two steps. The first step is to investigate the potential of phase change materials (PCMs) for use with thermoelectric modules in refrigeration system, in order to evaluate the effect of the PCM on the performance of the thermoelectric refrigeration, the system was constructed and tested for two different configurations. One configuration employed a conventional heat sink system (bonded fin heat sink) on the cold side of the thermoelectric modules. Another configuration was constructed using an encapsulated phase change material in place of the conventional heat sink unit. The performance of the two configurations were tested and compared. Results of tests of the latter system showed an improved performance as well as the cooling storage capability, which would be particularly useful for handling the peak loads, and overcoming losses during door openings and power-off periods. However to improve the storage capability, in particular during off-power periods, it was found necessary to integrate the PCM with a thermal diode, which would allow heat flow in one direction only. The second step is therefore to investigate the potential application of PCMs integrated with thermal diodes in the thermoelectric refrigerator. The thermoelectric refrigerator was reconstructed employing phase change material integrated with thermal diodes (thermosyphons) on the cold side of the thermoelectric modules and tested.

All the configurations used heat pipes embedded fins as the heat sink on the hot side.

The thermoelectric modules used in this system are obtained from Thermo Electric Devices (an UK supplier of Melcor cooling modules). These modules could maintain a temperature difference as high as 64°C between the hot and the cold side when operated at full capacity (i.e., at 14.4 V and 8.5 A DC) under no load conditions [Kin-ichi Uemura, 1995]. In most of the tests carried out on the thermoelectric refrigeration system under consideration, the maximum temperature difference between the cold and the hot junctions was 43°C, i.e., about 67% of the maximum design. The temperature difference could be increased by increasing the input energy, or by cascading the thermoelectric modules. All the tests were carried out with each module operated at 7.5 V and 3.5 A DC, which achieve the required temperature difference.

The experimental investigation in the two steps is described in section 6.3 and section 6.4 respectively.

6.3 Experimental Investigation of the Thermoelectric Refrigeration System Employing a Phase Change Material

6.3.1 Description of the experimental system

Details of the thermoelectric refrigeration system tested in this study are shown in Fig.6-1. The system comprises a refrigeration cabinet (420mm×420mm×380mm), six thermoelectric modules (type PT-12-40), and three (heat pipe, embedded fin) heat sink units on the hot side of the thermoelectric modules. The refrigeration system was first tested with a bonded fin heat sink unit mounted on the cold side of the thermoelectric modules as a cold heat sink. In the second test, an encapsulated PCM replaced the bonded fin heat sink unit. The encapsulated PCM used in this test is known as "ClimSel C7" and was obtained from Climator AB, Sweden (www.climator.com). The product consists of a mixture of sodium sulphate, ammonium chloride and potassium chloride with additives to prevent super-cooling. The salt mixture has a transition temperature point of 7°C and specific gravity of 1.42-kg/l. The encapsulated PCM has a latent heat fusion of 36 Wh/kg and a storage capacity of 50 Wh/kg in the temperature range 2.5–20°C.

The six thermoelectric modules were mounted side by side and were electrically connected in series. A metallic space block made of aluminum was placed between the cold plates of the thermoelectric modules and the cold side heat sink. The thermal contacts between the thermoelectric modules and heat sink units were improved by applying a thin film of thermal grease.

The heat sink on the hot side of the thermoelectric modules was made of a heat pipe, embedded-fin system of a thermal resistance 0.012°C W^{-1}. Three of these units were mounted on the hot side. Each of these units is capable of dissipating a maximum of 200 W, when mounted vertically. However, when mounted horizontally, it can handle only 150 W. Therefore a small fan was used to provide forced air convection on the hot side heat sink. Tests were carried out with this fan on, and off, in order to investigate its significant on the performance of the cooling system.

The refrigeration cabinet was insulated on the inside by a 25mm thick polystyrene plate, and held in place by an extruded PTFE sheet of thickness 3mm.

Power input to the thermoelectric modules was provided by a 400W DC power supply system.

When DC current is applied to thermoelectric refrigeration systems described in Figure 6-1, the thermoelectric modules absorb heat from the metallic block inside the refrigeration cabinet, and dissipate heat to the outside heat sink, thus create cold and hot side.

On the hot side, the working fluid in the evaporator end of the heat pipe, embedded-fin heat sink, evaporates and travels to the condenser end, where it condenses whilst dissipating heat. The heat is carried away by air convection. The working fluid returns to the evaporator by the capillary head of the heat pipe wick of the embedded-fin heat sink. On the cold side of the system, the bonded fin heat sink or PCM cools down whilst dissipating heat to the cold side of the thermoelectric modules. In the PCM system, the PCM dissipates energy, first as sensible heat, and when the phase change temperature is reached as latent heat. This maintains the refrigeration cabinet at the required

temperature, i.e., the transition temperature of the PCM, with any further cooling stored as latent energy. Photographs of the tested thermoelectric refrigeration prototype system are shown in Figures 6-2, and 6-3.

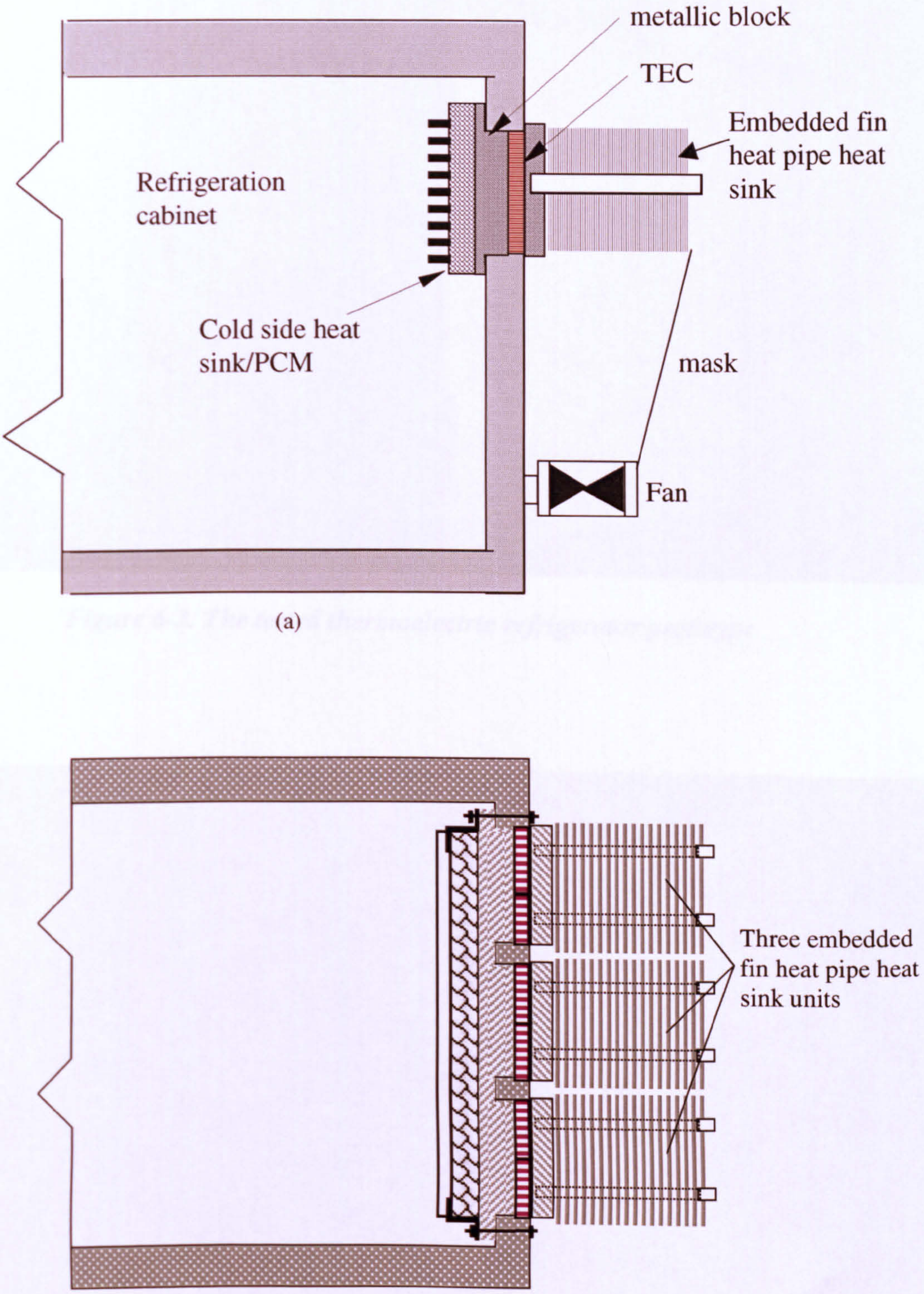

Figure 6-1. Schematic description of an experimental refrigeration system from different views (a) vertical section (b) horizontal section

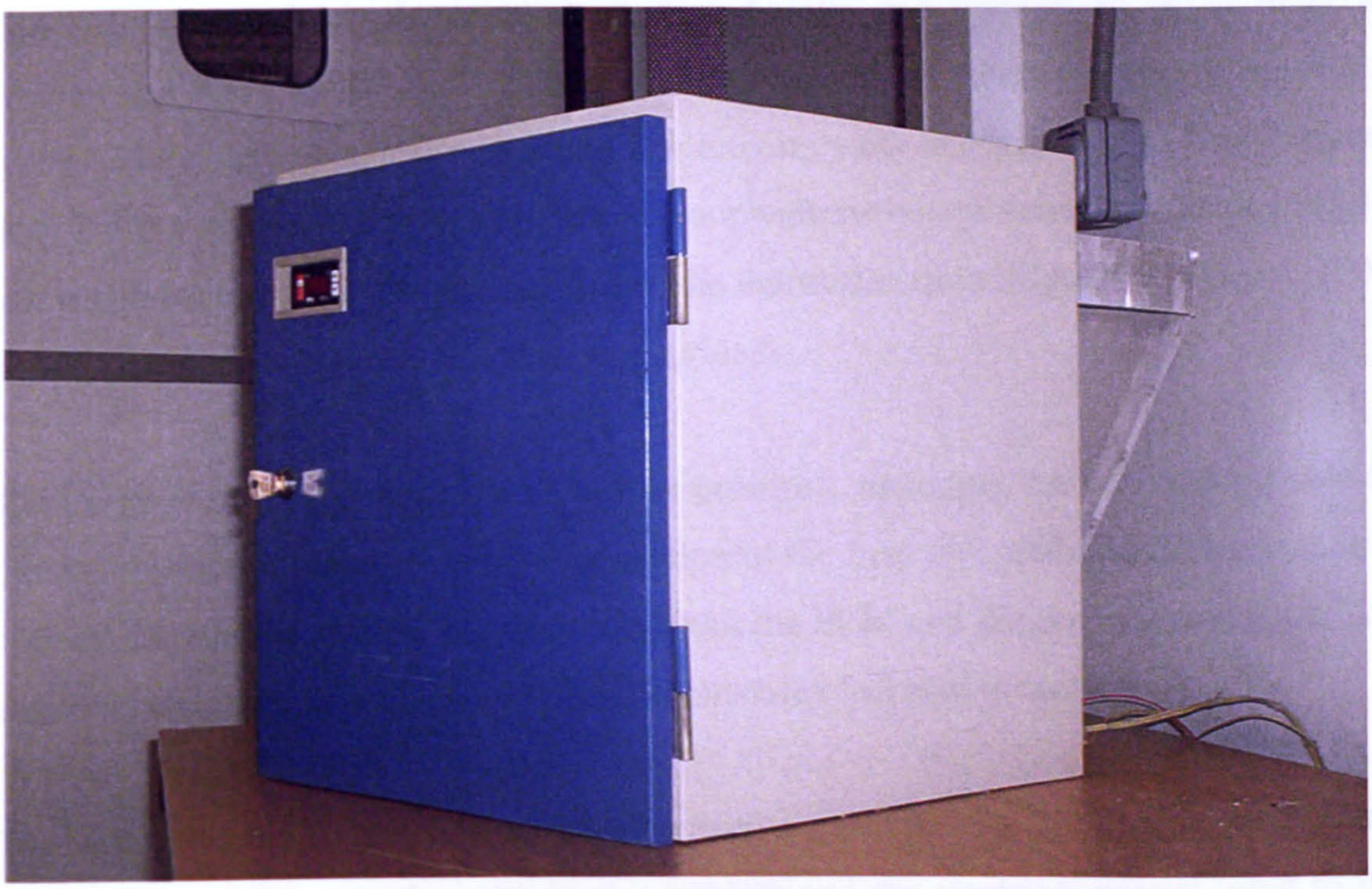

Figure 6-2. The tested thermoelectric refrigerator prototype

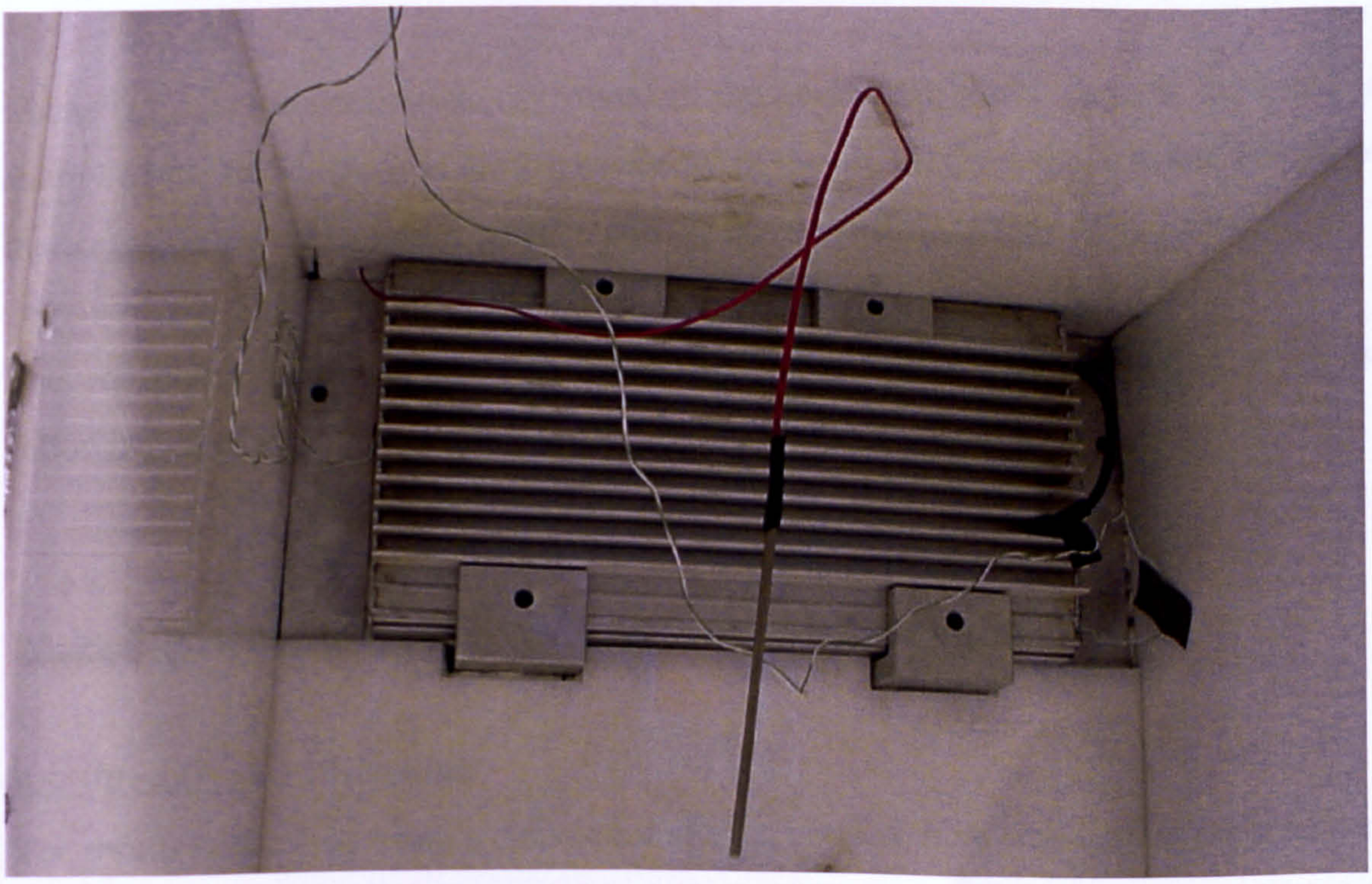

Figure 6-3. Encapsulated PCM as a cold heat sink.

6.3.2 Test Methodology

Since the aim of the study was to examine the potential of PCMs for use with thermoelectric modules, the system was tested with, and without PCM, in order to evaluate the effect of the PCM on the performance of the thermoelectric refrigeration system. The intention was also to use as few moving parts as possible, e.g., heat removal fans. For this reason, tests were also carried out with the heat removal fan on, and off, to investigate its effect on the performance of the thermoelectric refrigeration system. 1500 ml of water was used to simulate the cooling load.

The temperatures were measured at various positions, including the cold and hot side of the thermoelectric modules, condenser section of the heat pipe-embedded fins heat sink system, the interior of the refrigeration cabinet, the PCM and the environmental air. The electrical energy input to the thermoelectric modules was also measured.

The performance of the refrigeration system was evaluated by calculating the cooling energy dissipated inside the refrigeration cabinet and the electrical energy input to the thermoelectric modules. The cooling energy produced by the system was estimated using the following equation:

$$Q_{c,e} = Q_{allum} + Q_{spcm} + Q_{lpcm} + Q_w + Q_a \tag{6-1}$$

where Q_{allum} is the cooling energy stored in the aluminum block, Q_{spcm} is the sensible energy of the PCM, Q_{lpcm} is the latent energy of the PCM, Q_a is the sensible energy of the air inside the refrigeration cabinet, and Q_w is the sensible energy of the water.

The coefficient of performance of the refrigeration system was calculated using the following equation:

$$COP = Q_{c,e} / Q_{input} \tag{6-2}$$

Where Q_{input} is the electrical energy input to the thermoelectric modules.

6.3.3 Results and Discussion

The results of the tests using a conventional (fins bonded) heat sink system are presented in Figure 6-4, Figure 6-5, Figure 6-6 and Figure 6-7. Figure 6-4 shows the testing with

the heat removal fan off. It is seen that the cold side temperature dropped by 12 degrees and then increased, the system can not work normally and the temperature inside the cabinet increase slightly rather than decrease. Figure 6-5 shows the test with the heat removal fan on. It is seen that with the heat removal fan on, the system can work efficiently. After 90 minutes, the maximum temperature difference between the hot and cold side was reached. The temperature inside the cabinet did not drop too much due to the short period of the testing. If another small fan was used to increase the convection inside the cabinet, the temperature inside the cabinet can drop quickly and a test shown in Figure 6-6 illustrates this. To further illustrate the significant of the fan on the performance of this system, the hot side and the cold side temperatures are compared with the heat removal fan (on the hot side) on, and off, and this is shown in Figure 6-7. As shown in Figure 6-7, with fan off, the cold side temperature dropped by a few degrees and then increased, following the same pattern as the hot side temperature. Although the temperature difference between the hot and the cold side was almost equal, both when the fan was switched on, and off, the temperature of the hot side continued to increase, as did that of the cold side, until the condition of the maximum temperature difference for the given electrical input was reached. This is because the heat on the hot side can not be removed effectively and therefore the hot side temperature rose continuously, the cold side temperature also continued to increase due to the maximum temperature difference for the given electrical input was reached.

The above tests and analysis showed that it is necessary for the system to use heat removal fan on the heat pipe-embedded fins heat sink units. All the following tests shown in this chapter used the fan on the heat pipe-embedded fins heat sink units. Using of the small fan inside cabinet can speed up the cooling process but is not necessary, and did not apply to any the following tests.

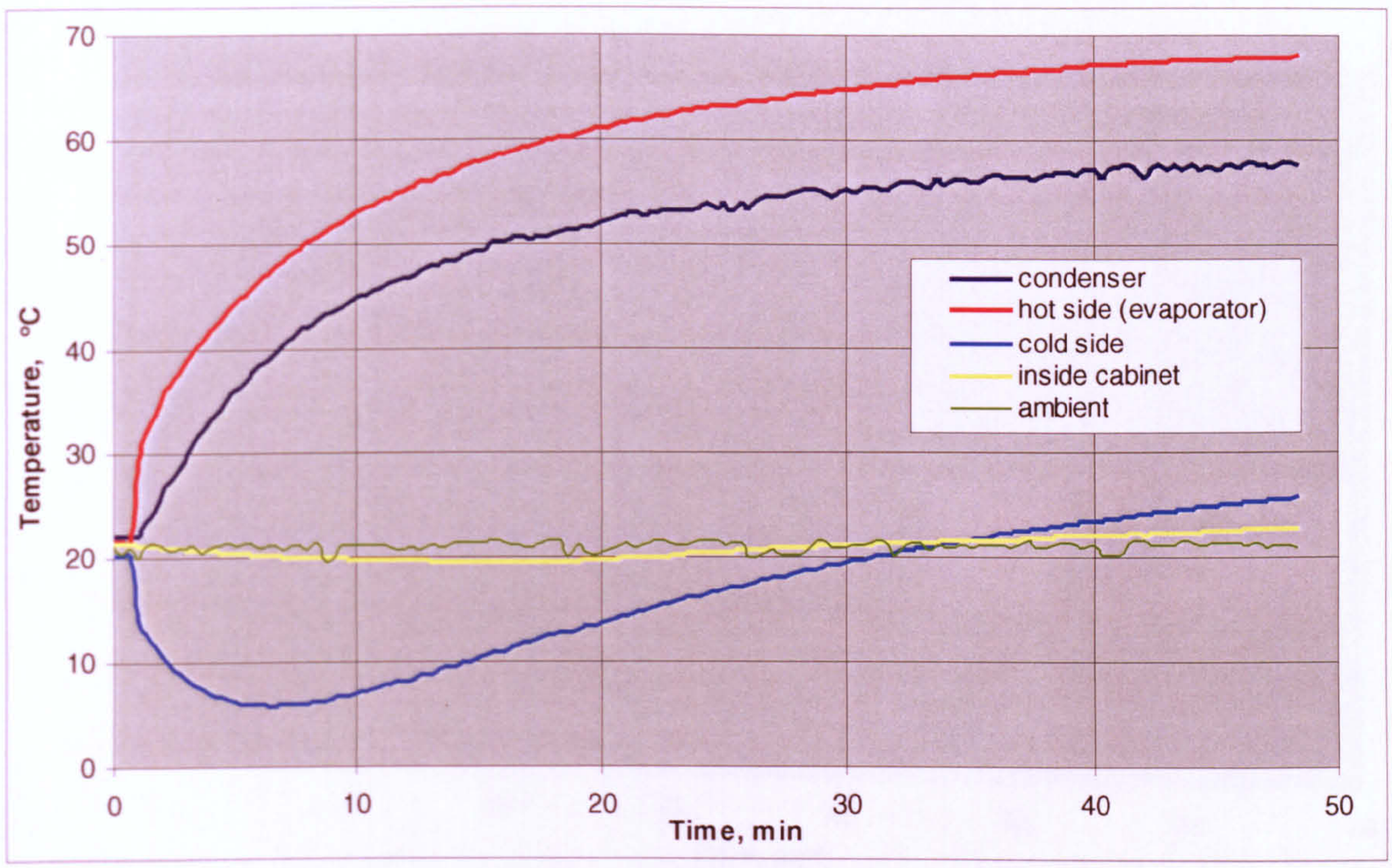

Figure 6-4. Variation of the temperatures with time on the condition of fan off for the bonded fins heat sink system

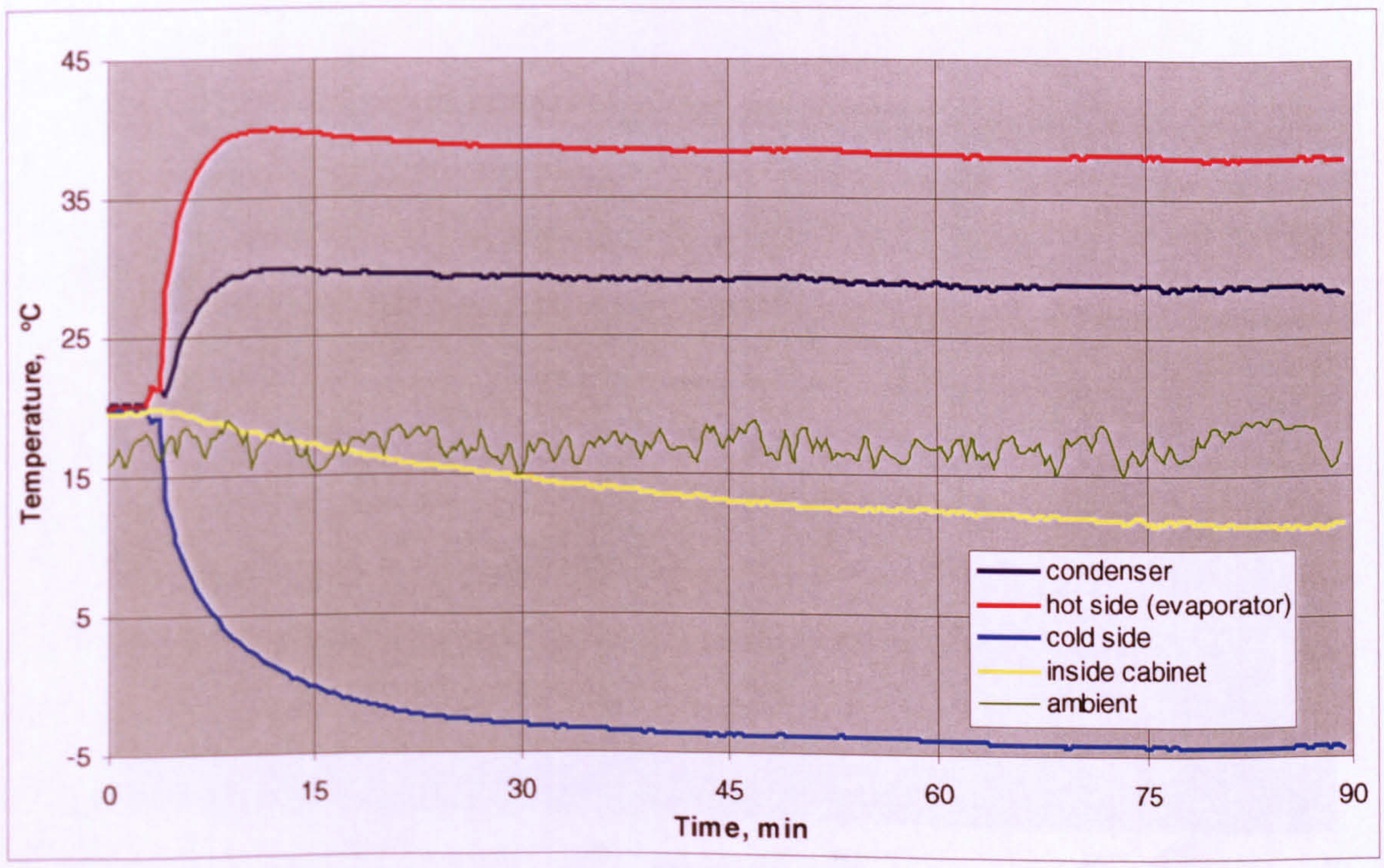

Figure 6-5. Variation of the temperatures with time on the condition of fan on for the bonded fins heat sink system

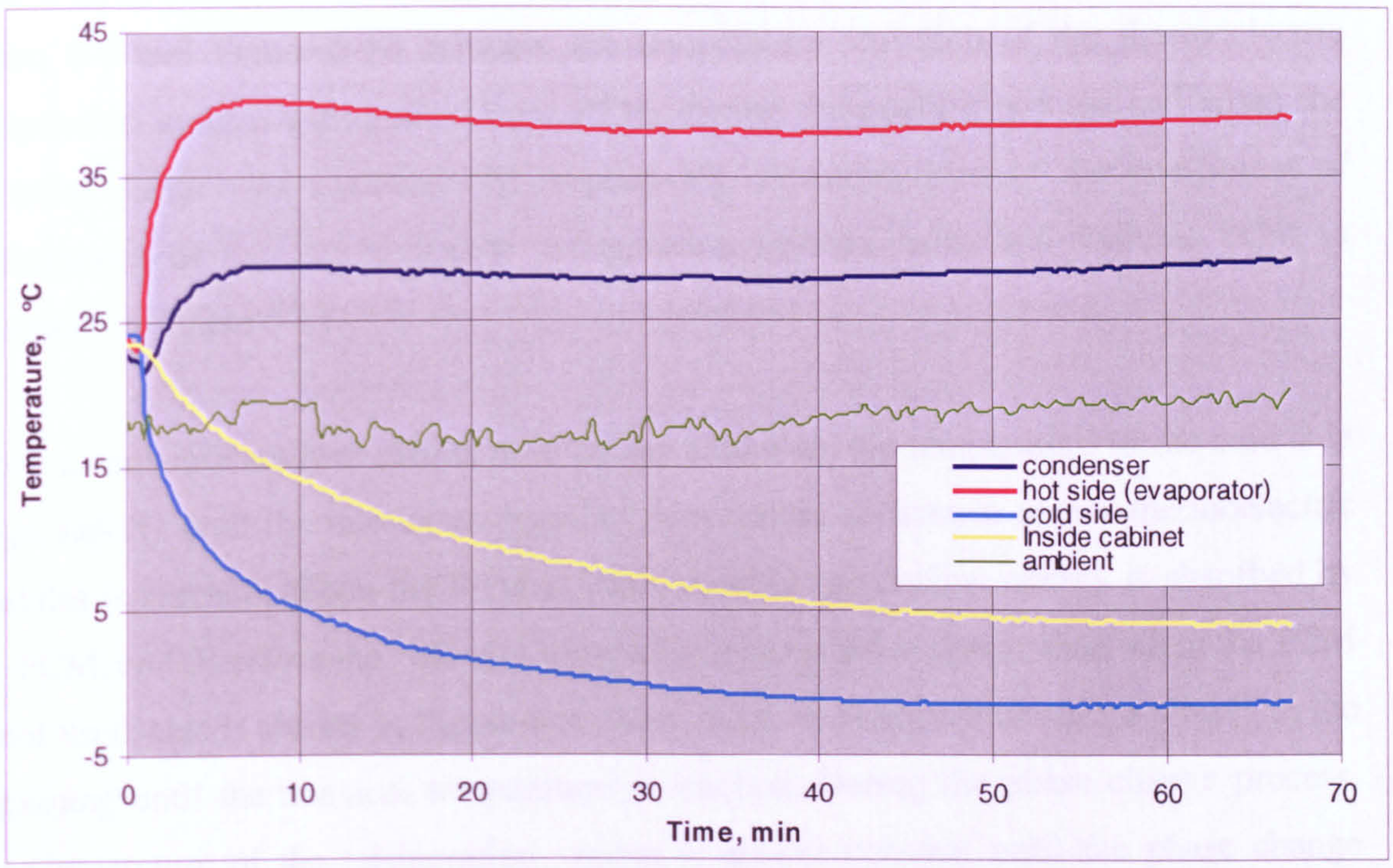

Figure 6-6. Variation of the temperatures with time on the condition of improved convection inside the cabinet for the bonded fins heat sink system.

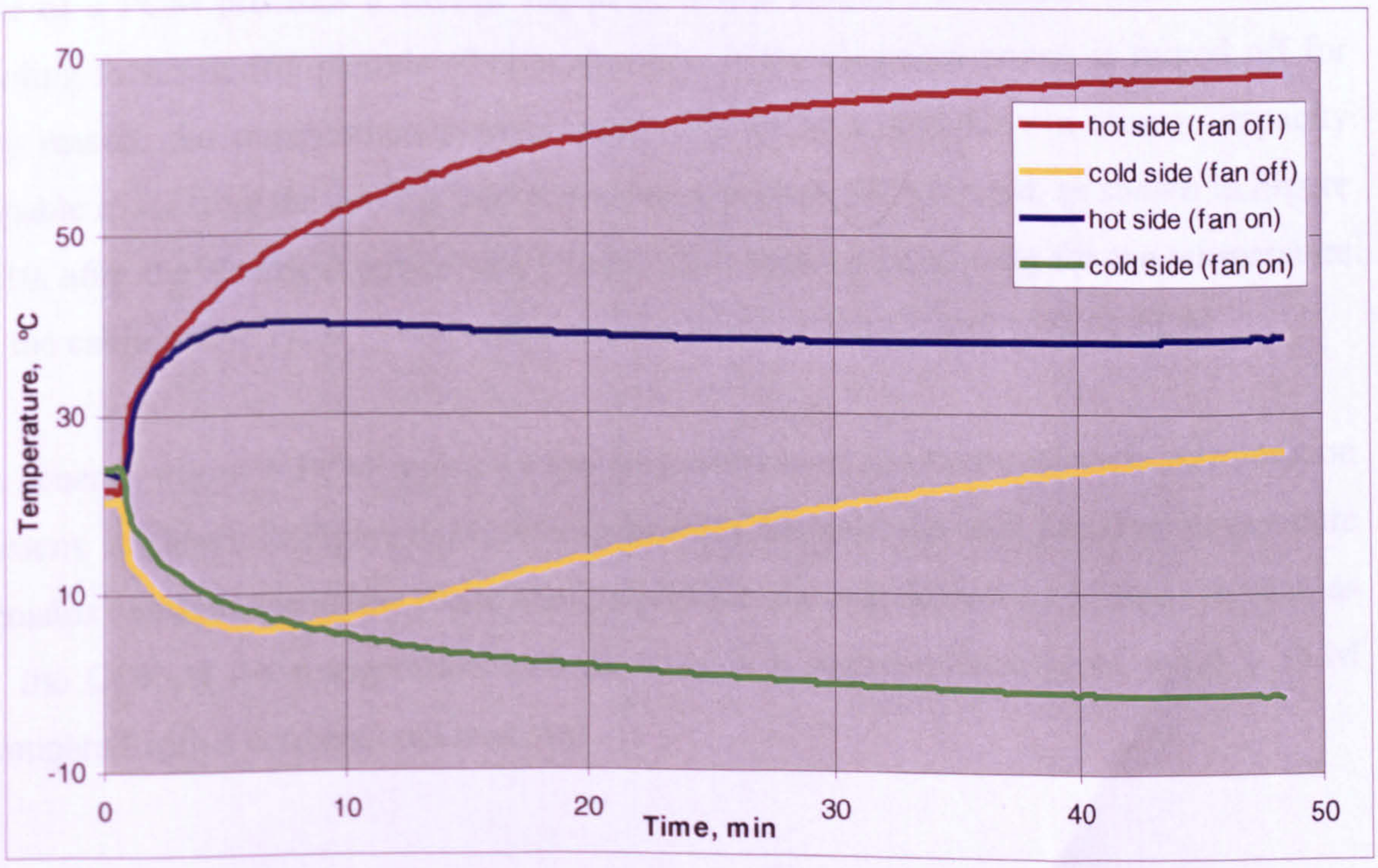

Figure 6-7. Variation of thermoelectric module hot and cold side temperatures with, and without, a heat removal fan for the bonded-fins heat sink system.

Figure 6-8 shows a test using the encapsulated PCM replaced the bonded heat sink unit. Figure 6-9 and Figure 6-10 compare the temperature variation of the thermoelectric refrigeration system with and without PCM, during the cooling process and when the electrical power was switched off, respectively. A comparison of the coefficient of performance of the thermoelectric refrigeration systems with and without PCM is presented in Figure 6-11.

When a conventional heat sink is used on the cold side, the temperature of the cold side drops rapidly until the maximum possible temperature difference across thermoelectric modules is reached. When the PCM is used, most of the cooling energy is absorbed by the PCM, and therefore the cold side temperature drops more slowly than when the PCM is not used; this is shown in Figure 6-9. With PCM, the temperature drops slowly at the beginning until the transient temperature is reached. During the phase change process, the temperature of the refrigeration system is almost constant until the phase change process is complete, as shown in Figure 6-9. This helps to keep the temperature difference across the thermoelectric modules to a minimum, thus improving its performance.

Use of a PCM provides a storage capacity, which helps to overcome peak loads and cooling losses during periods of door opening. If the electrical power is turned off for any reason, the refrigeration system employing PCM would have a storage capacity capable of meeting the cooling load for a longer period. For example, as shown in Figure 6-10, after the electrical power was turned off, it took twice as long for the temperature in the cabinet with PCM to rise to the same value as in the cabinet with no PCM.

In general, use of a PCM improves the performance of the thermoelectric refrigeration system, as shown in Figure 6-11. As can be seen, because the cold junction temperature remains constant during the phase change process, the rate of cooling is also constant, as is the COP of the refrigeration system. This is a major advantage of using a PCM compared with a conventional heat sink.

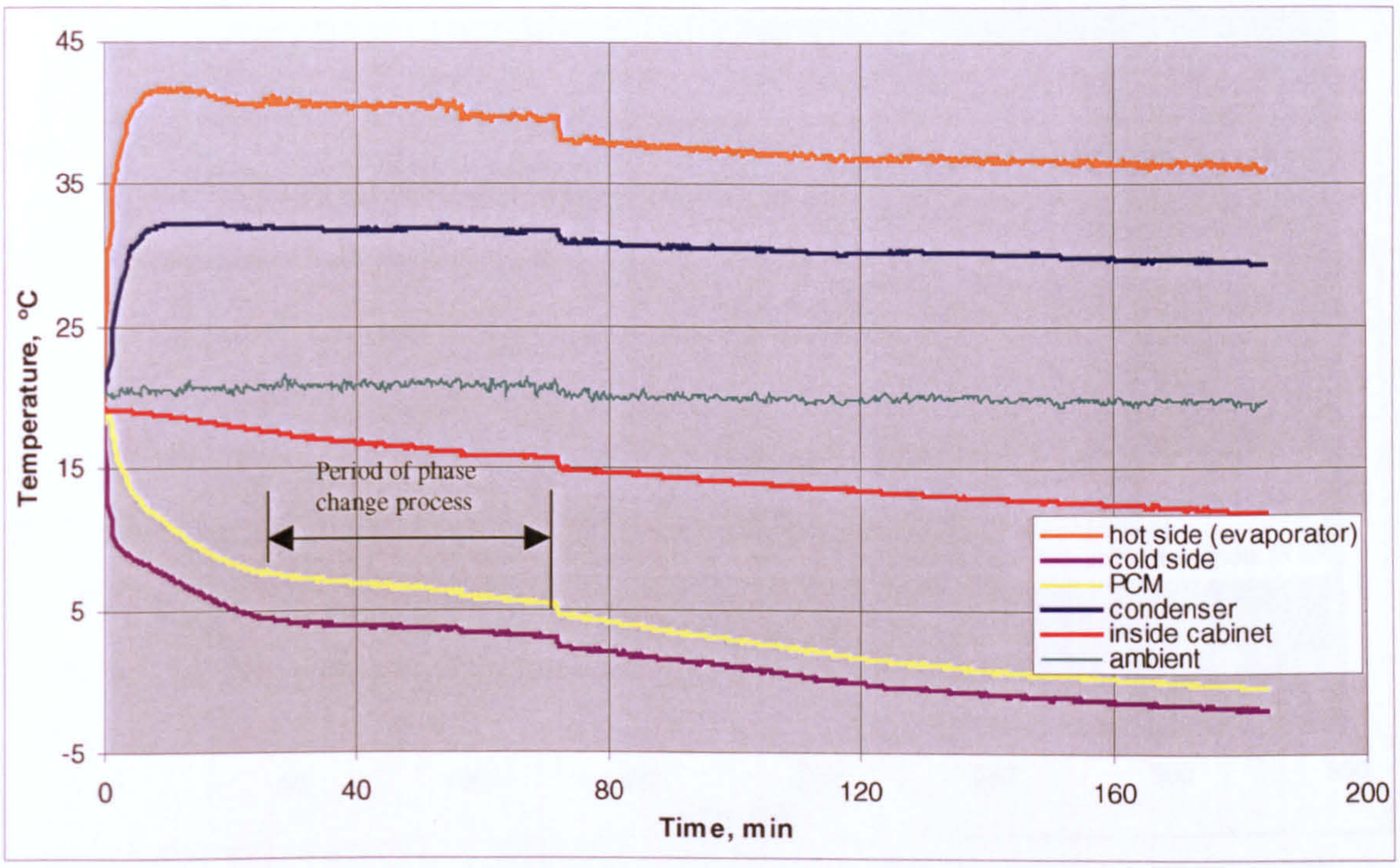

Figure 6-8. Variation of the temperatures with time for the PCM system

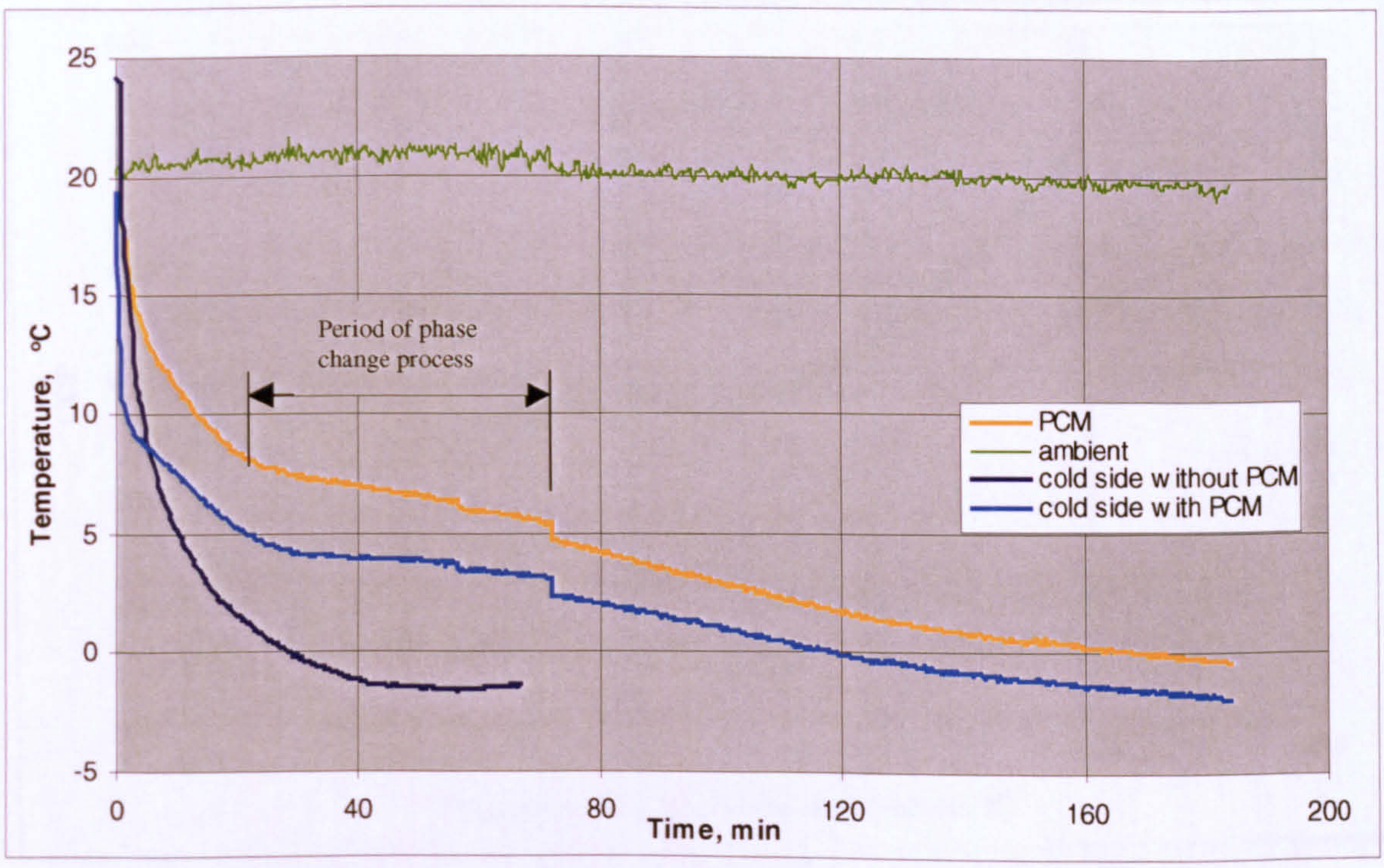

Figure 6-9. Variation of cold side and PCM temperatures during the cooling process for the tests with and without PCM.

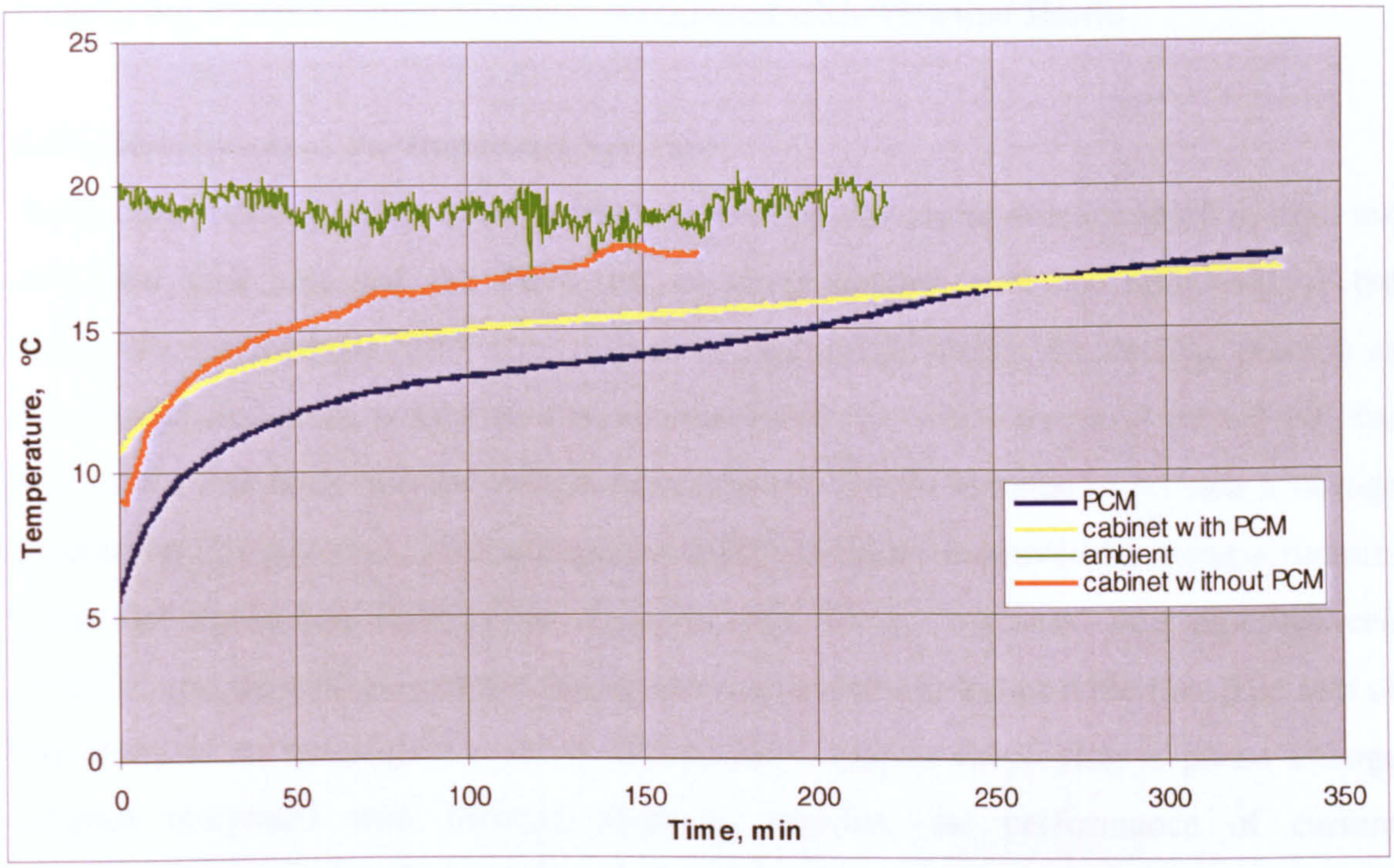

Figure 6-10. Variation of cabinet and PCM temperatures for the tests with, and without, PCM, after the power was switched off.

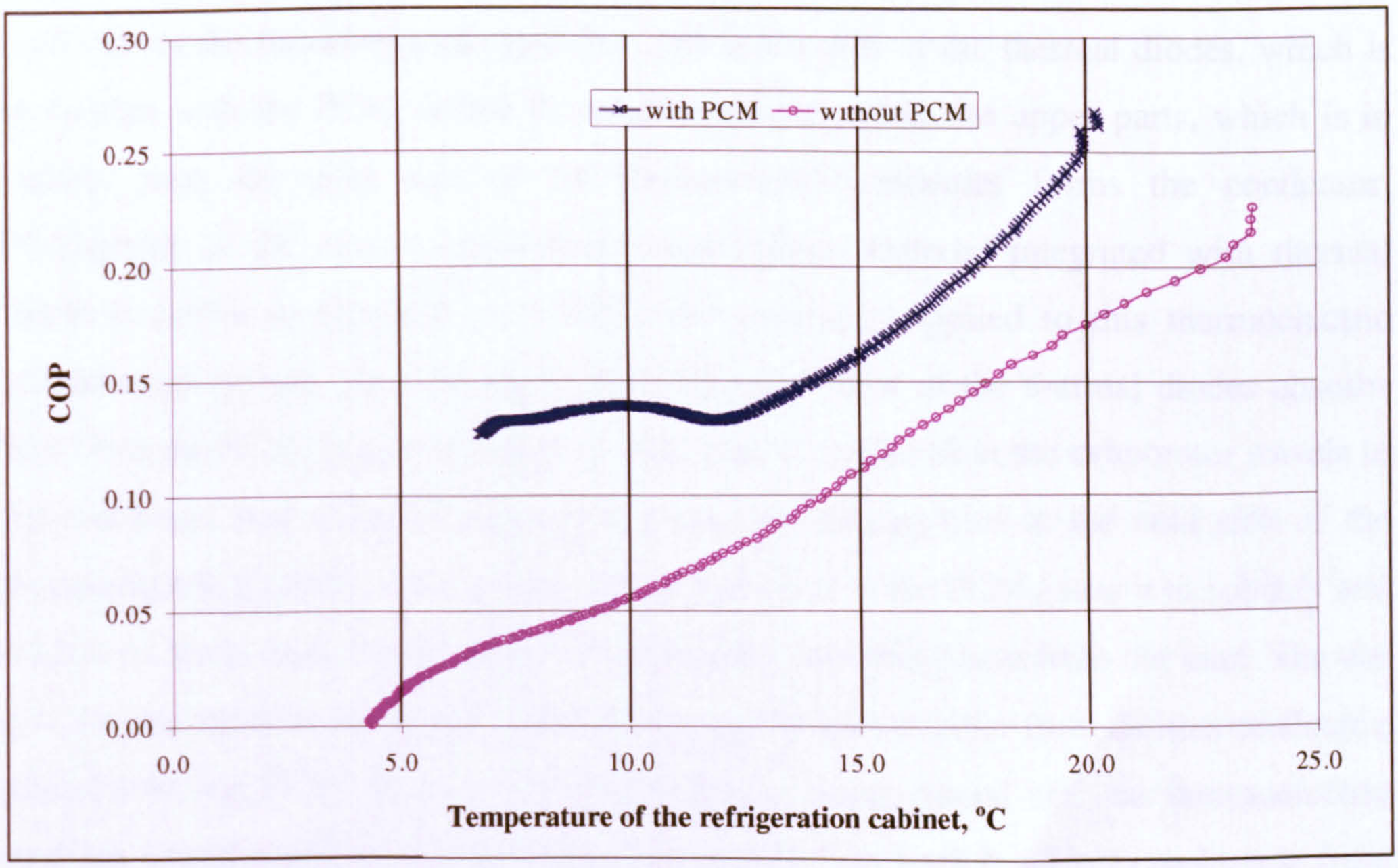

Figure 6-11. Comparison between performance of thermoelectric refrigeration system, with and without, PCM.

6.4 Experimental Investigation of the Thermoelectric Refrigeration System Employing Phase Change Material Integrated with Thermal Diode

6.4.1 Description of the Improved System

In the above arrangement of the refrigeration system illustrated in section 6.3, both the cold heat sink unit and the PCM are in direct contact with the cold side of the thermoelectric modules. This arrangement is appropriate during the cooling process as the thermal resistance is kept to a minimum. However, when power is turned off, the heat would leak back into the refrigeration cabinet. The PCM helps to provide a storage capacity in this situation. This storage capability could be improved by using a thermal diode that allows heat flow in one direction only. Using "wickless" heat pipe between the PCM and the cold side of the thermoelectric modules could provide this. The aim of this study is to investigate a novel refrigeration system employing a phase change material integrated with thermal diode to improve the performance of current thermoelectric modules. The refrigeration system was reconstructed, as shown in Fig.6-12. The only difference between the system in Figure 6-1 and that in Figure 6-12 is that, in the latter, the encapsulated PCM is not directly attached to cold side of the thermoelectric modules. The thermal diodes were inserted between the PCM and the cold side of the thermoelectric modules. The lower part of the thermal diodes, which is in contact with the PCM, forms the evaporator end, while the upper parts, which is in contact with the cold side of the thermoelectric modules forms the condenser. Photograph of the system employing phase change material integrated with thermal diode is shown in Figure 6-13. When DC current is applied to this thermoelectric refrigeration system, the working fluid in the evaporator of the thermal diodes absorbs heat from the PCM, producing cooling. The vapour produced in the evaporator travels to the condenser end where it condenses, whilst dissipating heat to the cold side of the thermoelectric modules. The cooling effect dissipated to the PCM cause it to solidify and release its latent heat. The PCM would melt while absorbing heat from the load. The use of a thermal diode in the system would enhance the heat transfer from the thermoelectric modules to the PCM. In an event of the power being turned off, the thermoelectric modules would cease operation and the heat would flow back by direct conduction from the hot side to the cold side of the thermoelectric modules, due to the temperature gradient. However, the operation of the thermal diode between the thermoelectric

modules and the PCM would cease because the cooling would not be sufficient to cause the vapour from the evaporator to condense, and thus would prevent heat leakage to the PCM via the thermoelectric modules. Due to the thermal diode can only transfer heat from the metal block to PCM, the evaluation of the performance of this system is the same as that of the system employing PCM directly attached to the cold side of thermoelectric modules, see Eq (6-1) and Eq (6-2).

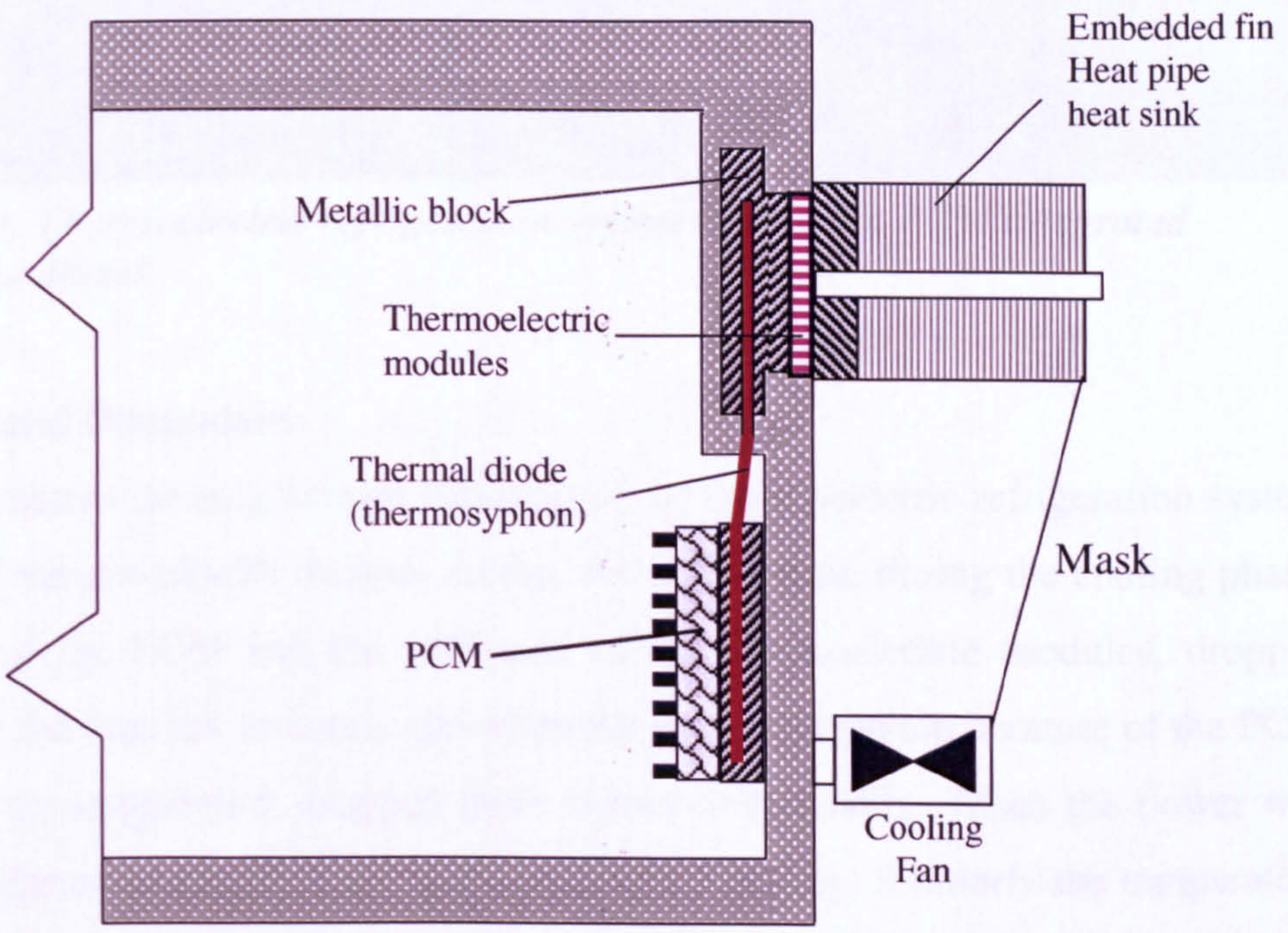

Figure 6-12. Schematic description of a thermoelectric refrigeration system employing PCM integrated with thermal diodes.

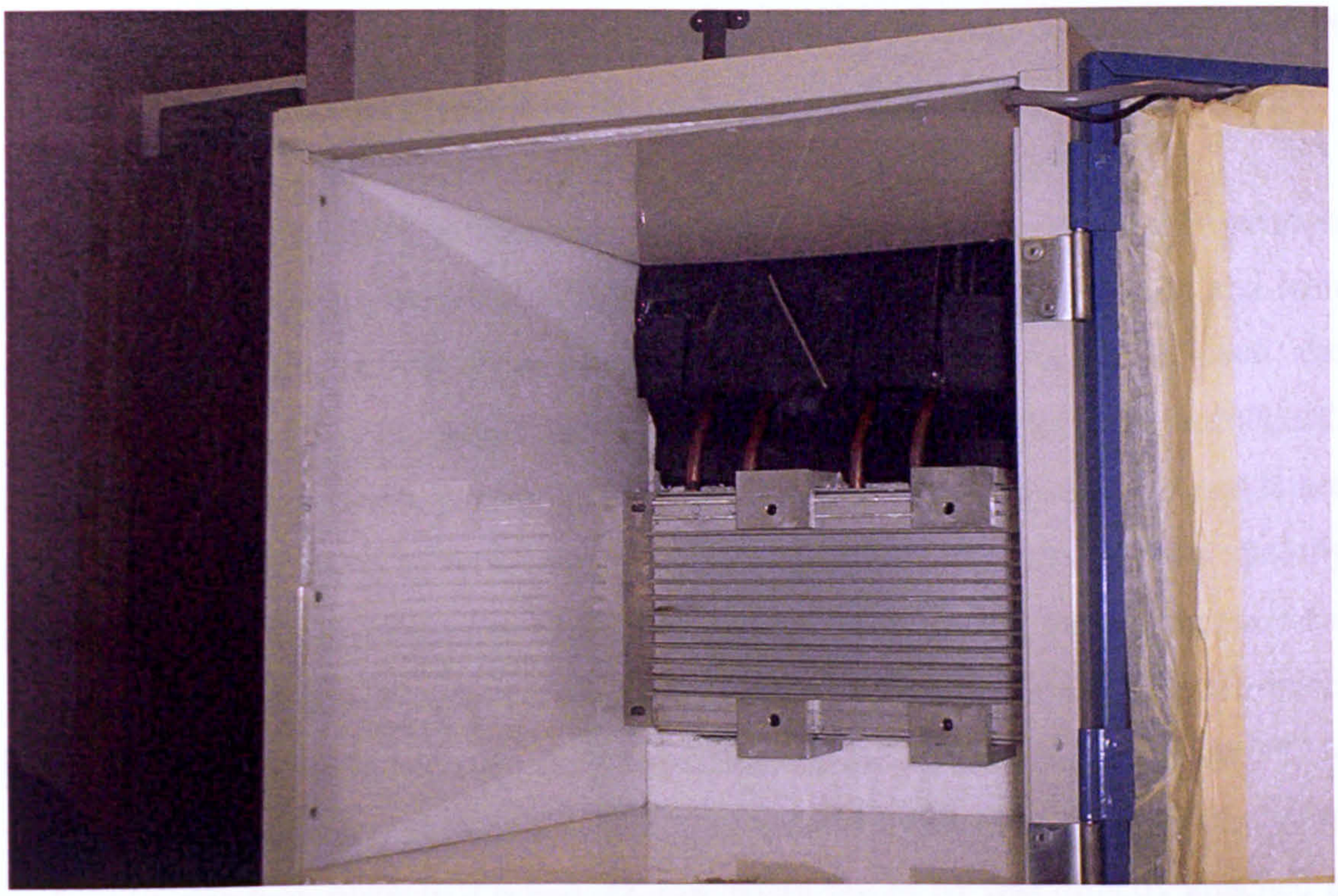

Figure 6-13. Thermoelectric refrigeration system employing PCM integrated with thermal diodes

6.4.2 Results and Discussions

Figure 6-14 presents the temperature variation of the thermoelectric refrigeration system with the PCM integrated with thermal diodes. As can be seen, during the cooling phase, temperatures of the PCM and the cold side of the thermoelectric modules, dropped rapidly during the first few minutes, and when the phase change temperature of the PCM was reached, the temperature dropped more slowly and steadily. When the power was switched off, the temperature of the hot side dropped rapidly. Similarly the temperature of the cold side increased rapidly to approach the hot side temperature near the ambient temperature. On the other hand, the PCM temperature and the refrigeration cabinet temperature increased steadily and slowly to approach the ambient in 4 h period after the power was switched off.

Without the thermal diodes (thermosyphons), the temperature of the PCM and the temperature of the refrigeration cabinet would have increased more rapidly. Inclusion of the PCM and the thermal diodes caused both the cooling and the heating processes to take place slowly due to the effect of the large energy storage capacity of the PCM.

Introduction of thermal diodes provided a thermal resistance to the heat transfer, which was an advantage when the power was switched off, as will be explained.

Figure 6-15 compares the PCM temperature variation of the thermoelectric refrigeration system with PCM directly attached to the cold side of thermoelectric modules and with PCM integrated with thermal diodes, during the cooling phase. As can be seen, the temperature of the PCM dropped more slowly, when thermal diodes were introduced. Similarly, when the power was switched off, the thermal diodes caused the temperature of the PCM to rise more slowly, compared to a situation when the PCM is directly attached to the cold side of the thermoelectric modules. This can be seen in Figure 6-16, which compares the temperature variation of the PCM with and without thermal diode, after the power was switched off. The temperature of the PCM increased from 2°C to 13.5°C in 5 h, when the PCM was integrated with thermal diodes, while the same temperature rise took place in 2 h and 20 min, when the PCM was directly attached to the cold side of the thermoelectric modules. In section 6.3, it was known that, replacement of the conventional heat sink system (bonded-fins heat sink) with a PCM, allowed twice as much time for a temperature in the refrigeration cabinet to rise to the same value compared to a refrigeration cabinet without PCM, after the power was switched off. It is worthy mentioning that, apart from the insulation that was used around the condenser section of the thermal diodes, the refrigeration cabinet insulation in all the tests was generally the same. Therefore, it could be concluded that, the temperature of a thermoelectric refrigeration system which incorporates PCM and thermal diodes, would take more than four times as long time to rise to the same value when conventional heat sink system is used, after the power was turned off. This is a major improvement on the performance of the thermoelectric refrigeration system.

The introduction of the thermal diodes, however did not contribute positively to the improvement of the COP of the thermoelectric refrigeration system, in place a slight reduction in COP was observed. Figure 6-17 compares COPs of the thermoelectric refrigeration system in three cases, i.e., without PCM, with PCM directly attached to thermoelectric modules and with PCM integrated with thermal diodes. It can be seen that, the COP drops steadily at lower temperatures, when conventional heat sink is used. However, the COP was improved significantly when PCM was introduced. It can be

observed that, the COP is almost constant during the phase change process as shown in Figure 6-17. This is because the cold side temperature is almost constant, resulting in a steady cooling rate. In general, use of PCM improves the performance of the thermoelectric refrigeration system, and provides a cooling storage capability, which is further improved by integration of the PCM with thermal diodes.

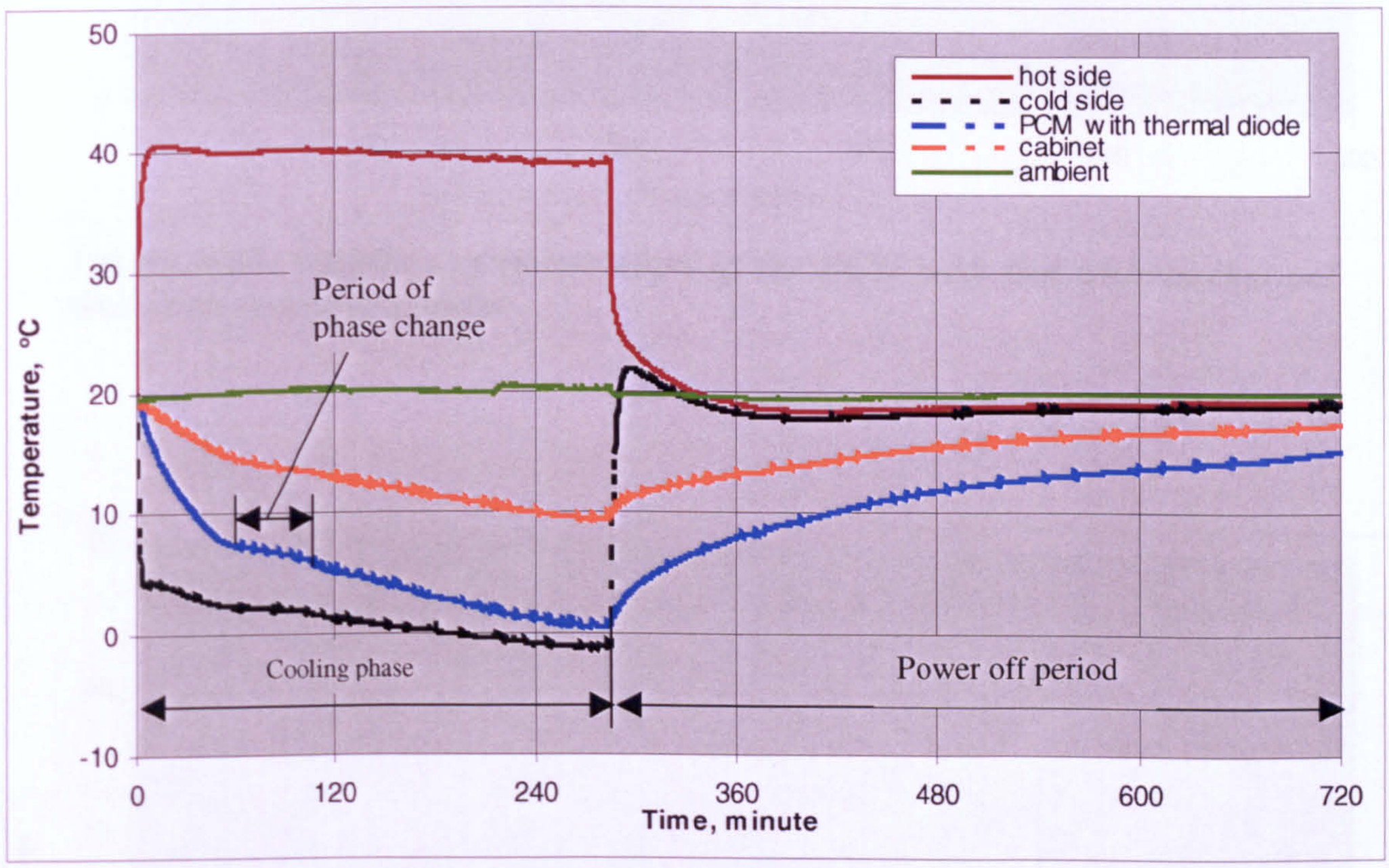

Figure 6-14.Temperature variation of the thermoelectric refrigeration system employing PCM integrated with thermal diode

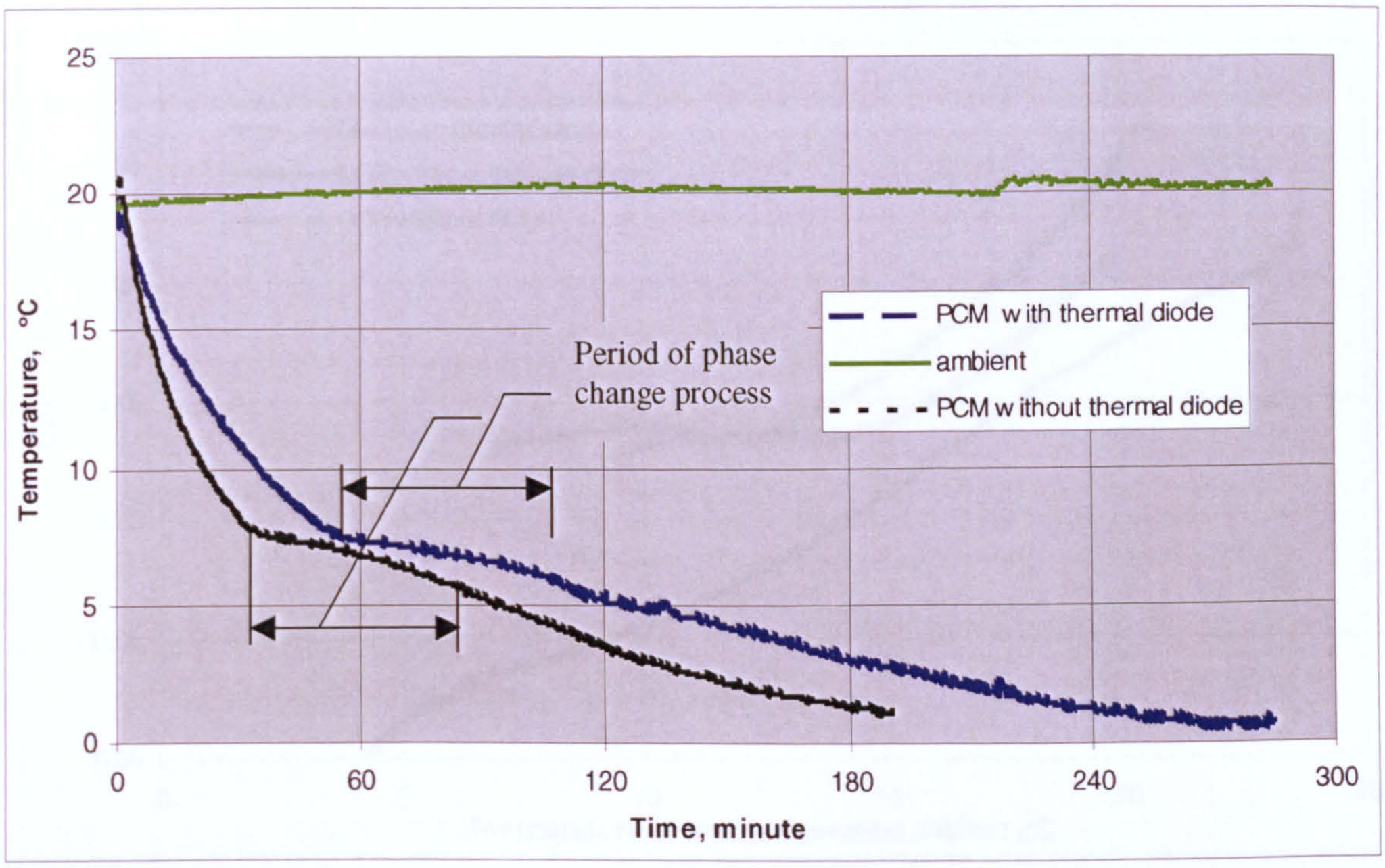

Figure 6-15. Variation of temperature of the PCM with and without thermal diode during cooling phase

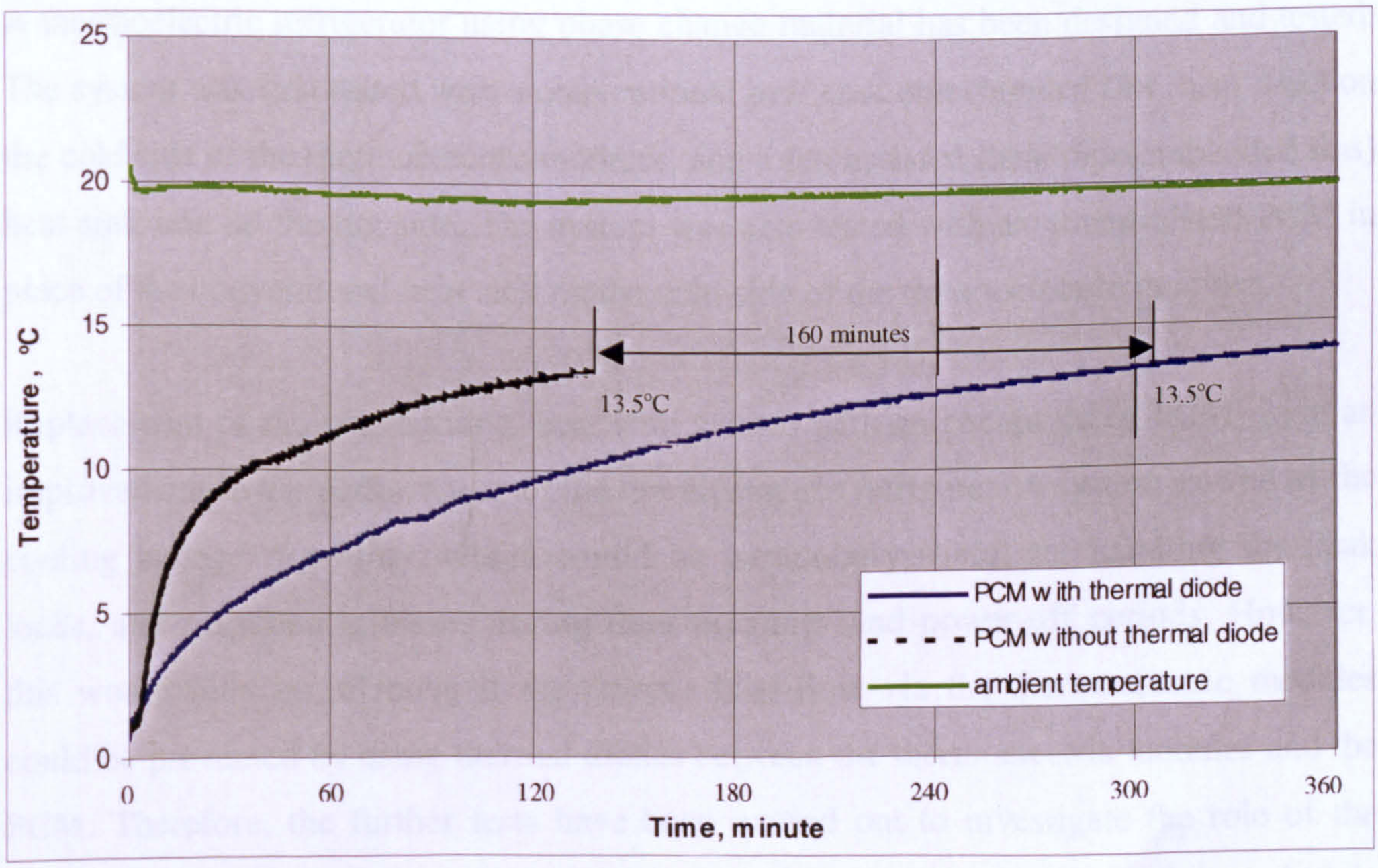

Figure 6-16. Variation of the temperature of the PCM with and without thermal Diode after the power was switched off

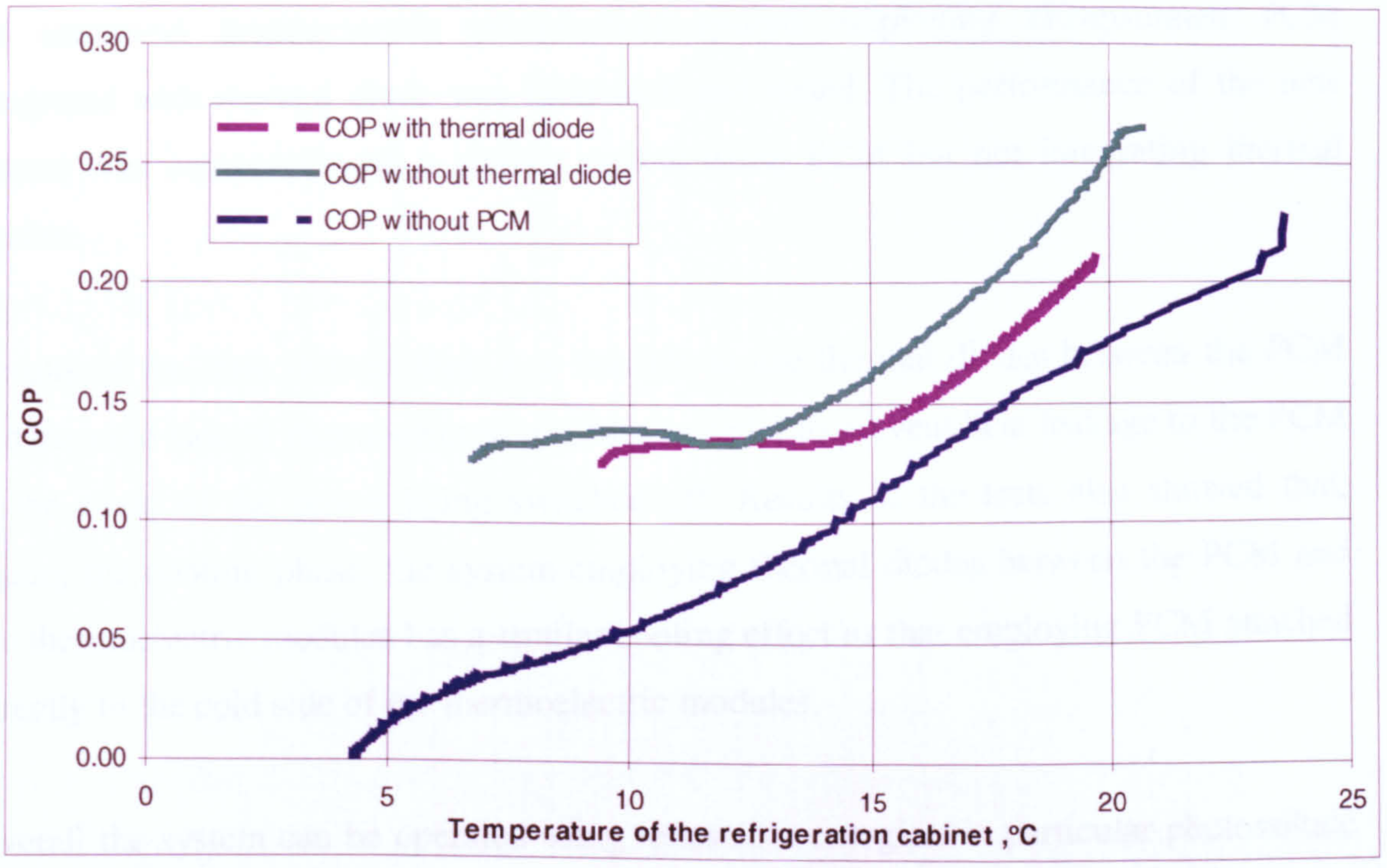

Figure 6-17. Comparison of the COP of thermoelectric refrigeration system with and without PCM and thermal diode.

6.5 Conclusion

A thermoelectric refrigerator using phase change material has been designed and tested. The system was first tested with a conventional heat sink unit (bonded fins, heat sink) on the cold side of the thermoelectric modules, and a fan-assisted (heat pipe-embedded fins) heat sink unit on the hot side. The system was also tested with an encapsulated PCM in place of the conventional heat sink on the cold side of the thermoelectric modules.

Replacement of the conventional heat sink system with an encapsulated PCM, gave an improvement in the performance of the thermoelectric refrigeration system as well as the cooling storage capability, which would be particularly useful for handling the peak loads, and overcoming losses during door openings and power-off periods. However, this would only be effective if the reverse heat flow via the thermoelectric modules could be prevented by using thermal diodes between the thermoelectric modules and the PCM. Therefore, the further tests have been carried out to investigate the role of the thermal diode (thermosyphon) and its effect on the performance of the thermoelectric refrigeration system.

An improved thermoelectric refrigeration system employing encapsulated PCM integrated with thermal diode was fabricated and tested. The performance of the new system was compared with a similar system using PCM but not integrating thermal diodes.

Results of the tests showed that, it is feasible to use thermal diodes between the PCM and the cold side of thermoelectric modules in order to prevent heat leakage to the PCM in the event of the power being switched off. Results of the tests also showed that, during the cooling phase, the system employing thermal diodes between the PCM and the thermoelectric modules has a similar cooling effect as that employing PCM attached directly to the cold side of the thermoelectric modules.

Overall the system can be operated using renewable energies, in particular photovoltaic solar energy which produces DC electricity, and is well suited for food and medicine storage.

Chapter 7. Conclusions and Further Work

7.1 Summary of the Work

This research investigated novel thermoelectric refrigeration systems, which include a building integrated thermoelectric heat pump and a thermoelectric refrigerator using phase change material. These systems can be driven by mains power (DC) or solar PV cells.

The research started from a review in relative to the several technical areas, including thermoelectric cooling technologies and their applications, research on improving coefficient of performance of thermoelectric cooling systems, heat pipe technology and heat pipe performance analysis, and photovoltaic solar cells and their applications. Technical progress in these areas was examined, and the innovative aspects of this research were identified compared to the current technical status.

The research investigated the thermoelectric module performance and finned heat sink performance. An optimum selection/design model of the thermoelectric modules was developed. The relation between optimum thermoelectric parameters and cooling/heating capacity, hot side/cold side temperature as well as geometry factor was investigated. An analytical model of the performance of the finned heat sink was developed. The relations between finned heat sink performance (heat transfer, efficiency and thermal resistance) and length of fins, number of fins and convective coefficient was investigated. These two models provided a basis for optimum selection/design of thermoelectric modules and finned heat sink.

The research also investigated the thermal performance of conventional heat pipe, including normal heat pipes, micro/miniature heat pipes, with/without wicks. Based on the investigation of the conventional heat pipes, a new type thermal diode was investigated for the two cases, i.e., using more liquid and using wick in the evaporator to keep the internal wall of the evaporator wet. An analytical model was developed to evaluate the heat transport capacity for the heat pipes. The new type thermal diode using more liquid to wet the internal wall of the evaporator was proposed. Variation of heat

transport capacity for the new type thermal diode with operation temperature, liquid fill level and channel geometry were investigated.

The research further involved the design, modelling, construction and testing of a novel thermoelectric heat pump, which can work in cooling and heating modes. A computer model was developed to analyse the heat transfer occurring in the heat pump. Modelling of the performance and required operating current of the heat pump was carried out under different operating and ambient temperatures, for both cooling and heating mode. The relation between the coefficient of performance and the operating condition as well as weather condition was explored. Laboratory tests were carried out to validate modelling predictions and examine the thermal performance of the heat pump. Comparison was made between the modelling and testing results, and the reasons for error formation were discussed. A correlation factor was determined to modify the predicted hot and cold side temperatures and this was used in the computer program to obtain more accurate modelling results.

The research work also involved the design, construction and testing of a thermoelectric refrigerator. The work intended to investigate the potential application of phase change materials (PCMs) in the thermoelectric refrigeration system. The system was first fabricated and tested using a conventional heat sink system at the cold side of the thermoelectric modules. In order to improve the performance and the storage capability, the system was reconstructed and tested using an encapsulated PCM as a cold sink. Results of testing of the latter system showed an improved performance compared with the former system. However to improve the storage capability, in particular during off-power periods, it was found necessary to integrate the PCM with the thermosyphons, which would allow heat flow in one direction only. Results of testing carried out on the system using PCM integrated with the thermal diodes showed considerable improvement in the storage capability of the thermoelectric refrigeration system compared with the previous ones.

7.2 Conclusions

Conditions for thermoelectric cooling/heating system to achieve maximum COP

For an application with fixed working temperatures T_h and T_c, the thermoelectric modules have an optimum current to achieve the maximum COP. To achieve maximum COP the optimum current should be input, i.e., the operating current of the thermoelectric modules should equal to the optimum current. For a specific working temperature T_h and T_c, a specific operating current is required to obtain the required cooling/heating capacity Q_c/Q_h. By using an appropriate number of thermoelectric modules or appropriate geometry factor, this operating current can equal the optimum current under this working temperature (hot/cold side temperatures of the thermoelectric modules) and therefore the maximum COP can be obtained.

The required number of thermoelectric modules for optimum current and COP increases with the cooling/heating capacity. The optimum current and optimum COP are determined by thermoelectric material property coefficients, geometry factor and working temperatures T_h and T_c, they have no relationship with the cooling capacity. The required number of the thermoelectric modules for optimum current and COP decreases with the increase of the hot side temperature and increases with the increase of the cold side temperature. To achieve optimum COP, the required number of thermocouples varies with the geometry factor, which determines the type of the thermoelectric modules. The larger the geometry factor, the fewer thermoelectric modules are required.

Heat transfer capacity and efficiency of the finned heat sink

Due to the high intensity heat flux, the thermoelectric modules can not work independently. They have to use heat sink to dissipate heat.

The heat transfer capacity and efficiency of finned heat sink varies with its geometry parameters as well as convective coefficient. The heat transfer capacity increases quickly with the length of fins while the length of fins is within a certain value, 8cm for selected finned heat sink for this investigation on thermoelectric heat pump, and it does not increase obviously while the length of fins is larger than around 8cm. The efficiency decreases with the increase of the length of fins. The heat transfer capacity increases straight with the number of fins. The efficiency decreases with the increase of the number of fins while the number of fins is within a certain value, 15 for selected finned heat sink for this investigation on thermoelectric heat pump, and it does not decrease

obviously while the number of fins is larger than 15. Although the high density of fin indicate a good performance as above analysis, it is suggested that appropriate number of fins should be chosen considering its resistance on coolant. The heat transfer capacity increases quickly with the increase of the convective coefficient and efficiency decreases with the increase of the convective coefficient.

Heat transport capacity of the new type thermal diode

The maximum heat transport capacity is the index evaluating heat transfer capacity of a heat pipe, which is governed by six limits, i.e., the sonic limit, the entrainment limit, the boiling limit, the viscous limit, the capillary limit as well as the filled liquid mass limit.

The new type thermal diode was investigated for two cases: one uses more liquid in evaporator to keep the internal surface of evaporator wet and another uses capillary wick to distribute the liquid from the bottom to the whole internal surface of the evaporator. The maximum heat transport capacity of the thermal diode for both cases increase with the working temperatures. The maximum heat transport capacity of the thermal diode for both cases increase with increasing cross section diameters. The maximum heat transport capacity of the thermal diode without wick remains constant when the liquid fill level varies. The maximum heat transport capacities of the thermal diode without wick, dominated by entrainment limit, are much greater than that of with wick under the various working temperatures, liquid fill levels and cross section diameters.

For the maximum heat transport capacities, n-pentane is superior to HFE-7100 in this investigation.

Thermoelectric heat pump

A thermoelectric heat pump prototype were designed and constructed to work in two modes, i.e., cooling mode and heating mode. The thermal performance of the heat pump system was investigated using the computer modelling and experimentally. It was found by both modelling and testing results that the COP and required DC current varies with cooling capacities (in cooling mode), heating capacities (in heating mode) and ambient temperature. In cooling mode, the COP decrease and the DC current increase with the increase of the cooling capacity and the ambient temperature. In heating mode, the COP

decrease and the DC current increase with the increase of the heating capacity, the COP increase and the DC current decrease with the increase of the ambient temperature. The COP of the heat pump is influenced greatly by the efficiency of the heat removal on the hot side of the thermoelectric modules. Using evaporation of water on the hot side heat sink can improve the COP in cooling mode significantly.

The testing results were compared with the theoretical predictions, and it was found that the distinct differences existed between the theoretical and testing values. The experimental COPs are lower and required currents are larger than modelling predictions. The main reason for this is the calculation of the thermal resistance of thermal diode in modelling was simplified due to the existing difficulty of calculating the thermal resistance of the new type thermal diode with a complex structure. Another reason for this is the difference between the designed heat sinks and the practical heat sinks. These cause the larger difference between the working temperatures in modelling and those in tests. The reasons for the difference between modelling and experimental results also include the limit of the model's accuracy as well as the manufacturing tolerances of the thermoelectric modules. These treatments were not taken into account in modelling development and processing. To enable the model to predict the heat pump performance at a reasonable accuracy, a correlation factor for working temperatures in modelling was determined and applied to the computer model and modified modelling results were obtained. The modified modelling results are much more close to the testing results, the differences between the COPs in modelling and in testing is within 0.2.

The required scale for an office of $15m^2$ in a building in Scotland was estimated based on the theoretical and experimental evaluations. The estimation was carried out for the system both using evaporation of water and not using evaporation of water in cooling mode. An COP of around 0.5 in cooling mode was determined. The estimated scale for the office is 150 pieces of CP2-127-06 thermoelectric modules with the area of $0.54m^2$ while not using the evaporation of water in cooling mode, and 106 pieces of CP2-127-06 thermoelectric modules with the area of $0.38m^2$ while using the evaporation of water.

Thermoelectric refrigerator using phase change material

A thermoelectric refrigerator system was designed, constructed and tested. To investigate the effect of the phase change material and thermal diode on the performance of the thermoelectric refrigeration system, the system was constructed and tested in three different configurations. The first configuration use a conventional heat sink unit (bonded fins heat sink) on the cold side of the thermoelectric modules. The second configuration use encapsulated PCM in place of the conventional heat sink on the cold side of the thermoelectric modules. The third configuration employing encapsulated PCM integrated with thermal diodes (thermosyphons) on the cold side. For the three configuration, a fan-assisted (heat pipe-embedded fins) heat sink unit was used on the hot side.

Results of the tests showed that, replacement of the conventional heat sink system with an encapsulated PCM, gave an improvement in the performance of the thermoelectric refrigeration system as well as the cooling storage capability, which would be particularly useful for handling the peak loads, and overcoming losses during door openings and power-off periods. However, this would only be effective if the reverse heat flow via the thermoelectric modules could be prevented by using thermal diode between the thermoelectric modules and the PCM, i.e., using the third configuration.

Results of the tests also showed that, it is feasible to use thermal diodes between the PCM and the cold side of thermoelectric modules in order to prevent heat leakage to the PCM in the event of the power being turned off. Results of the tests also showed that, during the cooling phase, the system employing thermal diodes between the PCM and the thermoelectric modules has a similar cooling effect as that employing PCM attached directly to the cold side of the thermoelectric modules.

7.3 Further work

Although substantial work has been carried out during this research, there are still quite a few opportunities to develop this thermoelectric heat pump and this thermoelectric refrigerator in order to improve the system's performance further. These may be indicated as follows:

Thermoelectric heat pump

It was noticed that reducing the hot side temperature of the thermoelectric modules would increase the COP significantly in cooling mode. Therefore, the configuration of the cranked thermal diode should be improved in order to remove the heat from the hot side more efficiently. Figure 8-1 shows a suggested improved configuration of the cranked thermal diode. The condenser (in cooling mode) constitutes of tubes connected with headers and the tubes are banded with fins, this configuration could increase the heat dissipating area and is easy to manufacture. The evaporator (in cooling mode) are still flat panel with the holes inside the panel and could be relevant small due to the less heat flow cold side (in cooling mode), the area could just match the total area of thermoelectric modules. This configuration is also suitable for working in heating mode.

The thermal resistance of the cranked thermal diode could be investigated by using CFD, by which the accurate thermal resistance could be predicted. The system analysis could be more accurate and therefore the practical system could obtained the designed optimum (maximum) COP. This would improve the performance greatly.

Evaporation of water is a very effective method to reduce the temperature of the heat sink. A circulation system for use of evaporation of water in the thermoelectric refrigeration system could be developed and used in the system to improve the COP.

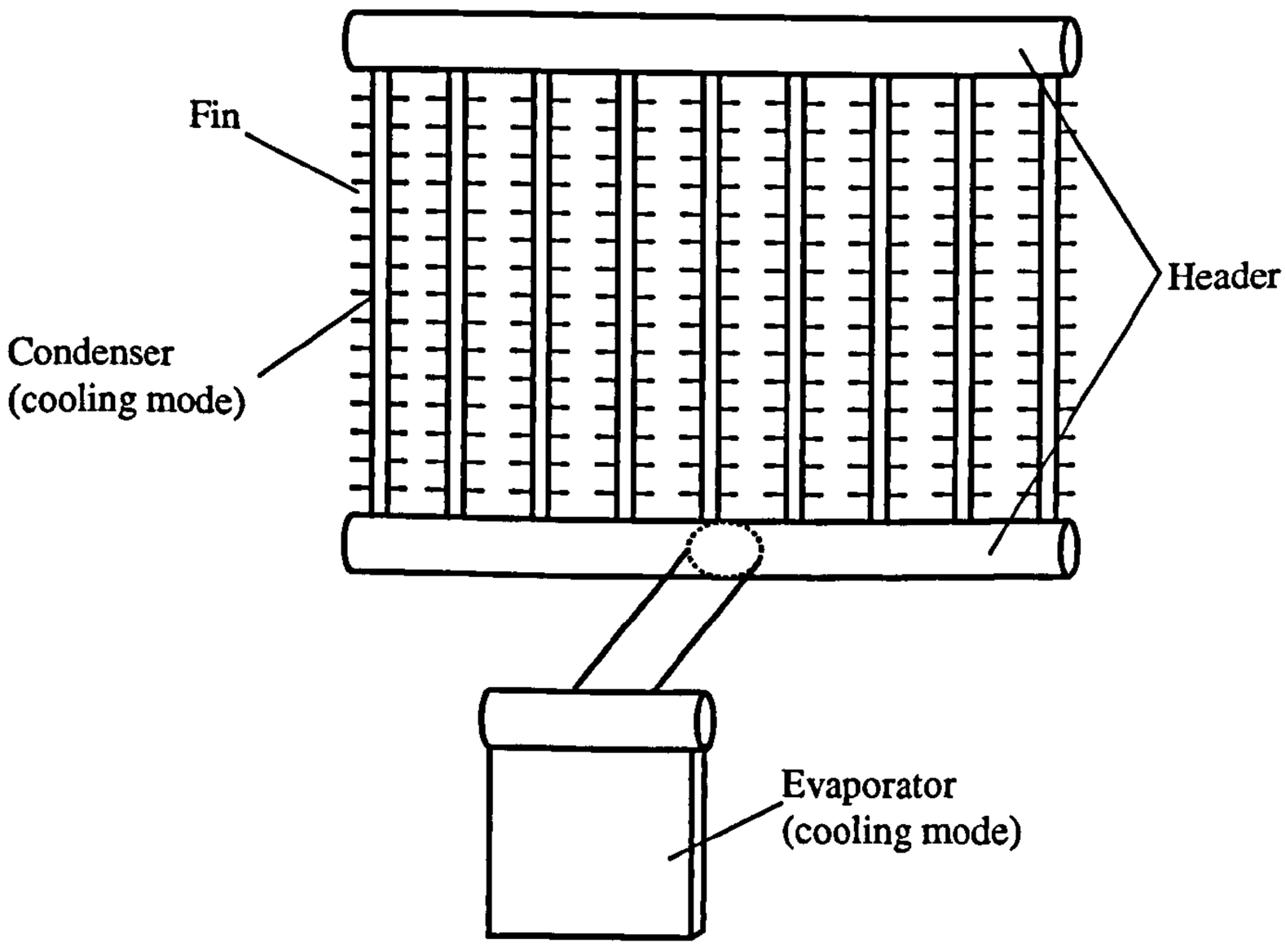

Figure 7-1. Schematic diagram of the improved configuration of new type thermal diode

Thermoelectric refrigerator

Due to the larger temperature difference between the hot and cold side of thermoelectric modules in the thermoelectric refrigerator, the COP of the system is much lower. The hot side heat sink system could be improved to reduce the hot side temperature and therefore improve the COP. This improvement could be achieved by developing a heat pipe heat sink system that could be mounted on the hot side vertically.

Combination of PV and the refrigeration system

Further investigations of the combining the PV into the thermoelectric refrigeration system could be carried out. The further investigations should include the optimum design of the PV system for a specific thermoelectric refrigeration system application, performance modelling and experimental testing.

References

A

Abhat A (1982) Performance investigation of a long, slender heat pipe for thermal energy storage application, J. Energy 6, pp.6-16.

B

Babin B.R., Peterson G. P., and Wu D. (1989) Analysis and testing of a micro heat pipe during steady state operation, American Society of Mechanical Engineers, New York, Paper 89-HT-17.

Babin B.R., Peterson G. P., and Wu D. (1990) Steady-state modelling and testing of a micro heat pipe, Journal of Heat Transfer 112, pp. 595-601.

Bale G et al (1999) Cooled CdZnTe detectors for X-ray astronomy, Nuclear Instruments and Methods in Physics Research Section A: Accelerators, Spectrometers, Detectors and Associated Equipment 436 (1999) pp.150-154.

Boehmer A. P et al (1963) Thermoelectric refrigerator, United States Patent, 3177670.

Bojic M et al (1997) Thermoelectric cooling of a train carriage by using a coldness-recovery device, Energy 22 (5) pp. 493-500.

Brown W.K et al (1965) Refrigerator-package arrangement, United States Patent, 3280573.

D

Duffie J A and Beckman W A (1991), Solar Engineering of Thermal Processes, John Wiley & Sons NewYork. London. Sydney. Toronto, TJ810.D8

Dunn P.D. and Reay D.A.(1982) Heat pipes, 3rd ed., Pergamon Press, New York.

F

Fahrenbruch A. L and Bube R. H (1983) Fundamentals of solar cells-photovoltaic solar energy conversion, Academic Press, Inc, New York.

Faghri, A. (1995) Heat Pipe Science and Technology, Taylor &Francis, Washington, DC, pp.11-110.

Fan C. Y, Air Conditioning System, Building Industry Press, China, 1983.

G

Gao M et al (1999) Cooling performance of integrated thermoelectric microcooler. Solid-state electronics 43 pp.923-929

Gao M, et al (2000) Improved model for calculating the coefficient of performance of a Peltier module, Energy Conversion and Management, Vol 41, pp.163-171.

Gilley, et al (1999) Thermoelectric refrigerator with evaporating/condensing heat exchanger. United States Patent, No. 6003319.

Groll M, Rösler S (1992) Operation principles and performance of heat pipes and closed two-phase thermosyphons, J.Non-Equilib. Thermodyn. Vol. 17 pp. 91-151

Guyer E.C (1988) Handbook of Applied Thermal Design, McGraw Hill, New York.

H

Hara T, et al (1998) Cooling performance of solar cell driven thermoelectric cooling prototype headgear, Applied Thermal Engineering, Vol. 18, pp.1159-1169

I

Iacullo R. S (1996) Thermoelectric intercooler cooling turbocharged air. United States Patent, 5547019.

J

Jeong S et al (1994) Optimum temperature staging of cryogenic refrigeration system, Cryogenics, Vol. 34, No. 11, pp.923-933.

Jones A.D and Underwood C.P (2001) A thermal model for photovoltaic systems, Solar Energy, Vol.70, Issue 4, pp. 349-359

K

Kin-ichi Uemura (1995) Commercial Peltier modules, in: D.M.Rowe (Ed.), Thermoelectric Handbook, CRC Press Inc., Boca Bato, FL, pp.621-631

Kim C.M et al (2001) Air conditioner for individual cooling/heating, United States Patent Application, 20010005990, kind code, A1.

Kraus A. D. and Bar-Cohen A. (1983) Thermal Analysis and Control of Eletronic Equipment, McGraw-Hill, New York.

L

Lienhard John H (2001) A Heat Transfer Textbook, Phlogiston Press, Cambridge, Massachusetts, USA.

Lindenblad N. E et al (1954) Thermoelectric refrigerator. United States Patent, 2837899

Lindler K.W (1998) Use of multi-stage cascades to improve performance of thermoelectric heat pumps, Energy Conversion and Management. Vol. 39, pp.1009-1014.

M

Morrow R.C (2000) Biomass production system (BPS) plant growth unit, Advance in Space Research: the Official Journal of the Committee on Space Research (COSPAR), Crabb, TM, 26 (2) pp.289-298.

R

Redus R.H et al (2001) Improved thermoelectrically cooled X/γ-ray detectors and electrobics, Nuclear Instruments and Methods in Physics Research Section A: Accelerators, Spectrometers, Detectors and Associated Equipment, Vol. 458, pp.214-219

Riffat S. B.(2000) European Commission, Energy, Environmental and Sustainable Development Programme, NNE5-1999-20114, Hybrid solar collector/CHP system.

Riffat S. B., Doherty P.S. and Abdel Aziz E.I.(2000) Performance testing of different types of liquid flat plate collectors, International Journal of energy Research, 24, pp.1203-1215.

Riffat S.B, Qiu G (2004) Comparative investigation of thermoelectric air-conditioners versus vapour compression and absorption air-conditioners, Applied Thermal Engineering (to be published in 2004)

Rowe D.M (1995) Handbook of Thermoelectrics, CRC Press Inc.

Rowe D.M et al.(1998) Evaluation of thermoelectric modules for power generation, Journal of Power Sources 73 pp. 193-198

S

Sanz-Bobi M. A, et al (1996) Thermoelectricity applied to the cryoconcentration of orange juice, 15th International Conference on Thermoelectrics, pp.259-263

Scruggs M.K et al (2001) Thermal-electrically cooled photodetector, United States Patent Application, 20010032922, kind code, Al.

Sofrata H (1996) Heat rejection alternatives for thermoelectric refrigerators, Energy Conversion and Management. Vol. 37 pp.269-280

T

Takaoka M., Motai T., Sakaya M., Mochizuki M., Mashiko K., and Ito M. (1985) Development of long heat pipes and heat pipe products, Fujikura Technical Review, No.14, Fujikura Ltd., Tokyo, Japan.

V

Venkatasubramanian R, et al (2001) Thin-film thermoelectric devices with high room-temperature figures of merit, Nature, Vol. 413, pp.597-602.

Viorel Badescu (2003) Dynamic model of a complex system including PV cells, electric battery, electrical motor and water pump, Energy, Vol. 28, Issue 12, pp. 1165-1181.

W

Webb-RL, et al (1998) Advanced heat exchange technology for thermoelectric cooling, Journal of Electric Packing, Vol. 120 No.1, pp.98-105.

Welling Jr T. E, et al(1997) The effect of thermoelectric cooler mounting orientation on cooling efficiency. Aes-vol.37, Proceedings of the ASME Advanced Energy Systems Division ASME pp.303-307

Z

Zhao X (2002) Design of an Energy Efficient Timber System at a Sawmill in Scotland, Heat Pump Association 7th Annual Student Award.

Zhuang J. et al. (1989) Heat Pipe and Heat Pipe Heat Exchanger, First ed., The Press of Jiaotong University, Shanghai, China, pp.127-147.

Zwaan Bob van der and Rabl Ari, Prospects for PV: a learning curve analysis, Solar Energy, Vol. 74, Issue 1, pp. 19-31

Appendix A

Thermoelectric material property coefficients

Material Property Coefficients

$$\alpha=(\alpha_0+\alpha_1 T_m+\alpha_2 T_m^2)x10^{-9} \qquad \text{(volts/Kelvin)}$$

α_0=22224.0

α_1=930.6

α_2=-0.9905

$$p=(p_0+p_1 T_m+p_2 T_m^2)x10^{-8} \qquad \text{(ohm cm)}$$

p_0=5112.0

p_1=163.4

p_2=0.6279

$$k=(k_0+k_1 T_m+kT_m^2)x10^{-6} \qquad \text{(watt/(cm Kelvin))}$$

k_0=62605.0

k_1=-277.7

k_2=0.4131

$Z=\alpha^2/(pK)$ (Kelvin^{-1})

Appendix B

Module types and their geometry factors (G)

Module type	G
FC 0.45 -xx- 05	0.016
FC 0.6 -xx- 06	0.024
FC 0.6 -xx- 05	0.030
FC 0.65 -xx- 04	0.040
CP 0.8 -xx- 0.6	0.042
CP 0.8 -xx- 05	0.052
CP1.0 -xx- 08	0.050
CP1.0 -xx- 06	0.061
CP1.0 -xx- 05	0.079
CP1.4 -xx- 10	0.077
CP1.4 -xx- 06	0.118
CP1.4 -xx- 045	0.171
CP2 -xx- 10	0.184
CP2 -xx- 06	0.282
CP2.8 -xx- 06	0.473
CP5 -xx- 10	0.778
CP5 -xx- 06	1.196

Appendix C

Publication list during this research

1. **A Novel Thermoelectric Refrigeration System Employing Heat Pipes and a Phase Change Material, an Experimental Investigation, S.B.Riffat, S.A.Omer and Xiaoli Ma, Renewable Energy (23), 2001, 313--323**

Abstract

This paper presents results of tests carried out to investigate the potential application of heat pipes and phase change materials for thermoelectric refrigeration. The work involved the design and construction of a thermoelectric refrigeration prototype. The performance of the thermoelectric refrigeration system was investigated for two different configurations. The first configuration employed a conventional heat sink system (bonded fin heat sink) on the cold side of the thermoelectric cells. The other configuration used an encapsulated phase change material in place of the conventional heat sink unit. Both configurations used heat pipe embedded fins as the heat sink on the hot side. Replacement of the conventional heat sink system with an encapsulated phase change material was found to improve the performance of the thermoelectric refrigeration system. In addition, it provided a storage capability that would be particularly useful for handling peak loads and overcoming losses during door openings and power-off periods. Results showed that the heat sink units employing heat pipe embedded fins were well suited to this application. Results also showed the importance of using a heat pipe system between the cold junction of the thermoelectric cells and the cold heat sink in order to prevent reverse heat flow in the event of power failure.

2. Experimental Investigation of a Thermoelectric Refrigeration System Employing a Phase Change Material Integrated with Thermal Diode (Thermosyphons), S.B.Riffat, S.A.Omer and Xiaoli Ma, Applied Thermal Engineering (21) 2001 , 1265-1271

Abstract

This paper presents results of tests carried out to investigate the potential application of phase change materials (PCMs) integrated with thermosyphons in a thermoelectric refrigeration system. The work involved design, fabrication and test of a 150 W thermoelectric refrigeration system. The system was first fabricated and tested using a conventional heat sink system (bonded fin heat sink system) at the cold heat sink. In order to improve the performance and the storage capability, the system was reconstructed and tested using an encapsulated PCM as a cold sink. Results of tests of the latter system showed an improved performance compared with the former system. However to improve the storage capability, in particular during off-power periods, it was found necessary to integrate the PCM with a thermal diode, which would allow heat flow in one direction only. Results of tests carried out on the new system showed considerable improvement in the storage capability of the thermoelectric refrigeration system compared with the previous ones. Overall the system suits operation with renewable energies, e.g., solar energy.

3. Thermoelectrics: A Review of Present and Potential Applications, S.B.Riffat and Xiaoli Ma, Applied Thermal Engineering, (23) 2003, 913-935

Abstract

Thermoelectric devices are solid state devices. They are reliable energy converters and have no noise or vibration as there are no mechanical moving parts. They have small size and are light in weight. As refrigerators, they are friendly to the environment as CFC gas or any other refrigerant gas is not used. Due to these advantages, the thermoelectric devices have found a large range of applications. In this paper, basic knowledge of the thermoelectric devices and an overview of these applications are given. The prospects of the applications of the thermoelectric devices are also discussed.

4. **Improving the Coefficient of Performance of Thermoelectric Cooling System: A review, S.B. Riffat and Xiaoli Ma, International Journal of Energy Research. 2004; 28: 753-768.**

Abstract

This paper reviews research carried out to improve the coefficient of performance of thermoelectric cooling systems during the past decade. This includes development of new materials for thermoelectric modules, optimisation of module design and fabrication, system analysis and heat exchange efficiency. Several conclusions are drawn.

5. Experimentation of a Novel Thermoelectric Heat Pump System, S.B.Riffat and Xiaoli Ma, International Journal of Ambient Energy, (accepted to be published)

Abstract

This paper presents results of tests carried out to investigate a passive technology based on integration of a thermal diode and thermoelectric modules for a novel heat pump. The system is very compact and suitable for incorporation within the building structure. The heat pump uses thermoelectric modules to produce cooling or heating, and a new type of thermal diode to transfer heat in or out of the building, and prevents reverse heat flow in the event of power failure. Following design and construction of a thermoelectric heat pump prototype, its performance was investigated for two different modes, i.e., cooling and heating, under various operating conditions and environmental temperatures. Results showed that reducing the temperature of the condenser of the thermal diode could provide a significant improvement of the efficiency of the thermal diode and the coefficient of performance (COP) of the system in cooling mode. This can be achieved using the evaporation of water on the heat sink attached to the condenser. The experimental results showed that the new type of thermal diode worked effectively in both cooling and heating modes.

6. Optimum Selection (Design) of Thermoelectric Modules for Large Capacity Heat Pump Applications, S.B.Riffat and Xiaoli Ma, International Journal of Energy Research, (proof approved in publish list)

Abstract

Thermoelectric modules should be selected or designed to meet the specific cooling/heating requirements of a particular application and in most cases, the cooling /heating capacity and the working temperatures (hot and cold side temperature of thermoelectric devices) are known. Computer modelling can be used to assist the selection process by determining the relationships between the cooling/heating requirements and optimum thermoelectric parameters thermoelectric modules suited to large capacity thermoelectric heat pump applications.

7. Performance Simulation and Experimental Testing of a Novel Thermoelectric Heat Pump System, S.B. Riffat and Xiaoli Ma, (completed)

Abstract

A computer model has been developed to simulate the performance of a novel thermoelectric heat pump system. The modelling was carried out to simulate the performance of a small prototype system. Results were obtained for various operating and weather conditions, and these were compared with experimental results carried out for the fabricated prototype system. Reasons for differences between the modelling results and test results were analysed, and the computer model was modified. More accurate modelling results were then obtained. The work provides a basis for analysis and design of the thermoelectric heat pump system.